STELLENBOSCH UNIVERSITY

A Kinetic and Thermodynamic Study of Procyanidin Oligomer Conformation by ^{1}H NMR and DFT

Author

S.J. O'Kennedy

Supervisor

Dr W.J. Gerber

Co-Supervisors

Prof. A.J. De Villiers

Dr D.J. Brand

December 2015

Declaration

By submitting this thesis/dissertation electronically, I declare that the entirety of the work contained therein is my own, original work, that I am the sole author thereof (save to the extent explicitly otherwise stated), that reproduction and publication thereof by Stellenbosch University will not infringe my third party rights and that I have not previously, in its entirety or in part, submitted it for obtaining a qualification.

Date: December 2015

Special Thanks

Prof. A.J. De Villiers	Thank you for your humour, conversation, assistance, financial support, academic drive and mentorship.
Bernard Dippenaar	Thank you for your assistance with the application and submission of scripts to and from the CHPC.
Danie van Niekerk	Thank you for your insights, humour, transport and assistance in any manner of office related labour.
Dr D.J. Brand	Thank you for your ready support, expertise and assistance with any and all matters concerning NMR.
Elsa Malehrbe	Thank you for the assistance in the NMR labs beyond the call of duty and an eternally positive and friendly attitude.
Hannelize Kritzinger	Thank you for your love, friendship, support, conversation, understanding, hardheadedness, academic drive, assistance, transport, emergency assistance, gifts, food and every day I can share with you. You have meant more to me than I can ever show.
John O'Kennedy	Thank you for assistance, friendship, advice, transport, financial support and humour. Brotherhood can never be replaced.
Prof. K. Koch	Thank you for a positive attitude, assistance, advice, constructive presentation criticism and the academic role model that you are to the chemistry students.
Lambertus O'Kennedy	Thank you for your support, advice, eternal pride in me, financial support, sporadic phone calls and guiding hand. You will always be my advisor and role model.
Dr Martha Kallili	Thank you for your eternal optimism, assistance and mentorship in practical chromatography and selflessness in your assistance.
Nicolas Walters	Thank you for your friendship, humour, conversation, advice, midnight hours of keeping me company during long NMR experiments, positive attitude and giving

	personality. Your friendship has carried me through two degrees.
Shafiek Mohammed	Thank you for all the administration, assistance with experimental equipment and chemical procurement. This department would not function without you and the rest of the technical and administrative staff.
Suzette O'Kennedy	Thank you for your eternal faith in me, your culinary creations that always come back after a visit, your insights into life and the role you have played in my upbringing. I can never repay the love and dedication you have shown.
Dr T.E. Geswindt	Thank you for all the transport, humour, conversation, mentorship, assistance and advice.
Dr W.J. Gerber	Thank you for your assistance, understanding, insight, mentorship, financial support, advice, humour and academic drive. Without you this study would never have been possible.
God	I give eternal thanks to the creator for my wits, good health and the opportunities I have been given. May I play a positive role in this world as homage.

Table of Contents

List of Figures and Tables

List of Terms and Acronynms

Acetylation	The synthetic reaction for the addition of an acetyl moiety
ADF	Amsterdam density functional
Astringency	The physical experience of dryness or puckering of the mouth during the consumption of tannin-containing substances, such as wine.
BCP	Bond critical point
BSSE	Basis set superposition error
CCP	Cage critical point
Chirality	The geometric property of a rigid object (or spatial arrangement of points or atoms) of being non-superimposable on its mirror image
Colloid	With reference to the formation of fine aggregating particles
COSMO	Conducter-like screening model
Counterpoise corrections	BSSE energy corrections in a DFT calculation
Dimer	Two monomeric units in either a non-covalent interaction (uncharged or ionic) or a bonded covalent molecule
DFT	Density functional theory
ESI	Electrospray ionization
ESP	Electrostatic surface potential
FFT	Fast Fourier transform
FID	Free induction decay
FT-NMR	Fourier transform nuclear magnetic resonance
HILIC	Hydrophiliic interaction chromatography
HMBC	Heteronuclear multiple bond correlation spectroscopy
HPLC	High performance liquid chromatography
HSQC	Heteronuclear single quantum coherence spectroscopy
Hydrophilic	Polar and attracted to polar molecules like water
Hydrophobic	Non-polar and repulsed by polar molecules like water

MD	Molecular dynamics
Micelles	Spherical (usually) surfactant aggregates with hydrophobic surfaces on the inside and hydrophylic moieties on the outside of the 'sphere'
MM	molecular mechanics
Monomers	A single unit of an oligomer, aggregate or a fraction of a molecule in fraction analysis
MS	Mass spectrometry
NCI	Non covalent interaction
NMR	Nuclear magnetic resonance
NOE	Nuclear Overhauser effect
NOESY	Nuclear Overhauser effect spectroscopy
Oligomers	A molecule of intermediate relative molecular mass, the structure of which essentially comprises a small plurality of units derived, actually or conceptually, from molecules of lower relative molecular mass. Used in this text to refer to low relative molecular weight polymers of procyanidin monomers.
PES	Potential energy surface
Procyanidins	Flavanoids belonging to the proanthocyanidins family and the principal molecules studied in this text
QM	Quantum mechanics
QTAIM	Quantum theory of atoms in molecules
QTOF	Quadropole time of flight
RCP	Ring critical point
RDG	Reduced density gradient
ROESY	Rotational frame nuclear Overhauser effect spectroscopy
RP	Reversed phase
SCF	Self-consistent field
SCRF	Self-consistent reaction field
UHPLC	Ultra high pressure liquid chromatography
WFT	Wave functional theory

3DRISM	Three dimensional reference site interaction model

Nomenclature of Equations

E_0	The electronic minimum energy of a molecule
$\Delta G^{\ddagger}$	Gibbs free energy of activation
$\Delta G^{0}{}_{rxn}$	Standard Gibbs free energy of reaction
$\widehat{H}$	The Hamiltonian operator
$\Delta H^{\ddagger}$	Enthalpy of activation
$\Delta H^{0}{}_{rxn}$	Standard enthalpy of reaction
ρ	The electron density
$\Delta S^{\ddagger}$	Entropy of activation
$\Delta S^{0}{}_{rxn}$	Standard entropy of reaction
$\widehat{T}$	The kinetic energy of the molecule
$\widehat{V}_{ee}$	The energy of the electron-electron repulsions
$\widehat{V}_{Ne}$	The energy of attraction and repulsion between the electrons and their environment, which includes the nuclei and any external magnetic or electronic fields
ψ	The wave function

Summary

Two procyanidin dimers, four trimers and single tetramer, pentamer and hexamer species were isolated by preparative liquid chromatography from fresh cocoa beans. The most abundant procyanidin dimer was identified as procyanidin B2 by means of UHPLC-ESI-TOF-MS and one- and two-dimensional hetero- and homonuclear NMR spectroscopy. The effect of aggregation was discounted based on DOSY NMR experiments in conjunction with the Einstein-Stokes equation. The hydrodynamic radius of the molecule (8.5 Å) is too small for aggragation. Line shape analysis of variable temperature ^{1}H NMR procyanidin B2 spectra by a custom developed program (NMRfit) yielded first order kinetic reaction parameters for the conformational interchange. The calculated $\Delta H^{\ddagger}_{forward}$ is 57.03 ± 3.92 kJ.mol^{-1}, $\Delta H^{\ddagger}_{reverse}$ is 53.36 ± 3.82 kJ.mol^{-1}, while $\Delta S^{\ddagger}_{forward}$ is -0.3454 ± 14.76 J.mol^{-1}K^{-1} and $\Delta S^{\ddagger}_{reverse}$ is -4.398 ± 14. 39 J.mol^{-1}K^{-1}. The thermodynamic parameters for the conformational interchange reaction are: ΔH^{0}_{rxn} = 3.670 ± 0.217 kJ/mol and ΔS^{0}_{rxn} = 4.053 ± 1.57 J.mol^{-1}K^{-1}. The conformational geometries and standard reaction Gibbs free energies were calculated via DFT. Current conformational models reported in literature for procyanidin B2 were found to be insufficient. Four conformers were identified in this text, as opposed to only two conformers reported previously. The new conformations have been named: fully compact (FC), fully extended (FE), partially compact (PC) and partially extended (PE). Intramolecular interactions that include hydrogen bonds were shown to occur to varying degrees within each conformer. The resulting electronic stability hierarchy was found to be FC>FE>PC>PE with two of the three functionals used in the calculations. However, it was found that the entropy component of the Gibbs free energy plays a significant role in determining the thermodynamic distribution. The conformations with the most internal interactions were also found to be less available to solvent interactions due to a decrease in the polarization of their hydroxyl moieties and the reduced availability of the solvation sites, due to a closed conformation. The final Gibbs free energy hierarchy (PC>FE>PE>FC) indicates that the PC and FE conformers are the two conformers visible on NMR spectra. Finally, the distribution of conformers is shown to approach 1:1 in increasing solvent polarity.

Opsomming

Twee procyanidin dimere, vier trimere en enkel tetrameer, pentameer en heksameer spesies is geïsoleer deur middel van preparatiewe chromatografie vanaf vars Kukao bone en die mees vollop procyanidin dimeer is identifiseer as procyanidin B2 deur middel van UHPLC-ESI-TOF-MS eksperimente en een- en twee-dimensionele hetero- and homokern KMR spektroskopie. Die effek van aggregasie was weglaatbaar gewys deur middel van DOSY KMR eksperimente in samewerking met die Einstein-Stokes vergelyking. Die berekende hidrodinamiese radius van die molekule (8.5 Å) is te klein vir aggregasie om teenwoordig te wees. Analiese van die KMR lyn vorme deur middel van 'n selfgeskrewe program (NMRfit) het eerste orde reaksie parameters gelewer. Die berekende $\Delta H^{\ddagger}_{vorentoe}$ is 57.03 ± 3.92 kJ.mol^{-1}, $\Delta H^{\ddagger}_{terugwaarts}$ is 53.36 ± 3.82 kJ.mol^{-1}, terwyl $\Delta S^{\ddagger}_{vorentoe}$ -0.3454 ± 14.76 J.mol^{-1}K^{-1} is en $\Delta S^{\ddagger}_{terugwaarts}$ -4.398 ± 14. 39 J.mol^{-1}K^{-1} is. Die termodinamiese parameters is bepaal as: ΔH^{0}_{rxn} = 3.670 ± 0.217 kJ/mol en ΔS^{0}_{rxn} = 4.053 ± 1.57 J.mol^{-1}K^{-1}. Die konformasie geometrieë en Gibbs vrye energieë van konformasie was bereken deur middel van DFT. Huidige konformasie modelle rapporteer in literatuur vir procyanidin B2 is onvoldoende bewys, aangesien vier konformere identifiseer is in die teks, in teenstryd met die twee konformere wat voorheen bepaal is. Die nuwe konformere is "fully compact" (FC), "fully extended" (FE), "partially compact" (PC) en "partially extended" (PE) benoem. Intramolekulêre interaksies, insluitend waterstofbindings, is gewys om plaas te vind in verskillende hoeveelhede binne elke konformeer. Gevolglik is die elektroniese hierargie van die konformere FC>FE>PC>PE vir twee van die drie "functionals" gebruik in die berekeninge. Die entropie komponente van Gibbs vrye energieë is egter gewys om 'n merklikke invloed te hê op die termodinamiese verspreiding van konformeer stabiliteit. Die konformere met die meeste interne interaksies is ook gewys om minder beskikbaar te wees vir interaksies met die oplosmiddel as gevolg van minder gepolariseerde hidroksiel funksionele groepe en steriese hindernis. Die finale Gibbs vrye energie hierargie (PC>FE>PE>FC) dui aan dat the PC en FE konformasies die sigbare konformere is op die KMR spectra en die berekende energieë van oplossing dui aan dat die equilibrium konstante na een streef soos die polariteit van die oplosmiddel toeneem.

Chapter 1. General Introduction

1.1 Introduction to Procyanidins

Procyanidins are organic and oligomeric phenolics of the proanthocyanidin family, also called condensed tannins. Table 1.1 shows the family of proanthocyanidins as redrawn from Ferreira *et al.* [1] to be used in conjunction with Figure 1.1.

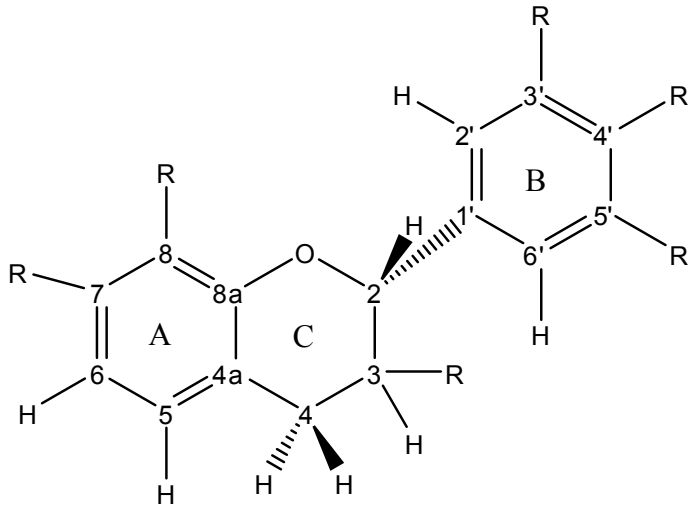

Figure 1.1. General structure of a proanthocyanidins with R representing various substituents (refer to Table 1.1 for classification of proanthocyanidins and substituents)

Table 1.1. Nomenclature and hydroxylation patterns corresponding to each group of proanthocyanidins [1]

		Hydroxylation pattern						
Proanthocyanidin	**Monomer**	**3**	**5**	**7**	**8**	**3'**	**4'**	**5'**
Procassidin	Cassiaflavan	H	H	OH	H	H	OH	H
Probutinidin	Butiniflavan	H	H	OH	H	OH	OH	H
Proapigeninidin	Apigeniflavan	H	OH	OH	H	H	OH	H
Proluteolinidin	Luteoliflavan	H	OH	OH	H	OH	OH	H
Protricetinidin	Tricetiflavan	H	OH	OH	H	OH	OH	OH
Prodistenidin	Distenin	OH	OH	OH	H	H	H	H
Propelargonidin	Afzelechin	OH	OH	OH	H	H	OH	H
Procyanidin	Catechin	OH	OH	OH	H	OH	OH	H
Prodelphinidin	Gallocatechin	OH	OH	OH	H	OH	OH	OH
Proguibourtinidin	Guibourtinidol	OH	H	OH	H	H	OH	H
Profisetinidin	Fisitinidol	OH	H	OH	H	OH	OH	H
Prorobinetinidin	Robinetinidol	OH	H	OH	H	OH	OH	OH
Proteracacinidin	Oritin	OH	H	OH	OH	H	OH	H
Promelacacinidin	Mesquitol	OH	H	OH	OH	OH	OH	H

Procyanidins are part of the flavanol sub-family of proanthocyanidins and are present in various plant species and products such as baobab fruit [2], bayberry [3], grape seed [4], wine [5], cocoa beans [6] and high tannin beverages, e.g. tea [7]. 'Procyanidin' can be directly translated as 'before cyanidin'; the name originates from the transformation of procyanidin to cyanidin that occurs under acidic conditions as a depolymerization reaction [8]. The color of a solution containing procyanidins changes from colourless to red or purple as cyanidin is formed.

Catechin and epicatechin, the procyanidin monomers, have 2*R*, 3*S* and 2*R*, 3*R* configurations of the C2 and C3 carbons respectively. Figure 1.2. shows the general structure and nomenclature of a procyanidin. The oligomeric procyanidins are formed by various combinations of catechin and epicatechin linked through the C8(A), C6(A) and C4(C) carbon atoms [9]. Procyanidins are notoriously difficult to separate and identify chromatographically due to this diastereomeric and chiral complexity.

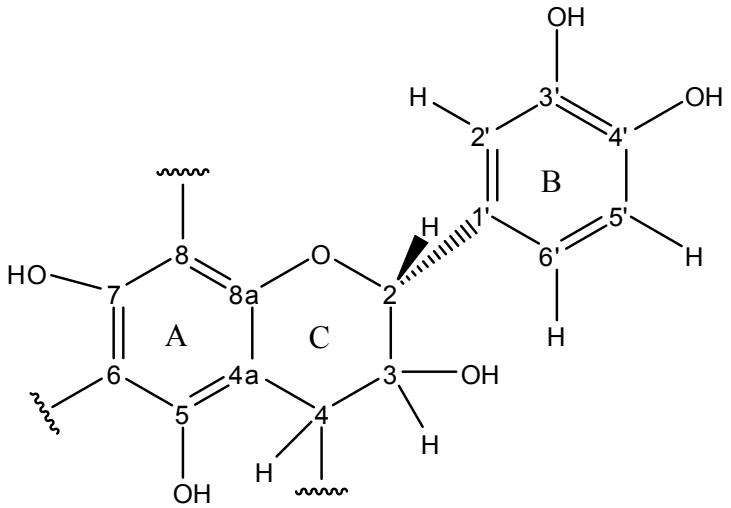

Figure 1.2. General structure and intermonomeric bonding positions of procyanidins

Procyanidins are of interest due to the medicinal and sensory properties that they possess. The medicinal properties claimed for procyanidins in general include wound healing [10], anti-inflammatory [11], anti-oxidant [12], anti-radical [13] and anti-cancer [6] activities.

1.2 Astringency and Intermolecular Self-Association Reactions of Procyanidins

Astringency is the physical experience of dryness or puckering of the mouth during the consumption of tannin-containing substances such as wine. This phenomenon is attributed to the association capacity of tannins to form colloids [14]. The procyanidin oligomers aggregate, when present in sufficiently high concentrations, to form micelles [15]. Micelles are usually ball-shaped surfactant aggregates with hydrophobic surfaces on the inside and hydrophilic moieties on the outside of the 'sphere'. These procyanidin micelles associate with proline-rich saliva proteins and precipitate out of the saliva solution. This causes the lubrication of the mouth to be lessened, leading to the perception of astringency [16]. The perception of astringency is of high interest to the tannin beverage industries, which include the wine, cocoa, coffee and tea industries [14].

The mechanism of astringency occurrence depends on the extent of self-association of procyanidins, which in turn depends on the solvent and the procyanidin's stereochemistry, conformation, concentration and degree of polymerization [15]. Procyanidins have been found to aggregate with the $IB7_{14}$ saliva protein [16], which may occur via two different mechanisms that depend on the extent of procyanidin aggregation. If the procyanidin is not present in a micelle, it interacts with three specific sites on the $IB7_{14}$ protein, but when micelles have been formed, the procyanidin micelles form random hydrophobic stacks around the proteins [16]. The association constants between $IB7_{14}$ and various procyanidins and the critical micellar concentrations (CMC) of various procyanidins at room temperature in deuterated water and 10% deuterated ethanol are shown in Table 1.2 and 1.3, respectively. These constants were determined via nuclear magnetic resonance spectroscopy (NMR). The binding affinity of procyanidins is ranked as C1>B2>B4>B1>B3 [16], where C1 is epicathechin4S->8epicatechin4S->8epicatechin. It was noted that in creating a tight complex between $IB7_{14}$ and procyanidins, the conformational dynamics of the protein are reduced and the structure is in the form of a type II helix [17]. This result suggests that the B2 procyanidin and procyanidin oligomers of higher degree of polymerization, present in relatively large concentrations, are the principal culprits for the astringency phenomenon. It was further noted that the conformation of the procyanidin plays an important role in this process and that the extended procyanidin conformer binds more favourably with the

protein than the compact conformer [16]. Pianet *et al.* reported that the monomers have a different micellar formation dynamic than the oligomers, where the monomers aggregate time dependently and precipitate out of solution [15]. The dimers and higher molecular weight oligomers associate to a certain size and remain stable in solution when above the critical micelle concentration [15]. Addition of 10% ethanol to the solution significantly increases the CMC and decreases the size of the micelles to half their original value [15].

Table 1.2. Association constants of various procyanidins with the $IB7_{14}$ saliva protein at 298 K in deuterated water and ethanol at pH 7 [15]

	D_2O M^{-1}	D_2O/EtOD (90:10) M^{-1}
Catechin	53±10	45±5
Epicatechin	39±8	37±2
Epigallocatechin Gallate	44±5	39±8
B1	7±2	7±2
B2	7±1	6±1
B3	6.5±1	6±1
B4	7±2	6±1
C2	5±1	5.5±1

Table 1.3. Critical micelle concentrations of various proanthocyanidins at 298 K in deuterated water and ethanol at pH 4 [15]

	D_2O mM	D_2O $g.L^{-1}$	D_2O/EtOD(90:10) mM	D_2O/EtOD(90:10) $g.L^{-1}$
Catechin	<5	1.5	<5	1.5
Epicatechin	9±2	2.6±0.6	16±1	5.5±0.3
Epigallocatechin Gallate	6±2	2.7±0.9	10±2	4.5±0.9
B1	17±3	10±1.5	27±5	16±3
B2	18±3	10.5±1.5	28±8	16±4
B3	24±4	14±2	19±3	11±1.5
B4	17±4	10±2	26±5	15±3
C2	15±2	13±1.5	26±6	22±5

The addition of carbohydrates to a saliva solution inhibits the formation of protein-procyanidin aggregates [18, 19]. It was reported that both hydrophobic and hydrophilic interactions between carbohydrates and trypsin enzymes or saliva proteins allow for ternary complexes to form, which competed with the tannins for protein binding [19]. Pectin is the most effective in competing with the tannins [19].

1.3 Redox Reactions of Procyanidins

1.3.1 Oxidative Decay of Procyanidins

Procyanidins' high anti-oxidant capacity leads to their oxidative decay as a function of time. De Frietas *et al.* showed that procyanidins undergo significant to complete decay between 20 to 60 days in oxidizing environments including oxygen feed and a metal catalyst [4].

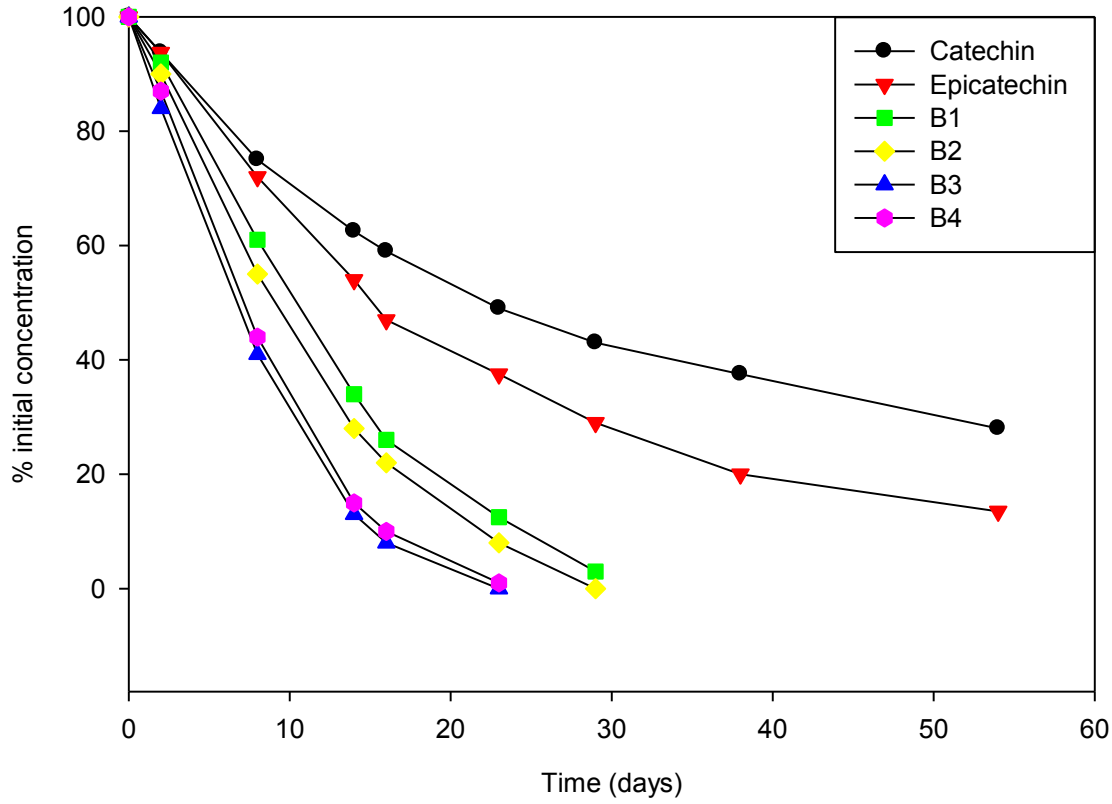

Figure 1.3. Procyanidin decay as a function of time in a 12% ethanol/ water (v/v) mixture in the presence of metal catalysis and oxygen sparging [4]

The authors reported that galloylation of procyanidins significantly reduces the rate of oxidative decay, which is attributed to the π-π stacking of the aromatic galloyl and catechol rings that reduce the availability of the molecules to undergo oxidation reactions [4]. The study does not specify the rate constants, nor does it suggest a mechanism for the catalyzed oxidative decay. Nevertheless, it is important to store procyanidin samples in an inert atmosphere in order to avoid oxidative decay.

1.3.2 Anti-oxidation Properties of Procyanidin

The anti-oxidant and radical scavenging capacity of procyanidins are of interest for several medicinal reasons. The anti-oxidation reaction is proposed to occur by stopping chain reactions of lipid oxidation by scavenging the radical initiator in living organisms [12]. The capacity of an anti-oxidant is expressed by its ability to capture radicals in solution. Various methods for quantification of the anti-oxidant capacity of chemicals are available [12], which include the trolox equivalent anti-oxidant capacity (TEAC), oxygen radical absorbance capacity (ORAC), total radical anti-oxidant parameter (TRAP) and ferric-ion reducing anti-oxidant power (FRAP) assays [20]. Another way of quantifying the capacity of an anti-oxidant is to determine the concentration necessary to reduce a standard amount of 2,2-diphenyl-1-picrylhydrazyl (DPPH) by half (EC_{50}), shown in Table 1.4 [21].

Table 1.4. Anti-oxidant capacity of procyanidins [21]

Compound	EC_{50} (mg.L^{-1})	EC_{50} (µM)	% purity
(+)-catechin	73±2(6)	251±7(6)	99.9
(-)-epicatechin	61±2(2)	210±7(6)	99.9
dimer B1	49±2(5)	85±3(5)	89.4
dimer A2	400±5(4)	692±8(4)	91.2
dimer B2	117±4(5)	202±7(5)	92.7
dimer B3	50±2(5)	87±(3)	93.8
dimer B4	100± 3(5)	173±5(5)	88.9

Zhang *et al.* found EC_{50} values for epicatechin and procyanidin B2 were 2.87 and 2.06 mg.L^{-1} [3], respectively, which differs by an order of magnitude from the data reported by Saint-Cricq *et al.* [21]. It is unclear which values are more reliable and which would need to be revaluated. Groupy *et al.* [22] proposed that the kinetics of radical scavenging reactions may be more important than the ability to transfer labile H atoms to radicals. Their study characterized a wide array of dietary flavanols' stoichiometry and rate constants of the first H-abstraction, by addition of DPPH, using UV-Vis spectroscopy.

Although the methods used to quantify anti-oxidation and free radical scavenging capacity are diverse, the general consensus found by Groupy *et al.* [22], Zhang *et al.* [3] and Saint-Cricq *et al.* [21], is that procyanidins are effective anti-oxidants and that conformation plays an important role in the process.

1.3.3 Health Benefits of Procyanidins

Foo *et al.* coated a surface containing *α*-Gal(1→4)*β*-Gal receptors, as found on the exterior of uroepithelial cells, with a procyanidin-containing cranberry extract to inhibit the adhesion of P-fimbriated *Escherichia coli (E. Coli)* to the membrane. Consequently, procyanidins were shown to prevent P-fimbriated *E. Coli* from attaching to urinary tract walls, thereby preventing urinary tract infection [11].

Certain proanthocyanidins have been found to aid the wound healing process. *Paraptadenia rigida* bark is extensively used in Brazilian traditional medicine for its wound healing and anti-inflammatory properties [10]. Schmidt *et al.* separated four proanthocyanidins from the bark of this species and the extracts contained epigallocatechin-(4β→8)-epigallocatechin-3-O-gallate, epigallocatechin-(4β→8)-4'-O-methylgallocatechin, epicatechin-(4β→8)-4'-O-methylgallocatechin and 4'-O-methylgallocatechin(4α→8)-bis-methylepigallocatechin, which are hypothesized to the aid in wound healing due to their anti-oxidant capacity [10].

Due to the antiradical properties of procyanidins derived from *Ginkgo beloba* leaf, Qa'dan *et al.* claimed that procyanidins may be effective in the treatment of mild cognitive disorders such as tinnitus and dementia [23].

1.4 Procyanidin Structure and Conformational Interchange Reactions

According the IUPAC gold book, the definition of a molecular conformation is: "The spatial arrangement of the atoms affording distinction between stereoisomers which can be interconverted by rotations about formally single bonds…"

1.4.1 Analysis of Procyanidin Structure

The primary method for the analysis of procyanidins' structure and conformation is the use of acetylation and esterification along with ^{1}H NMR spectroscopy, circular dichroism (CD) and fast atom bombardment mass spectrometry (FAB-MS) or electrospray ionization mass spectrometry (ESI-MS). However, modern two dimensional NMR techniques have been shown to be sufficient to characterize the structure and stereochemistry of dimeric procyanidins, including their major rotameric conformations [9]. De Bruyne et al. also

reported that the addition of cadmium nitrate to a procyanidin solution in trace amounts causes the NMR resonance peaks to narrow, leading to higher resolution spectra [24].

According to Esatbeyoglu *et al.* [25] the assignment and structural determination of procyanidin is primarily done using two dimensional ^{1}H NMR spectroscopy. Various sources report NMR resonance frequency chemical shifts for procyanidins obtained from several organic sources that can be used as references for identification of procyanidins [5, 11, 24-26]. Moreover, the use of nuclear Overhauser effect spectroscopy (NOESY) and rotational frame nuclear Overhauser effect spectroscopy (ROESY) allows for spatial assignment of procyanidin stereochemistry and conformation, as well as the structural assignments. Esatbeyoglu *et al.* assigned the chemical shifts of two B-type procyanidin dimers and eight C-type procyanidin trimers [25], making their report a good reference source for resonance frequency chemical shift values.

The interflavanoid bond formed between monomeric groups of flavanoids can occur in one of two positions; either between the 4(C) and 8(D) carbon atoms of the monomer (leading to dimers B1 to B4) or between the 4(C) and 6(D) carbon atoms (yielding dimers B5 to B8); the structures are illustrated in Figure 1.4. Combination of these bonding patterns generates a multitude of possible higher chiral oligomeric procyanidins. The interflavanoid bond is not only shared through the 4th pyran ring carbon, but can additionally be formed as a H2β-> O7 interflavanoid bond, thereby forming procyanidins denoted as the ‘A’ dimers [11]. The A-type interflavanoid bond leads to reduced rotational freedom and is of limited interest in this study.

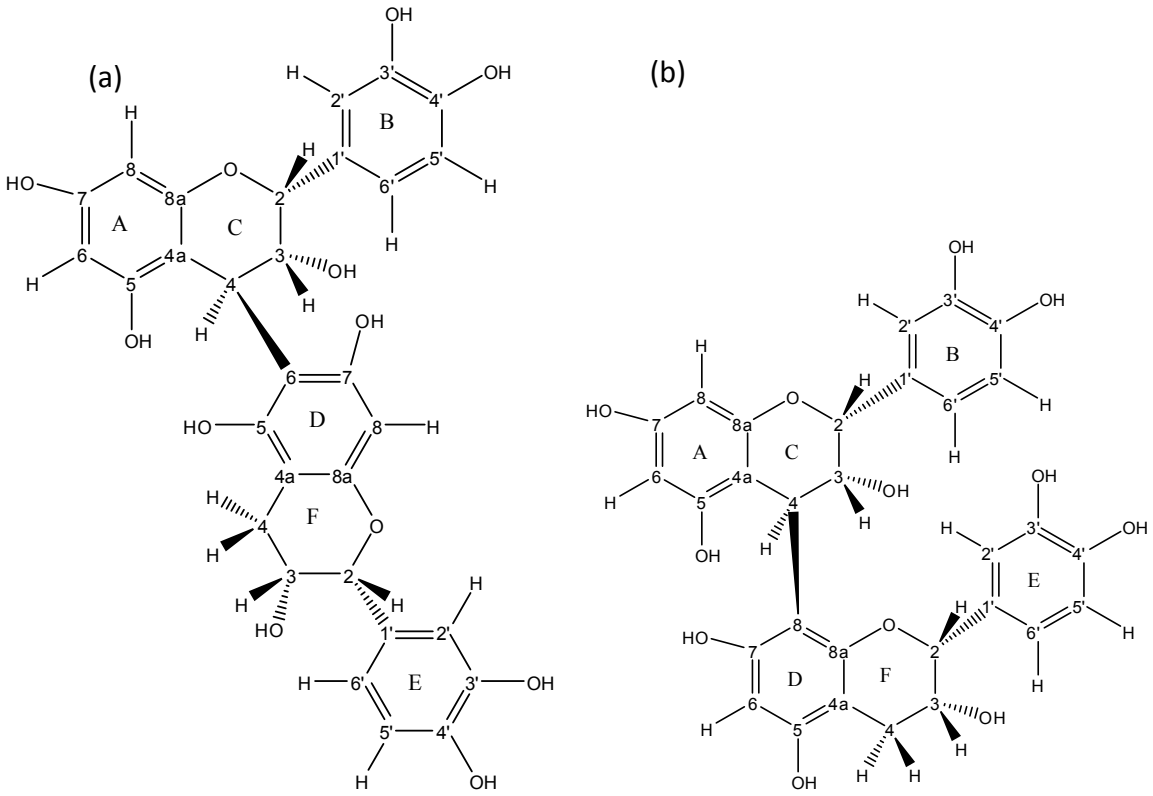

Figure 1.4. Skeletal representation of (a) procyanidin B5 (epicatechin4S->6epicatechin) and (b) procyanidin B2 (epicatechin4S ->8epicatechin)

1.4.2 Procyanidin conformational interchange

The rotation of the aromatic B- and E rings is most probably much lower in energy compared to rotation about the interflavanoid bond and should be rapid even at low temperatures. The time scale for these types of rotations falls in the fast exchange regime for ^{1}H NMR, meaning that different conformers cannot be distinguished, *vida infra*. It has also been suggested that the aromatic B- and E rings can form intramolecular π-π stacking interactions in larger oligomers and oligomeric gallates [16].

The pyran ring has been found to assume either a half-chair or couch conformation, depending on the oligomer [27]. Similarly, the conformation of the pyran ring can be characterized by the position of its *ß*-OH group as quasi-axial or equatorial [24] using two dimensional NMR techniques, through space associations in NOESY and ROESY experiments [28]. The C3(C)-C4(C)-C8(D)-C8a(D) interflavanoid bond between monomer units in a dimer is a rotational axis that leads to several possible conformations. These rotamers exist in a dynamic equilibrium in solution.

A ^{1}H NMR study of procyanidin, obtained from cocoa, was conducted by Kahn *et al.* in order to determine whether the interflavanoid bond is located at the 4(C)*S*->8(D) or 4(C)*S*->6(D) position [9]. According to Kahn *et al.* a compact conformer has any positive (C3(C)-C4(C)-C8(D)-C8a(D)) interflavanoid dihedral angle and the extended conformer has any negative (C3(C)-C4(C)-C8(D)-C8a(D)) interflavanoid dihedral angle. The exact angle varies between procyanidin oligomers and chiralities [27]. They also found that the most abundant dimeric procyanidin found in cocoa is procyanidin B2 and deduced from molecular mechanics (MM) MM3+ forcefield calculations that they either assumed the extended or compact conformation, with the hydroxyl moieties on the pyran rings preferring the quasi-axial positions for both conformers [9]. These conformations have been recalculated by us using the AM1 semi empirical calculation in Spartan '08 and are shown in Figure 1.5.

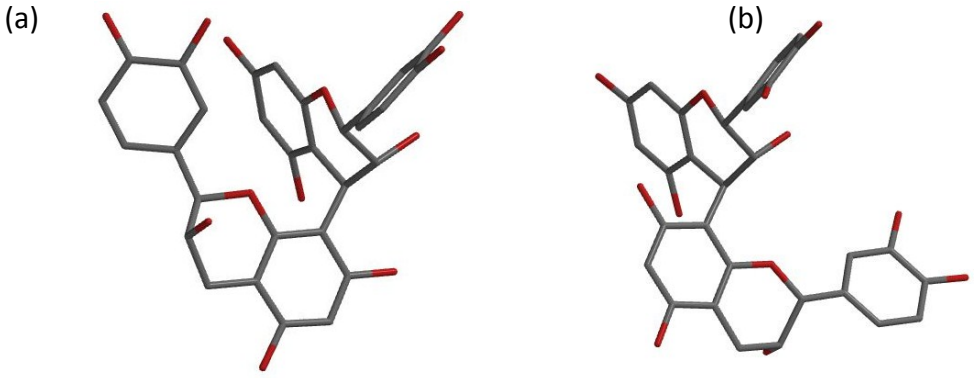

Figure 1.5. Tube representation of the (a) compact and (b) extended procyanidin conformers of procyanidin B2 recalculated in Spartan '08 by use of the AM1 semi-empirical method

Terascou *et al.* calculated the exchange rate between conformations of two dimers, B1 and B4 in water at room temperature using exchange spectroscopy (EXSY) NMR data (Table 1.5) and their respective equilibrium distributions (Table 1.6) [27].

Table 1.5. Conformational interchange rate constants of procyanidin B1 and B4 at 298 K in water [27]

	B1	**B4**
$k_1(s^{-1})$	0.34 ± 0.04	0.16 ± 0.03
$k_{-1}(s^{-1})$	3.38 ± 0.43	0.54 ± 0.09

Table 1.6. Equilibrium procyanidin conformer abundance percentages in 10% ethanol in water [27]

	Conformer ratio (compact:extended)
B1	95 : 5
B2	55 : 45
B2g[a]	98 : 2
B3	95 : 5
B4	76 : 24

a) B2g denotes a galloylated B2 dimer

The conformer ratios are very different for each chirality and as such shows that chirality plays an important role in the conformational stability of each dimer. According to Terascou *et al.,* the identified dimer conformers have a positive or negative ±90^{o} dihedral angle around the C3(C)-C4(C)-C8(D)-C8a(D) interflavanoid bond as found by MM3+ force field calculations. A similar ±180^{o} angle between the two conformers' dihedral positions is also proposed by Kahn *et al.* [9]. Table 1.7 depicts the equilibrium distribution of the quasi-axial and -equatorial conformations of the pyran ring as well as the conformation of the interflavanoid bond in aqueous phase as calculated by MM and observed by NMR spectroscopy [27]. It should be noted that B2g denotes a B2 dimer with a galloyl functional group attached to the aromatic B- or E ring.

Table 1.7. %Abundance of conformations of dimeric procyanidins in water as determined by MM or NMR [27]

Conformation (C-F)	**Eq-Eq**	**Eq-Ax**	**Ax-Eq**	**Total**
(B1) Compact exp.	83.7	5.7	2.6	92
Compact th.	96.7	0.2	1.9	98.8
Extended exp.	7.3	0.5	0.2	8
Extended th	0.4	0	0.8	1.2
(B2) Compact exp.	53.4	0	1.6	55
Compact th.	96.2	0.3	1.6	98.1
Extended exp.	43.7	0	1.3	45
Extended th	0.95	0.05	0.9	1.9
(B2g) Compact exp.	86.5	11.5	0	98
Compact th.	99.6	0	0.3	99.9
Extended exp.	1.8	0.2	0.9	2
Extended th	0.07	0	0.03	0.1
(B3) Compact exp.	75	14.3	4.7	95
Compact th.	98	0.2	0.9	99.3
Extended exp.	4	0.8	0.2	5
Extended th	0.7	0	0	0.7
(B4) Compact exp.	70	9	4	83
Compact th.	96.5	1.1	0.6	98.2
Extended exp.	14	1	2	17
Extended th	1.7	0.1	0	1.8

a) B2g denotes a galloylated B2 dimer

Similarly, it was found that procyanidin trimers assume either compact or extended conformations in various combinations [29]. These conformations have been modeled using MM and the different conformers are named extended-extended, extended-compact, compact-extended or compact-compact as an extension of the names given to the dimer conformers [29]. A similar set of conformations could be expected for higher oligomers.

The conformations of procyanidins also affect their intermolecular interactions and ability to associate with other compounds [14, 16, 30]. The presence of a galloyl group bound to procyanidins has been shown by de Berke *et al.* to improve copigmentation strength and complexation ability between oenin (malvidin-3-O-glucoside) and procyanidins in a wine model solution [30]. The study employed UV-Vis spectrophotometry in conjunction with MM to determine the copigmentation constants in order to correlate the copigmentation with expected complex structures [30]. Copigmentation was shown to be highly dependent on the procyanidin conformation and the conclusion was that the galloyl moiety in galloylated procyanidins has the ability to form π-π stacking interactions between the aromatic rings or the galloyl groups of the flavanoids and oenin [30].

Solid state NMR analysis of the procyanidin monomer epicatechin has also been performed by Fronczek *et al.* [28]. Epicatechin was crystalized and analyzed by solid state NMR. The X-ray crystal structure was determined as orthorhombic, $P2_12_12_1$, a= 670.8(1), b = 1329.1 (3), c= 1426.2 (4) pm, Z=4, D_c=1.516 g.cm^{-3}, R= 0.041 from 1624 observations [28]. This study found intermolecular hydrogen bonds between procyanidin hydroxyl groups in the crystal structure with the aromatic B ring in the equatorial position. The heterocyclic ring's hydroxyl moiety was in an quasi-axial conformation [28].

In a study performed by Kolodzei *et al.,* catechin-3-O-rhamnosyl-(4α->8)-catechin conformation was determined by NOESY. Their conclusion was that two rotamers exist in major and minor quantities, similar to those found for procyanidin dimers, and conformational analysis suggested that the conformational interchange reaction is independent of additional substitution at the 3-O position [31].

A recent study investigated the interaction between the procyanidin monomer, catechin, and cytosine using DFT at B3LYP level [32]. The authors extensively investigated

the intermolecular hydrogen bonding structures for lowest energy intermolecular interaction to infer the most likely interaction [32], but did not perform comprehensive conformational studies of these interacting molecules.

Mendoza-Wilson *et al.* computatationally investigated, at DFT level, the free radical scavenging abilities of procyanidins by removing their respective protons or hydrogen atoms in all expected exchange positions in order to discern the most likely mechanism of free radical scavenging. Additionally, this study attempted to determine the best free radical scavengers between a few case molecules, which included monomers, dimers or trimers. The identified conformational geometries only included two conformations which were referred to as compact and extended. The structure corroborated previous studies and reported interflavanoid dihedral angles of 102.77° for procyanidin B1-compact, -82.43° for B1-extended, 97.55° for procyanidin B2-compact and -81.12° for procyanidin B2-extended [33]. Furthermore, the study also found that conformational effects were of paramount importance in terms of free radical scavenging activity [33].

Conformational studies have been performed by Schmidt *et al.* using MM+ force field calculations, which showed that three structures (epigallocatechin-(4β→8)-epigallocatechin-3-O-gallate, epigallocatechin-(4β→8)-4'-O-methylgallocatechin and epicatechin-(4β→8)-4'-O-methylgallocatechin) assumed conformations where their B and E rings are in quasi-equatorial positions, while the fourth 4'-O-methylgallocatechin-(4α->8)4'-O-methylgallocatechin assumed both rotameric conformations in a stable distribution [10]. The carbon backbones of these molecules are very similar to procyanidins and as such are expected to exhibit similar conformational behaviour.

Due to the limited conformational DFT studies present in literature, a more in-depth study of the conformational geometry as determined by DFT versus MM is necessary and is addressed in chapter 4 of this study.

1.5 Kinetic Exchange Effects on NMR Line Shapes

The line widths of NMR resonance signals are determined by the transverse (T_2) spin relaxation rates of the corresponding nuclei, the magnetic field strength and the presence of motional averaging effects such as chemical exchange or conformational interchange [34]. In the case of motional averaging effects, the underlying physical processes occur in the

spectral time scale between 10^{-3} to 10^{-7} seconds, depending on the chemical shift difference between the specific resonance peaks of interest and the strength of the main magnetic field of the spectrometer. Figure 1.6 shows the effect of a symmetrical first order exchange reaction on the line widths and chemical shifts of a set of NMR peaks as generated by the Bloch-McConnell equation [35]. The data used in these figures were calculated with the custom developed program (NMRfit), *vida infra*. Figure 1.6 a shows the resonance peaks of a system that exchanges at a negligibly small rate (*i.e*. k≈0). At this slow exchange rate, the peak shape is entirely independent of the exchange. Figure 1.6 b shows that when increasing the rate of exchange, the peak widths broaden with a corresponding decrease in peak maxima. This broadening is a direct result of chemical exchange of the two species averaging the phase of the resonances of the respective peaks. As the exchange rate is further increased, the peaks observably shift towards each other as is illustrated in Figure 1.6 c. The individual resonance frequency chemical shifts remain unchanged, but the dephasing of the exchanging peak resonances gives the NMR line shapes the appearance of shifting towards the average of the two symmetrical chemical shifts. Broadened frequency domain peaks are shown to correspond to fast relaxation of the free induction decay (FID) in the same figure, due to the destructive interference effects of the dephased peaks. At sufficiently high exchange rates the different peaks coalesce to become a single broad peak, Figure 1.6 d**,** as the chemical exchange is fast enough to appear as a single peak on the NMR time scale. Upon further increase of the exchange rate, the single peak starts to sharpen until it reaches the fast exchange rate regime where no chemical exchange can be observed on the NMR spectral time scale and the peaks are represented by a single peak with an averaged chemical shift [34].

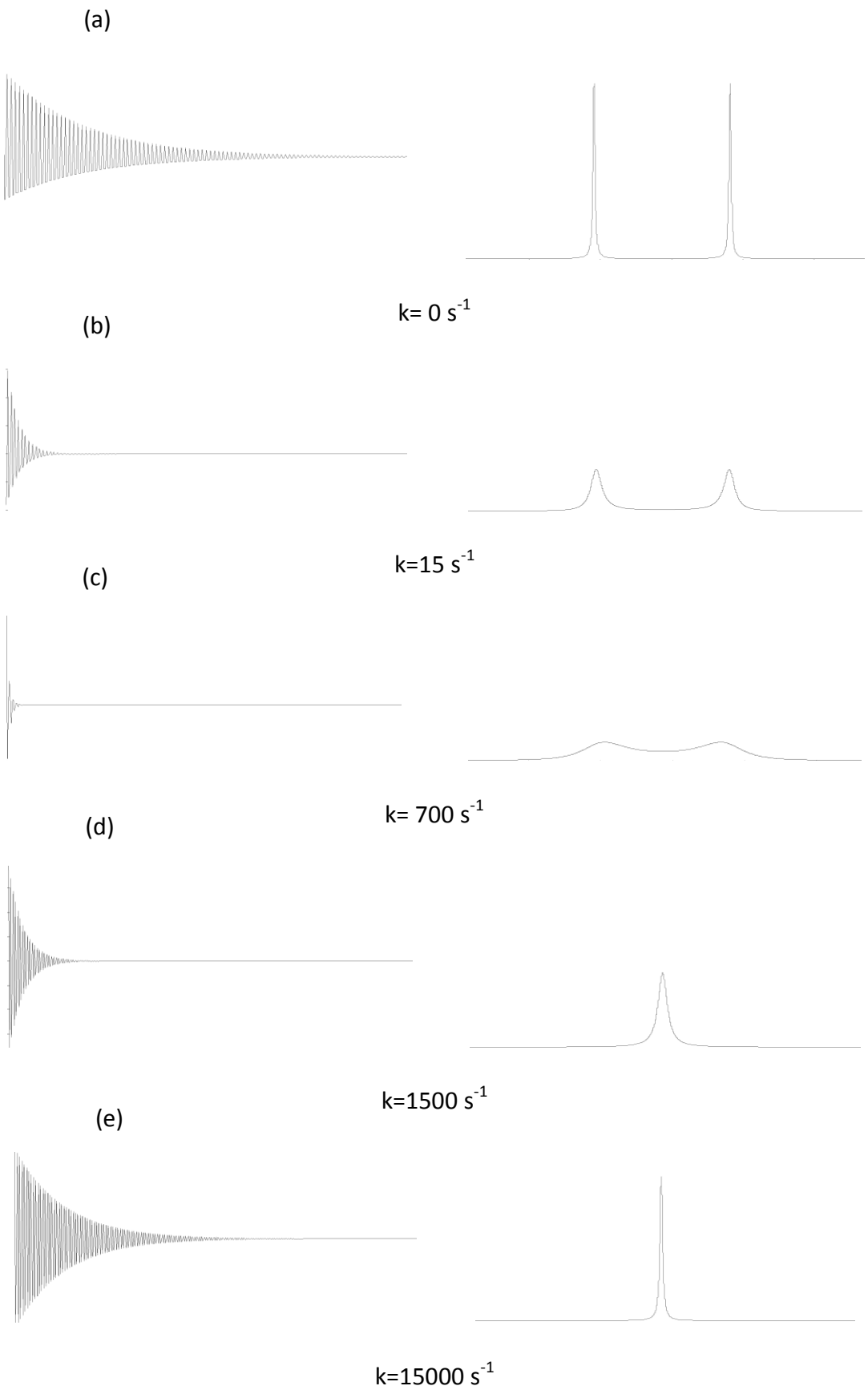

Figure 1.6. Representation of NMR symmetrical exchange line shapes at various exchange rate constant values as calculated using the Bloch McConnell equation

The symmetrical first order chemical exchange line shapes are given by equation 1.1**.**

$$S(\Omega) = \frac{1}{2}\left(1 - \frac{ik}{R}\right)\mathcal{L}(\Omega; \bar{\Omega} + R, \lambda + k) + \frac{1}{2}\left(1 + \frac{ik}{R}\right)\mathcal{L}(\Omega; \bar{\Omega} - R, \lambda + k) \quad (1.1)$$

In equation 1.1 $\mathcal{L}$ denotes a lorentzian lineshape defined by

$$\mathcal{L}(\Omega; \Omega^0, \lambda) = \frac{1}{\lambda + i(\Omega - \Omega^0)} \ .$$

Asymmetrical first order two site chemical exchange is a more complicated case of chemical exchange where the species are not present in equal abundance. In an asymetrical exchange the areas of the exchanging peaks correspond to the distribution of the species at equilibrium and the broadening of the individual peaks is biased towards the higher abundance species' resonance frequency. The species are in a dynamic equilibrium. Therefore, if the peak of the reactant is larger than the product, the rate constant of the forward reaction must be smaller than that of the reverse reaction and the smaller peak will be more dephased and broadened than the larger peak to an extent that is proportional to the equilibrium constant. The final resonance peak chemical shift of the coalesced peak is determined by the average of the chemical shifts weighted by the equilibrium constant, *i.e.* is closer to the chemical shift of the larger peak proportional to the equilibrium constant as shown in equation 1.2. The higher the initial separation of the resonance peaks, the greater the kinetic constants are required to be for line broadening to occur.

$$\Omega_{peak} = \frac{[A]_{eq}\Omega_A^0 + [B]_{eq}\Omega_B^0}{[A]_{eq} + [B]_{eq}} = \frac{\Omega_A^0 + K\Omega_B^0}{1 + K} \quad (1.2)$$

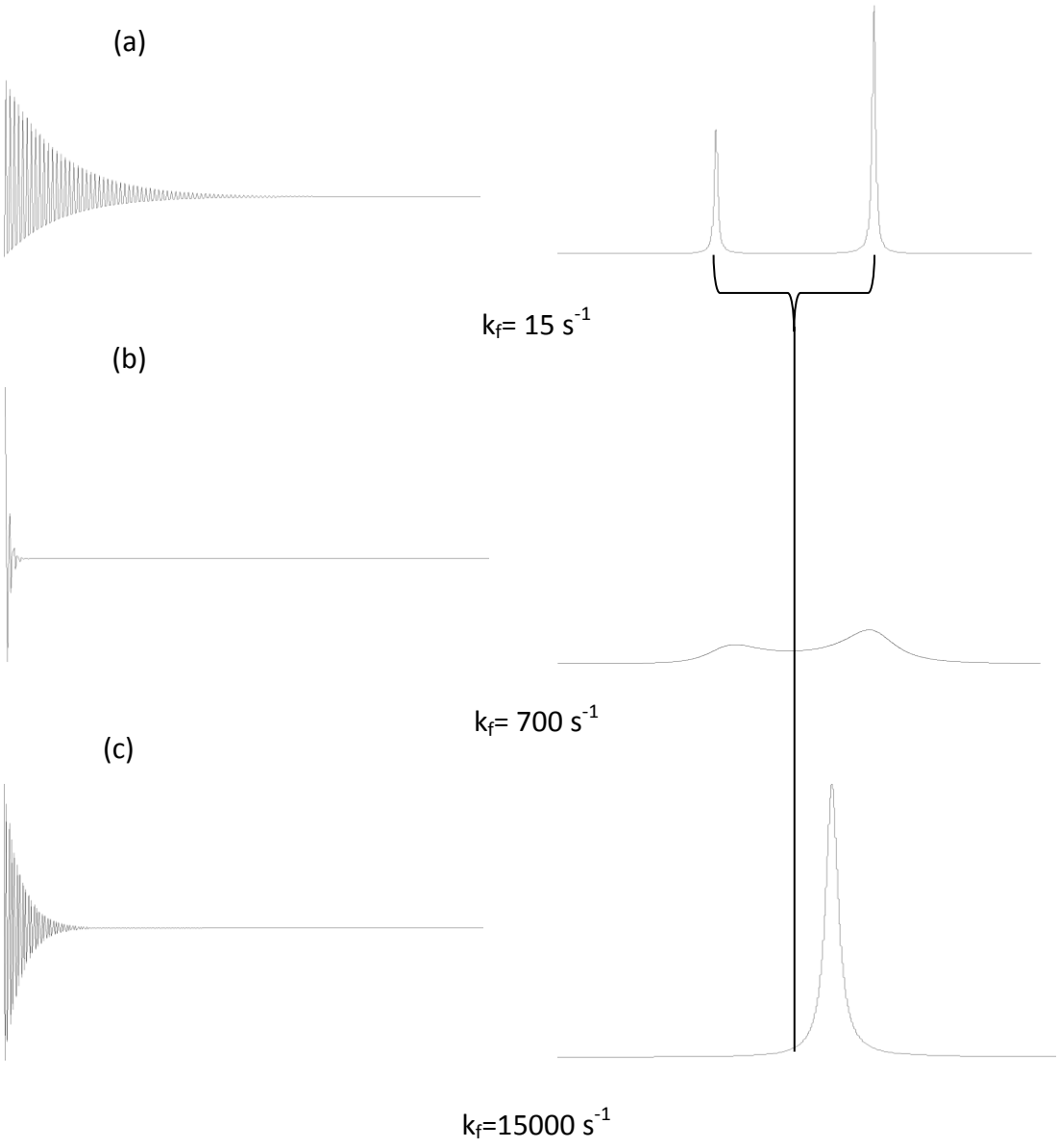

Figure 1.7. NMR line shape illustration of asymmetric exchange at various exchange rate constant values as calculated using the Bloch-McConnell equation

1.6 Computational Methods

1.6.1 Quantum Mechanics

The foundation of modern quantum mechanics is the Schrödinger equation. The time-independent non-relativistic form of the Schrödinger equation is shown in equation 1.3**.**

$$\hat{H}\psi_i(\vec{x}_1, \vec{x}_2, \ldots \vec{x}_n, \vec{R}_1, \vec{R}_2, \ldots \vec{R}_n) = E\psi_i(\vec{x}_1, \vec{x}_2, \ldots \vec{x}_n, \vec{R}_1, \vec{R}_2, \ldots \vec{R}_n) \quad (1.3)$$

$\hat{H}$ is the Hamiltonian operator and is equated to the energy (*E*) of the molecule by use of the wave function (ψ_i). The molecule consists of M nuclei with R spatial vectors to define the 3M spatial coordinates of said nuclei. There are 3N x vectors to define the spatial coordinates of the electrons with N spin coordinates. The Hamiltonian operator (equation 1.3) yields all of the energy components of the molecule by being applied to the wave function and can be simplified by the Born-Oppenheimer approximation. This approximation assumes that the nuclei move so slowly compared to the electrons that they are regarded as stationary. Therefore, with the addition of the Born-Oppenheimer approximation, the kinetic energy of each nucleus is zero. Thereby, the Hamiltonian in equation 1.3 is simplified to the electronic Hamiltonian, equation 1.4.

$$\hat{H}_{electronic} = -\frac{1}{2}\sum_{i=1}^{N}\nabla_i^2 - \sum_{i=1}^{N}\sum_{A}^{M}\frac{Z_A}{r_{iA}} + \sum_{i=1}^{N-1}\sum_{j>1}^{N}\frac{1}{r_{ij}} = \hat{T} + \hat{V}_{Ne} + \hat{V}_{ee} \quad (1.4)$$

And

$$\hat{H}_{electronic}\psi_{electronic} = E_{electronic}\psi_{electronic} \quad (1.5)$$

The $\hat{T}$ operator in equation 1.4 represents the kinetic energy and the $\hat{V}_{ee}$ operator represents the energy of the electron- electron repulsions. $\hat{V}_{Ne}$ represents the attraction and repulsion between the electrons and their environment, which includes the nuclei and any external magnetic or electronic fields. Due to the removal of the nuclear energy from the equation, the nuclear energy must be added to the electronic energy in order to calculate the total energy of the molecule.

$$E_{total} = E_{electronic} + E_{nuclear} \quad (1.6)$$

The consequence of equation 1.6 is that the wave function must be defined in order to determine the energy of the molecule. However, the wave function only assumes meaning when squared. The square of the wave function defines the probability (normalized to 1) to find an electron within a volume defined by the integral shown in equation 1.7.

$$\int \ldots \int |\psi_{electronic}(\vec{x}_1, \vec{x}_2, \ldots \vec{x}_N)| d\vec{x}_1 d\vec{x}_2 \ldots d\vec{x}_N = 1 \quad (1.7)$$

From equation 1.7, the definition of the electron density is derived, which is the probability of finding an electron within any distance $\vec{r}$ from the nucleus with N-1 electrons occupying the surrounding space in their respective spin states. The electron density is defined in equation 1.8.

$$\rho(\vec{r}\ ) = N \int \dots \int |\psi_{electronic}(\vec{x}_1, \vec{x}_2, \dots \vec{x}_N)| d\vec{x}_1 d\vec{x}_2 \dots d\vec{x}_N \tag{1.8}$$

The variation principal allows for the determination of the zero point energy (E_0) that represents the lowest possible energy that a molecule can assume by the optimization of its geometrical configuration with minimization of the electronic energy as the optimization criteria. The optimization is done by a systematic trial and error method where a trial wave function is generated and tested.

1.6.2 Density Functional Theory (DFT)

DFT implements the Born-Oppenheimer approximation and is derived from the Kohn-Sham calculations. In a Kohn-Sham calculation, the electrons are considered as non-interacting entities of identical density and the total energy of the electron densities are described and determined by the relationship between the energy and density. In the Kohn-Sham definition of these hypothetical non-interacting electrons, the self-consistent field (SCF) potential and energy of these electrons is an intrinsic property of the electrons, not an approximation, and is uniquely determined by the electron density by minimization of the SCF potential. Thus, the energy corresponding to the electron density of a system is determined. The energy of the electron interactions ($\hat{V}_{ee}$) lost by the hypothetical property of non-interaction, as compared to a wave functional interaction energy definition, is corrected during this self-consistent field minimization.

A functional is a mathematical definition of a set of functions that describes a vector field. In other words, a functional describes the entire set of functions and returns a value to a function, thereby describing any system of the functions that it contains. DFT implements functionals to replace the wave function in order to approximate the Schrödinger equation. The functional receives a function and returns a value. The purpose of this operation is to minimize the functional calculated self-consistent field and in turn find the lowest possible energy (E_0). In order for the answer to be meaningful, the resulting wave function must be continuous in all dimensions and it's square must be integrable, equation 1.9.

$$E_0 = min_{\psi \to N} E[\psi] = min_{\psi \to N} \langle \psi | \hat{T} + \hat{V}_{Ne} + \hat{V}_{ee} | \psi \rangle \quad (1.9)$$

By use of this methodology a self-consistent field (SCF) is generated and is the basis for most electronic calculations in modern DFT.

1.6.3 DFT Methodology Used in This Study

The density functional analysis implemented in this text was used mainly for the purpose of conformational analysis. In order to study the conformations of procyanidin B2, a methodology for optimal computational efficiency was implemented. Initial less time-consuming functionals and basis sets were implemented for the generation of a potential energy surface (PES) in Gaussian 09 (G09) revision B0.1. The generation of the potential energy surface was done by use of a relaxed scan, where the conformation of the molecule geometry was partially optimized with the interflavanoid dihedral angle rotation as the scan coordinate. The purpose of this scan was to find the lowest electronic energy interflavanoid bond dihedral angle. After the initial PES minima were identified, full geometry optimizations were done for increasingly computationaly intensive functionals (Hartree Fock, local density approximation (LDA) and consequently the GGA and B3LYP hybrid functionals) and higher basis sets (3-21, 6-31, 6-31+g* and 6-311++g**) until the geometries have converged at B3LYP, PBE and PBE-D2 functional level with the 6-311++g** basis set. The equilibrium geometries of the conformations were then confirmed and the Gibbs free energy of conformation determined by implementation of frequency calculations using the respective functionals in order to confirm that the conformations are indeed minima on the PES. The geometries optimized in G09 were subsequently re-optimized in the Amsterdam Density Functional (ADF) suite, with the PBE functional and TZ2P basis set, and the frequencies calculated. These equilibrium conformers were used in all the calculations (electrostatic surface potentials and 3DRISM) implemented in ADF.

1.6.4 Basis Set Superposition Error (BSSE)

The BSSE is the result of density functional theory's atomic basis sets that overlap in three dimensional space and thereby overestimate the system's electronic energies. Counterpoise corrections can be employed to counteract these errors in the Gaussian 09 suite. The BSSE is mostly of interest for small basis sets and tends to decrease for larger basis sets, but it is of most interest where there are closed-shell interactions and steric

clustering [36], as is the case for procyanidins. Counterpoise calculations generally consider molecules (monomers) that form electronically interacting complexes (dimers). However, it is possible to consider a counterpoise calculation for intramolecular interactions, but the 'monomer' selection must be non-arbitrary in order to carry meaning. Several studies have been performed on intramolecular counterpoise corrections [37-39]. The interaction energy between interacting 'monomers' can be calculated by equation 1.10, where '*E*' refers to the electronic energy. The superscripts refer to the basis set to be used and the subscript refers to the monomer's geometry that was used during the calculation. The brackets refer to the structure used for the calculation (*i.e.* the A monomer, B monomer or interacting system of monomers).

$$\Delta E_{int}(AB) = E_{AB}^{AB}(AB) - E_{A}^{A}(A) - E_{B}^{B}(B) \tag{1.10}$$

In order to correct this interaction energy, the BSSE for each basis set needs to be calculated and subtracted from the total system.

$$E_{BSSE}(A) = E_{A}^{AB}(A) - E_{A}^{A}(A), \tag{1.11.1}$$

$$E_{BSSE}(B) = E_{B}^{AB}(B) - E_{B}^{B}(B), \tag{1.11.2}$$

The assumption made when using equations 1.11.1-2 is that there is no geometrical change between the monomers and that of the combined dimer molecule. The more intensive case where conformational change is added is not of interest for this study and consequently omitted from this discussion. The counterpoise corrected energy of the dimer can now be calculated by subtracting the BSSE's of each monomer, equation 1.12.

$$\Delta E_{int}^{CP} = E_{AB}^{AB} - E_{A}^{AB} - E_{B}^{AB} \tag{1.12}$$

1.6.5 Solvation Computation Techniques

The effect of solvation on procyanidin molecules has not been studied in depth in any of the reviewed literature. The solvation effects on conformational geometry and energies are essential to understand conformational interchange in solvent phase. By the use of implicit solvation models in DFT, an initial approximation of the effect of solvation can be calculated to compare the effect of polar solvents with less polar solvents [40, 41]. The methodology for implementation of the implicit solvent model used here was the re-

optimization of the gas phase calculated geometries of the conformations in each self consistent reaction field (SCRF) implicit solvent. Frequency calculations were conducted on the re-optimized geometries in order to determine the Gibbs free energy of conformation and confirm the equilibrium geometry in the above-mentioned solvent. However, more thorough techniques exist that can approximate the packing of solvation molecules explicitly around the analyte. A three dimensional reference site interaction model (3DRISM) allows for MM solvent molecules to be explicitly used in iterative solvation calculations. By use of 3DRISM, the statistical average of solvent-solute interaction, geometrical distribution of the interactions and solvation energy can be determined in order to approximate macro-fluid parameters [42].

1.6.6 Electron Density Topology Analyses

The quantum theory of atoms in molecules (QTAIM) and the non-covalent interaction (NCI) Index are two methods that can be used to study the electron densities of a molecule as an extension to DFT, that allow for the in-depth study of the bonding structure and interactions within the molecule.

1.6.6.1 Quantum Theory of Atoms In Molecules (QTAIM)

The QTAIM allows for the identification of the bonding structure in molecules and non-covalently bound structures by analysis of the electron density, ρ(r) [43]. The electron density of atoms and molecules is a quantum mechanical definition referring to the probability of an electron to occupy a point in space out of all the electrons in a molecule. Therefore, it is a probability density scalar field that is scaled to the number of electrons in a given molecule [43]. The electron density can be determined by using the number of electrons in each orbital (n_i) and the wave function (ψ) as shown in equation 1.7 and is simplified for this discussion, as shown in equation 1.13.

$$\rho(r) = \sum n_i |\psi_i(r)|^2 \tag{1.13}$$

The electron density is not an actual density or concentration of electrons within a given volume, but is often understood mnemonically as such, as it allows understanding of nuclear and electronic topology. The geometry and topology of electron clouds in molecular orbitals allow for the understanding of bonding as a fundamental phenomenon in molecular structure [43].

The atoms in molecules (AIMs) theory uses electron density as generated from experiment or density functional theory (DFT) to describe, assign and rationalize bonding in molecules. The understanding enabled by AIMs surpasses that which can be mnemonically inferred from just the electron density by using mathematical operations on the electron density. By deriving the electron density in three dimensions, a gradient vector field is generated that can indicate slope and direction of electron depletion or accumulation. This gradient vector field is crucial in understanding the flux direction of an electron field and is often used to understand attractive and repulsive forces in molecules [43]. The gradient vector field is defined mathematically as:

$$\nabla\rho(r)_c = \frac{\partial\rho(r)}{\partial x} + \frac{\partial\rho(r)}{\partial y} + \frac{\partial\rho(r)}{\partial z} \tag{1.14}$$

Similarly, a second derivative in three dimensions is designated the Laplacian of the electron density. This new derived property is used for determination of local charge concentration or depletion and is one of the most accessible of the theoretical properties in assigning bond character [43]. The Laplacian of the electron density is defined in equation 1.15.

$$\nabla^2\rho(r)_c = \frac{\partial^2\rho(r)}{\partial x^2} + \frac{\partial^2\rho(r)}{\partial y^2} + \frac{\partial^2\rho(r)}{\partial z^2} \tag{1.15}$$

The Laplacian indicates whether electron density is locally concentrated or depleted by determining whether $\nabla^2\rho(r)_c < 0$ or $\nabla^2\rho(r)_c > 0$, respectively. This allows rationalization of shared-shell or closed-shell interactions in bonding [43]. A closed-shell interaction is an interaction between atoms where the electrons are not shared between orbitals to a substantial degree and a shared-shell interaction is an interaction where electrons are shared between orbitals to a substantial degree [43].

Critical points (CPs) in AIMs theory refers to maxima and minima in the electron density topology or stated alternatively, a CP is a zero in three dimensions in the gradient vector field. Critical points are denoted by a *(r,s)* system where *r* is the rank of the critical point with regards to the number of non-zero 2nd order derivatives and *s* is the sum of the signs of the three eigen values of the 2nd order derivative matrix of the electron density [43]. By investigation of the second eigen value at the critical points, an interaction can be interpreted to be accumulating electron density or to have a depletion in electron density.

Bader rationalized that an accumulation in the electron density is a negative charge accumulation between the positively charged nuclei and therefore an attractive interaction [43]. Similarly, an electron depletion indicates a repulsion and a destabilizing interaction. Interpretation of the first and third eigen values of the Laplacian allows for the characterization of the linear or curved (which usually indicates bond strain) geometry of an interaction.

According to AIMs theory, a bond is designated by the presence of a bond critical point (BCP) which occurs along a bond path. A BCP is a point in a molecule where there is a one dimensional minimum and a two dimensional maximum in electron density. Looking at this mathematical explanation geometrically, a BCP is a point on a plane of minimum electron density between two atoms at the point where a bond path between the two intersects the plane. A bond path is a line of maximum electron density between two atoms intersecting plane of two dimensional zero in the gradient vector field of electron density, which is called an inter-atomic surface (IAS). A BCP is consequently denoted by (3,-1) as it is a one dimensional minimum and a two dimensional maximum in electron density. A simple example of the electron density and Laplacian topology at a BCP is shown in Figure 1.8 for the covalent bond in a diatomic hydrogen molecule. The contour plot of the Laplacian clearly shows a negative Laplacian around the covalently bonded nuclei, showing that a covalent bond has a electron density accumulation at the BCP [43].

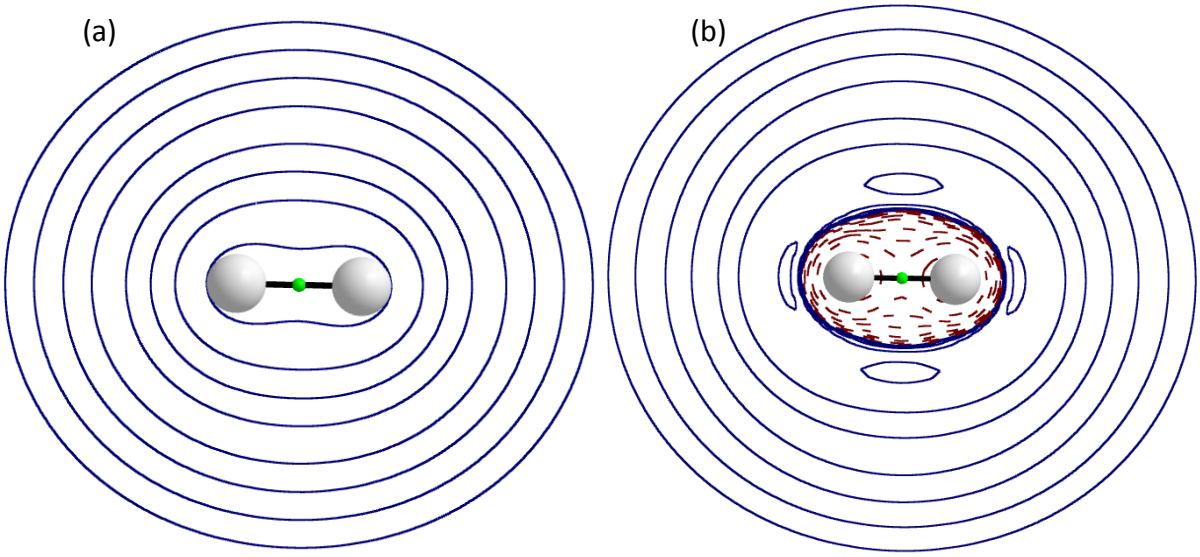

Figure 1.8. Ball and stick diagram of H_2 with a contour plot of (a)the electron density and (b) the Laplacian of the electron density at the covalent bond as calculated by B3LYP/6-311++g** basis set in Gaussian 09 revision B.01. Red dashed lines indicate negative contours and blue lines indicate positive contours.

A ring critical point (RCP) is a point surrounded by a ring of bond paths of arbitraty length. It is expected that a ring critical point is indicative of electron depletion as the electron density is concentrated in the bonds and bonding interactions of the ring; however, in the case of phenol rings or other double bond containing rings, the electron density can be more concentrated at the center and allow for π-interactions as a result of negative charge accumulation. An RCP is denoted (3,+1) as it is a two dimensional minimum and one dimensional maximum in electron density. A typical example of a ring critical point is illustrated in Figure 1.8 in the center of a benzene ring. The contour plot of the Laplacian of the electron density indicates a electron accumulation in between the covalent bonds, but in contrast to the hydrogen atoms in Figure 1.8 b there is a positive Laplacian shell surrounding the carbon atoms of the benzene ring in Figure 1.8 b, which illustrates the separation between the inner and outer electron shells of the carbon atom. Unfortunately the carbon spheres representing the nuclei obscure the negative Laplacian of the inner electron orbital shell, but the contour plot in Figure 1.8 a shows a electron accumulation surrounding the carbon atoms. However, there is a illustrative depletion in electron density at the center of the ring corresponding to the RCP.

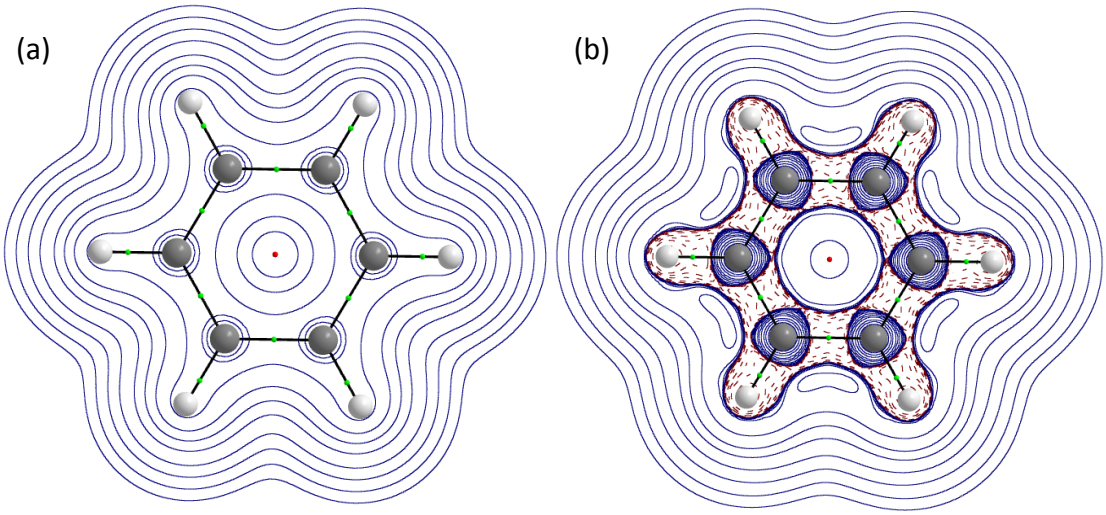

Figure 1.9. Ball and stick diagram of benzene with a contour plot of the (a) electron density and the (b) Laplacian of the electron density at the covalent bond as calculated by B3LYP/6-311++g** basis set in Gaussian 09 revision B.01. Red dashed lines indicate negative contours and blue lines indicate positive contours.

A cage critical point (CCP) is similar to an RCP as it is contained by a chain of bonds or bonding interactions, but is surrounded by a three dimensional cage instead of a two dimensional ring. A CCP is denoted (3,+3) as it is a three dimensional minimum in electron density. A classical theory atomic nucleus appears as a nuclear attractor (NA) in AIMs theory and is denoted (3,-3) as it is distinguished by a three dimensional maximum in electron density [43].

BCPs can be characterized by a set of variables into classes of shared interactions or closed-shell interactions [44]. Figure 1.10 shows the bond classes and parameters associated with each bonding regime as redrawn from Bianchi *et al.* [44]. For a procyanidin only covalent, polar covalent and van der Waals bonds (including hydrogen bonds) are expected. A H_2 covalent bond is clearly not polarized and the electron density according to a B3LYP calculation is equal to 0.261. The associated Laplacian at the H_2 bond is equal to -1.058, indicating a shared-shell interaction. Similarly, the electron density of a benzene ring C-C covalent bond is high. The partial double bonds of the benzene ring share the electron density around the ring, allowing for a relatively high electron density at the BCP of 0.309. The Laplacian of the electron density is also negative (-0.967) at the BCP of a benzene C-C bond as is expected for covalent bonds. The H-C bonds on benzene are slightly polarized and have a slightly higher single bond electron density of 0.281 due to electron density

migration from the protons and clearly corresponds to polarized covalent bonds with a Laplacian of the electron density equal to -0.862. The G_b parameter shown in Figure 1.10 represents the kinetic energy associated with the interaction and V_b corresponds to the associated potential energy [44]. The sum of the kinetic and potential energies yields the E_b parameter. For the H_2 covalent bond G_b approaches zero and V_b is equal to -0.264 and agrees well with the requirements for a covalent bond as indicated in Figure 1.10. Similarly, the G_b for the benzene C-C bonds are 0.0997 and far smaller than the corresponding $|V_b|$ of 0.415. Finally, the benzene carbon-hydrogen slightly polarized covalent bond is characterized by a G_b of 0.0386 which is far smaller than the $|V_b|$ of 0.319 associated with the bond. Also in agreement with the characteristics expected according to the classification scheme in Figure 1.10, the V_b values of al three bonds are negative.

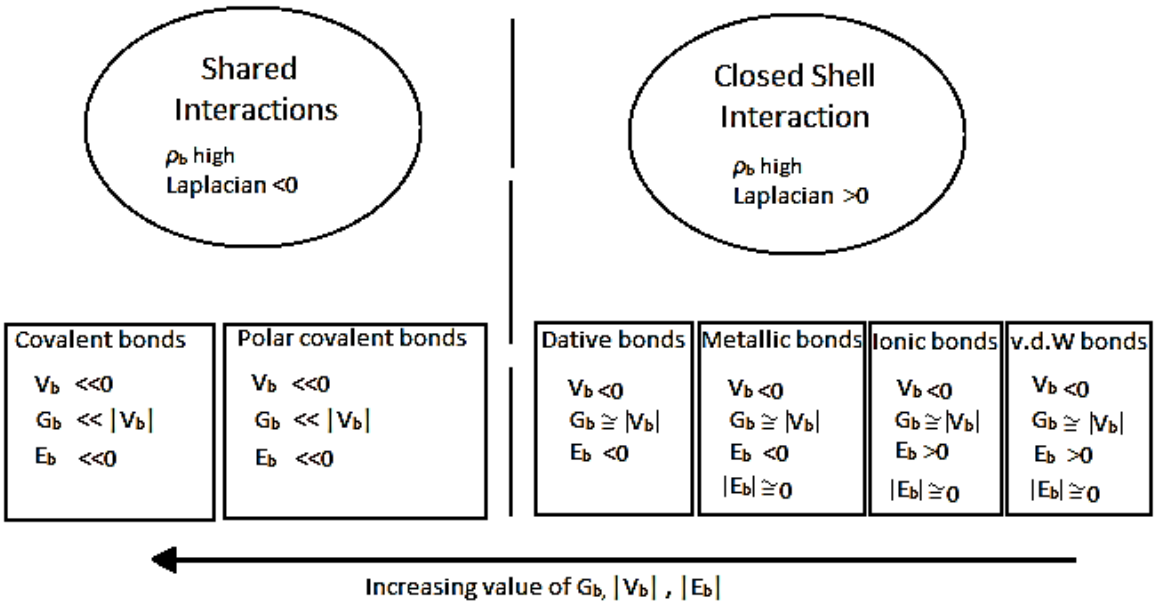

Figure 1.10. Bond classification schematic according to QTAIM parameters [44]

It is sensible that a closed-shell interaction would have a low electron density at the BCP, however, care should be taken as short bond lengths may convolute this distinction as the electron density is more compressed. An in-depth distinction is made in AIMs so that differentiation between weak van der Waals bonds, ionic bonds and gas clusters can be made. A parameter to take into account when classifying bonds is the ellipticity of the bond, which indicates the extent to which the bond is elongated in one direction in comparison to

another, which is interpreted as an indicator of structural stability or strain in the presence of a RCP or the π-bonding character of a BCP.

According to Bader, hydrogen bonds are defined as having a BCP with an electron density between 0.002 and 0.04 au, a Laplacian value between 0.15 and 0.02, mutual penetration of the bond path between the hydrogen and the acceptor atom, loss of charge of the hydrogen atom, energy destabilization of the hydrogen atom, decrease in the dipolar polarization of the hydrogen atom and a decrease in the atomic volume of the hydrogen atom [43]. When interpreting closed-shell interactions of non-hydrogen atoms, it is a good start to look at the Laplacian and electron density, which provides a general indication of electron density as a determining factor for van der Waals interactions. However, it has been shown that closed-shell interactions can have high electron densities in cases of short bond lengths, but are shown to have negative Laplacians irrespectively. Therefore, the full spectrum of parameters should be evaluated in order to classify a bond.

1.6.6.2 Non-covalent Interaction (NCI) Index

The NCI index is an extension of the analysis employed in QTAIM that is calculated by determining a reduced density gradient (RDG) and comparing it to the sign of the second eigen value of the Laplacian ($Sign(\lambda_2)$) [45]. The eigen value of the Laplacian is multiplied with the electron density on the independent axis in order to separate various interactions along the independent axis.

$$RDG = \frac{1}{2(3\pi)^{1/3}} \frac{\nabla\rho}{\rho^{4/3}} \tag{1.16}$$

By using the NCI index, interactions can be determined that would appear as BCPs, as well as some that do not form the BCP minima, and as a result a more in-depth study of the interactions of the molecule can be performed [45]. The repulsive interactions can also be determined in more depth than those indicated by simple CCPs and RCPs. By definition, a repulsive interaction in NCI is an interaction that falls on the positive side of the $Sign(\lambda_2)\rho$ parameter and an attractive interaction on the negative. Using the electron density of interaction, the interactions' NCI parameters can be correlated to the QTAIM analysis. Visual molecular dynamics (VMD) molecular visualiser can be used to represent the NCI values on an isosurface in three dimensional space [45].

1.6.6.3 Van der Waals forces

The closed-shell bonding interactions detected by QTAIM and NCI theory in organic molecules often include van der Waals bonds. However, Figure 1.10 does not show the forces involved in the formation of these interactions. Van der Waals forces are devided into three separate forces namely Keesom, Debye and London forces [46]. The Keesom force is an attractive or repulsive force between two permanent dipoles existing within a molecule like that found between a hydroxyl oxygen atom and an opposing hydroxyl hydrogen atom. By contrast, a Debye force is found between one permanent dipole and an unpolarized atom within the molecule. The unpolarized atom undergoes an induced dipolarization of opposite polarity as a result of the proximity of the permanent dipole of the opposing moiety, thereby causing a Debye force between the two. The final van der Waals force is the London dispersion force which is often mistakenly used interchangeably with the van der Waals force term. Atomic and molecular electron clouds are contuously in motion and form resonant instantaneous dipoles [46]. When these electron clouds are proximate and can form resonant opposing dipoles the atoms or atoms within molecules experience the attractive London force. Therefore, the London dispersion force is a weak, long range force formed between two unpolarized atoms. The term van der Waals interaction refers to an interatomic instance of electronic destabilization or stabilization by the van der Waals forces and is by definition a closed-shell interaction [46].

1.7 Aims and Objectives

The aim of this project is to study of the kinetics and thermodynamics of the conformational interchange reactions of the major conformers of selected procyanidin B2. The separation of procyanidin oligomers in various organic tannin containing media, already a challenging task due to the large number of dimers, may be further complicated by the conformational interchange and aggregation reactions that tannin molecules undergo. The aggregation of these molecules is fairly well documented in literature, but the conformational interchange reactions are insufficiently documented and the conformations of these reactions are, as of yet, not sufficiently investigated. In order to achieve this aim, the following objectives are set for this study:

- To obtain pure procyanidins for analysis, it is proposed to separate procyanidin dimers from fresh cocoa beans on a preparative scale by use of two-dimensional preparative high performance liquid chromatography (HPLC), including both hydrophiliic interaction chromatography (HILIC) HPLC and a reversed phase (RP) HPLC steps. This is necessary due to the lack of commercially available standards.
- The separated fractions are to be analyzed by ^{1}H NMR, ^{13}C NMR and mass spectrometry for confirmation of analyte purity and for structural assignment.
- The ^{1}H NMR analysis of the samples will also be conducted at various solvent compositions and temperatures in order to determine the relavant interchange or aggregation kinetic and thermodynamic parameters in different solvent environments.
- A kinetic analysis of the variable temperature (VT) ^{1}H NMR spectra will be performed using a program that will be written by the author for the purpose of this study.
- The possibility of aggregation interactions will be investigated by ^{1}H DOSY NMR.
- Quantum mechanical (QM) DFT and limited wave functional theory (WFT) (as included in hybrid functionals) calculations will be performed in order to

study the conformational geometries and energies involved in any relevant reactions.

- The results of the NMR experiments and energies calculated by DFT calculations will be correlated and the intramolecular interactions will be studied in detail using the quantum theory of atoms in molecules (QTAIM) and the non-covalent interaction (NCI) index.
- The effects of solvation energy on the equilibrium distribution of conformations will be studied by computational techniques, including implicit solvation models (SCRF) and the three dimensional reference interaction site model (3DRISM).

Chapter 2. Experimental Results and Discussion: Isolation and Characterization of Procyanidins

2.1 Introduction

In order to investigate the kinetics and thermodynamics of procyanidin conformational interchange, pure components have to first be obtained before structural analysis and data processing can proceed. Procyanidins can be obtained by synthesis or by isolation from natural products of which grape seeds and cocoa are of the most abundant sources. Synthetic procedures can be difficult and expensive as the diastereomeric and oligomeric composition are hard to regulate and separation of the desired product is also necessary to ensure purity. Extraction and purification is the simpler route as no complicated synthetic steps are necessary and direct separation (which is necessary for most synthetic methods as well) is the main process. The purification of procyanidins is most often achieved via chromatographic separation. After isolation has been completed, an in-depth analysis is necessary to confirm the purity and identification of the sample. Once the sample has been confirmed as the desired molecule, the study of its properties can commence.

Structural analysis of procyanidins has been conducted in various studies by ^{1}H NMR. The NMR analysis allows for 2D or 3D structural determination as well as the identification of phenomena of chemical exchange and aggregation. The effect of chemical exchange is observed in the line shapes of the NMR spectra by peaks that broaden and change in chemical shift. Similarly, aggregation broadens and shifts the peaks, but occurs as a concentration and temperature dependent phenomenon, in contrast to chemical exchange which is purely temperature dependent.

2.2 Procyanidin Procurement

2.2.1 Synthesis

Synthesis of procyanidins is a multistep and complex process and many avenues of approach have been taken in the past [47-49] in order to generate the various chiral and

oligomeric procyanidin molecules. The main challenge in synthetic procedures for generation of procyanidins is to create a highly stereo-selective and oligomer-selective processes to avoid difficult separations. As early as 1966, procyanidins have been synthesized by condensation of phloroglucinol and catechin with flavan-3,4-diol under acidic conditions [47]. A few semisynthetic approaches exist that employ the condensation of extracts. Köhler and associates developed one such an approach to simultaneously degrade higher oligomers and polymers to increase dimeric yield [48]. The study employs high-speed countercurrent chromatography for separation of the various chiral dimeric species [48].

Stepwise condensation is often employed for procyanidin synthesis, as it allows for the generation of a desired specific oligomer. Oyama *et al.* proposed a synthetic method with stepwise self-condensation using 3,4-cis-acetoxy-3-O-acetyl-4-dehydro-5,7,3',4'-tetra-O-benzyl-(+)-catechin and (-)-epicatechin as the key building monomer [49]. The study reported high regio- and stereo-selectivity in the presence of equimolar tetramethylsilyl trifluoromethanesulfonate (TMSOTf) [49].

Cala *et al.* reported a synthetic method that proceeds with the step-wise addition of monomeric groups in order to create a desired degree of polymerization. The documented process involves benzylation in order to protect phenolic OH sites, followed by oxidation of the 4C position of either cathechin or epicatechin and subsequent bromination in order to create a site for the polymerization step to take place. The reaction requires a $TiCl_4$ catalyst and can be repeated step-wise to synthesize the oligomer of choice. This synthetic method only produces oligomers of identical monomeric groups selectively and cannot produce mixed monomer oligomers like B1 selectively [14].

Tuckmantel *et al.* developed a benzylated method and implemented the use of Dess-Martin periodinane to oxidize the chiral C4-H to OH an subsequently into a carbonyl group, which could readily be transformed into the C4-OH with opposite chirality [6]. The study included methods for galloylation and other more advanced syntheses for production of galloyated species [6].

Saito *et al.* developed a method for stereo-selective gram scale synthesis of procyanidin B3 [50]. Benzylated 2,3-Dichloro-5,6-Dicyanobenzoquinone (DDQ) oxidation is implemented, followed by a Lewis acid condensation of which the product is acetylated. The

product is then purified by column chromatography [50]. The study reports high stereo-selectivity and gram scale yields [50].

A rare earth metal catalyzed equimolar condensation was proposed by Mohri *et al.* [51] and employed the use of a Yb(OTf) catalyst to produce all four of the 4→6 dimeric procyanidins (B1, B2, B3 and B4) [51]. The synthesis is stereo-selective with 62%, 76%, 64%, 59% yield for B1 to B4 reported (respectively) from benzylated catechin and epicatechin as substrates [51].

2.2.2 Chromatographic Isolation of Procyanidins

The separation of procyanidins from plant extracts is currently the main method for procuring sufficient amounts of the compounds in high purity. This is routinely executed by extraction from the plant material (cocoa, grape seeds, wine, bark and more) followed by some form of preparative chromatography [2, 30, 31, 47]. The chromatographic separation of procyanidins is most often conducted using a reversed phase column. However, Lozano *et al.* demonstrated anion-exchange chromatography separation of catechin conjugates from underivatized polyphenols and other oligomeric materials [52]. The method excluded the catechin conjugate containing compounds by using a low percentage of organic solvent. Upon the addition of a salt the uncharged polyphenols eluted. In the absence of these salts the uncharged polyphenols would be retained by the matrix. It was proposed that cation-π interactions between the quaternary amino group on the resin and the electron rich faces of the flavanols' aromatic rings might explain the observation [52].

2.3 Procyanidin Extraction and Chromatographic Purification

Due to the complexity and level of difficulty involved in procyanidin synthesis, extraction and separation for sample preparation and purification was utilized in this study. All solvents used are Merck HPLC grade 99.93% with the exception of water where MilliQ (12.8 MΩ at 298K) was used and the deuterated solvents used for NMR. Raw cocoa beans were peeled and flash frozen in liquid nitrogen. The frozen beans were milled to a fine powder and the powder was collected. The cocoa powder (2.0 g) was extracted with three times 9 mL hexane to remove the natural fats. The remaining solid cake was dried under a stream of nitrogen gas and the hexane liquid fractions were discarded. The solid cake was extracted three times with 3 mL of a 70:30 acetone/water (v/v) mixture and then with a 3

mL of a 70:30 methanol/water (v/v) mixture three times. The water/acetone and water/methanol extraction was done in order to collect the polar organic compounds from the cocoa powder cake. Procyanidins are polar due to the numerous OH groups present and are thus retained in this fraction. The procedure was repeated until appreciable amounts of each procyanidin oligomer could be separated (determined to be approximately 10 mg of each after separation). The methanol/water and acetone/water fractions were then combined and centrifuged at 5000g in order to remove the remaining suspended solids. The supernatant was decanted and filtered through a 0.45 µm hydrophilic polyvinylidene difluoride filter membrane (Millipore, Milford, MA, USA) in order to remove particulates that could clog HPLC columns. The remaining liquor was dried in a rotary evaporator to remove the methanol before freeze drying at a temperature of -40 °C. The freeze dried powder was kept at 4.0 °C in a nitrogen atmosphere.

2.4 Preparative High Performance Liquid Chromatography (HPLC)

The freeze dried powder was reconstituted (0.01g/mL) in a 70:30 acetonitrile/water (v/v) mixture for injection in HPLC. Preparative HPLC experiments were performed on a modular Waters (Waters, Milford, MA, USA) system equipped with two 510 pumps controlled by a Waters Automated Gradient Controller and a manual Rheodyne injector fitted with a 1000 µL loop. Detection was performed using a Hewlett Packard 1050 variable wavelength detector set to 280 nm (Hewlett Packard, California, USA), and data wes acquired using DAx 8.0 data acquisition software (Van Mierlo software, Amsterdam, The Netherlands). The method used for the separation of procyanidin fractions of increasing levels polymerization was adapted from Hammerstone *et al.* [26, 53]. For the separation of procyanidins present in the extract a preparative Develosil (Nomura Chemicals, Japan) hydrophilic interaction chromatography (HILIC) column with dimension of 20.0 X 150 mm, 10 µm particle size with a DIOL packing was used. Each run duration was 65 min and the flow rate was kept at 7 $mL.min^{-1}$. The mobile phases consisted out of an acetonitrile and water solvent gradient. Th average injection volume was 500 µL. Table 2.1 shows the solvent gradient and Figure 2.1 shows a typical chromatogram for the preparative separation obtained from cocoa.

Table 2.1. HILIC-HPLC solvent gradient

Time elapsed (min)	Flow rate (mL.min^{-1})	% ACN	% H_20
Initial	7	96	4
50	7	60	40
55	7	0	100
60	7	0	100
62	7	96	4

The HILIC-HPLC experiments allowed for quantitative separation of oligomers up to hexamers. Each of the peaks labeled in Figure 2.1 correspond to all isomeric procyanidins of the same degree of polymerization [26, 53].

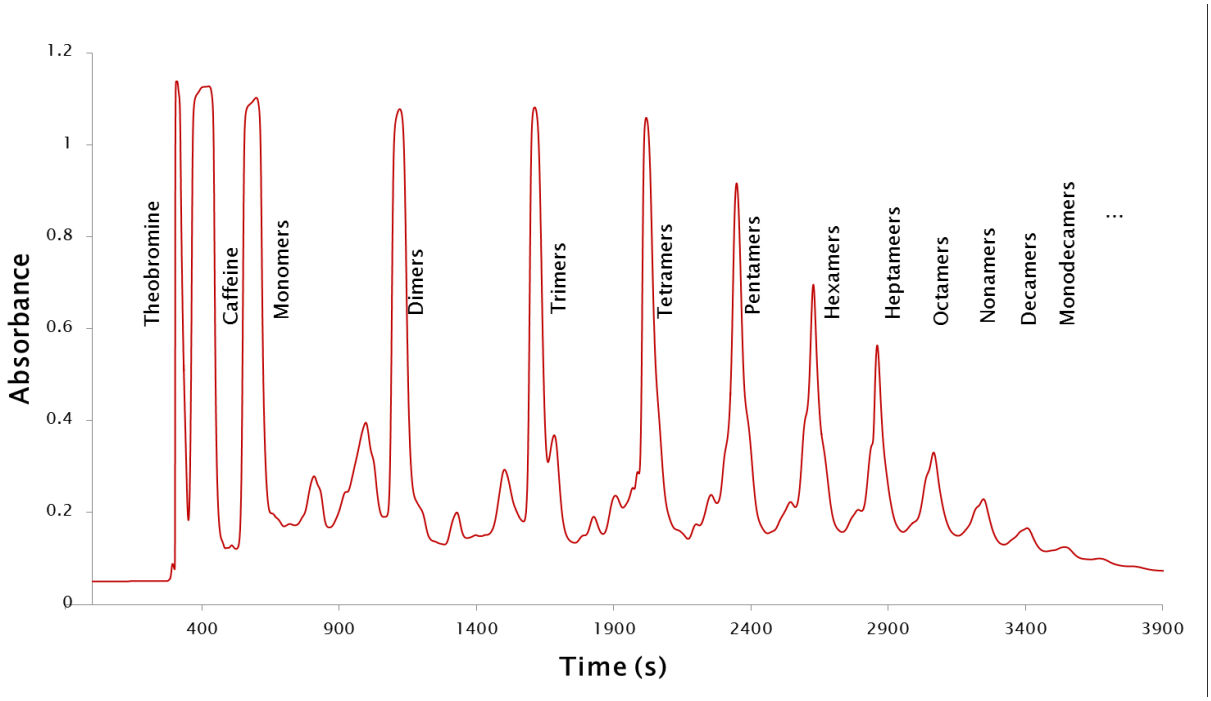

Figure 2.1. Preparative HILIC-HPLC chromatogram of a cocoa extract with UV detection at 280 nm, preparative Develosil (Nomura Chemicals, Japan) hydrophilic interaction chromatography (HILIC) column with dimension of 20.0 X 150 mm, 10 µm particle size with a DIOL packing, 7 mL.min^{-1} flow rate, 500 µL injection volume and H_2O and ACN mobile phases with gradient details as specified in Table 2.1

The monomer, dimer, trimer, tetramer, pentamer and hexamer peaks were manually collected and corresponding fractions for 40 injections were combined and freeze dried. Higher oligomeric peakswere not collected due to bad resolution and lower levels of those compounds.

The resulting fractionated concentrate powders were dissolved in a 70:30 acetonitrile and methanol(v/v) mixture and re-injected onto a C18 reversed phase (RP)

column (Phenomenex 250 X 10, 10 µm, Gemini C18) in order to separate the oligomeric procyanidins of the same degree of polymerization as displayed in Figure 2.2. The mobile phase consisted of acetonitrile and 0.1 % formic acid solution. The run time was kept at 72 min with a flow rate of 3 $mL.min^{-1}$. The solvent gradient is displayed in Table 2.2.

Table 2.2. RP -HPLC solvent gradient

Time elapsed (min)	Flow rate (mL.min-1)	% ACN	% FA
Initial	3	2	98
0.82	3	2	98
34.03	3	18	82
56.72	3	25	75
65.23	3	100	0
70.88	3	2	98

As an example, Figure 2.2 shows the RP-HPLC chromatogram obtained for the dimeric procyanidin fraction, which displays the two dominant dimer isomers that were collected. The Finally the major peaks were collected, the organic solvents evaporated and the extracts freeze dried for storage at 4.0°C under a nitrogen atmosphere. The complete set of uncharacterized separated fractions for which sufficient amounts were obtained includes two dimers, four trimers, one tetramer, one pentamer and one hexamer. The RP-HPLC stacked chromatogram of two runs is shown in Figure 2.2. chromatograms of the remaining oligomeric RP-HPLC chromatograms fractions are not included in this text and the purity of these fractions can be assessed from the UHPLC-MS TIC chromatograms in appendix A.2.

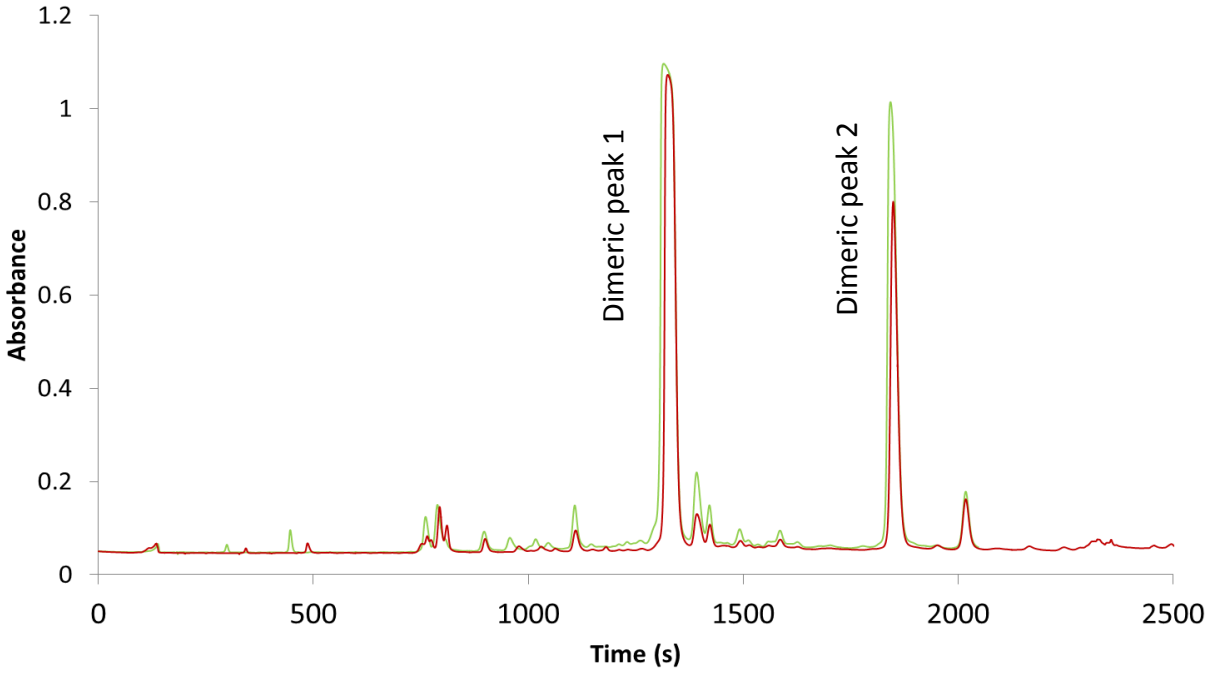

Figure 2.2. Stacked semi-preparative reversed phase HPLC chromatograms at 280 nm of two experimental runs showing two dimer peaks isolated from cocoa

2.5 Ultra High Pressure Liquid Chromatography-Electrospray-Ionization-Time-of-Flight Mass Spectrometry (UHPLC-ESI-TOF-MS)

The purpose of the UHPLC-ESI-TOF-MS experiments were to confirm analyte identity estimate analyte purity for procyanidin oligomers. The isolated fractions were dissolved in separate vails containing a mixture of 10 % (v/v) methanol and water. RP-UHPLC-MS analyses were performed on an Acquity UPLC system equipped with a binary pump, autosampler, column oven, photodiode array (PDA) detector hyphenated to a Waters Synapt G2 quadrupole time-of-fight (Q-TOF) instrument (Waters, Milford, MA, USA) in negative ionization mode using a Kinetex C18 50 X 4.6 mm, 2.6 µm column. Data was acquired using MassLynx v.4.1 software (Waters, Milford, MA, USA). Procyanidin C1 and B1 standards were bought from Phytolab GmbH & co. KG and also analyzed for comparison. The mobile phase consisted of acetonitrile and a 0.1 % formic acid solution at 50 °C. A 10µl injection volume was eluted during a 15 min gradient run (Table 2.3).

Table 2.3. UHPLC-MS solvent gradient

Time elapsed (min)	Flow rate (mL.min^{-1})	% 0.1% FA	% ACN
initial	0.8	98	2
0.13	0.8	98	2
5.4	0.8	78	18
9	0.8	75	25
10.35	0.8	0	100
11.25	0.8	0	100
12.6	0.8	98	2

A 1:1 split in the flow between the UHPLC and the mass spectrometer used. The MS parameters included a source temperature 120 °C, desolvation temperature of 275 °C, cone gas flow (N_2) of 50 mL.min^{-1}, desolvation gas flow rate (N_2) of 650 mL.min^{-1} and scan range 200-2000 m/z. The instrument was calibrated with a sodium formate solution. The major dimer peak fraction (at retention time of 1330 seconds on the RP chromatogram) was analyzed as the study's primary analyte and showed a deprotonated molecular *m/z* 577.1351 (accurate mass *m/z* 577.1346, Δppm of 0.9), with an empirical formula of a $C_{30}H_{26}O_{12}$. A small amount of $[2M-H]^-$ aggregate was also observed at *m/z* 1155.280 as seen in Figure 2.4. The analyte showed high purity on the total ion current (TIC) and UV chromatograms (Figure 2.4). The isolated procyanidin oligomers are reported in Table 2.4. The results of the remaining MS TIC chromatograms and mass spectra attached in appendix A.2.

Table 2.4. Mass spectrum predicted and experimental m/z in negative ionization mode for various procyanidins separated from cocoa

Molecule	chemical formula	$[M-H]^-$ theoretical (m/z)	$[M-H]^-$ experimental (m/z)	Δppm[a]	$[M-2H]^{-2}$ experimental (m/z)
B1	$C_{30}H_{25}O_{12}^-$	577.1346	577.1355	0.9	none
B2	$C_{30}H_{25}O_{12}^-$	577.1346	577.1355	0.9	none
second dimer	$C_{30}H_{25}O_{12}^-$	577.1346	577.1355	0.9	none
C1	$C_{45}H_{37}O_{18}^-$	866.2058	865.1982	3.6	none
First trimer	$C_{45}H_{37}O_{18}^-$	866.2058	865.1984	1.0	432.2674
second trimer	$C_{45}H_{37}O_{18}^-$	866.2058	865.1981	2.4	432.1920
third trimer	$C_{45}H_{37}O_{18}^-$	866.2058	865.1980	10.5	432.2551
fourth trimer	$C_{45}H_{37}O_{18}^-$	866.2058	865.1982	1.3	432.2432
tetramer	$C_{60}H_{49}O_{24}^-$	1155.2770	1153.2612	2.0	576.3330
pentamer	$C_{75}H_{61}O_{30}^-$	1444.3482	1441.3254	211.2	720.3860
hexamer	$C_{90}H_{73}O_{36}^-$	1733.4195	1729.3883	500.8	864.4421

(a) Theoretical/experimental *m/z* difference in parts per million

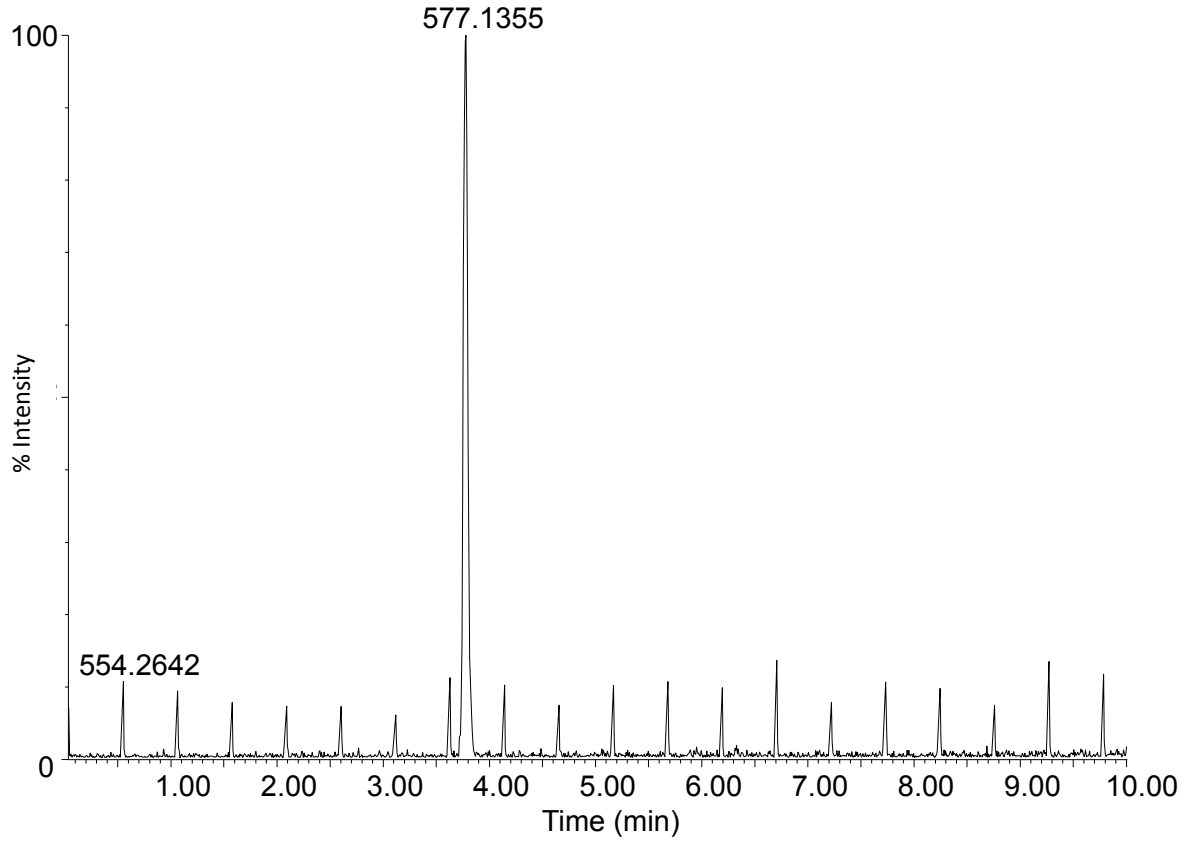

Figure 2.3. Base peak ion (BPI) chromatogram obtained for the UHPLC-MS analysis in negative ionization mode of the procyanidin dimer isolated from cocoa

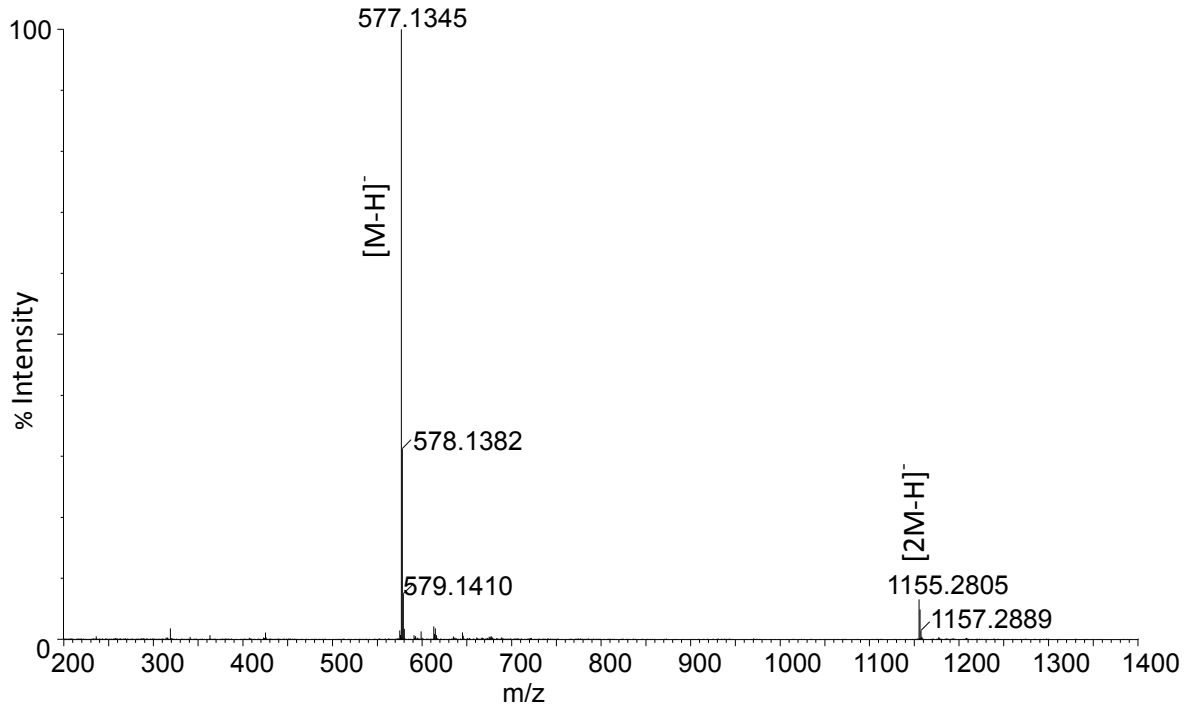

Figure 2.4. Mass spectrum in negative ionization mode of the main procyanidin dimeric fraction separated from cocoa

2.6 Nuclear Magnetic Resonance (NMR) Spectroscopy

The main procyanidin dimer isolated by the abovementioned procedure was dissolved in acetonitrile-D_3 and several ^{1}H and ^{13}C spectra were recorded in an Agilent-Inova 600 MHz nuclear magnetic resonance instrument. Variable temperature one dimensional ^{1}H spectra were recorded incrementally (5 K) between 253 K and 303 K. Correlation spectroscopy (COSY), rotational-frame nuclear Overhauser effect spectroscopy (ROESY), diffusion ordered spectroscopy (DOSY), heteronuclear multiple bond correlation spectroscopy (HMBC) and heteronuclear single quantum coherence spectroscopy (HSQC) as well as one dimensional ^{13}C experiments were performed at 253 K. Variable temperature one dimensional ^{1}H experiments were also performed in acetone-D_6 on procyanidin C1 and B1 samples bought from Phytolab GmbH & co. KG. Due to the temperature range (253 K – 353 K) of the indirect-detection with z-pulsed-field-gradient (IDPFG) probe available on the 600 MHz spectrometer, an Agilent-Inova 400MHz spectrometer equipped with a broad band pulsed-field-gradient (PFG) probe was used for a second set of experiments which included one dimensional ^{1}H, ROESY, COSY, HMBC, HSQC and ^{13}C experiments in acetonitrile-D_3 at 238 K.

The stacked VT ^{1}H NMR spectra of procyanidin B2 in acetonitrile-D_3 are displayed in Figure 2.5. From initial inspection of the ^{1}H spectra, line broadening and shifting is evident as the temperature is increased. Literature reports that the line broadening and shifting is due to extensive conformational interchange between the compact and extended conformations as determined by a positive or negative interflavanoid dihedral angle of the C3(C)-C4(C)-C8(D)-C8a(D) bonds respectively [27, 24].

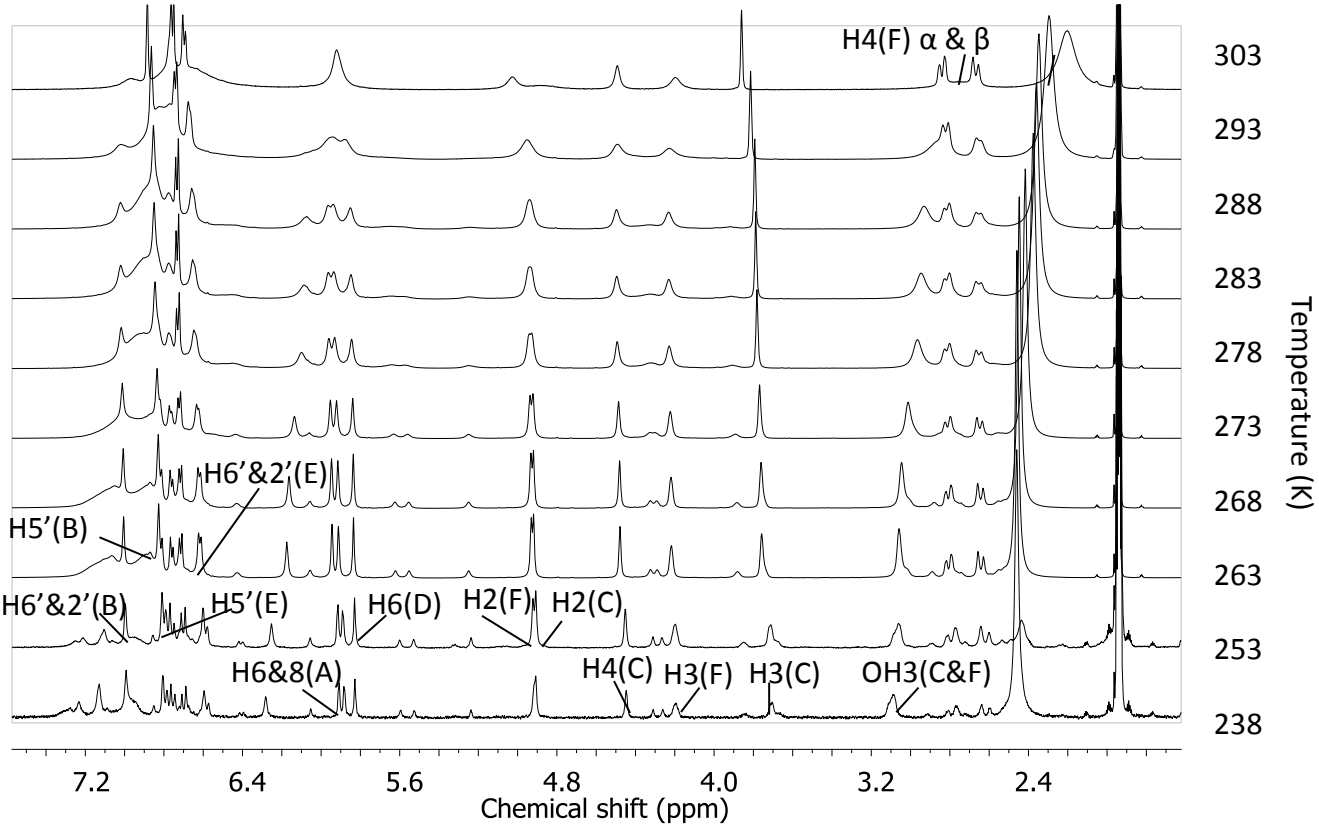

Figure 2.5. Stack plot of variable temperature ^{1}H NMR spectra of procyanidin B2 in acetonitrile-D_3

The conformations were recalculated by use of semi-empirical methods via the Spartan '08 program to compare with literature. High geometrical agreement was found with Terascou *et al.* [27].

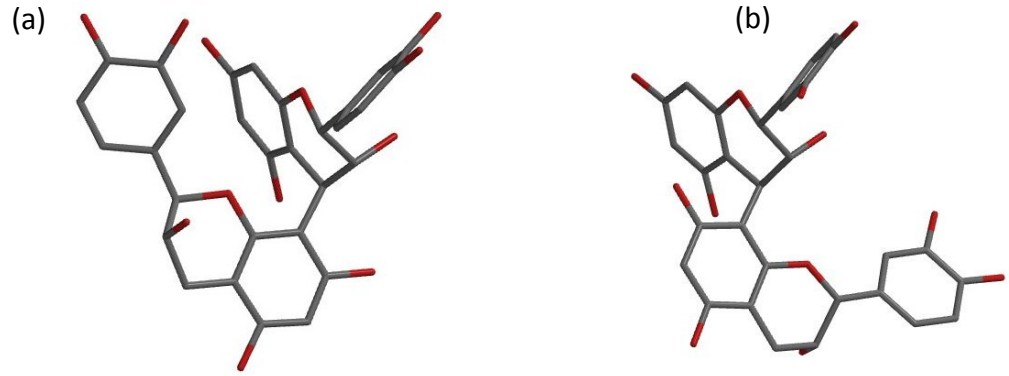

Figure 2.6. Tube representation of the (a) compact and (b) extended procyanidin B2 conformers recalculated in Spartan '08 by use of the AM1 semi-empirical method

Aggregation interactions may also contribute to the observed line broadening [14]. To investigate this possibility, the diffusion of B2 was measured in acetone-D_3 at 253 K via a ^{1}H DOSY experiment using an Agilent-Inova 600 MHz intrument. The critical micelle concentrations (CMC) for water/alcohol mixtures (wine like solutions) have been determined previously and are reported by Pianet *et al.* [15]. The solutions investigated by Pianet *et al.* contained up to 10 % ethanol in water and the CMC concentrations were found to be 18 ± 3 mM in pure D_20 and 28 ± 8 mM in 10% deuterated ethanol in D_20. The concentrations used in this study were far lower than the CMC reported by Pianet *et al.* [15], but the aggregation characteristics for B2 in non-polar solvents are not described in the reviewed literature. Additionally, no literature was found reporting the conformational exchange rate of B2 in deuterated acetonitrile. The aggregation characteristics were analyzed in acetone as it is a less polar solvent than acetonitrile and should consequently contribute to aggregation of procyanidin more readily than acetonitrile. To eliminate the possibility of aggregation contributing to the line broadening in the ^{1}H NMR spectra, a DOSY experiment was performed in acetone-D_6 at 253 K. The DOSY experiment allows for the measurement of the diffusion rate of a molecule, from which the hydrodynamic radius of the molecular particles in solution can be determined. This allows for correlation with expected molecular sizes in order to determine whether aggregation takes place. The resulting DOSY spectrum is shown in Plate 2.1 and the diffusion constant was determined as 4×10^{-6} $cm^2.s^{-1}$. The A molecular hydrodynamic radius of 8510 Å was calculated by using the Einstein-Stokes equation (equation 2.1).

$$D = k_B \frac{T}{6\pi\eta r} \tag{2.1}$$

The experimental temperature was 253 K and the kinematic viscosity of acetone is linearly proportional to temperature until close to its melting point of 178 K. Using tabulated viscosity values from the Dortmund databank [54] an acetone viscosity of $5.44x10^{-7}$ $m^2.s^{-1}$ at 253 K was obtained and used in the Einstein-Stokes equation.

$$4x10^{-10} = \frac{k_B(253.15)}{6\pi(5.44x10^{-7})r}$$

$$\Rightarrow \quad r = 8.51x10^{-7}m = 8510\ \text{Å}$$

A hydrodynamic radius of 8510 Å indicates aggregation. However, from the DOSY experiment the diffusivity for acetone is determined as $1.74x10^{-9}$ $m^2.s^{-1}$. By using the same calculation on the hydrodynamic radius of acetone (≈2.2 Å) a diffusivity of $1.62x10^{-6}$ $m^2.s^{-1}$ is calculated. The ratio of the calculated and measured hydrodynamic radii were calculated and used to correct the calculated hydrodynamic radius of procyanidin B2. The calculation standardized in this way yields a hydrodynamic radius of 8.5 Å or a hydrodynamic diameter of 19 Å, which roughly corresponds to the hydrodynamic diameter of the full extended (16.6 Å) conformer as measured from atomic cores of the furthest hydrogens as calculated in the DFT chapter of this text, *vida infra*. The Einstein-Stokes equation assumes spherical shape in the particle modeled and as such is a fairly rough approximation, but the agreement is good. The three dimensional geometry of the procyanidin largely depends on its conformation, but would not be approaching any sort of spherical shape and that deviation from the model is expected to be the reason for deviation from the calculated hydrodynamic radius. The good agreement between the density functional theory molecular radius and Einstein-stokes hydrodynamic radius suggests that no aggregation of procyanidin B2 takes place at 253 K in deuterated acetone. Additionally, the duplication of signals observed as well as the signals shifting towards each other as seen in the temperature dependent spectra, Figure 2.5, between the minor and major peaks corresponds to slow conformational interchange on the NMR time scale. Therefore, the broadened line shapes are not attributed to aggregation. Moreover, at higher temperatures, intermolecular aggregation becomes less and peak narrowing should occur in contrast to our data. Aggregation becomes less at higher temperatures due to the increased kinetic energy of each molecule that allows them

to more readily overcome the intermolecular interactions formed by aggregates. Additionally, different concentrations procyanidin B2 ($1.4x10^{-2}g.l^{-1}$ and $1.0x10^{-2}$ $g.l^{-1}$) in acetone were analyzed by ^{1}H NMR spectroscopy and showed no visible resonance frequency shift.

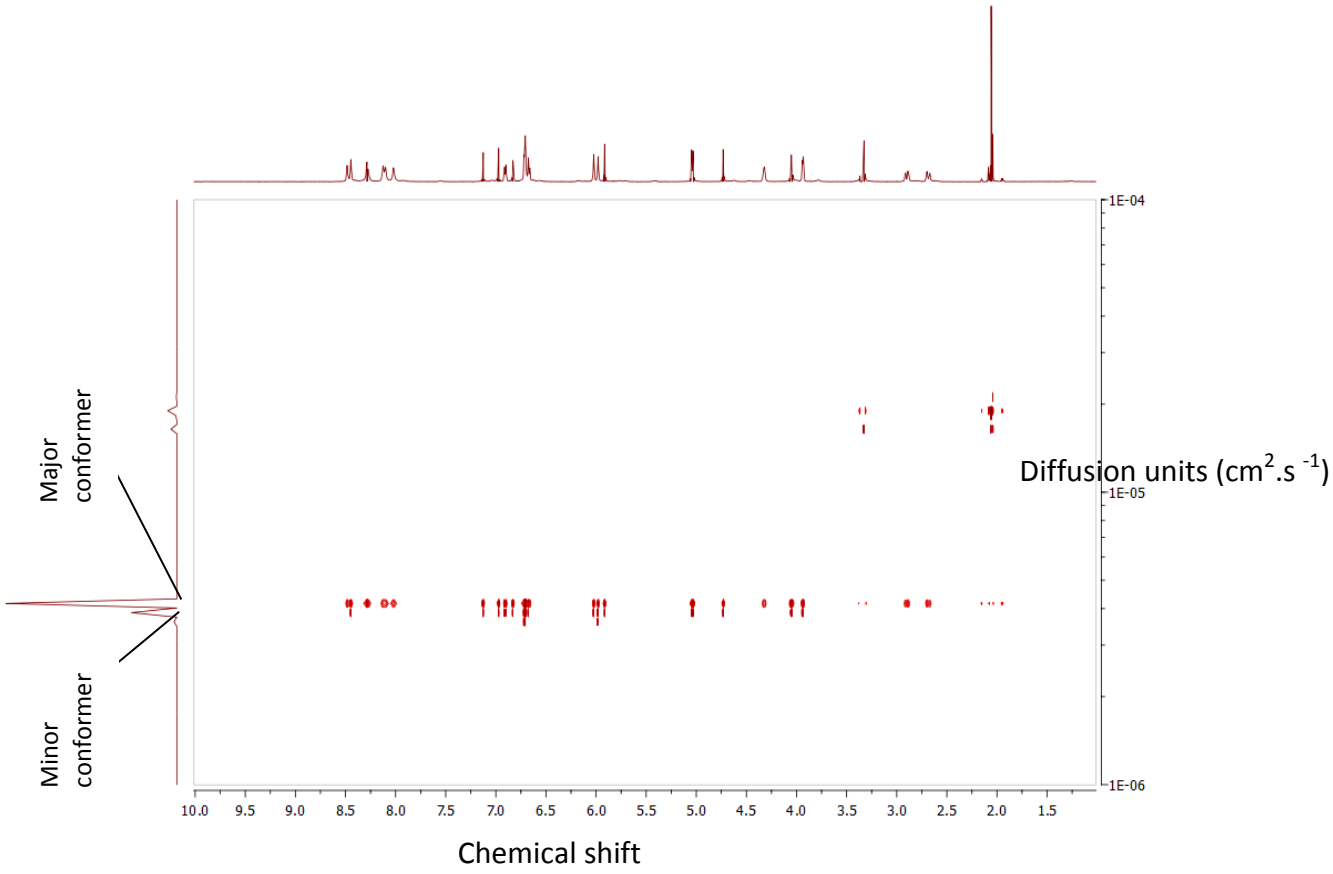

Plate 2.1. DOSY spectrum of procyanidin B2 in acetone-D_6 at 253 K

The assignment of the ^{1}H and ^{13}C NMR signals was achieved by utilizing one and two dimensional NMR techniques including COSY, ROESY, HMBC, HSQC, 1D ^{13}C at 238 K and variable temperature 1D ^{1}H NMR experiments between 303 and 238 K in acetonitrile-D_3. Although deuterated acetonitrile has a melting point of 228 K, it was found to be undesirable to reduce the temperature below 238 K as the spectrum starts to broaden as a result of increasing viscosity of the solvent and consequently increasing the T_2 relaxation rate. The ^{1}H NMR spectrum at 253 K in acetonitrile-D3 as determined in a 600MHz Agilent-Inova instrument is shown in Figure 2.7. Extensive broadening of the OH peaks is observed as a result of exchange with a residual water peak (2.45 ppm) as assigned from water chemical shift data, and has been suppressed by using a standard water presaturation

experiment. The saturation of the water resonance peak in ^{1}H NMR was also performed on a 400MHz instrument at 238 K, and was extended to all two dimensional experiments except the DOSY experiment. The convoluted aromatic protons between 6 and 8 ppm was also given clarity by the suppression of the OH and water peaks during the presaturation experiments, thereby decreasing the convolution of the aromatic proton resonance signals. The water suppression also supresses the hydroxyl groups' protons as the hydroxyl moieties' protons exchange with the water in the sample.

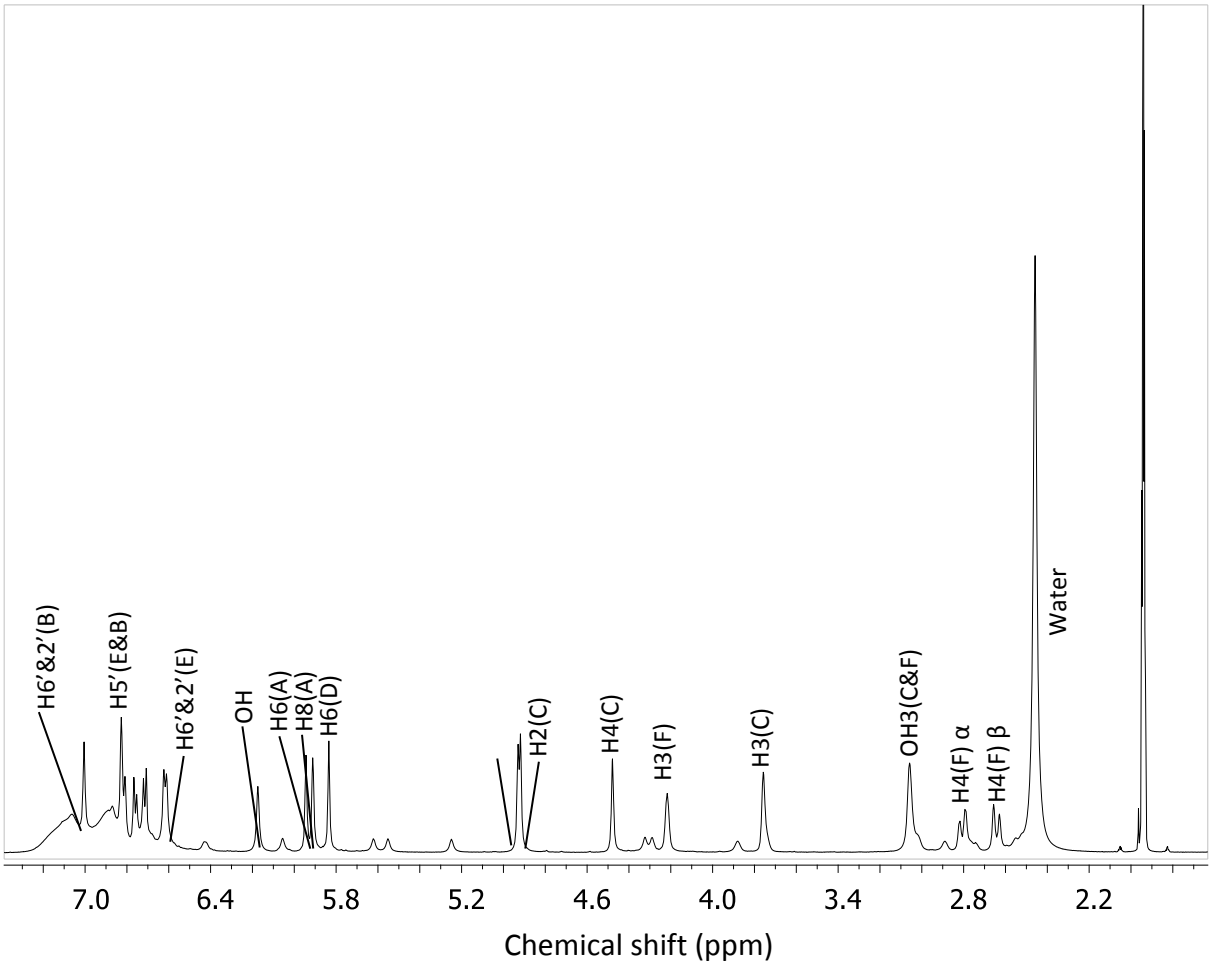

Figure 2.7. ^{1}H NMR spectrum of procyanidin B2 at 253 K in acetonitrile-D_3

The ^{1}H NMR spectra allows identification of the two H4(F) protons as a doublet of doublets in the aliphatic region at 2.79 (dd, J = 16.5, 3.3 Hz H4(F)α) and 2.62 (d, J = 16.5 Hz H4(F)β). These two protons are furthermore identified by the geminal coupling they display, which is unique within the B2 molecule. The COSY spectrum, Plate 2.2, displays a vicinal

coupling between aliphatic H2(C), H3(C) and H4(C) and H2(F), H3(F) and H4(F) ring protons in their respective spin systems. Here the H2(F) and H3(F) protons can be distinguished by their coupling to the H4(F) protons and each other. Plate 2.2 only shows the aliphatic region of the COSY experiment. The full COSY spectrum is shown in Supplementary plate 1 in the appendix.

It is possible to assign the relative stereochemistry of the F-ring protons via the ROESY, which shows that the alpha H4(F) proton associates stronger with the H3(F) and H2(F) protons, confirming the lower unit as an epicatechin unit. The H4(C) has strong COSY cross peaks with the corresponding H2(C) and H3(C) protons, assigning the vicinal spin system of the C-ring. Even at 238 K the resolution of all the ^{1}H spectra is not resolved enough to clearly distinguish the smaller coupling constant of the H4 β (F) doublet of doublets. Also, the H2 protons on the respective units have a similar shift and are only distinguishable by high resolution ^{1}H NMR experiments and may interchange chemical shift values at various solvent compositions and temperatures as found for B2 in acetone, acetonitrile and reported in water by Terascou *et al.* [27]. The aliphatic assignments via the COSY experiments at 238 K in deuterated acetonitrile are shown in Table 2.5.

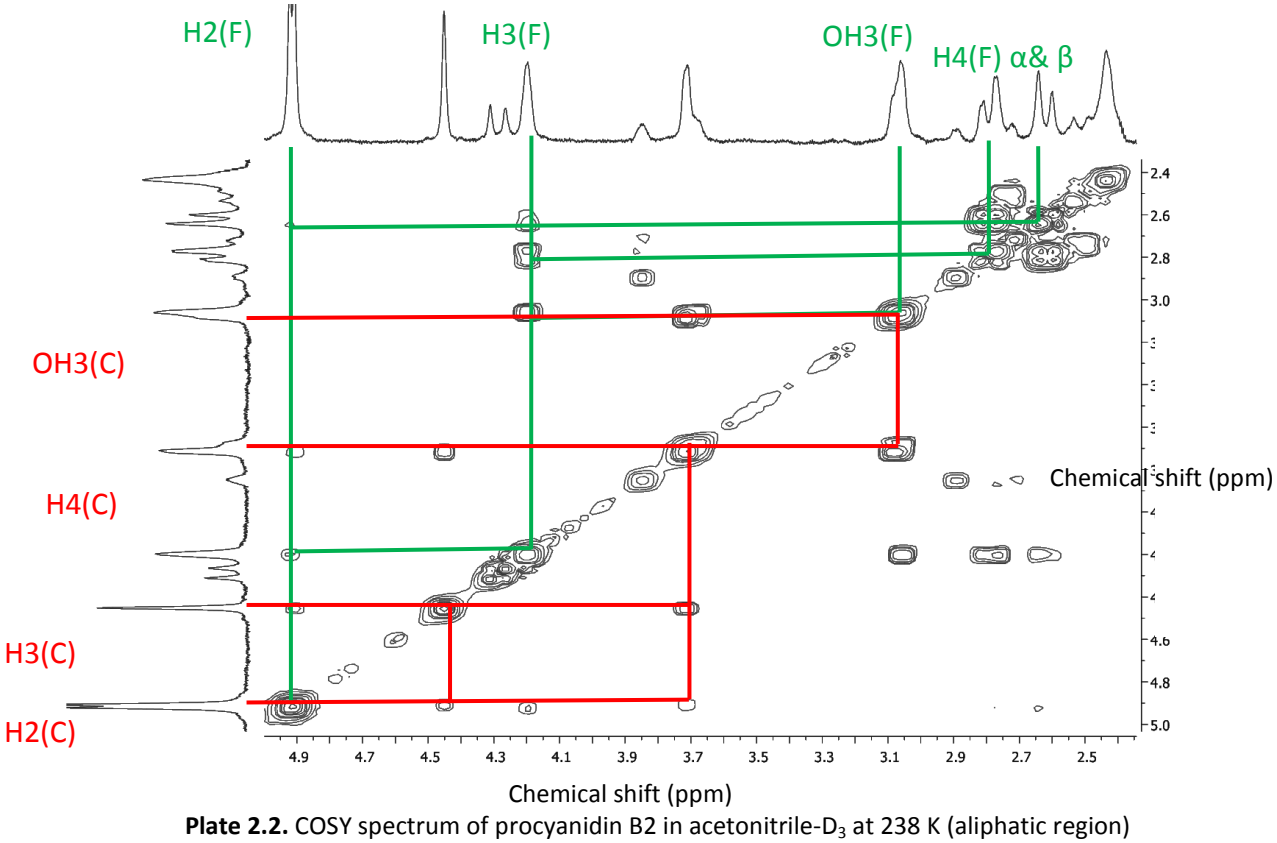

Plate 2.2. COSY spectrum of procyanidin B2 in acetonitrile-D_3 at 238 K (aliphatic region)

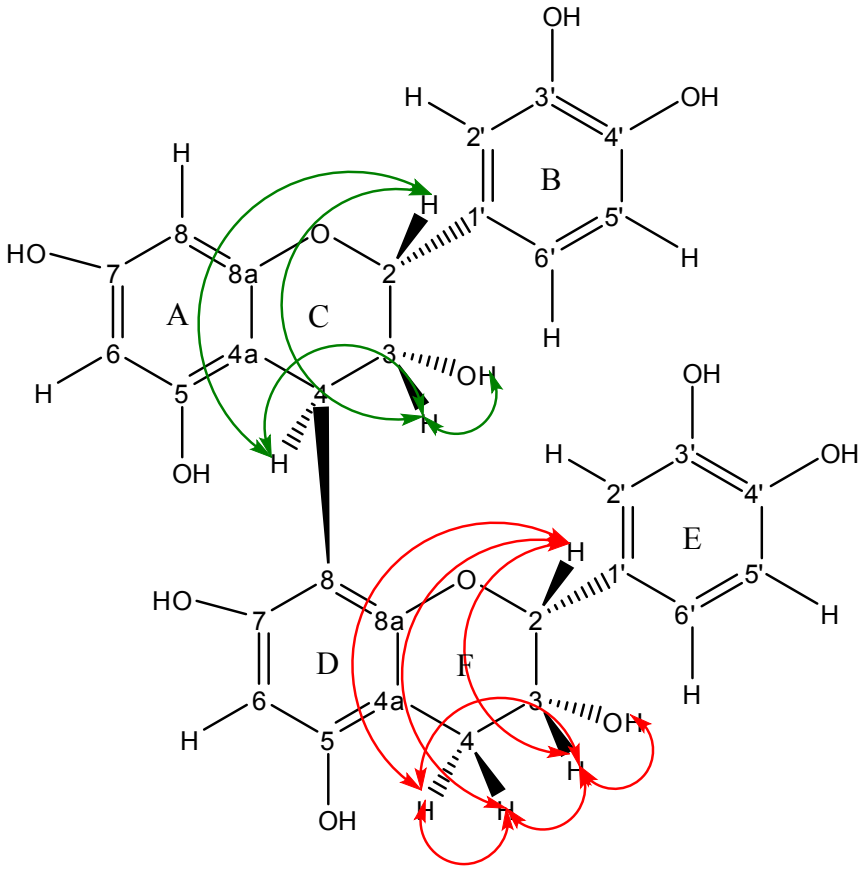

Figure 2.8. Representation of procyanidin B2 showing the COSY vicinal coupling patterns as depicted on Plate 2.2

The aromatic proton resonances are highly convoluted and more difficult to assign when compared to the aliphatic proton signals. The A and D ring protons do not show any cross peaks on the COSY spectrum with their own spin systems, except between their closest aromatic neighbours where considerable peak overlap complicates the assignment. The meta-coubled doublets at 5.9 ppm can only be assigned to the aromatic protons H6(A)/H8(A) at 5.91 ppm (d, J= 1.76 Hz) and 5.89 ppm (d, J= 1.76 Hz) as they do not correspond to the B and E ring ABX spin systems. Therefore, the 5.83 ppm singlet must correspond to the H6(D) proton. The A ring H6 and H8 protons are very difficult to differentiate, even from the NOE associations observed in ROESY experiment, Plate 2.3. Due to conformational exchange it is observed in the ROESY spectra that all the proton resonance signals share off-diagonal slow tumbling effect peaks with the minor conformational isomer [34].

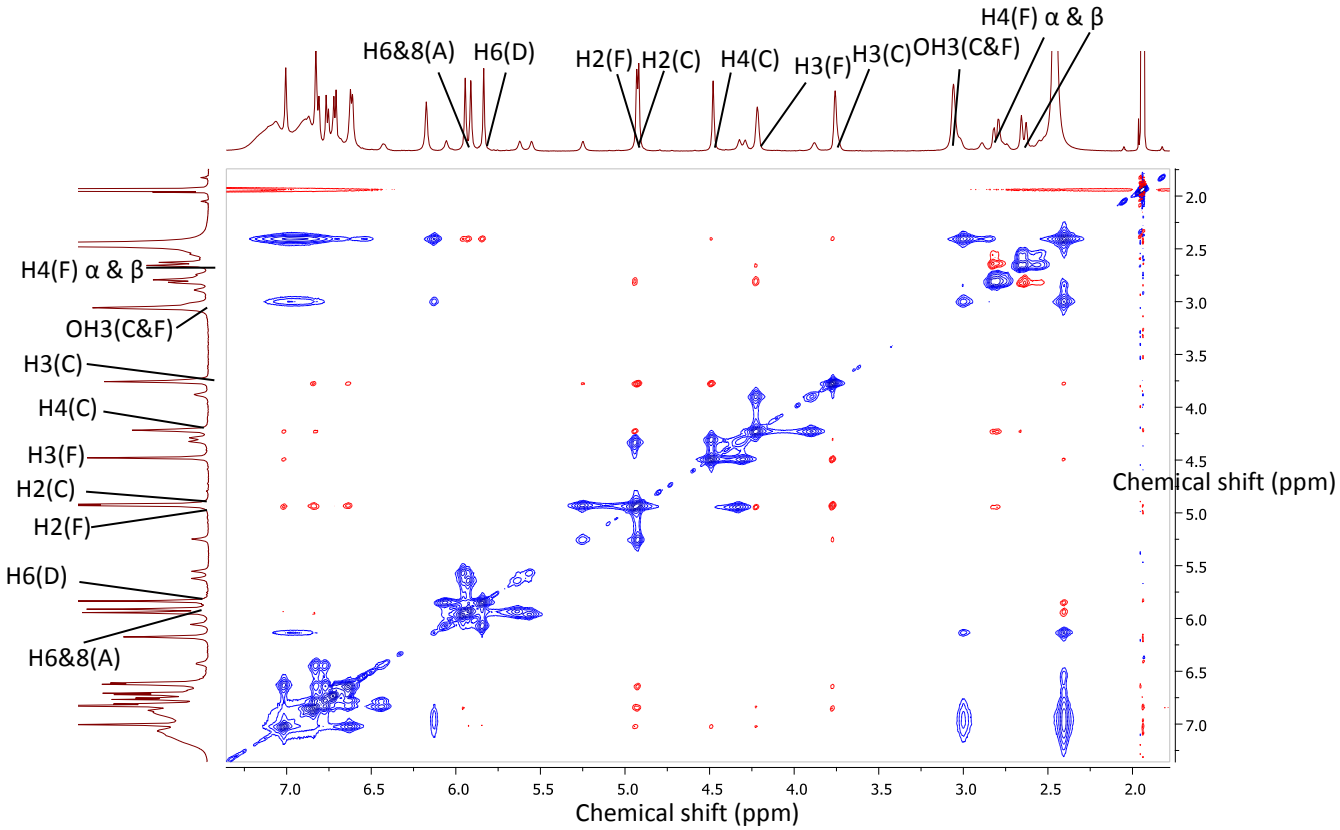

Plate 2.3. ROESY spectrum of procyanidin B2 in acetonitrile-D_3 at 253 K

It is very difficult to determine or correlate conformational geometry solely by NMR as the NOE's are often overlapping and the conformational freedom is too complex. However, extensive density functional theory (DFT) conformational analysis has been performed for this study on procyanidin B2, *vida infra*. These optimized DFT structures can be used to identify the experimental conformations in solutions and are discussed in exceeding detail in the DFT section of this text, chapter 4. According to the Gibbs free energies calculated by DFT in chapter 4 at 298 K, the conformations that are visible in acetonitrile are what this study will henceforth refer to as partially compact (PC) and fully extended (FE). Two more conformations exist that are energetically unfavourable in acetonitrile solutions according to self consistent reaction field (SCRF) solvation modeling in Gaussian 09 suite, as reported in chapter 5.

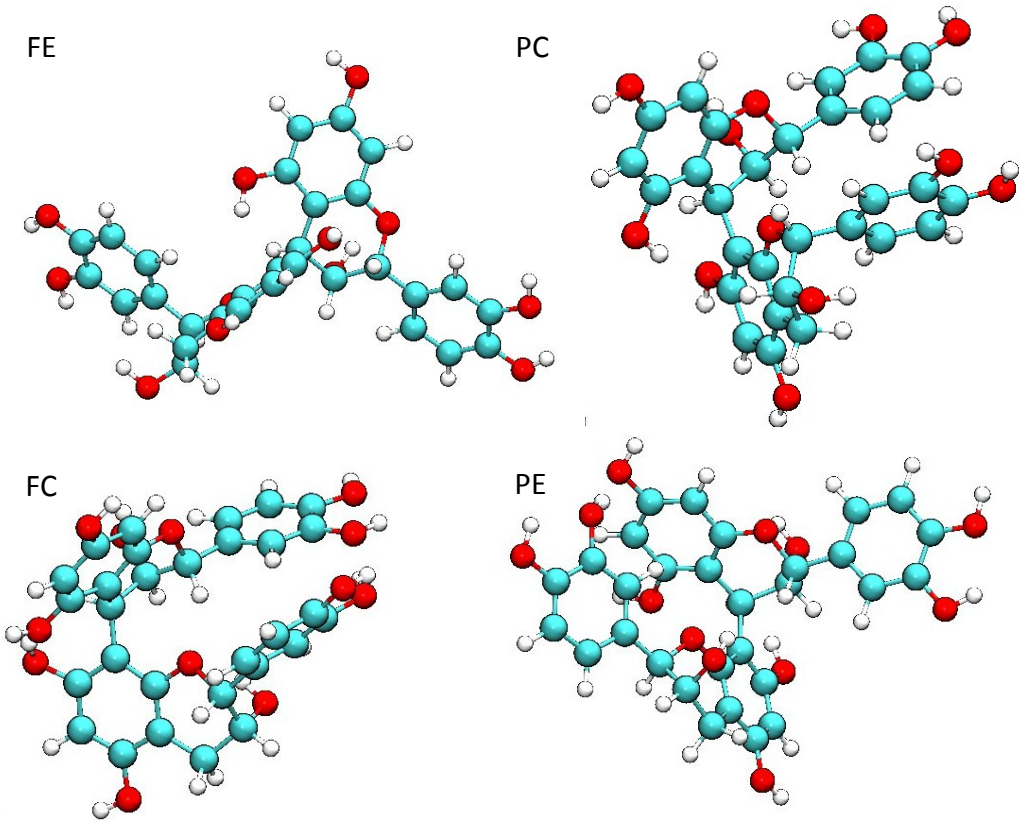

Figure 2.9. Ball and stick representation of DFT conformers (fully extended (FE) , fully compact (FC), partially extended (PE) and partially compact (PC)) as calculated in Gaussain 09 B.01 with theB3LYP functional and 6-311++g** basis set

It was attempted to correlate the DFT conformational interactomic distances with the corresponding NOE interactions detected by the ROESY experiment. However, the only NOE's shared between opposing monomeric units are between those of the H2(C) and H2(F) with the opposing aromatic protons and hydroxyl protons. Unfortunately the resonance signals of these protons are overlapping and unclear. Consequently the NOEs were abandoned in determining the conformation. Nevertheless, the PC conformer is energetically favoured as deduced by DFT calculations. Thus, the major conformer is postulated to be the PC conformer and the minor conformer to be the FE conformer in accordance with the DFT conformational energies, *vida infra*. The final proton resonance frequency chemical shift values of both the major and minor conformers are reported in Table 2.5.

Table 2.5. ^{1}H chemical shift assignments for procyanidin B2 in acetonitrile-D_3 at 253 K

Ring		Major conformer	Minor Conformer	Ring		Major conformer	Minor conformer
A	5			D	5		
	6	5.94/5.91 ppm (bs)[a]	5.552/5.624 ppm (s)		6	5.83 ppm (s)	6.057 ppm (s)
	7				7		
	8	5.94/5.91 ppm (bs)	5.552/5.624 ppm (s)		8		
	8a				8a		
	4a				4a		
B	1′			E	1′		
	2′	6.99 ppm (s)	6.609/6.94 ppm (s)		2′	6.59 ppm	6.61/6.77 ppm (s)
	3′				3′		
	4′				4′		
	5′	6.830 ppm (s)	6.41 ppm (s)		5′	6.830 ppm	6.41 ppm (s)
	6′	6.99 ppm (s)	6.609/6.94 ppm (s)		6′	6.59 ppm	6.61/6.77 ppm (s)
C	2	4.919 ppm (s)	5.249 ppm (s)	F	2	4.93 ppm	4.324 ppm (s)
	3	3.758 ppm (s)	3.758 ppm (s)		3	4.218 ppm	3.88 ppm (s)
	4	4.479 ppm (s)	4.287 ppm (s)		4 α	2.642 ppm (dd, J=16.5,3.3 Hz)	2.55 ppm (m)
					4 β	2.805 ppm (d, J=16.5 Hz)	2.75 ppm (m)

[a]s=singlet, bs=broad singlet, m=multiplet, d=doublet, dd=doublet of doublets. All shifts are given relative to internal standard CD_3CN.

The ^{13}C NMR resonance signals were assigned using HMBC and HSQC spectra (Figure 2.10). By use of the HSQC experiment (Plate 2.4), the assignment of the carbons with directly bonded hydrogen atoms was achieved. The H4(F)(β & α) protons at 2.642 ppm and 2.805 ppm are unfortunately not visible on the HSQC spectrum due to the limited amount of procyanidin B2 available.

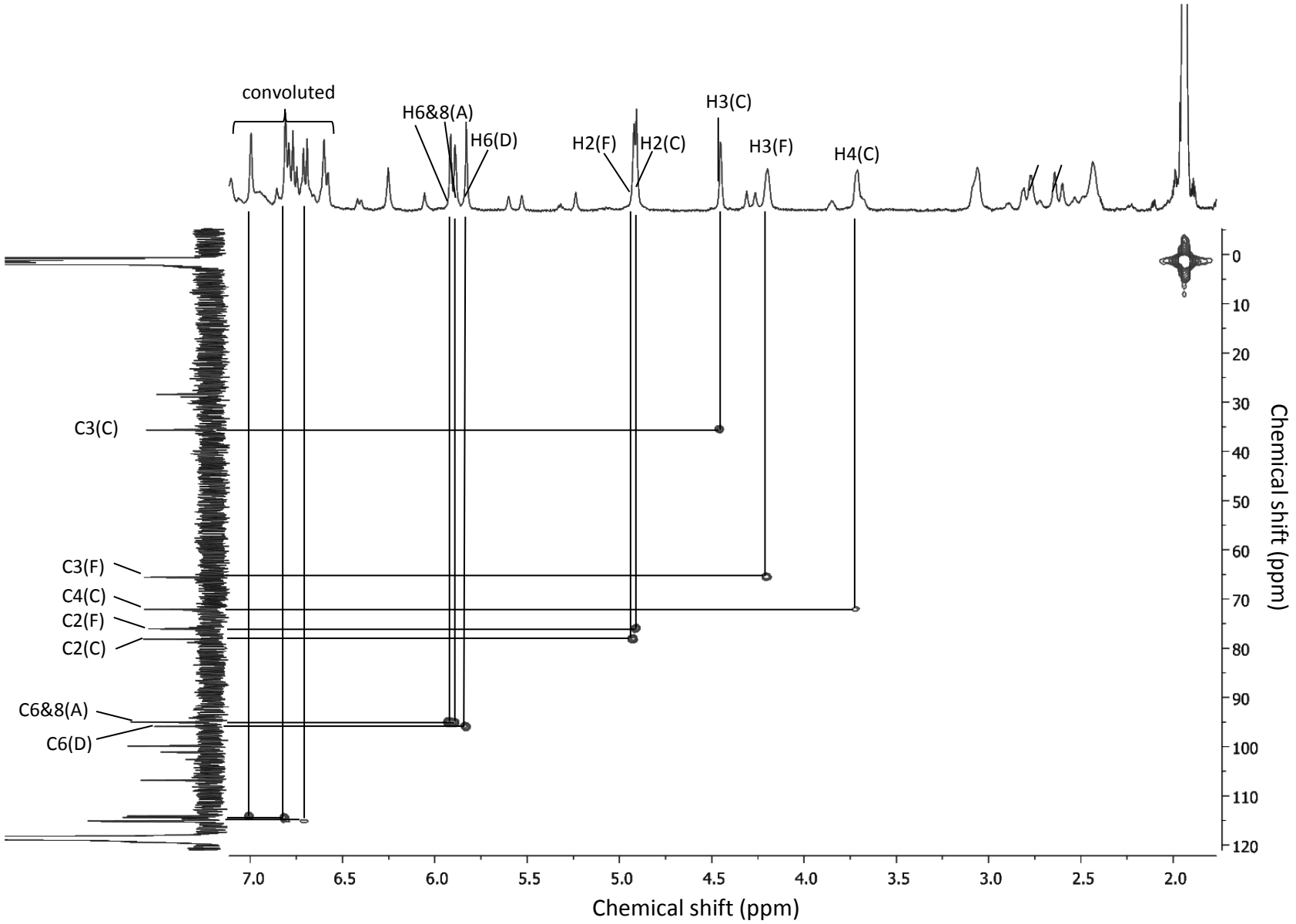

Plate 2.4. HSQC spectrum of procyanidin B2 in acetonitrile-D_3 at 253 K

The HMBC spectrum, Plate 2.5, displays the carbon atoms that have already been determined by the HSQC experiment and these are used for the identification of the $^{2}J_{H\text{-}C}$, $^{3}J_{H\text{-}C}$ unprotonated carbon atoms. It is easiest to assign the resonance signals of unprotonated carbon atoms that are adjacent to protonated carbon atoms, like those of the C6(A) & C8(A) at 157.003 ppm and 157.3 ppm respectively (which remain ambiguous like their bonded hydrogen atoms). The C4(C) carbon is assigned as the 131.862 ppm resonance due to its long range $^{2}J_{HC}$ and $^{3}J_{HC}$ coupling with the H3 (C) and H2 (C) protons respectively. The H2(C) and H2(F) protons show coupling to the C2', C6' and C1' carbons on their respective B and E rings. Finally, the aromatic region with its highly overlapping proton spectrum can't be entirely assigned at this resolution due to broad HMBC peaks that overlap over most of the aromatic C shifts and due to the fact that the HMBC experiment is proton detected and the cross-peaks resemble the resolution of the proton spectra. However their assignment has been performed as completely as possible. The complete assignment is given in Table 2.6.

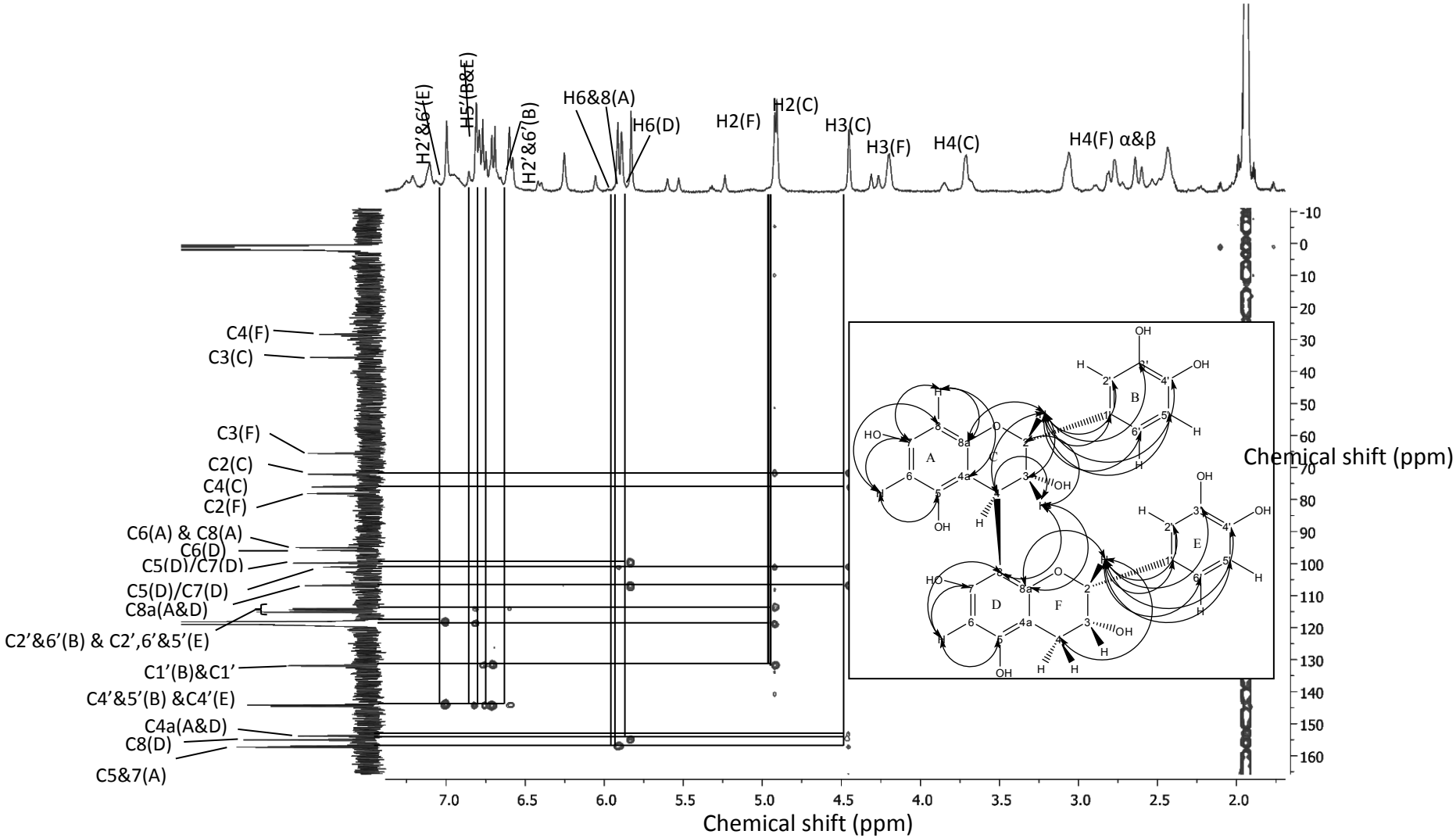

Plate 2.5. HMBC spectrum of procyanidin B2 in acetonitrile-D_3 at 253 K

Table 2.6. ^{13}C chemical shift assignments (ppm) for procyanidin B2 in acetonitrile-D_3 at 253 K

Ring		Major conformer	Ring		Major conformer
A	5	157.003/157.3	**D**	5	99.882/106.822
	6	94.978		6	95.927
	7	157.003/157.3		7	99.882/106.822
	8	95.076		8	154.995
	8a	101.13		8a	101.13
	4a	153.77		4a	153.77
B	1	131-132	**E**	1	131-132
	2	114-116		2	114-116
	3	118.17		3	118.85
	4	143-145		4	143-145
	5	143-145		5	114-116
	6	114-116		6	114-116
C	2	76.045	**F**	2	78.147
	3	35.699		3	65.63
	4	72.186		4	28.53

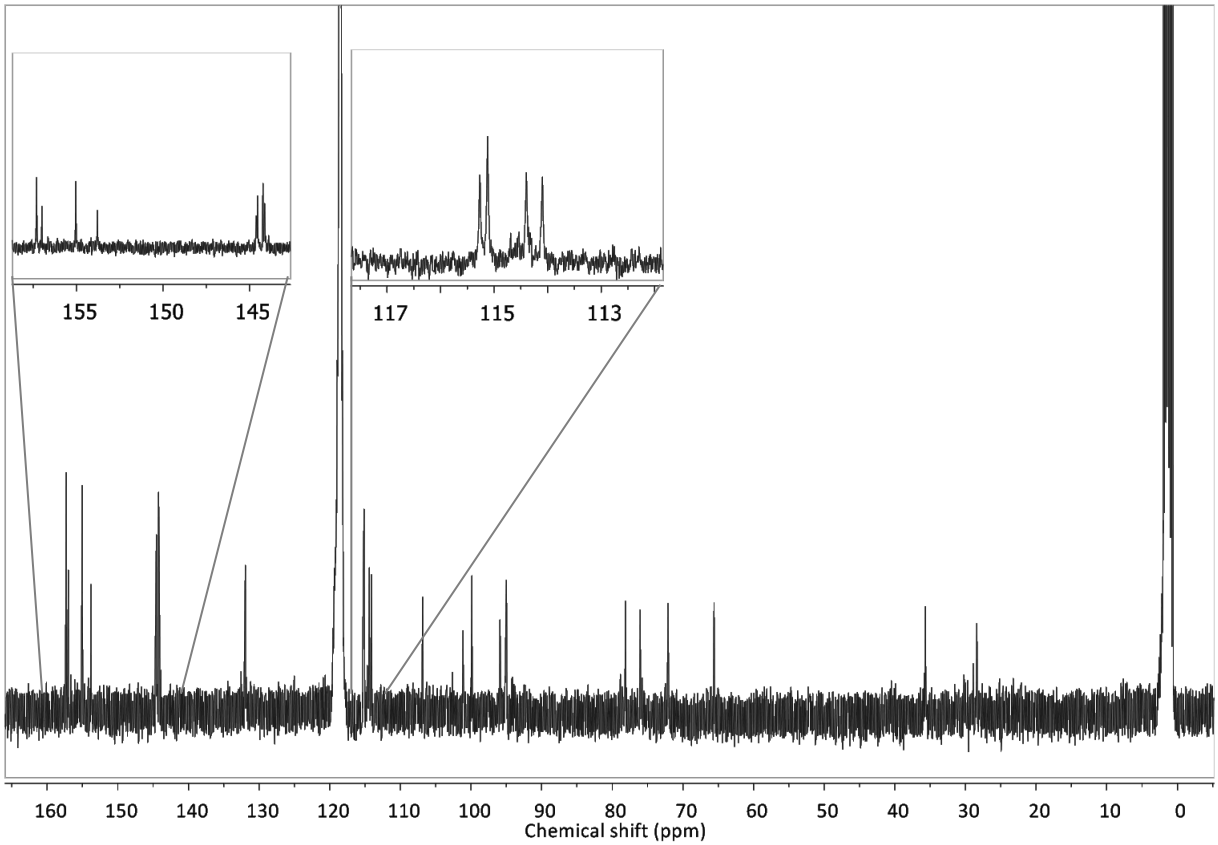

Figure 2.10. ^{13}C NMR of procyanidin B2 in acetonitrile-D3 at 253 K

Chapter 3. Procyanidin B2 Conformational Interchange Kinetics

3.1 Introduction

Procyanidin B2 was isolated by preparative chromatography from cocoa and the purity of the analyte was confirmed by ^{1}H NMR and UHPLC-ESI-TOF-MS experiments. Homo- and heteronuclear two dimensional NMR techniques were performed for structural and chiral assignment of the isolated procyanidins.

In acetone and water/ethanol mixtures Kahn *et al.* [9] and Terascou *et al.* [27] respectively found that only two conformers for all B-type procyanidin dimers could be detected by means of ^{1}H NMR. In water the ratio of the B2 conformers was found to be approximately 1:1 [27] and in acetone the one conformer dominates in a 9:1 ratio. The ^{1}H NMR spectra of B2 exhibited line broadening as a function of temperature, which corresponds to conformational interchange on the slow exchange NMR timescale. The thermodynamic distribution of the B2 conformers changes as a function of solvent polarity. In polar solvents, aggregation of procyanidins occurs readily above the critical aggregation concentration [15] (similar to the critical micelle concentration) which could also contribute to NMR resonance line broadening in NMR experiments. However, the exhistence of such aggregation effects for procyanidin B2 has been discounted by ^{1}H DOSY NMR experiments in the previous chapter. The aim of this chapter is to discuss and interpret variable temperature (VT) ^{1}H NMR data of the B2 dimer followed by a kinetic and thermodynamic analysis of the data.

There are existing software packages (DNMR, iNMR, gNMR, EXSYcalc, and MEXICO) that can analyze NMR resonance line broadening caused by chemical exchange reactions and determine the kinetic constants. However, both DNMR and gNMR are rather complex, counter-intuitive and unfriendly to new users with limited user support. Due to the steep learning curve for DNMR and gNMR, these software suites are not commonly used. iNMR is only supported on Apple computers and is proprietary software that is not currently available in our research group. However, iNMR is advertised to include the capacity for

spectral processing of one and two dimensional spectra and includes a line shape analysis function for the determination of rate constants. EXSYcalc is a fit program that only works on a set of ROESY experiments, which are resource intensive to run and analyze, because of the time required for such a set of ROESY experiments. Finally, MEXICO is a Matlab (MATLAB 6.1, The MathWorks Inc., Natick, MA, 2000) program that is poorly supported by the research group that originally wrote it and does not work with newer versions of the Matlab suite. As a result the decision was made to write an in-house application using Matlab to suit our needs and to extend the program in future to model more complex chemical systems, e.g. second order kinetics.

3.2 Computational Details

Conformational interchange of B2 is assumed here to be a reversible first order reaction, Reaction scheme 3.1.

$$A\,(Major) \underset{k_{-1}}{\overset{k_1}{\rightleftharpoons}} B(Minor)$$

Reaction scheme 3.1. First order conformational interchange reaction

which can be written in differential form as:

$$d\,[A]/dt = -k_1[A] + k_{-1}[B] \qquad (3.1.1)$$
$$d\,[B]/dt = \;\; k_1[A] - k_{-1}[B] \qquad (3.1.2)$$

and in matrix form as:

$$\frac{d}{dt}\begin{bmatrix}[A]\\[B]\end{bmatrix} = \begin{bmatrix}-k_1 & k_{-1}\\ k_1 & -k_{-1}\end{bmatrix}\begin{bmatrix}[A]\\[B]\end{bmatrix} .$$

At equilibrium

$$\frac{d[A]}{dt} = \frac{d[B]}{dt} = 0 = k_1[A_{eq}] - k_{-1}[B_{eq}]$$
$$and \;\; \frac{[B_{eq}]}{[A_{eq}]} = \frac{k_1}{k_{-1}} \quad .$$

Then it follows that

$$\Delta A(t) = ([A] - [A_{eq}]) = \Delta A(0)\mathrm{e}^{-k_{ex}t} = \Delta A(0)\mathrm{e}^{-(k_1+k_{-1})t}$$

and the k_{ex} is characterized by a single timescale and is equal to the sum of k_1 and k_{-1}

$$\tau_{ex} = \frac{1}{k_{ex}}.$$

Various analytical techniques exist that can be used to measure reaction kinetics, but NMR is arguably the simplest method to analyze conformational exchange in procyanidins [9]. NMR line shape analysis has been clearly mathematically defined by Bloch and McConnell *et al.* [35, 55].

3.2.1 Derivation Of The Bloch-McConnell Equation

The Bloch equation for a species in a B_0 field has the following form

$$\frac{d}{dt}\begin{bmatrix}\hat{E}\\ \widehat{M_z}\\ \widehat{M^+}\\ \widehat{M^-}\end{bmatrix} = \begin{bmatrix} & & & \\ R_1\widehat{M_{z0}} - R_1 & & & \\ & i\omega - R_2 & & \\ & & -i\omega - R_2 & \end{bmatrix}\begin{bmatrix}\hat{E}\\ \widehat{M_z}\\ \widehat{M^+}\\ \widehat{M^-}\end{bmatrix}.$$

The equation describes the magnetic relaxation of a species to equilibrium from an excited state [56]. Here Ê is the identity operator and R_1 and R_2 are the transversal and longitudinal relaxation rates respectively. The identity M_{z0} represents the equilibrium magnetization along the external field B_0. When considering only the transverse component we find:

$$\widehat{M^+} = \widehat{M_x} + i\widehat{M_y}$$

Then for two chemical species or sites

$$\frac{d}{dt}\begin{bmatrix}\widehat{M_A^+}\\ \widehat{M_B^+}\end{bmatrix} = \begin{bmatrix} i\omega_A - R_2 & \\ & i\omega_B - R_2\end{bmatrix}\begin{bmatrix}\widehat{M^+}\\ \widehat{M^-}\end{bmatrix}.$$

Solving the equation we find

$$\begin{bmatrix}\widehat{M_A^+}(t)\\ \widehat{M_B^+}(t)\end{bmatrix} = e\begin{bmatrix} i\omega_A - R_2 & \\ & i\omega_B - R_2\end{bmatrix}t\begin{bmatrix}\widehat{M_A^+}(0)\\ \widehat{M_B^+}(0)\end{bmatrix},$$

which leads to

$$\widehat{M^{+}}(t) = \widehat{M_A^{+}}(0)e^{(-R_{2,A}+i\omega_A)t} + \widehat{M_B^{+}}(0)e^{(-R_{2,B}+i\omega_B)t} .$$

This solution yields the Free Induction Decay (FID) signal as found in Fourier Transform Nuclear Magnetic Resonance (FT-NMR). The Fourier transform of the FID yields the NMR frequency spectrum. However, this only includes the natural line broadness of the free induction decay signal and not the effects of chemical exchange or conformational interchange. To introduce the effect of chemical exchange (*e.g.* conformational interchange) into the Bloch equations we use magnetization intensity as a metric for the abundance of each species. Combining the differential forms of the change in species abundance equations (3.1.1 and 3.1.2) with the Bloch equation yields:

$$\frac{d}{dt}\begin{bmatrix}\widehat{M_A^{+}}\\ \widehat{M_B^{+}}\end{bmatrix} = \left[\begin{bmatrix}-R_{2,A}+i\omega_A & \\ & -R_{2,B}+i\omega_B\end{bmatrix} + \begin{bmatrix}-k_1 & k_{-1}\\ k_1 & -k_{-1}\end{bmatrix}\right]\begin{bmatrix}\widehat{M_A^{+}}\\ \widehat{M_B^{+}}\end{bmatrix}.$$

This equation is called the Bloch-McConnell equation and can be simplified to

$$\frac{d\vec{M}}{dt} = \left[i\hat{\omega} - \hat{R} + \hat{k}\right]\vec{M}$$

and

$$\vec{M} = \begin{bmatrix}\widehat{M_A^{+}}\\ \widehat{M_B^{+}}\end{bmatrix}, \hat{\omega} = \begin{bmatrix}\omega_A & \\ & \omega_B\end{bmatrix}, \hat{R} = \begin{bmatrix}R_{2,A} & \\ & R_{2,B}\end{bmatrix} \text{and} \hat{k} = \begin{bmatrix}-k_1 & k_{-1}\\ k_1 & -k_{-1}\end{bmatrix}.$$

A solution to this equation is:

$$\vec{M}(t) = e^{[i\omega-\hat{R}+\hat{k}]t}\vec{M}(0) \qquad (3.2)$$

and

$$\begin{bmatrix}\widehat{M_A^{+}}(t)\\ \widehat{M_B^{+}}(t)\end{bmatrix} = \begin{bmatrix}a_{11}(t)a_{12}(t)\\ a_{21}(t)a_{22}(t)\end{bmatrix}\begin{bmatrix}\widehat{M_A^{+}}(0)\\ \widehat{M_B^{+}}(0)\end{bmatrix}.$$

with

$$a_{11} = \frac{1}{2}\left[\left(1 - \frac{i\Delta\omega - \Delta R_2 + k_1 - k_{-1}}{(\lambda_+ - \lambda_-)}\right)e^{-\lambda_- t} + \left(1 + \frac{i\Delta\omega - \Delta R_2 + k_1 - k_{-1}}{(\lambda_+ - \lambda_-)}\right)e^{-\lambda_+ t}\right];$$

$$a_{22} = \frac{1}{2}\left[\left(1 + \frac{i\Delta\omega - \Delta R_2 + k_1 - k_{-1}}{(\lambda_+ - \lambda_-)}\right)e^{-\lambda_- t} + \left(1 - \frac{i\Delta\omega - \Delta R_2 + k_1 - k_{-1}}{(\lambda_+ - \lambda_-)}\right)e^{-\lambda_+ t}\right]$$

$$a_{12} = \frac{k_{-1}}{(\lambda_+ - \lambda\text{-})}\left[e^{-\lambda_- t} - e^{-\lambda_+ t}\right] \quad ; \quad a_{21} = \frac{k_1}{(\lambda_+ - \lambda\text{-})}\left[e^{-\lambda_- t} - e^{-\lambda_+ t}\right]$$

$$\Delta\omega = \omega_B - \omega_A, \Delta R_2 = R_{2,B} - R_{2,A}\ .$$

The Eigen values are

$$\lambda_\pm = \frac{1}{2}\left[\left(-i\omega_A - i\omega_B + R_{2,A} + k_{ex}\right) \pm \left((i\Delta\omega - \Delta R_2 + k_1 - k_{-1})^2 + 4\mathrm{k}_1 k_{-1}\right)^{\frac{1}{2}}\right].$$

The exact positions and line widths of the spectra can be obtained from the imaginary and real parts of the equation, respectively. For mathematical simplicity the resonance frequency of A is taken as a reference point. This simplifies the equations by eliminating the resonance frequency shift of A and reducing the delta resonance frequency to resonance frequency B. This leads to:

$$\frac{d}{dt}\begin{bmatrix}\widehat{M_A^+}\\ \widehat{M_B^+}\end{bmatrix} = \begin{bmatrix}-R2,A - k_1 & k_1\\ k_{-1} & -R2,B + i\Delta\omega - k_{-1}\end{bmatrix}\begin{bmatrix}\widehat{M_A^+}(0)\\ \widehat{M_B^+}(0)\end{bmatrix}.$$

Upon further literature searches an analytical solution for the above system was found that yields both a time and a frequency domain solution at a fraction of the calculation cost [57].

$$\frac{d}{dt}\begin{bmatrix}\widehat{M_A^+}\\ \widehat{M_B^+}\end{bmatrix} = \begin{bmatrix}-\beta_A - k_1 & k_1\\ k_{-1} & -\beta_B - k_{-1}\end{bmatrix}\begin{bmatrix}\widehat{M_A^+}(0)\\ \widehat{M_B^+}(0)\end{bmatrix}$$

where

$$\beta_A = R_A - i\omega_A;\ \ \beta_B = R_B - i\omega_B$$

is the alternative nomenclature used for the analytical solution which is reduced to

$$\begin{bmatrix} \widehat{M_A^+} \\ \widehat{M_B^+} \end{bmatrix} = U \begin{bmatrix} \exp(\lambda_1 t) & 0 \\ 0 & \exp(\lambda_2 t) \end{bmatrix} U^{-1} \begin{bmatrix} \widehat{M_A^+}(0) \\ \widehat{M_B^+}(0) \end{bmatrix}, \tag{3.3}$$

where

$$U = \begin{bmatrix} \mathrm{a} & -\mathrm{b} \\ -\mathrm{c} & \mathrm{d} \end{bmatrix}$$

$$a = b = k_{-1}$$

$$c = \frac{1}{2}\left(\beta_A - \beta_B + k_1 - k_{-1} + D^{\frac{1}{2}}\right)$$

$$d = \frac{1}{2}\left(\beta_A - \beta_B + k_1 - k_{-1} - D^{\frac{1}{2}}\right)$$

$$D = (\beta_A - \beta_B + k_1 - k_{-1})^2 + 4k_1k_{-1}$$

$$\lambda_{1,2} = \frac{1}{2}\left(-(\beta_A + \beta_B + k_1 + k_{-1}) \pm D^{\frac{1}{2}}\right).$$

3.2.2 NMRfit Program Details

NMRfit is the name given to of the program written by the author in order to simulate and fit NMR one dimensional line shapes using the Bloch-McConnell equations [35] as a theoretical base. The program was written in Matlab (MATLAB 6.1, The MathWorks Inc., Natick, MA, 2000) and includes the capability for manual adjustment of the fit parameters by the user to approximate the line fit by inspection. This approximate fit can be used as an initial approximation to be improved upon by fitting the data with a Bloch-McConnell equation generated spectrum iteratively with a least squares non-linear Nelder Mead algorithm [58].

The aim of this application is not to replace existing spectral processing software, but to calculate the kinetic constants and equilibrium distributions of two-site chemical exchange in processed one dimensional spectra exported from an existing software package as an X-Y data ASCII text file.

In v12.0 (current version) the program is able to generate multiple peak sets of one dimensional two-site J-coupled (without second order effects) 1st order asymmetric exchanging resonance signals. Both asymmetric and symmetric exchange is supported.

Future versions are envisioned to include non-1st order reaction rate models, strong coupling effects and two dimensional spectrum analysis.

Equation 3.2 yields the FID signal as observed in FT-NMR. The Fourier transform of the FID yields the NMR frequency spectrum. Equation 3.2 is an analytical solution, but requires matrix exponential operations. The solution to the Bloch-McConnell equations could also be obtained numerically, but the calculation is expected to be orders of magnitude slower using the ordinary differential equation solving algorithms available in the Matlab libraries. To test the efficiency of the EXPM and ODE solution functions, the CPU clock times were measured to generate a NMR spectrum using the following set of parameters: $k_1 = k_2 = 15s^{-1}$; $M(0)_1 = M(0)_2 = 1$; $\omega_1 = 1$ ppm; $\omega_2 = 2$ppm; $R_2 = 0.5s^{-1}$; spectral width=2π ppm. The results obtained are shown in Figure 3.1.

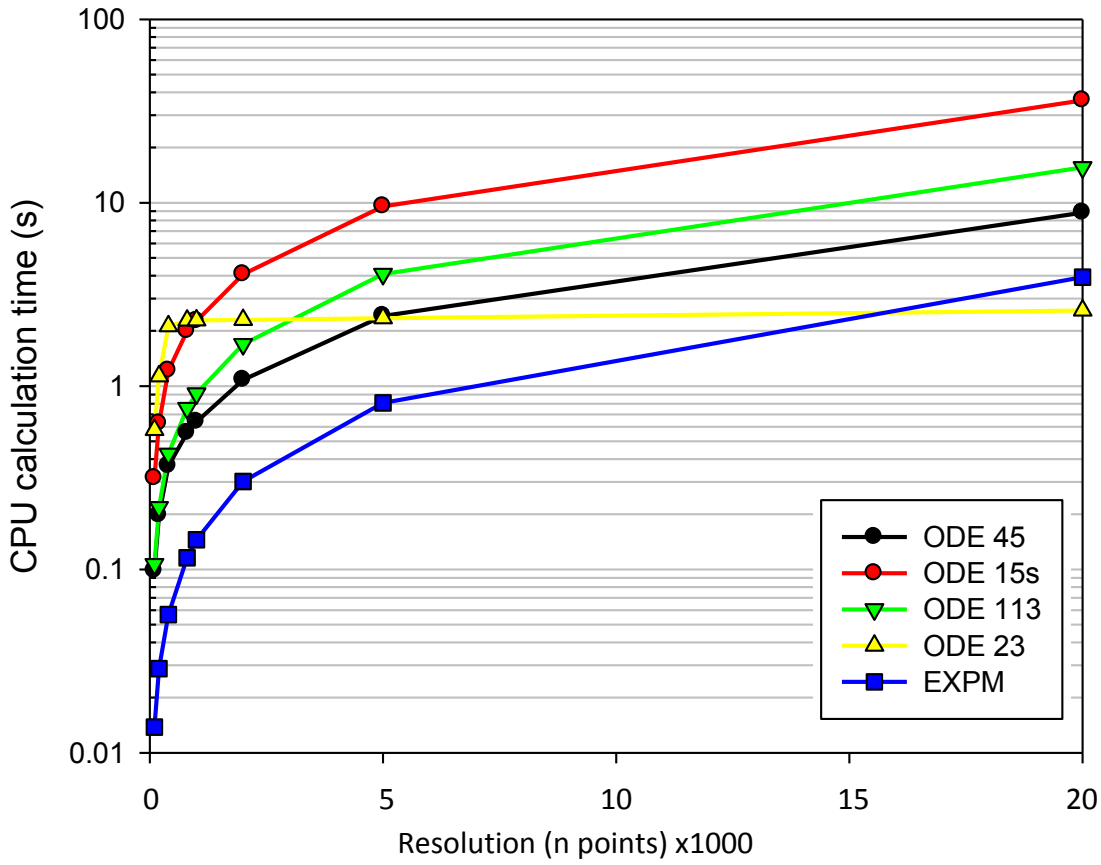

Figure 3.1. Comparison of calculation times for generation of two site exchange spectra using various ordinary differential solving methods

As can be seen from Figure 3.1, the EXPM method is by far the most efficient method to solve the Bloch-McConnell equation. Interestingly, ODE23 outperforms EXPM

when 15000 or more data points are used. ODE23, although efficient at high resolutions, has the lowest efficiency at lower resolutions. As calculation times of higher than 1s are highly undesirable and most test spectra will be generated with less than 10000 data points, EXPM was implemented. Using the approximate parameters extended by the user, the program generates a time domain with equation 3.2 and then uses a fast Fourier fransform (FFT) to transform the spectrum to the frequency domain.

A new analytical solution (equation 3.3) of the Bloch-McConnell equation has recently been published and has also been implemented in the program as an even faster alternative for calculation [57]. The analytical solution has been tested to be significantly faster than the functions shown in Figure 3.1 as it immediately generates the spectrum in the time domain form without having to solve ordinary differential equations iteratively, perform matrix exponent calculations and transform the spectrum to the frequency domain with an FFT [57]. The user has the choice to implement the faster analytical solution or the EXPM method.

3.2.3 Fast Fourier Transform

A fast Fourier transform is a discrete Fourier transform which is defined by

$$X_k = \sum_{n=0}^{N-1} x_n e^{-i2\pi k\frac{n}{N}};\ k = 0, \dots, N-1 \tag{3.4}$$

Where N is the number of points in the spectrum, x_n is the time domain function value at point n and X_k is the frequency domain function value at point k. A fast Fourier transform creates a frequency domain with N points from a time domain with N points, where the frequency range is determined by the sampling frequency. In terms of experimental NMR spectra the true sampling frequency is determined by the machine (e.g. 600 MHz). This frequency is actually the Larmor frequency of protons in a machine of a given magnetic field strength. However, this sampling frequency should not be confused with the terminology of the sampling frequency when referring to discrete Fourier transforms such as an FFT. The sampling frequency of the FFT is equal to the spacing between data points for a given resolution of the spectrum. When generating spectra by the Bloch-McConnell equation the sampling frequency is determined by the time domain spacing Ts (1/Fs) and not the magnetic field strength of the machine's main field. The experimental instrument sampling frequency is a changeable parameter specified by the

user in MHz units. However, line broadening is determined by the relaxation rate constant in conjunction with the sampling frequency, because the sampling frequency determines the timescale of the spectra.

The parameters that are available to the user in NMRfit v12.0 are the magnetization intensity at time 0 for asymmetrical exchange as well as the chemical shift of the species in ppm. The spectral width can also be adjusted for easier fitting of smaller fit regions or analysis of broad spectral regions. NMRfit has a function to generate multiplets which is available under the J coupling button. By specifying order of splitting (XC) of 2, a doublet is generated (assuming the coupling constant (JC) is not 0, in which case it will appear to be 1 peak). The multiplet generation is achieved by multiplying the FID of each set of peaks by a sine wave for each level of splitting with the coupling frequency as the frequency of each of the sine waves. Due to the Fourier transforms principal function of transformation of time domain resonances to their corresponding frequencies, the multiplication of any time resonance with a sine wave, splits that resonance peak in the frequency domain in two with the relavent splitting frequency of the sine waves used. Using multiple sine waves allows more complex splitting patterns to be generated. Unfortunately the program does not include a routine for the iterative fitting of J coupling parameters, but the parameters can be easily measured on the NMR spectra and specified by the user. Finally the spectrum resolution, sampling frequency, kinetic constants, longitudinal relaxation constant and optimization method parameters are also adjustable. Moreover, the Nelder Mead least square optimization algorithm is only programmed to optimize the magnetization intensity and kinetic constants for convergence to the best fit. The user must define the correct chemical shift and transversal relaxation rate constant ($R_2=1/T_2$) in order for the optimization to produce sensible results. These values are obtained at low temperature or at some set of conditions where the conformational interchange reaction rate is near zero. At such a low temperature or conditions the shift and line broadening due to chemical exchange will also be negligible and the relaxation constant (T_2) can be estimated by the half height peak width. The procedure for the operation of the program is described in more detail in the program structure section (3.2.5).

3.2.4 The Nelder Mead Algorithm

The Nelder Mead algorithm is a simplex optimization algorithm implemented in NMRfit for non-linear least-square optimization [59]. The criterion used in this application is the minimum mean square error (MSE) as is defined in equation 3.5**.**

$$MSE = \sum_{n=0}^{k-1} \frac{\left(f(n)-g(n)\right)^2}{k} \tag{3.5}$$

Here f(n) is the experimental data and g(n) is the calculated spectrum. Therefore, for any given set of magnetization intensities $\vec{M}(0)$ and kinetic constants $\hat{k}$ as defined in equations 3.2 and 3.3, an MSE can be computed with which to evaluate the quality of the fit. It should be noted that the square in this equation has two purposes. It corrects the error sign and creates a bias towards minimizing large differences instead of just linearly proportionate sums of errors. This means that the optimizations will tend to rather allow small accumulated errors spaced over the whole optimization range instead of having a single large error with no small accumulate errors.

The algorithm itself works by using a set of logical tests. Three triangularly spaced variable sets are generated at random distances from the initial point to randomize the initial triangle's dimensions. This random number generation is done within the bounds set by the user and is a fraction of the initial guess values. The initial step is illustrated in Figure 3.2 a. The next step is to calculate an MSE for each of the three variable sets in order to rank them as the best, good or worst values accordingly. A reflected point is calculated next by taking the reflection of the triangle away from its worst point over the axis of the line of the best and good points as seen in Figure 3.2 b. The reflection point is extended in order to see if continuing along its course yields continual improvement in the criterion as seen in Figure 3.2 c. This particular logical step was limited to one extension in order to retain the triangular shape integrity and prevent directional bias in NMRfit. Loss of triangular shape by excessive elongation limits the directional freedom of the algorithm and can lead to longer calculations times. If the projected point is not ranked higher than the worst point, the triangle contracts the worst and good points towards the best point as is shown in Figure 3.2 d. This algorithm is used to iterate for the optimization of the rate constants and the magnetic intensity constants in turns until the convergence criteria are met, the improvement in fit for each cycle becomes negligible or the cycle limit is reached.

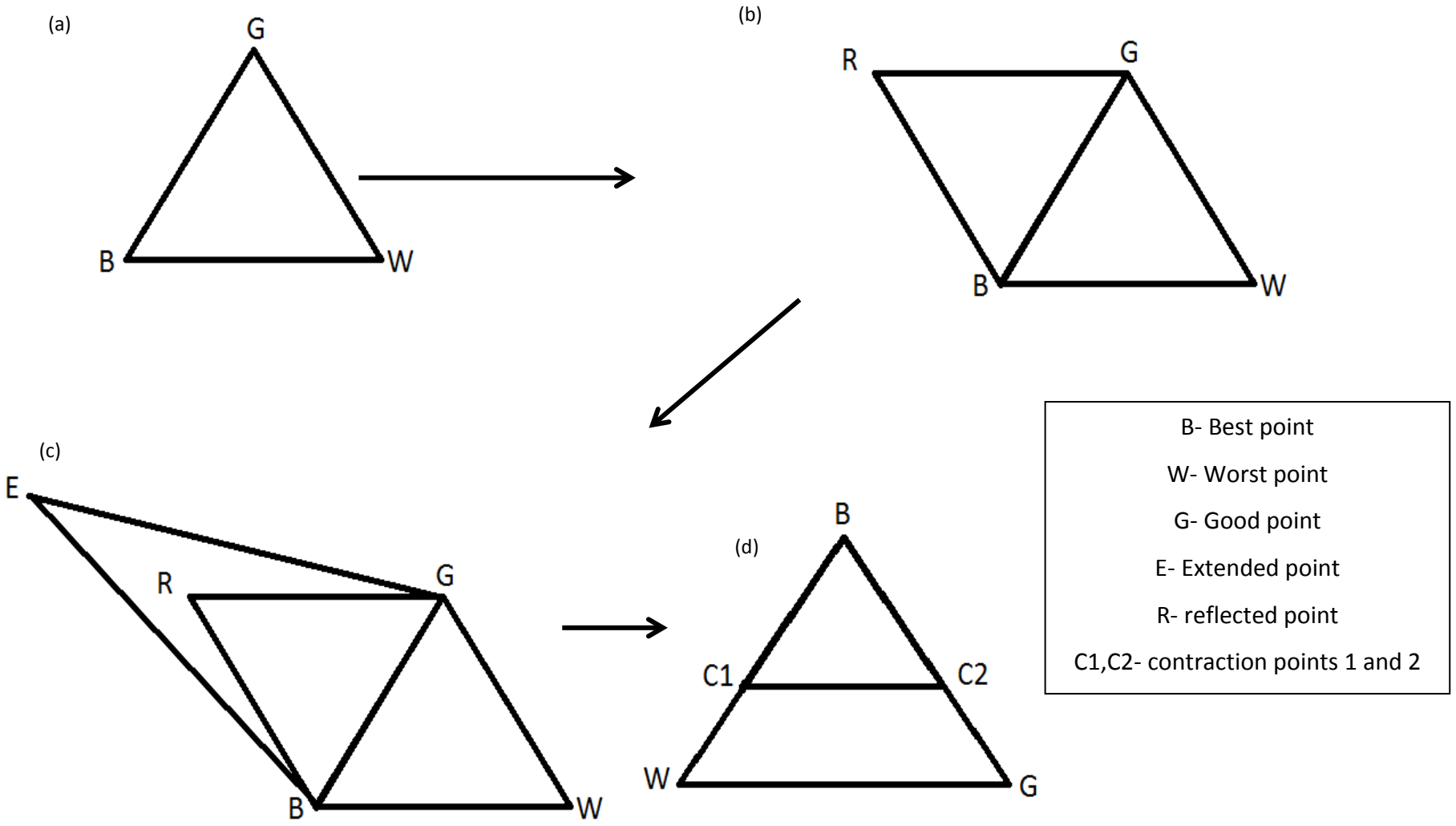

Figure 3.2. Schematic representation of the Nelder Mead algorithm

3.2.5 Program Structure

NMRfit has been written in order to have maximum control over the mathematical parameters, but be able to simply and efficiently make a least-squares non-linear fit of one dimensional NMR timescale exchange spectra for determination of the kinetic and thermodynamic parameters. The program is written to import a one dimensional NMR spectrum generated by any spectral processing suite in the form of an ASCII format file as a space delimited x-y data set. These files consist of two columns containing the chemical shift (in ppm units) and magnetic intensity (in arbitrary units). This spectrum is imported and it is left to the user to input the correct instrument frequency (eg. 400 MHz). The user also has to input a reasonable chemical shift for the peak set to be fit and the fit ranges to be analyzed. The fit ranges are the ppm ranges between which the MSE value will be evaluated. The relaxation time is also an important value for molecules that exchange slowly or fast in terms of the NMR timescale, *i.e.* resonance peaks that are relatively narrow, that are resolved or coalesced respectively. Similarly, the program does not automatically detect the multiplet structures, but these can be input by the user. The program does not have any method of approaching second order line shapes, *i.e.* "roofing". Second order effects are envisioned to be added in future versions.

The program itself is controlled using a central graphical user interface (GUI) named 'GUI.m'. All other .m files and functions are called by GUI.m. The spectrum generation .m file has changed over the course of program development and includes various .m files that offer various abilities. SGen(), SGen2(), SGen3() and AnalyticGen() are all functions written to generate spectra according to the Bloch-McConnell equations. SGen() generates a time domain spectrum (also known as a free induction decay signal (FID)) and uses a fast Fourier transform function (FFT() matlab function) on the FID to derive a frequency domain spectrum. The intensities of both of these spectra along with their frequency domain (ppm) x-axis values are returned to the calling function in the form of a matrix, Ma, which has the form [Mt; Mw; w]. Here Mt is the matrix containing the y-axis values of the FID, Mw is the matrix that contains the y-axis values of the frequency domain spectrum and w is the matrix that contains the x-axis chemical shift (ppm) from the frequency spectrum. SGen2() executes the same function but has the added capability of changing the spectral width in order to generate spectra with wider ppm ranges than the standard 6.28 ppm (2π ppm)

generated by SGen(). SGen3() allows the generation of spectra with the functionality of the previous SGen() and SGen2() along with the capability for multiplet specification and the ability to adjust the sampling frequency of the instrument. AnalyticGen() has all of the capabilities of SGen3() but is not generated solving the ordinary differential equation of the Bloch-McConnell equation by using the expm() Matlab function as stated earlier, but uses an analytical solution shown in equation 3.3 instead. The MSE values as described above are calculated in the MSEr.m file function and called by the various Nelder Mead fit functions corresponding to the implementation of each spectrum generation function. The implementation functions use the Nelder Mead simplex method to optimize the kinetic and magnetic intensity variables iteratively according to the MSE values and terminate when the parameters no longer change more than a value specified in the GUI by the user, the iteration limit is reached or the fit is good enough. The calculated values are then used to replace the initial values and the user can restart the iterative calculation from the calculated values if the fit is unsatisfactory. It should be noted that getMXY() (a function to get the x and y values from a spectrum) and SPlot2() (a function used to plot the frequency domain spectrum directly from the calculated values of a spectrum generation function) are both written exclusively for implementation by NMRfit. As of NMRfit v12.0 functionality for the generation of multiple exchanging peaks in an overlapping spectrum is available. The functionality also allows for the simultaneous optimization of one set of kinetic and magnetic intensity constants for multiple peak sets. The GUI includes a drop down menu for each method of optimization.

The program structure of callbacks, calls, returns and the distinction between personally generated content and Matlab content is sometimes very difficult to perceive. Therefore, a flow chart of the program structure is displayed in Figure 3.3. The documentation of the personally written functions themselves and their .m file contents are also added in appendix A.4. Callback functions are not seen as generated content and are merely associated with the GUI.

The program algorithm is illustrated by the following schematic:

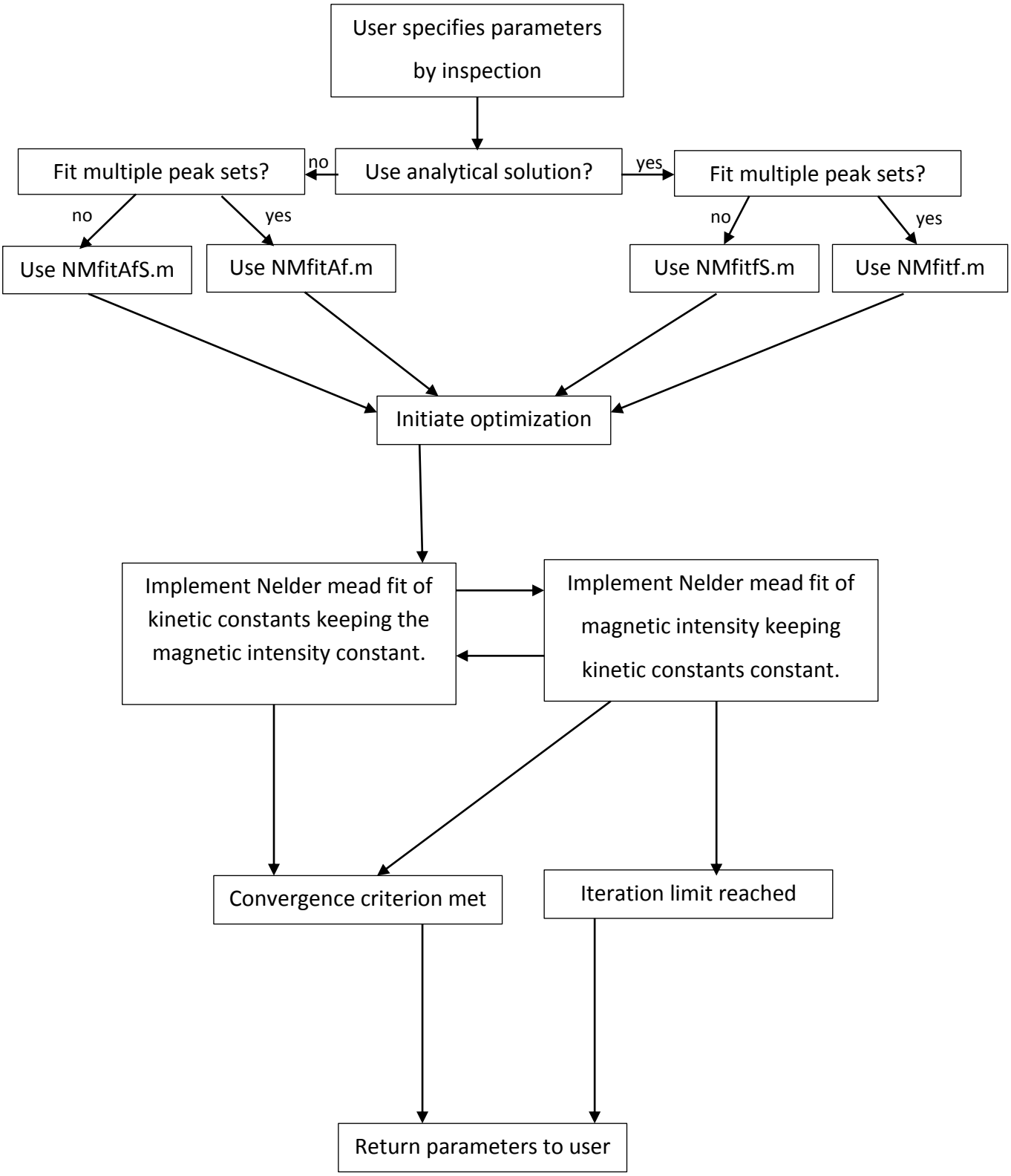

Figure 3.3. NMRfit program algorithm flow chart

3.3 Statistical Analysis of Model Errors

In order to quantify the error in the fit, the statistical error in the least squares model was used as defined by Miller [60]. For a least squares model the equation of a straight line is shown in equation 3.6.

$$a = \bar{y} - b\bar{x} \tag{3.6}$$

Where

$$b = \frac{\sum_i[(x_i-\bar{x})(y_i-\bar{y})]}{\sum_i(x_i-\bar{x})^2}.$$

In order to quantify the error in this model, the difference between the model and each individual experimental data point used for the fit needs to be considered. By use of the $S_{x/y}$ statistic shown in equation 3.7, a general indication of the error in the slope and intercept is gained.

$$S_{x/y} = \left[\frac{\sum_i(y_i-\hat{y})^2}{n-2}\right]^{\frac{1}{2}} \tag{3.7}$$

After the determination of $S_{x/y}$ the standard deviations S_b and S_a, of the slope and intercept respectively, can be determined.

$$S_b = \frac{S_{x/y}}{[\sum_i(x_i-\bar{x})^2]^{\frac{1}{2}}}; \quad b_t = b \pm S_b t \tag{3.8}$$

$$S_a = S_{x/y}\left[\frac{\sum_i {x_i}^2}{n\sum_i(x_i-\bar{x})^2}\right]^{\frac{1}{2}}; \quad a_t = a \pm S_a t \tag{3.9}$$

As our uncertainty in the model stems from the measurement of y_0 the error is determined by equation 3.10**.**

$$S_{x0} = \frac{S_{x/y}}{b}\left[\frac{1}{m} + \frac{1}{n} + \frac{(y_0-\bar{y})^{\frac{1}{2}}}{b^2\sum_i(x_i-\bar{x})^2}\right] \tag{3.10}$$

By using a t-statistic along with the error determined here a top and bottom error range for a certainty level can be determined.

$$x_{top} = \bar{x} + t.S_{x0} \tag{3.11.1}$$

$$x_{bot} = \bar{x} - t.S_{x0} \quad (3.11.2)$$

The 95% confidence interval, *i.e.* two standard deviations, was chosen for our purposes. The determined x_{top} and x_{bot} error ranges are input into the model for the determination of the y error range.

3.4 Conformational Interchange Kinetics

To investigate the possible conformational interchange reactions of procyanidin B2 a ^{1}H NMR variable temperature (238 K to 303 K) experiment was performed, illustrated in Figure 3.4. At temperatures below 273.15 K two sets of well resolved resonance signals are observed corresponding to two conformers of procyanidin B2, as has also been reported in literature [9, 27]. The major and minor conformers at 238.15 K are present in a ratio of approximately 4:1. When the temperature is increased, significant line broadening occurs and several resonances coalesce. The coalescence of certain resonances indicates that the conformational interchange between the minor and major conformers ranges from the slow to the fast chemical exchange regime on the NMR acquisition timescale.

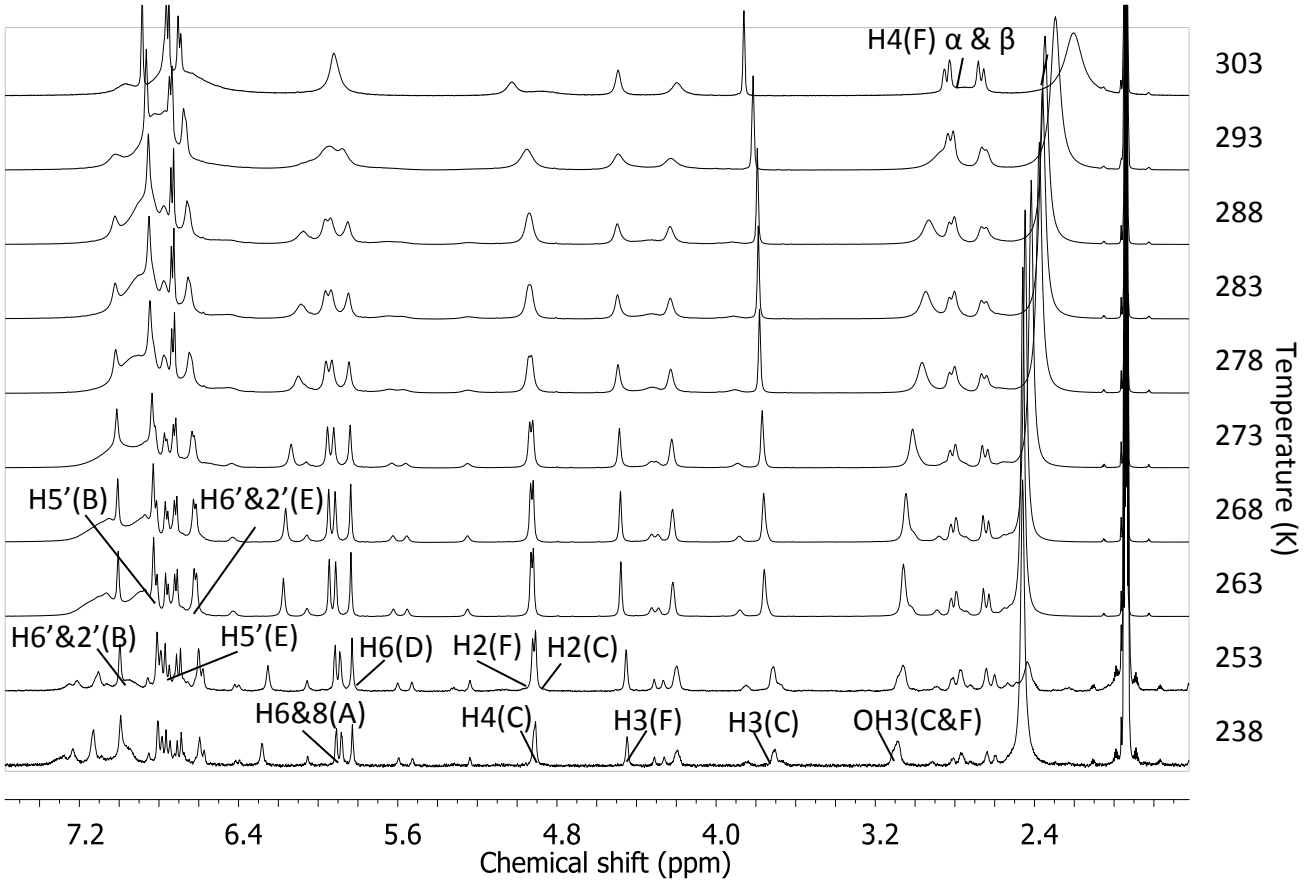

Figure 3.4. Stack plot of variable temperature ^{1}H NMR of procyanidin B2 in acetonitrile-D_3

In order to quantify the conformational interchange kinetics it is necessary to first identify which ^{1}H NMR minor resonance frequencies correspond to which major resonance frequencies. The identification of the corresponding minor and major resonance frequencies then allows for kinetic line shape analysis. Consequently, we performed a rotating-frame nuclear Overhauser effect spectroscopy (ROESY) experiment, Plate 3.1, to allow for the determination of nuclear Overhauser effects (NOE's). A ROESY experiment was implemented instead of a nuclear Overhauser effect spectroscopy (NOESY) experiment as the ROESY experiment is better suited to 'medium' sized molecules [61]. From the NOE's the spatial proximity of protons can be identified within an approximate 5 Å inter-atomic distance. Moreover, another feature of ROESY experiments is the appearance of slow tumbling off diagonal peaks. Due to the rate of conformational interchange, the slow tumbling peaks have an opposite phase to those of the NOE peaks. Therefore, the slow tumbling peaks appear as positive peaks along with the diagonal peaks, in contrast to the NOE peaks, which are negative [34]. From analysis of the ROESY spectrum it is clear which

minor conformer resonance frequencies correspond to which major conformer resonance frequencies by use of slow tumbling effect off-diagonal peaks. The assignment is shown in Table 2.5.

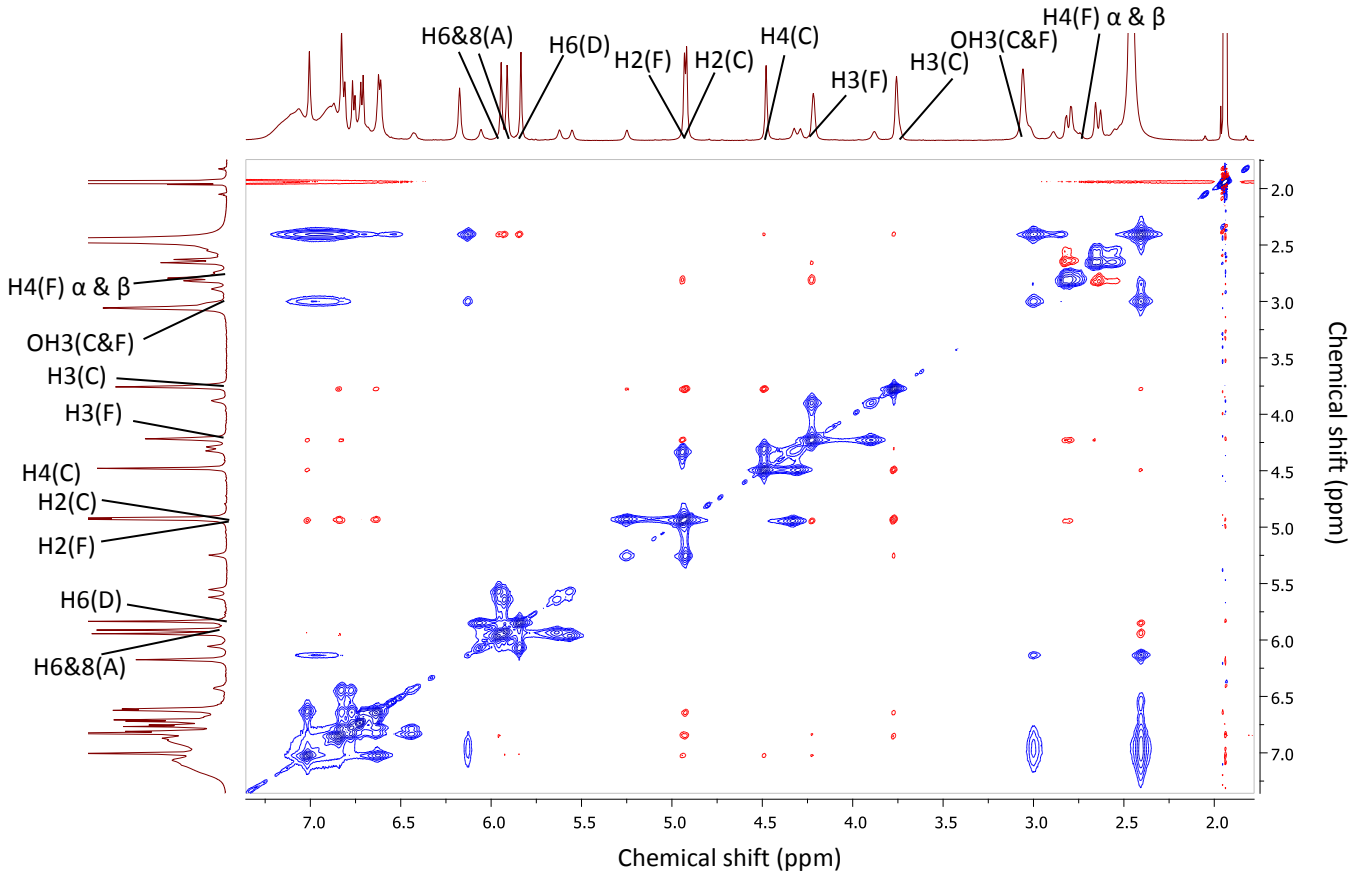

Plate 3.1. ROESY spectrum of procyanidin B2 in acetonitrile-D_3 at 253 K

Previous studies have shown that procyanidin B2 forms non-covalently bonded aggregates in water at relatively high concentrations [15, 16]. In order to test whether procyanidin B2 forms non-covalently bonded aggregates, we performed a ^{1}H DOSY experiment at 253 K in acetone-D_6 where the procyanidin B2 concentration was equal to $1.33x10^{-2}$ $\mu g.\mu L^{-1}$, the same concentration used for all of the NMR spectra. A diffusivity constant for procyanidin B2 of $4.0x10^{-6} cm.s^{-1}$ was obtained from the DOSY spectrum, Plate 2.1. Using the Einstein-Stokes equation (3.12) the hydrodynamic radius (r) is estimated at 8.5 Å, which corresponds to a single procyanidin molecule. This result has been discussed in further detail in chapter 2.

$$D = k_B \frac{T}{6\pi\eta r} \tag{3.12}$$

The conformational exchange reaction is shown in Reaction scheme 3.1, where A and B are the major and minor conformers respectively. The forward and reverse rate constants were calculated along with the magnetic intensities, using an in house program written in Matlab. The transversal relaxation rate (T_2) was estimated to be 0.5 s^{-1}, from the half height peak width using the ^{1}H NMR spectrum at 253.15 K. This T_2 value was used for all the VT NMR fits as the change in T_2 was assumed to be small in comparison to the conformational exchange rate at higher temperatures.

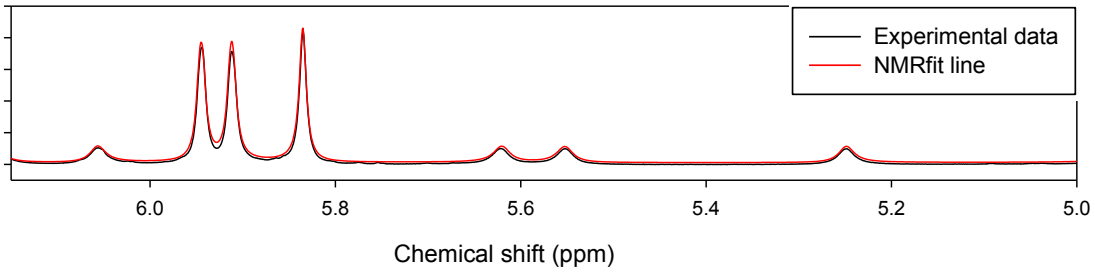

Figure 3.5. Bloch-McConnell least squares fit of procyanidin B2 in acetonitrile-D_3 at 253.15K

The initial fits were carried out on the 6.15 to 5.0 ppm region due to minimal peak overlap present in this region, Figure 3.5. The non-linear least-squares fits obtained for this region over the full temperature range are illustrated in Figure 3.7. A hydroxyl group proton resonance partially overlaps with the minor conformer resonance of H6(D) as temperature increases, but for the fit only the H6&8(A) protons' resonance signals were used for temperatures above 262 K. Thereafter, the conformational interchange rate constants and equilibrium magnetic intensities obtained from fits in the ppm range of 6.15 to 5.0 were used to calculate the VT ^{1}H NMR spectra between 2.5 ppm and 6.15 ppm, which showed good agreement with experimental data. The assumption of a constant relaxation rate, *i.e.* T_2 over the wide temperature range is validated by the good fits obtained, since only the conformational interchange rate constants and equilibrium magnetization intensity were optimized. The only exceptions to the fit are the hydroxyl groups that exchange with the residual water in the solvent and the second order effects observed for the H4(F) protons.

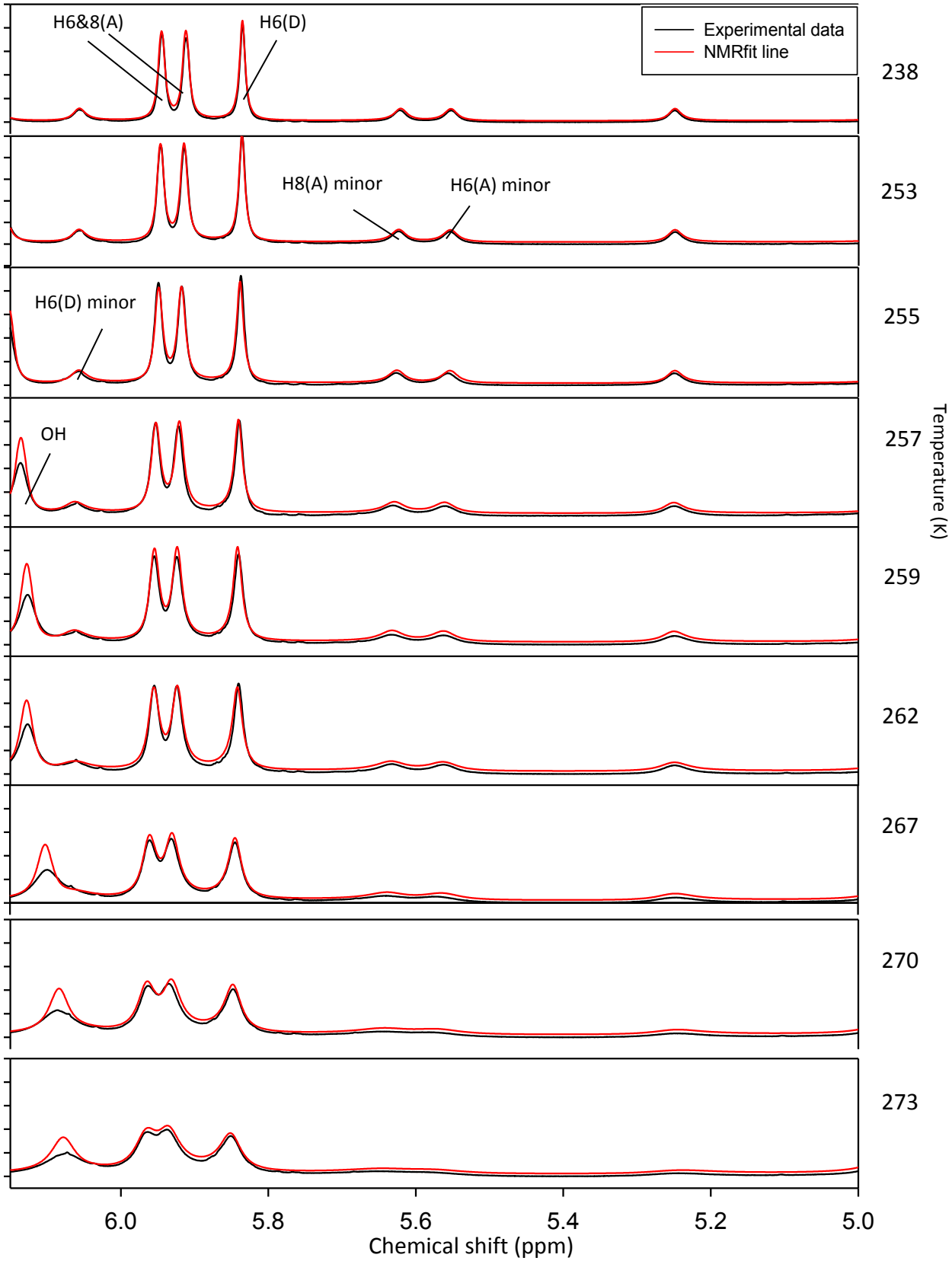

Figure 3.6. Bloch-McConnell least squares fit of procyanidin B2 in acetonitrile-D_3

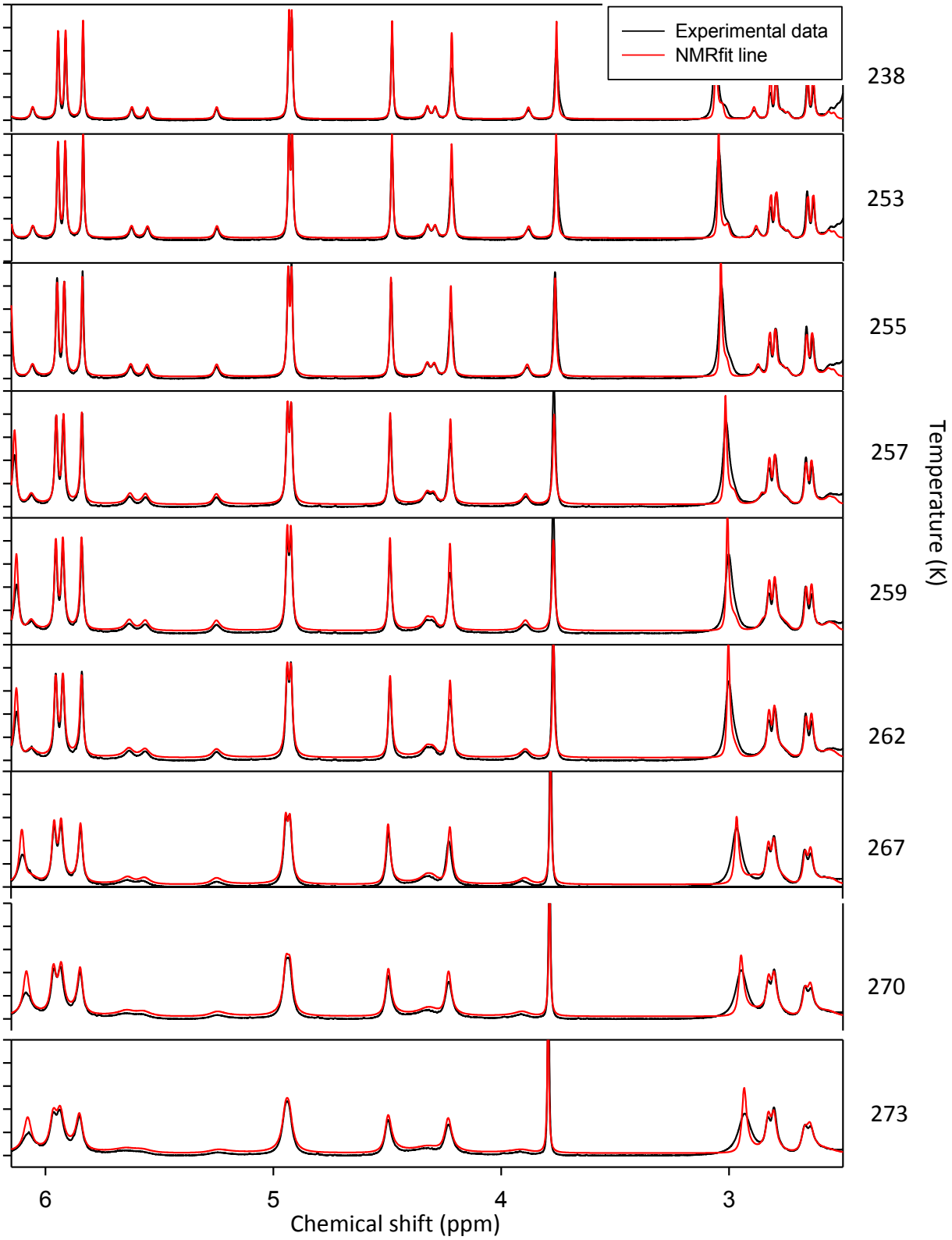

Figure 3.7. Full spectrum Bloch-McConnell least squares fit of procyanidin B2 in acetonitrile-D_3

An Eyering plot, Figure 3.8, of $\ln(k.T^{-1})$ vs. T^{-1}, as defined in equation 3.13, yielded linear trends for both reaction directions, validating the model that was fitted.

$$\ln\left(\frac{k}{T}\right) = -\frac{\Delta H^{\ddagger}}{RT} + \frac{\Delta S^{\ddagger}}{R} + \ln\left(\frac{k_B}{h}\right) \tag{3.13}$$

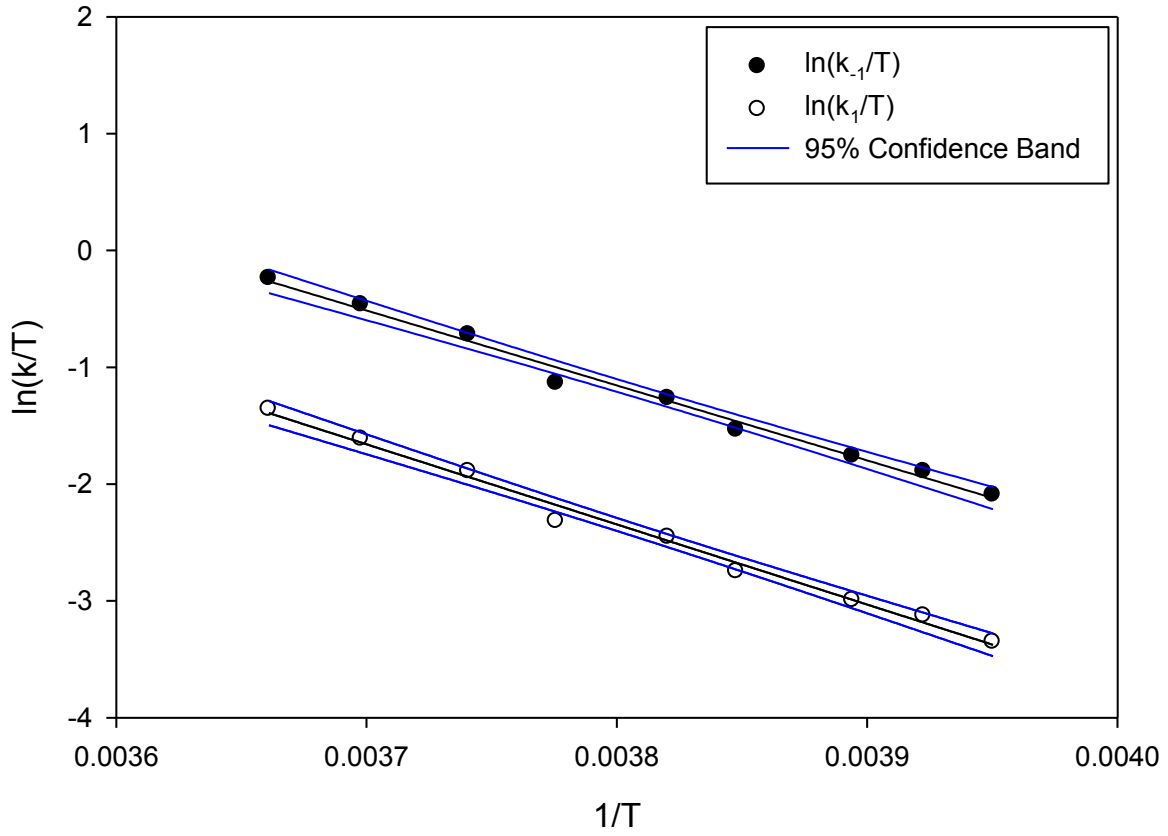

Figure 3.8. Eyering plot of procyanidin B2 forward and reverse conformational interchange reactions in acetonitrile-D_3

From the Eyering plot it is observed that the fitted data clearly follows a linear trend but not all of data points are contained within the 95 % confidence bands. These points are disregarded as outliers. The calculated activation enthalpies ($\Delta H^{\ddagger}$) and entropies ($\Delta S^{\ddagger}$) are listed in Table 3.2. As expected, relatively large positive enthalpies of activation were obtained, indicating a relatively large electronic energy barrier for conformational interchange to take place. The $\Delta S^{\ddagger}$ is difficult to interpret as the solvent component of $\Delta S^{\ddagger}$ can be pronounced and separation of the solvent component from the nuclear vibrational component of the activated state is ambiguous. However, the negative entropy of activation for both the forward and reverse reactions increase the Gibbs free energy of activation ($\Delta G^{\ddagger}$), *i.e.* the number of ways the molecule can distribute between quantum states for the

activated state is less compared to reactants or products. Therefore, the Gibbs free energy of activation for both reaction directions will increase with an increase in temperature, assuming that the enthalpy of activation remains independent of temperature. The $\Delta S^{\ddagger}$ for the forward reaction is less negative than the reverse reaction's $\Delta S^{\ddagger}$ and the forward reaction will be favoured with an increase in temperature. As the forward reaction becomes faster relative to the reverse reaction, the fraction of minor conformer will increase. However, when the temperature is high enough for the minor conformer to become dominant, the reaction will have reached a high enough reaction rate for the NMR resonance signals to become too coalesced to be distinguishable by ^{1}H NMR, as seen in the high temperature spectra in Figure 3.7. It should be noted that the error ranges for the $\Delta S^{\ddagger}$ are relatively large (a few times the absolute value of the $\Delta S^{\ddagger}$) due to the intercept of the Eyering plot that is relatively far from the centroid of the data points, thereby causing the uncertainty to be large.

Table 3.1. Activation parameters for the conformational interchange

	forward	reverse
$\Delta H^{\ddagger}$ (kJ.mol^{-1})	57.03 ± 3.915	53.36 ± 3.818
$\Delta S^{\ddagger}$ (J.mol^{-1}.K^{-1})	-0.3454 ± 14.76	-4.398 ± 14.39
$\Delta G^{\ddagger}$(273.15K) (kJ.mol^{-1})	57.12 ± 5.620	54.56 ± 5.479

From the ratio of the conformational magnetic intensities in the Bloch-McConnell equation (equation 3.3) the equilibrium constant for the temperature range was calculated. Moreover, at a temperature of 253.15 K the major and minor conformers' ^{1}H NMR H6&8(A) resonance signals at 5.94/5.91 ppm and 5.55/5.62 (as reported in Table 2.5) do not overlap. Therefore, the relative amounts of major and minor conformer at equilibrium can be measured directly via integration of the corresponding resonance signals. The ratio of reactant to product obtained and hence the equilibrium constant at 253.15 K is equal to 0.234. This agrees within experimental error with the equilibrium constant calculated (0.296 to 0.233) via non-linear least squares fitting using the program NMRfit. The error ranges were calculated as discussed by Miller [60]. These equilibrium constants correspond to the ratio of the forward and reverse reaction constants by setting the forward and reverse reaction rates (equation 3.1.1 and 3.1.2) equal. A plot of $\ln K_{eq}$ vs. T^{-1} (Figure 3.10), the van't Hoff equation numbered equation 3.7, yielded a linear trend from which the standard Gibbs

free energy of reaction (ΔG_{rxn}^{0}), standard enthalpy of reaction (ΔH_{rxn}^{0}) and standard entropy of reaction (ΔS_{rxn}^{0}) were calculated. The linear trend validates the reaction model fitted.

$$\ln(K_{eq}) = -\frac{\Delta H_{rxn}^{0}}{RT} + \frac{\Delta S_{rxn}^{0}}{R} \qquad (3.14)$$

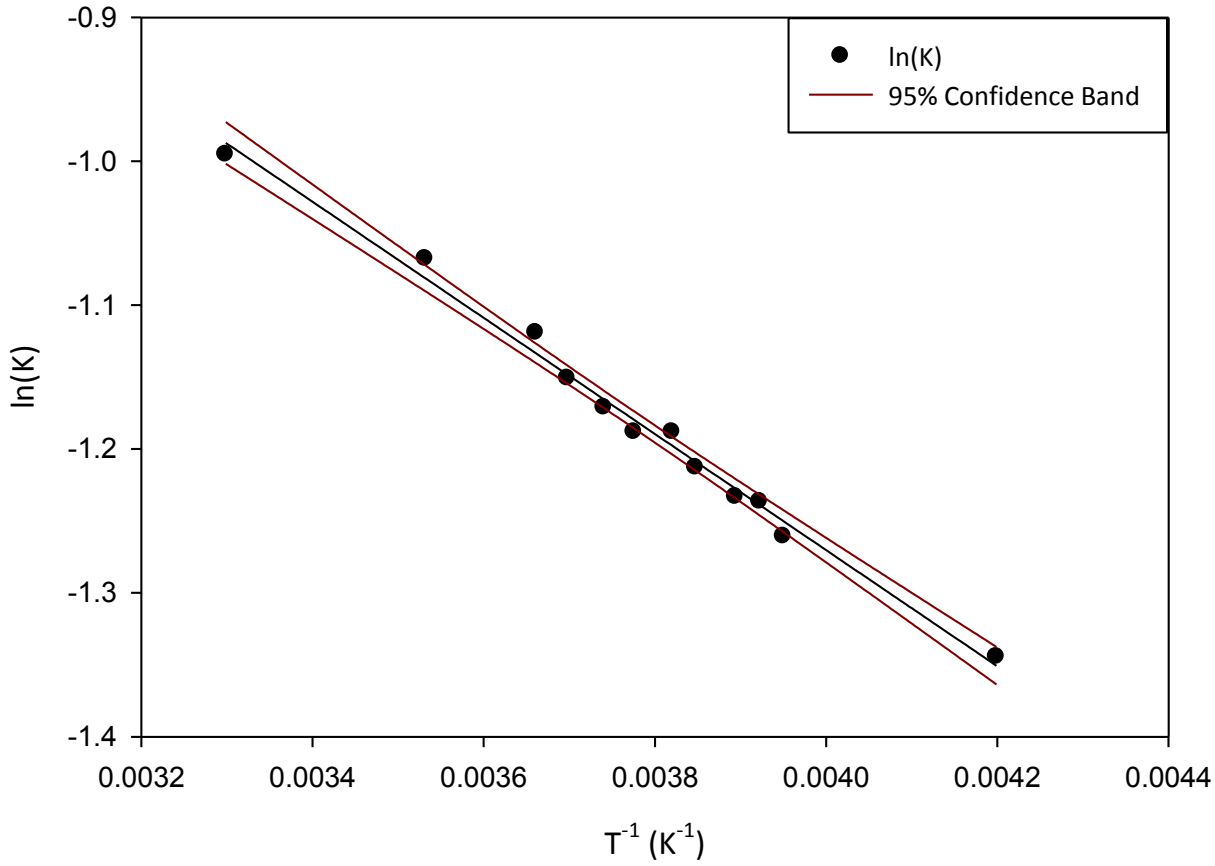

Figure 3.9. Van't Hoff plot of procyanidin B2 conformational interchange in acetonitrile-D_3

The van't Hoff plot is linear with three outlier data points. The standard enthalpy of reaction (ΔH_{rxn}^{0}) for the conformational interchange is 3.356 kJ.mol^{-1} and the standard entropy of reaction (ΔS_{rxn}^{0}) is 2.863 J.mol^{-1}.K^{-1}. The standard Gibbs free energy of reaction (ΔG_{rxn}^{0}) as calculated from the difference between the $\Delta G^{\ddagger}$(298K) for the forward and reverse reactions (3.273 kJ.mol^{-1}) and that calculated from the van't Hoff plot ΔH_{rxn}^{0} and ΔS_{rxn}^{0} (2.503 kJ.mol^{-1}) correlate to within experimental error. These results are tabulated with error ranges in Table 3.2.

Table 3.2 Standard reaction entropy, enthalpy and Gibbs free energy as determined from the van't Hoff plot

$\Delta \boldsymbol{S}^{\boldsymbol{0}}_{\boldsymbol{rxn}}$ (J.mol^{-1}K^{-1})	4.053 ± 1.565
ΔH^{0}_{rxn} (kJ.mol^{-1})	3.670 ± 0.2166
ΔG^{0}_{rxn}(298 K) (kJ.mol^{-1})	4.878 ± 0.3279

It was attempted to determine kinetic and thermodynamic constants for the conformational interchange reaction in acetone, but at the temperature used (298 K) there was an insufficient amount of the minor conformer for accurate analysis. The kinetic and thermodynamic constants of conformational interchange are expected to be entirely different in a different solvent system, as has been observed for the conformational interchange of procyanidin B1 and procyanidin B4 in water by Teracscou *et al.* [27]. The conformational interchange reaction constants in water for procyanidin B1 and B4 determined by EXSY, as shown in Table 3.3, are much smaller than the constants determined for procyanidin B2 in acetonitrile.

Table 3.3. Kinetic constants for procyanidin B1 and B4 in water at 298.15 K [27]

	B1	B4
k_1 (s^{-1})	0.34 ± 0.04	0.16 ± 0.03
k_{-1} (s^{-1})	3.83 ± 0.43	0.54 ± 0.09

From the thermodynamic constants shown by Terascou *et al.* [27], Table 1.6, it is clear that the distribution of the conformers approaches 1:1 in a polar solvent such as water. The minor conformer must therefore be stabilized by higher solvent polarity. However, it is possible that the dominant conformer could be a different conformer altogether than that formed by procyanidin B2 for a different molecule chirality, such as procyanidin B1 and procyanidin B4. The geometries of the various conformers have only been determined on a MM level of theory. DFT conformational analysis would be necessary to confirm the conformations of different chiral molecules and determine the features of the B2 molecule conformers.

Conclusion

An in house program has been created for the purpose of analyzing ^{1}H NMR chemical exchange line shapes. The program (NMRfit) has been implemented in the analysis of VT ^{1}H NMR spectra of procyanidin B2, which undergoes conformational interchange on the NMR timescale, and yielded good fits. The results of the least squares fit of the VT ^{1}H NMR spectra allowed for the construction of van't Hoff and Eyering plots which showed good linear trends with single anomalous data points in each fit. The Eyering and van't Hoff plots have allowed for the determination of the entropies, enthalpies and Gibbs free energies of activation and reaction, respectively. The entropy of reaction shows that the minor conformer's relative abundance increases with increasing temperature and the enthalpy shows that the forward reaction is slightly exothermic. The calculated standard reaction Gibbs free energy calculated agrees well with the relative abundance ratios of the conformers as estimated from the integration of the peaks of the NMR resonance signals. However, as of yet very little is known regarding the geometry of the conformations in question.

Chapter 4. A DFT Conformational Analysis of Procyanidin B2

4.1 Introduction

In relatively non-polar solvents two conformers of procyanidin B2 could be identified by means of ^{1}H NMR. Moreover, the rates at which these conformers interchange were also calculated as a function of temperature and consequently the thermodynamic parameters associated with the conformational interchange reaction were obtained. However, the geometrical features of these B2 conformers are unknown. Terascou *et al.* performed a MM calculation in the gas phase, using the MM3+ force field, and found two conformers that are thermodynamically stable named compact and extended. The compact conformer was found to be lower in standard Gibbs free energy of reaction by 12 kJ.mol^{-1} than its extended counterpart. This difference in standard Gibbs free energy of reaction compares relatively well with our experimentally determined ΔG^{0}_{rxn} of 4.9 kJ.mol^{-1} at 298 K. We therefore decided to repeat the MM calculations using the semi-empirical AM1 force field in the gas phase. The geometry of the compact and extended forms found (Figure 4.1) corresponds very well with those reported by Terascou *et al.* [27].

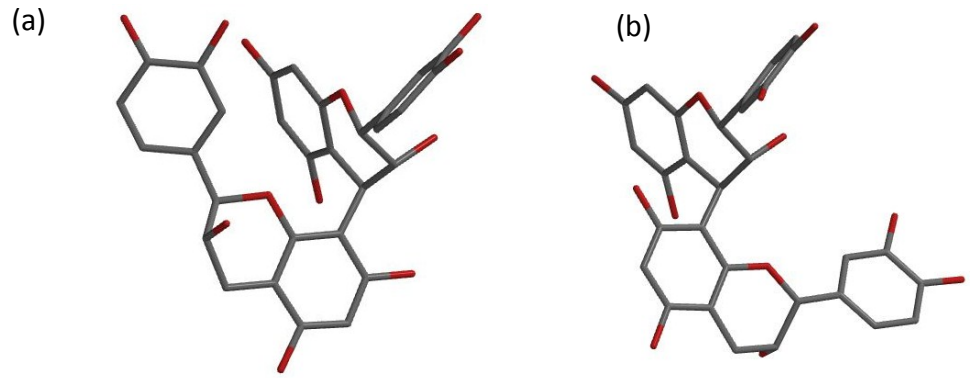

Figure 4.1. Tube representation of the (a) compact and (b) extended conformers of procyanidin B2 recalculated in Spartan '08 using the AM1 semi-empirical force field

From the semi-empirical calculation results it can be deduced that the compact form is thermodyanimically favoured and the ΔG^{0}_{rxn} for the conformational interchange reaction (compact to extended) is equal to 4.2 kJ.mol^{-1}. This compares unexpectedly well with our

experimentally determined ΔG^0_{rxn}. However, MM and semi-empirical computational approaches cannot properly take intramolecular bonding interactions into account and we suspect the relatively good agreement with regards to ΔG^0_{rxn}, found by us and Terascou *et al.,* to be fortuitous. Moreover, in a study conducted by Pianet *et al.* concerning the formation of colloids of several procyanidins (catechin, epicatechin, epigallocatechin gallate and procyanidins B1, B2, B3, B4 and C2), it was speculated that intramolecular interactions such as π-π stacking between phenol rings and the galloyl functional groups of galloylated procyanidins along with hydrogen bonding are the reasons why the compact conformation is thermodynamically favoured for most dimeric chiral molecules, including the galloylated procyanidins. This prompted us to investigate which conformations of procyanidin B2 are thermodynamically stable and also to identify possible intramolecular non-covalent interactions using a higher level of theory, namely DFT. To the best of our knowledge this is the first conformational study of procyanidin B2 using DFT.

4.2 Conformational Analysis Of Procyanidin B2 in the Gas Phase

Procyanidin dimers have several structural features that can result in a relatively large number of possible conformations. Relatively small energy changes are found for the quasi-axial and quasi-equitorial interchange reaction of the heterocyclic rings (ring C and F) as discussed by Kahn *et al.* [9]. The hydroxyl moieties can rotate and in the process can interact intramolecularly via hydrogen bonding or intermolecularly with solvent atoms. However, the rotation of only one OH can't be used as a basis for conformational analysis as procyanidin B2 has 10 hydroxyl moieties. If the rotation of all hydroxyl moieties were considered for conformational analysis there would be an unpractical amount of combinations in terms of computational resources required. Similarly, the phenol rings (ring B and E) can also rotate and in doing so generate several conformations. However, rotation about the interflavanoid bond has the largest influence on conformational geometry and was our primary interest. Therefore, a relaxed potential energy scan was performed for B2 about the (C3(C)-C4(C)-C8(D)-C8a(D)) interflavanoid bond dihedral angle in the gas phase at the B3LYP/6-31+g* level of theory. The resulting two dimensional potential energy surface (PES) is shown in Figure 4.2 and it is evident that there are four minima on the electronic PES. Subsequent relaxed PES scans in smaller dihedral angle steps around the 80 º and 270 º

regions improved the PES resolution and illustrated with greater clarity that at 80 º a minimum is found and at 270 º an inflection point occurs.

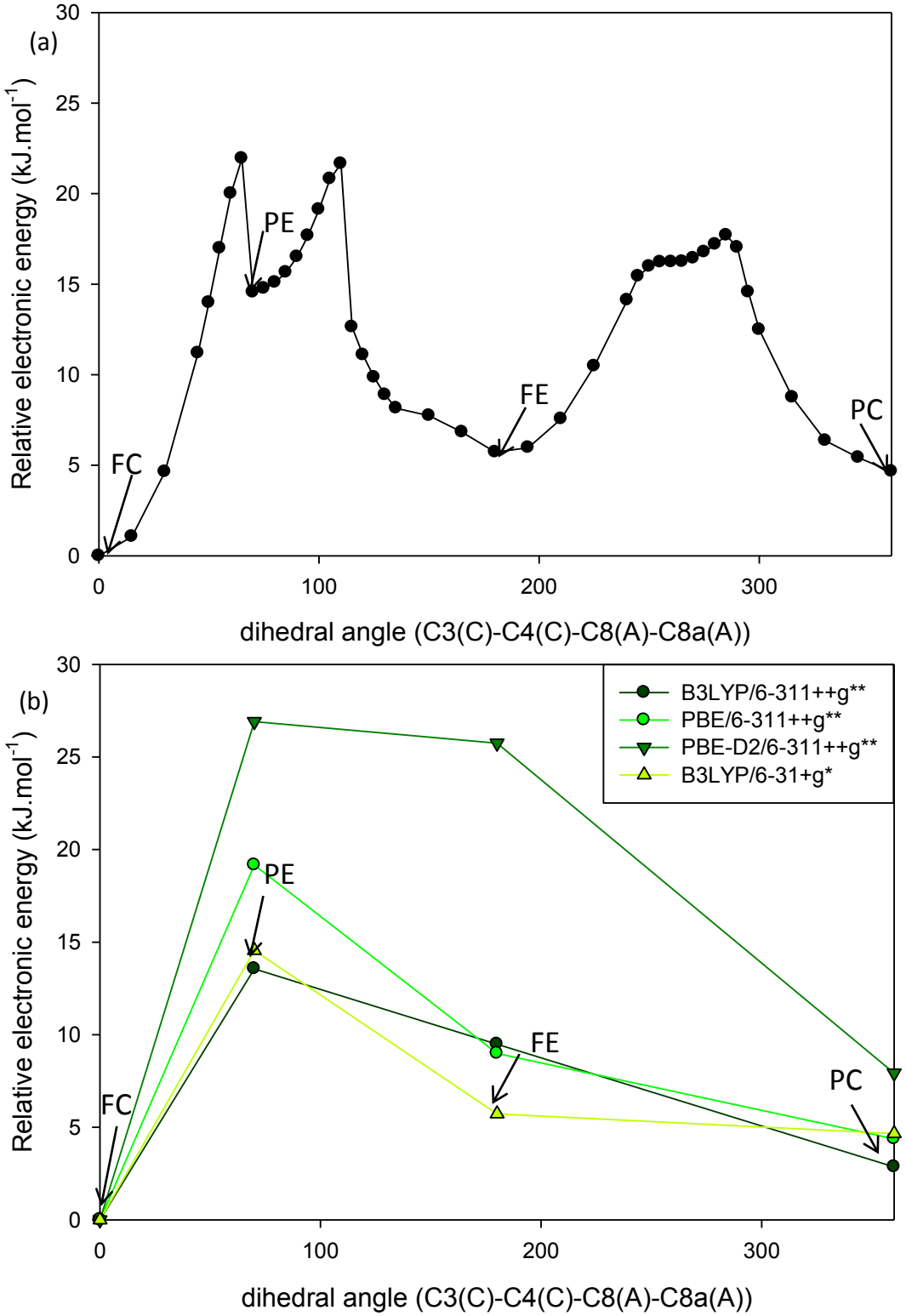

Figure 4.2. Potential energy surface, relative to the lowest energy conformation (FC), of the rotation of the C3(C)-C4(C)-C8(D)-C8a(D) dihedral bond angle (a) using B3LYP/6-31+g* with (b) the electronic energies of the reoptimized structures with varous functionals using the 6-311++g** basis set.

The geometries of the B2 conformations found on the PES, Figure 4.2, were re-optimized, shown in Figure 4.3, using three functionals (B3LYP, PBE and PBE-D2 functionals) and a larger basis set, 6-311++g**. Frequency calculations were done on each re-optimized geometry in order to validate that these structures are minima on the PES and to determine the standard Gibbs free energy of reaction between conformers. The four conformers are renamed here with the previous naming scheme in mind [9, 27] as fully-compact (FC), partially compact (PC), fully extended (FE) and partially extended (PE). The 'existence' of four conformations is in contrast to previous MM calculations where only 2 conformations were reported [9, 27] with a 180 ^{o} dihedral angle difference about the (C3(C)-C4(C)-C8(D)-C8a(D)) interflavanoid bond. It should be noted that the geometry of conformations found by MM and DFT differ significantly, as can be seen when comparing the structures shown in Figure 4.1. and Figure 4.3. A comparison of the electronic energies obtained for the set of conformers using PBE, PBE-D2 and B3LYP is shown in Figure 4.2 b**.** All the functionals yield the same trend with respect to electronic energy where the FC conformer is the lowest, indicating it is the most electronically stabilized, followed by the PC, FE and PE conformers. The difference in electronic energy for the four conformers agree within 5 kJ.mol^{-1} for the B3LYP and PBE functionals, whilst the FC electronic energy is considerably lower using the PBE-D2 functional compared to that found with the B3LYP and PBE functionals. Moreover, the change in basis set from 3-21 to 6-311++g** increased the electronic energy of the PE and FE conformers relative to the FC whilst the PC conformer's electronic energy remained largely the same.

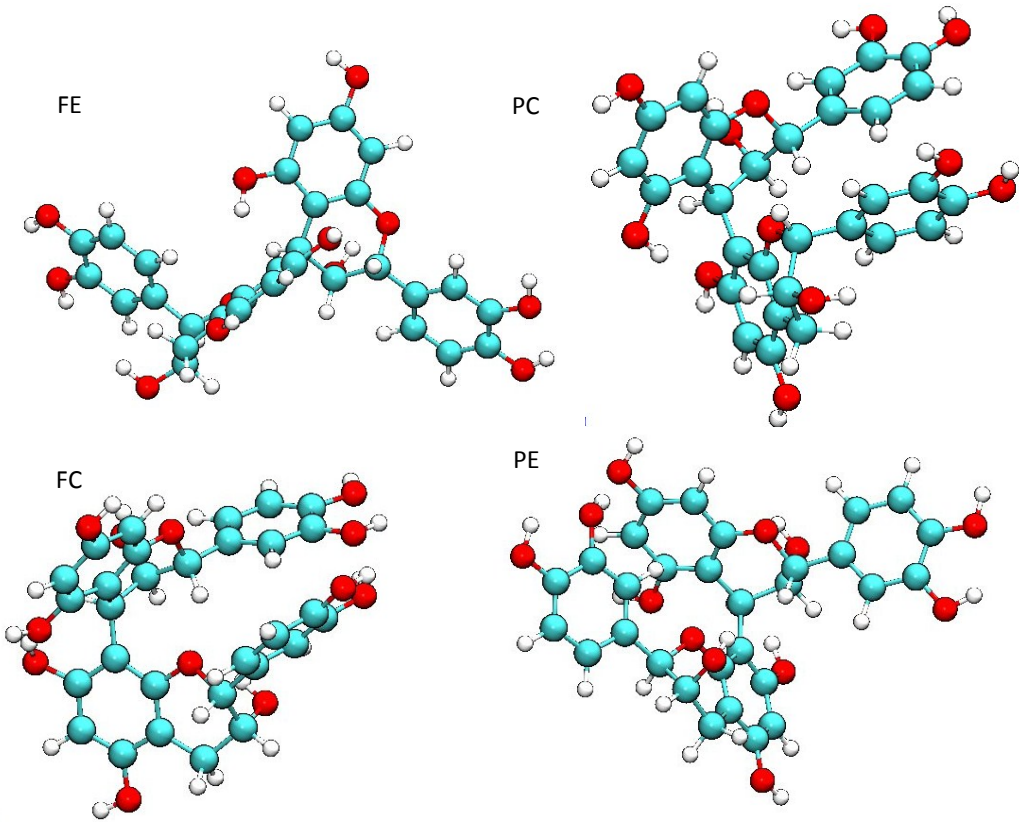

Figure 4.3. Ball and stick representation of procyanidin B2 conformers (fully extended (FE) , fully compact (FC), partially extended (PE) and partially compact (PC)) as found using the B3LYP functional and 6-311++g** basis set.

The geometry of the equilibrium structures found using the three different functionals for the PC and FC conformers are illustrated in Figure 4.4. The bond angles and lengths (*vida infra*) obtained with the B3LYP and PBE functionals vary only slightly from each other, in contrast with the PBE-D2 functional, for which the phenol groups are closer to each other compared to the PBE and B3LYP calculated geometries.

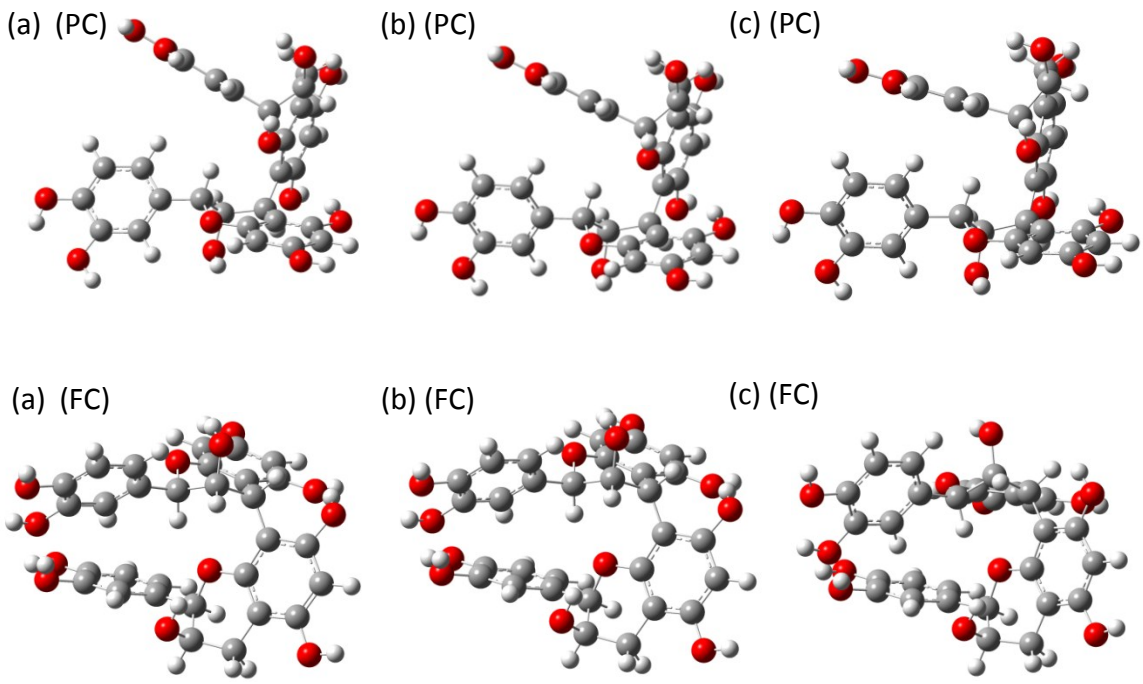

Figure 4.4. Comparison of the PC and FC conformer equilibrium geometries calculated by three DFT functionals, (a) B3LYP (b) PBE (c) PBE-D2, with the 6-311++g** basis set

A set of metrics of each gas phase conformer were chosen in order to convey the similiarity and/or dissimilarity between computed geometries using the various functionals (Table 4.1). The dihedral bond angles obtained with the B3LYP and PBE functionals for the respective procyanidin B2 conformations agree well with each other. However, with the PBE-D2 functional the dihedral bond angle for the FC conformer is rotated by 30 degrees with respect to the B3LYP and PBE functionals' calculated geometries, Figure 4.4. The interflavanoid bond length obtained with the PBE-D2 functional has a 0.002 to 0.008 Å reduction when compared to the B3LYP and PBE functionals' calculated geometries, indicating a more 'compact' geometry as a result of dispersion corrections (*vida infra*). The remaining metrics are in good agreement with minimal variation and the position of the heterocyclic rings is consistent for all functionals for their respective conformers. The position of the heterocyclic rings can be named boat, chair or half-chair, however this naming scheme has been deprecated and a new naming scheme where the position of the hydroxyl goup is quasi-equatorial (in the plane of the ring) or quasi-axial (perpendicular to the plane of the ring) is implemented in modern literature [27, 29].

Table 4.1. Metrics for measurement of procyanidin B2 conformational agreement as calculated using the B3LYP, PBE or PBE-D2 functionals with the 6-311++g** basis set

Conformation	Interflavanoid bond dihedral angle (°)	heterocyclic C ring OH position	heterocyclic F ring OH position	interflavanoid bond length (Å)	O1(F)- H2(C) (Å)
B3LYP					
Fully compact	62.17	quasi-axial	quasi-axial	1.537	2.033
Partially extended	108.17	quasi-axial	quasi-axial	1.531	3.04
Fully extended	-85.38	quasi-axial	quasi-equitorial	1.533	4.732
Partially compact	90.56	quasi-axial	quasi-equitorial	1.533	2.389
PBE					
Fully compact	61.84	quasi-axial	quasi-axial	1.535	2.014
Partially extended	108.12	quasi-axial	quasi-axial	1.528	3.071
Fully extended	-87.39	quasi-axial	quasi-equitorial	1.531	4.791
Partially compact	92.48	quasi-axial	quasi-equitorial	1.532	2.361
PBE-D2					
Fully compact	90.29	quasi-axial	quasi-axial	1.529	2.087
Partially extended	119.21	quasi-axial	quasi-axial	1.531	3.399
Fully extended	-88.68	quasi-axial	quasi-equitorial	1.527	4.671
Partially compact	90.45	quasi-axial	quasi-equitorial	1.529	2.26

The D2 dispersion was ‘added’ to the PBE functional, because the pure generalized gradient approximation (GGA) functional PBE is known to underestimate dispersion interactions [62]. However, in some cases Grimme D2 dispersion has been reported to overestimate dispersion interactions [63]. Unfortunately, the Grimme D3 dispersion correction is not available in the G09 B.01 revision used for the calculations in this study, which would have allowed for more accurate dispersion corrections.

By careful inspection of the DFT conformer geometries a few observations can be made concerning expected intramolecular interactions. The FC conformer, as the name suggests, is relatively compact and has several possible sites for intramolecular interactions. The FC conformer’s phenol moieties are folded in toward each other, which suggests possible hydrogen bonds between the oxygens and hydrogens of the hydroxyl groups. The FE conformer extends its phenol rings away from each other and has subsequently lost opportunities to form intramolecular interactions. The PC conformer is similar to the FC, as it has more opportunities for intramolecular stabilization, with the exception that it’s phenol rings are not sufficiently proximate for bonding interactions and as a result this conformer has less ‘electronic stabilization’ in that region. The PE conformer has the top monomeric

unit's heterocyclic ring interacting with the bottom monomeric unit's phenol ring, which can result in several intramolecular interactions similar to those postulated for the FC conformer. A more quantitative approach to investigate intramolecular interactions will be discussed in the next section.

4.2.1 Electron Density Topological Analysis Of The Gas Phase Procyanidin B2 Conformations

The FC conformer has the lowest electronic energy in the gas phase and we suspect that this is due to more extensive intramolecular interactions between the upper and lower monomeric units compared to the other conformers. A QTAIM analysis of the four conformers using the AIMSALL software suite yielded the molecular graphs illustrated in Figure 4.5. Green dots in Figure 4.5 refer to BCPs, which are minima in the electron density gradient in one dimension and maxima in two dimensions, i.e. a saddle point in the electron density. Moreover, the eigenvalues (λ_1, λ_2, λ_3) of the Hessian matrix at a BCP have the property that λ_1 and λ_2 are negative and λ_3 is positive, where $\lambda_1 < \lambda_2$. The red dots in Figure 4.5 represent RCPs, where the electron density topology forms a second order saddle point where $\lambda_1 < 0$, λ_2 and $\lambda_3 > 0$. The blue dots represent CCPs, where λ_1, λ_2 and $\lambda_3 > 0$. In Figure 4.5 the 'formal' covalent bonds are indicated by solid lines and the non-covalent intramolecular interactions by dotted lines.

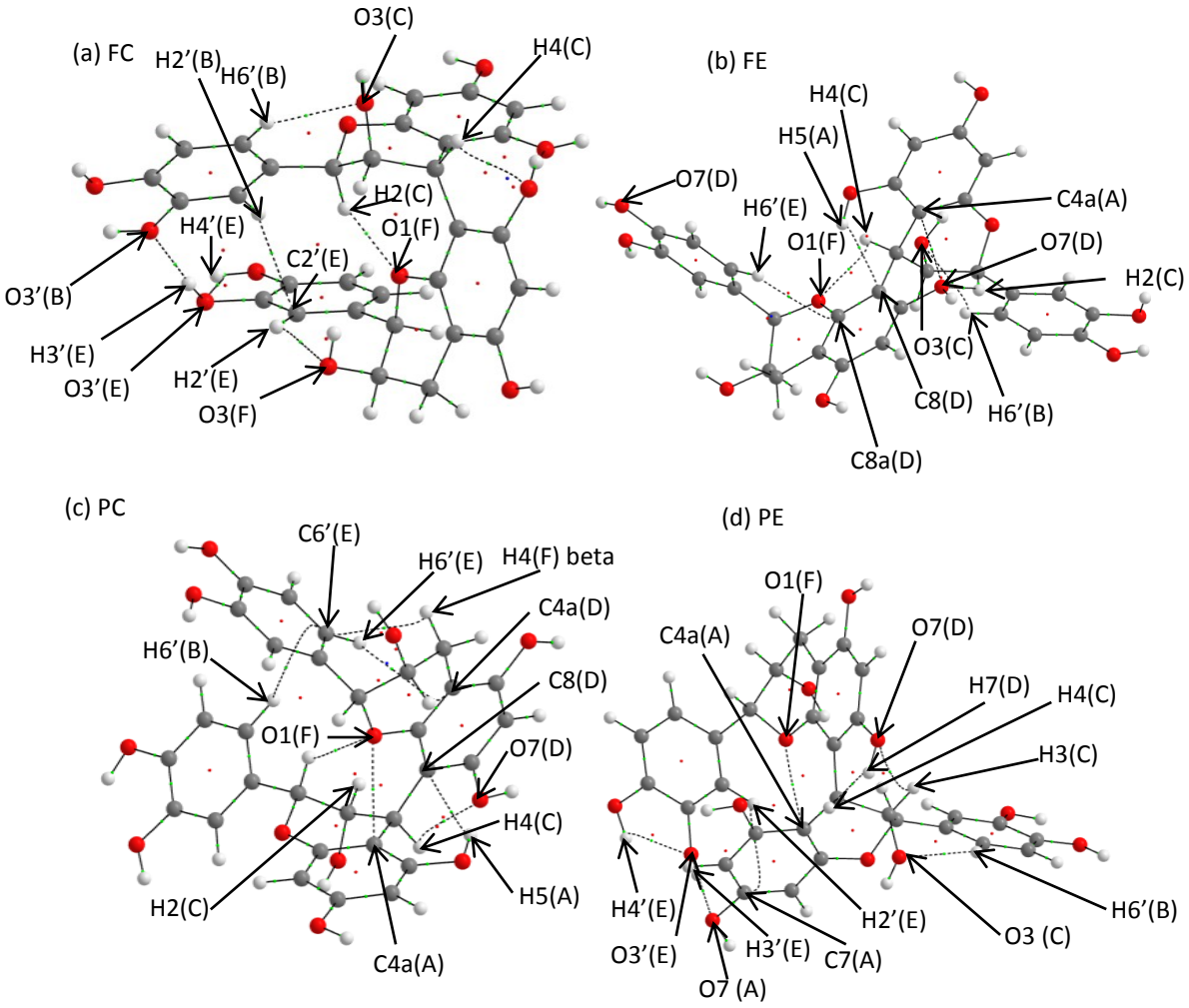

Figure 4.5. Ball and stick representations of various procyanidin B2 conformers ((a) fully compact (FC), (b) fully extended (FE),(c) partially compact (PC),(d) partially extended (PE)) calculated with B3LYP/6-311++g** in Gaussian 09 Rev. B.01 showing QTAIM bond paths with non covalent interactions indicated by dotted lines. BCP's are shown in green, RCPs in red and CCPs in blue.

The QTAIM analysis performed on the procyanidin B2 conformers yield a multitude of indices that can be used in the classification of bond character as described in chapter 1 section 1.6. The classification scheme in Figure 1.10 can be used in order to determine whether an interaction is a shared-shell or closed-shell interaction and if the electron density topology is indicative of covalent, dative, metallic, ionic or van der Waals character. According to this characterization scheme C=C, C-O, C-C, C-H and O-H bonds, represented by solid lines in Figure 4.5, satisfy the following criteria $\nabla^2\rho<0$, $V_b<<0$, $G_b<<|V_b|$, $E_b<<0$ and ρ_b high. These bonds are therefore shared interactions and classified in the range of polar covalent to covalent. The tables containing the above mentioned metrics for covalent bonds

for all four conformers and for all three functionals are included on the supplementary DVD accompanying this thesis [\AIM\SuppBCP.xls].

Table 4.2. QTAIM closed-shell interaction parameters for BCPs as calculated by using the B3LYP/6-311++g** functional for procyanidin B2 in the gas phase

	Nuclear Attractor	$\lambda 1$	$\lambda 2$	$\lambda 3$	ρ	$\nabla^2\rho$	G_b	V_b	E_b	ε
FC	C2'(E) - H2'(B)	-0.006	-0.004	0.034	0.008	0.023	0.005	-0.004	0.001	0.5
	O3(C) - H6'(B)	-0.013	-0.011	0.068	0.013	0.044	0.010	-0.008	0.001	0.2
	H2'(E) - O3(F)	-0.014	-0.012	0.073	0.014	0.046	0.010	-0.009	0.001	0.1
	O7(D) - H4(C)	-0.013	-0.008	0.094	0.017	0.073	0.015	-0.012	0.003	0.6
	O5(A) - H7(D)	-0.025	-0.023	0.122	0.020	0.074	0.016	-0.014	0.002	0.1
	O3'(B) - H3'(E)	-0.031	-0.028	0.142	0.022	0.084	0.018	-0.016	0.002	0.1
	O3'(E) - H4'(E)	-0.024	-0.012	0.124	0.021	0.089	0.020	-0.017	0.003	1.0
	O1(F) - H2'(C)	-0.030	-0.028	0.146	0.023	0.089	0.020	-0.017	0.003	0.1
	Nuclear Attractor	$\lambda 1$	$\lambda 2$	$\lambda 3$	ρ	$\nabla^2\rho$	G_b	V_b	E_b	ε
PE	C8(A) - H2'(E)	-0.005	-0.002	0.027	0.007	0.020	0.004	-0.003	0.001	2.3
	O7(D) - H3(C)	-0.005	-0.003	0.049	0.010	0.041	0.009	-0.007	0.002	0.6
	C4a(A) - O1(F)	-0.008	-0.007	0.058	0.012	0.042	0.009	-0.008	0.001	0.1
	H7(D) - H4(A)	-0.020	-0.013	0.095	0.017	0.062	0.014	-0.012	0.002	0.5
	O3'(E) - H4'(E)	-0.023	-0.010	0.120	0.020	0.087	0.019	-0.017	0.003	1.2
	O7(A) - H3'(E)	-0.036	-0.034	0.160	0.025	0.089	0.021	-0.019	0.002	0.1
	Nuclear Attractor	$\lambda 1$	$\lambda 2$	$\lambda 3$	ρ	$\nabla^2\rho$	G_b	V_b	E_b	ε
FE	C8a(D) - H6'(E)	-0.005	-0.001	0.032	0.008	0.026	0.005	-0.004	0.001	2.6
	H2(C) - C7(D)	-0.010	-0.009	0.054	0.010	0.035	0.008	-0.006	0.001	0.1
	H6'(B) - O3(C)	-0.007	-0.005	0.050	0.010	0.038	0.008	-0.007	0.001	0.3
	C7(D) – H4(A)	-0.013	-0.007	0.063	0.014	0.044	0.010	-0.008	0.001	0.9
	C4a(A) - C7(D)	-0.008	-0.007	0.060	0.012	0.045	0.010	-0.008	0.002	0.2
	H4(C) - O1(D)	-0.017	-0.007	0.105	0.018	0.080	0.017	-0.014	0.003	1.3
	Nuclear Attractor	$\lambda 1$	$\lambda 2$	$\lambda 3$	ρ	$\nabla^2\rho$	G_b	V_b	E_b	ε
PC	H6'(B) - C6'(E)	-0.002	-0.001	0.010	0.003	0.007	0.001	-0.001	0	0.9
	C4a(D) - H6'(E)	-0.005	-0.002	0.031	0.007	0.024	0.005	-0.004	0.001	1.6
	H4(D)beta - C6'(E)	-0.004	-0.002	0.033	0.008	0.027	0.006	-0.004	0.001	1.5
	H2(C) - O1(F)	-0.012	-0.011	0.063	0.012	0.039	0.009	-0.007	0.001	0.1
	C8(D) - H5(A)	-0.013	-0.008	0.065	0.014	0.044	0.010	-0.008	0.001	0.6
	C4a(A) - O1(F)	-0.009	-0.006	0.062	0.012	0.047	0.010	-0.009	0.001	0.4
	H4(C) - O7(D)	-0.015	-0.005	0.099	0.017	0.078	0.016	-0.013	0.003	2.1

Table 4.3. QTAIM closed-shell interaction parameters for BCPs as calculated by using the PBE/6-311++g** functional for procyanidin B2 in the gas phase

	Nuclear Attractor	$\lambda 1$	$\lambda 2$	$\lambda 3$	ρ	$\nabla^2\rho$	G_b	V_b	E_b	ε
FC	C2'(E) - H2'(B)	-0.007	-0.005	0.038	0.009	0.026	0.005	-0.004	0.001	0.5
	O3(C) - H6'(B)	-0.013	-0.011	0.067	0.013	0.043	0.010	-0.008	0.001	0.2
	H2'(E) - O3(F)	-0.015	-0.013	0.074	0.014	0.046	0.010	-0.009	0.001	0.1
	O8(D) - H4(C)	-0.013	-0.009	0.092	0.018	0.070	0.015	-0.012	0.003	0.5
	O5(A) – H7(D)	-0.027	-0.025	0.129	0.021	0.076	0.017	-0.015	0.002	0.1
	O3'(E) - H4'(E)	-0.026	-0.016	0.132	0.023	0.090	0.020	-0.018	0.002	0.7
	O1(F) - H1(F)	-0.031	-0.029	0.151	0.024	0.090	0.020	-0.017	0.003	0.1
	O3'(B) - H3'(E)	-0.036	-0.033	0.159	0.025	0.090	0.020	-0.018	0.002	0.1
	Nuclear Attractor	$\lambda 1$	$\lambda 2$	$\lambda 3$	ρ	$\nabla^2\rho$	G_b	V_b	E_b	ε
PE	C7(A) - H2'(E)	-0.005	-0.001	0.028	0.007	0.022	0.004	-0.004	0.001	3.7
	C4a(A) -O1(F)	-0.009	-0.007	0.059	0.012	0.043	0.009	-0.008	0.001	0.1
	O7(D) - H3(C)	-0.004	-0.001	0.050	0.011	0.045	0.009	-0.008	0.002	2.4
	H7(D) - H4(C)	-0.021	-0.014	0.100	0.019	0.064	0.014	-0.013	0.002	0.5
	O3'(E) - H4'(E)	-0.026	-0.016	0.132	0.022	0.090	0.020	-0.018	0.002	0.6
	O7(A)- H3'(E)	-0.039	-0.037	0.166	0.027	0.090	0.021	-0.020	0.001	0.1
	Nuclear Attractor	$\lambda 1$	$\lambda 2$	$\lambda 3$	ρ	$\nabla^2\rho$	G_b	V_b	E_b	ε
FE	C8a(D) - H6'(E)	-0.006	-0.003	0.038	0.009	0.030	0.006	-0.005	0.001	1.4
	H2(C) - O7(D)	-0.012	-0.011	0.061	0.012	0.038	0.008	-0.007	0.001	0.1
	H4(C) - O1(F)	-0.010	-0.008	0.059	0.012	0.041	0.009	-0.008	0.001	0.2
	C4a(A) - O7(D)	-0.008	-0.006	0.058	0.012	0.044	0.009	-0.008	0.002	0.3
	C8(D) - H5(A)	-0.017	-0.011	0.077	0.017	0.049	0.011	-0.010	0.001	0.5
	H6'(B) - O3(C)	-0.018	-0.008	0.106	0.018	0.080	0.017	-0.014	0.003	1.2
	Nuclear Attractor	$\lambda 1$	$\lambda 2$	$\lambda 3$	ρ	$\nabla^2\rho$	G_b	V_b	E_b	ε
PC	H6'(B) - C6'(E)	-0.003	-0.001	0.017	0.005	0.012	0.003	-0.002	0.001	1.3
	C8a(D) - H6'(E)	-0.005	-0.001	0.031	0.008	0.026	0.005	-0.004	0.001	4.1
	H4(F) - C6'(E)	-0.004	-0.001	0.033	0.008	0.028	0.006	-0.004	0.001	4.7
	H2(C) - O1(F)	-0.013	-0.012	0.064	0.012	0.040	0.009	-0.008	0.001	0.1
	H2'(B) - O3(C)	-0.015	-0.014	0.078	0.015	0.048	0.011	-0.009	0.001	0.1
	C8(D) - H6(A)	-0.016	-0.011	0.076	0.017	0.049	0.011	-0.010	0.001	0.4
	C4a(A) - O1(F)	-0.010	-0.007	0.066	0.013	0.049	0.011	-0.009	0.002	0.3

Table 4.4. QTAIM closed-shell interaction parameters for BCPs as calculated by using the PBE-D2/6-311++g** functional for procyanidin in the gas phase

	Nuclear Attractor	$\lambda 1$	$\lambda 2$	$\lambda 3$	ρ	$\nabla^2\rho$	G_b	V_b	E_b	ε
FC	C7(A) - C6'(E)	-0.003	-0.002	0.019	0.006	0.015	0.003	-0.002	0.001	0.5
	O3(C) - H6'(B)	-0.009	-0.007	0.05	0.01	0.033	0.007	-0.006	0.001	0.2
	C2'(E) - H2'(B)	-0.012	-0.008	0.058	0.013	0.039	0.008	-0.006	0.002	0.5
	C4a(A) - O1(F)	-0.01	-0.008	0.072	0.015	0.054	0.012	-0.01	0.002	0.2
	H2'(E) – O3(F)	-0.017	-0.016	0.088	0.016	0.055	0.012	-0.01	0.002	0.1
	H7(D) - H4(C)	-0.026	-0.02	0.113	0.021	0.066	0.015	-0.013	0.002	0.3
	O3'(B) - H3'(E)	-0.027	-0.025	0.125	0.02	0.073	0.016	-0.014	0.002	0.1
	O1(F) – H2(C)	-0.026	-0.024	0.126	0.022	0.076	0.017	-0.015	0.002	0.1
	O3'(E) - H4'(E)	-0.023	-0.012	0.122	0.021	0.087	0.019	-0.017	0.003	1
	Nuclear Attractor	$\lambda 1$	$\lambda 2$	$\lambda 3$	ρ	$\nabla^2\rho$	G_b	V_b	E_b	ε
PE	C6'(E) – H4(A)	-0.003	-0.001	0.017	0.004	0.013	0.003	-0.002	0.001	1
	C5(A) - C2'(E)	-0.004	-0.002	0.031	0.008	0.025	0.005	-0.004	0.001	0.6
	H2'(E) - O3(F)	-0.008	-0.007	0.045	0.01	0.031	0.007	-0.006	0.001	0.2
	O7(D) - H3(C)	-0.012	-0.007	0.073	0.014	0.055	0.011	-0.009	0.002	0.6
	C4a(A) - O1(F)	-0.015	-0.008	0.088	0.017	0.065	0.014	-0.012	0.002	0.7
	O3'(E) - H4'(E)	-0.026	-0.014	0.124	0.022	0.084	0.019	-0.017	0.002	0.9
	O7(A) - H3(D)	-0.048	-0.044	0.196	0.031	0.104	0.025	-0.025	0.001	0.1
	Nuclear Attractor	$\lambda 1$	$\lambda 2$	$\lambda 3$	ρ	$\nabla^2\rho$	G_b	V_b	E_b	ε
FE	H2'(E) – H4(A)	-0.003	-0.002	0.02	0.004	0.014	0.003	-0.002	0.001	0.6
	C4a(A) - H2'(E)	-0.009	-0.004	0.052	0.012	0.038	0.008	-0.006	0.002	1
	H6'(B) - O3(C)	-0.009	-0.007	0.058	0.012	0.041	0.009	-0.008	0.001	0.2
	H2(C) - O7(D)	-0.013	-0.012	0.068	0.013	0.043	0.009	-0.008	0.001	0.1
	C8(D) - H5(A)	-0.012	-0.003	0.063	0.014	0.048	0.01	-0.009	0.002	2.9
	C4a(A) - O7(D)	-0.009	-0.007	0.064	0.013	0.048	0.01	-0.009	0.002	0.2
	H4(C) - O1(F)	-0.017	-0.007	0.105	0.018	0.081	0.017	-0.014	0.003	1.4
	Nuclear Attractor	$\lambda 1$	$\lambda 2$	$\lambda 3$	ρ	$\nabla^2\rho$	G_b	V_b	E_b	ε
PC	H5'(B) - O4'(E)	-0.002	-0.001	0.015	0.003	0.011	0.002	-0.002	0.001	0.6
	H6'(B) - O5'(E)	-0.004	-0.001	0.03	0.008	0.025	0.005	-0.004	0.001	2.2
	H4(F) - C6'(E)	-0.006	-0.003	0.044	0.01	0.035	0.007	-0.006	0.002	0.9
	C4a(D) - H6'(E)	-0.008	-0.004	0.047	0.011	0.035	0.007	-0.006	0.002	1.1
	C7(D) – H5(A)	-0.016	-0.01	0.074	0.017	0.048	0.011	-0.01	0.001	0.6
	H2'(B) - O3(C)	-0.016	-0.014	0.079	0.015	0.049	0.011	-0.01	0.001	0.1
	H2(C) - O1(F)	-0.017	-0.015	0.083	0.016	0.051	0.011	-0.01	0.001	0.1
	C4a(A) - O1(F)	-0.011	-0.009	0.075	0.015	0.055	0.012	-0.011	0.002	0.2

Tables 4.2 to 4.4 list the eigenvalues, electron densities (ρ), Laplacian ($\nabla^2\rho$), kinetic energy densities (G_b), potential energy densities (V_b), total electronic energy densities (E_b= G_b + V_b) and the bond elepticities (ε) for the bonding interactions indicated by dotted lines on Figure 4.5 at the BCPs. The relatively low electron densities and positive lapacians at the

BCPs indicate that all these bonding interactions are closed-shell interactions. Moreover, it is also observed from Table 4.2 to 4.4 that $V_b < 0$, $G_b \equiv |V_b|$, $E_b > 0$ *and* $|E_b| \approx 0$, which would imply from the classification scheme in Figure 1.10 that these bonding interactions are van der Waals in nature.

As discussed in chapter 1, hydrogen bonds are defined as a BCP with an electron density between 0.002 and 0.04 au, a Laplacian value between 0.02 and 0.15, mutual penetration of the bond path between the hydrogen and the acceptor atom (meaning that the bond path must pass directly from one nuclear attractor to another), loss of charge of the hydrogen atom, energy destabilization of the hydrogen atom, decrease in the dipolar polarization of the hydrogen atom and a decrease in the atomic volume of the hydrogen atom [43]. From Table 4.2 to 4.4 it is observed that all the intramolecular interactions' electron densities at the BCPs range between 0.002 and 0.04 au. The Laplacian of the electron density of most of the interactions vary within the 0.02 to 0.15 range. The O8(D) - H4(C) in the FC conformer as calculated using the PBE functional is an example of the typically expected Laplacians for hydrogen bonds, with the exception of a few relatively low electron density interactions like the H6'(B) - C6'(E) in the PC conformer calculated using the PBE functional. All interactions discussed from a QTAIM standpoint have mutual bond path penetration and the electron density accumulation at the BCP indicates that the hydrogen atom charge and dipolar polarization decreases. This electron density decrease will inevitably also lead to a reduction of the atomic volume. Consequently, the interactions listed in the tables that include hydrogens conform to the definition of a hydrogen bond as set out by Bader [43].

If the electronic closed-shell van der Waals interactions are taken as the reason and rationale for assignment of the electronic energy hierarchy of conformers, the larger energy polar van der Waals interactions are of most interest. The energy of interactions is not defined within QTAIM and a interacting quantum atoms (IQA) investigation would be necessary to obtain that information. Unfortunately, IQA calculations on molecules of procyanidin B2 size are beyond the calculation resources of this study. However, more polar hydrogen bonds can be rationalized to be stronger than non-polar van der Waals interactions due to the coulombic element of the interaction causing an attractive Keesom force. Consequently, the highest energy closed-shell interactions are expected to be the

polar O to H interactions. When considering the PC and FC conformers, the interflavanoid bond dihedral angle is similar, but only the H4(C) - O7(D) interaction is communal to the conformations. The H4(C) - O7(D) interaction is clearly strained in the PC conformer as the electron density is slightly lower and the ellipticity of the interaction is 2.1, in contrast to the 0.6 elipticity value found for FC using the B3LYP functional. The dissimilarity in electronic interaction networks is unexpected and indicates that the conformations have different stabilization mechanisms. By examining the relatively high energy intramolecular interactions it should become clear where the highest electronic stabilization occurs. The PC conformer has two polar van der Waals O to H interactions in contrast the FC conformer which has seven. The PE conformer has three polar van der Waals O to H interactions and the FE conformer also only has three. The FE conformer's internal stabilization includes three polar van der Waals O to H interactions that are found in the H2(C)-O7(D), H6'(B)-O3(C) and H4(C)-O1(F) interactions near the interflavanoid bond. Therefore, it is unexpected that the FC and FE conformers should be as close in electronic energy as found on the PES shown in Figure 4.2. The red and blue dots in Figure 4.5 illustrate ring critical points (RCP) and cage critical points (CCP), respectively, and are indicative of steric strain [43]. FC, with 15 RCPs and 1 CCP, clearly has more electronic destabilization from cage and ring critical points than FE, with 13 RCPs and no CCPs , but is still similar in energy on the PES, most probably as a result of the amount of polar van der Waals O to H closed-shell interactions that are formed. However, the FE conformer is 'minimally' stabilized by intramolecular electronic interactions, i.e. less than the other conformers. Quantification of the destabilization caused by RCPs and CCPs is difficult. However, high electron density is expected to be indicative of a stronger repulsion [43, 45]. Consequently, FE has comparatively low electronic destabilization from CCPs and RCPs.

When dispersion corrections, as implemented in the PBE-D2 functional, are taken into account, there are several geometrical parameters that change compared to the optimized geometries obtained with the PBE and B3LYP functionals. Most notably the interflavanoid bond dihedral angle for the FC conformer is rotated by 30 °. Changes in geometry will also affect the electron density topology which in turn will cause several differences to appear in the QTAIM results for the procyanidin B2 conformers. The molecular graphs obtained for the FC and PC conformers using the PBE and PBE-D2

functionals are illustrated in Figure 4.6. Firstly, the dispersion correction for all conformers results in one extra intramolecular van der Waals interaction, Tables 4.3 and 4.4. Several bond paths (BP) are now between different atoms, e.g. for the FC conformer with dispersion correction BPs are now present between C7(A) –C6'(E), C4a(A)-O1(F), H7(D)-H4(C), O1(F)-H2(C) and O3'(E)-H4'(E), which are absent in the PBE functional geometry optimized FC conformation. Eight of the nine intramolecular van der Waals interactions have electron densities at the BCPs (Table 4.4) in the hydrogen bond range which presumable lower the electronic energy compared to the other conformers analyzed using PBE-D2. This may also explain why the difference in the electronic energy between the FC and other conformers, Figure 4.2 b, is relatively large compared to that obtained with the PBE and B3LYP functionals. From the PC conformer's intramolecular interactions it is clear that the addition of dispersion corrections allows for more interactions to form. An interaction is noted in the C4a(A) to O1(F) position and a carbon to phenol ring interaction is noted between the E ring and the C8(A) position. The A to E ring carbon interaction may be rationalized as a phenol ring π - π interaction, but in such a case the misalignment of the rings brings the validity of the interaction into further question.

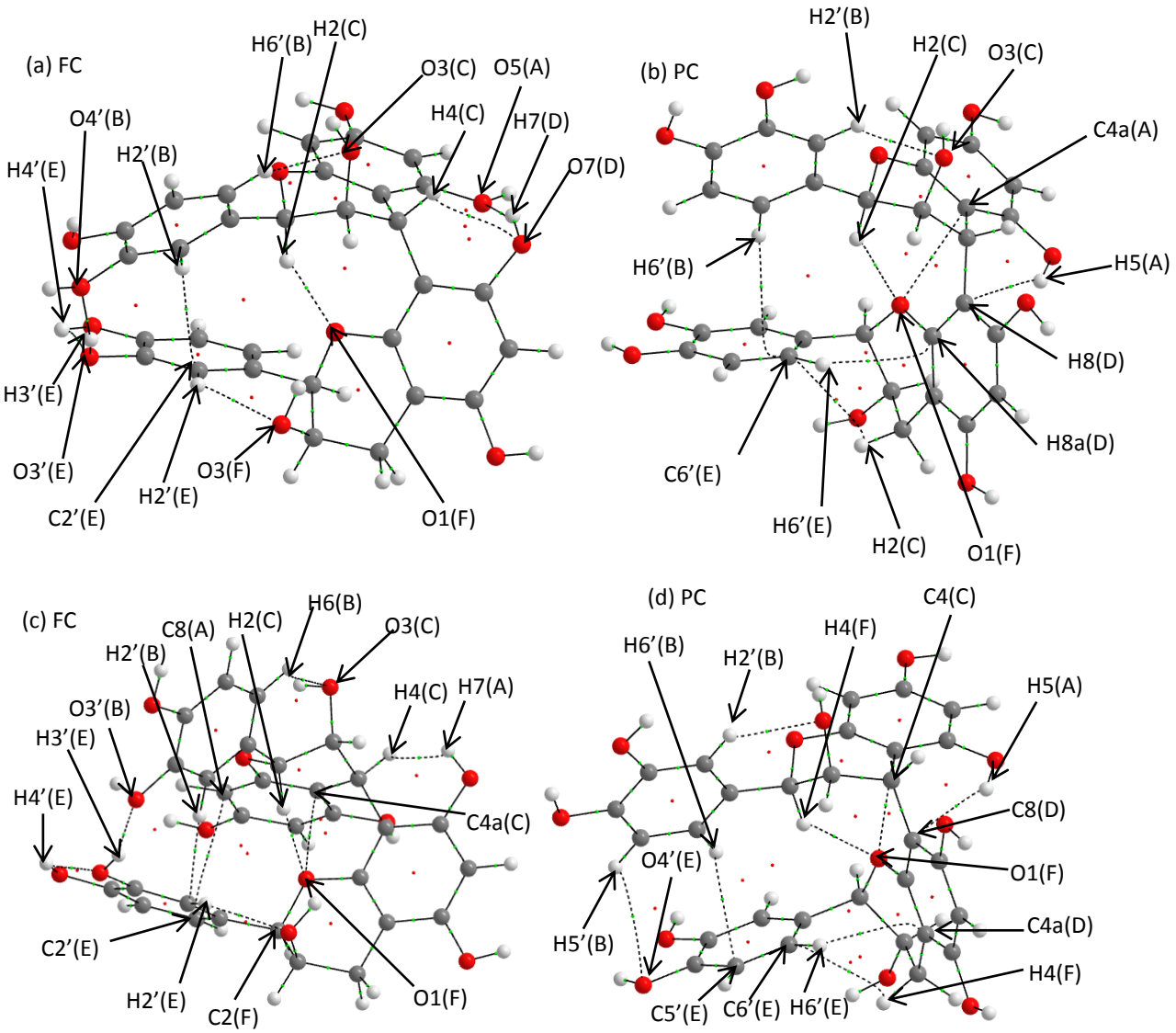

Figure 4.6. Ball and stick representations of QTAIM bonding interactions in procyanidin B2 conformers with (a) and (c) indicating an FC conformer and (b) and (d) indicating a PC conformer. ((a) and (b) are calculated with the PBE/6-311++g** functional and (c) and (d) are calculated with the PBE-D2/6-311++g** functional in Gaussian 09 Rev. B0.1)

Interestingly, it is observed for the FC conformer that the H7(A) to H4(C) intramolecular van der Waals interaction has an electron density of 0.02 at the BCP, which is comparable to a 'standard' example of a hydrogen bond [43]. At first glance it is counter intuitive that a positively charge polarized hydrogen atom could form a 'full' strength hydrogen bond with another positively charge polarized hydrogen atom. However, this type of intramolecular van der Waals interaction is similar to σ-hole bonding found in intermolecular halogen bonding [64]. The anisotropy of the charge polarization around the halogen, e.g. CH_3Cl , results in regions that are lower in electron density (at the tip of the atom) and regions of higher electron density around the bond axis. The charge polarization

leads to intermolecular electrostatic attraction (Keesom force) or, in the case of apolarized moiety approaching an unpolarized moiety, induces a dipole (Debye force) [65, 66]. Noteably, a hydrogen bond is formed between the H5'(B) and O4'(E) atoms, which is expected to be highly stabilizing by the Keesom force. It is rationalized that the H4(C) to H7(C) interaction is formed by an induced dipole (a Debye force) or London dispersion force [65, 66]. The electrostatic surface potential of the H4(C) to H7(A) region is of interest due to the controversial nature of 'like' charge polarized moieties that form interactions. From the ESP it is observed that the H4(C) hydrogen is not as strongly charge accumulated as the H7(A) hydrogen that has some electron density shared with the oxygen of its hydroxyl moiety. This allows for the deduction that the dipolarization of the hydrogens is not present to such an extend that there is significant coulombic repulsion between the hydrogen atoms in question.

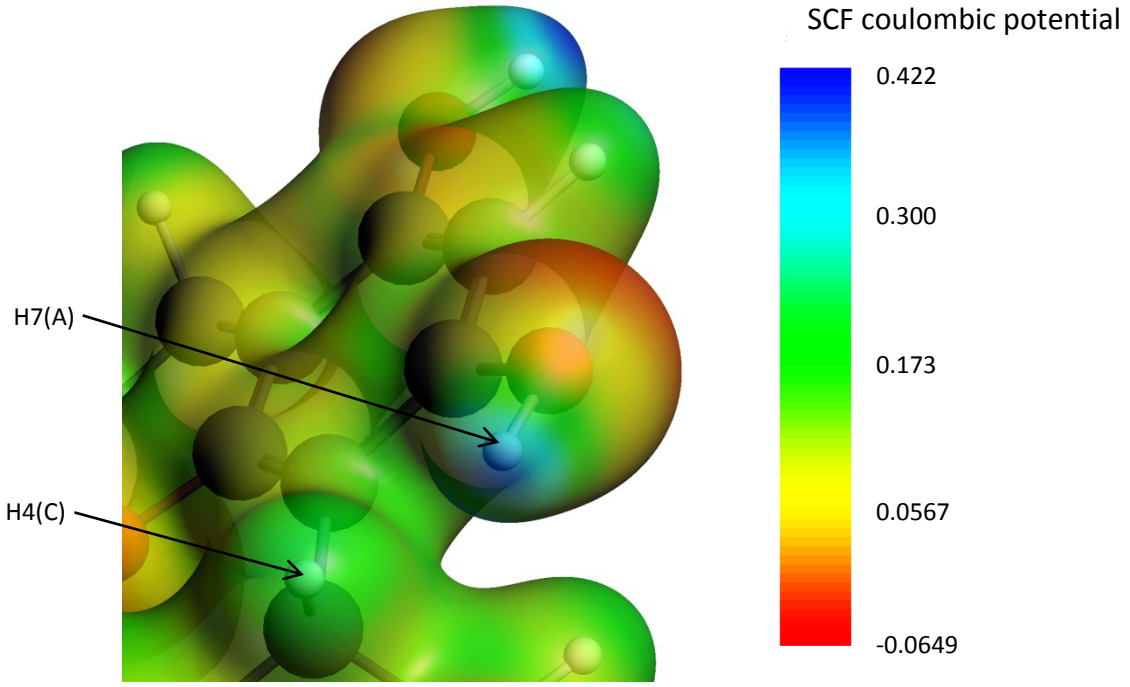

Figure 4.7. Electrostatic surface potential isosurface of the FC conformer as calculated with the PBE/TZ2P functional in ADF suite

In a recent study by Lane *et al.* [67] "Are Bond Critical Points Really Critical for Hydrogen Bonding?" the authors argue that QTAIM criteria are too stringent to decide when two or more atoms are bonded. It was suggested by Lane *et al.* that an analysis of the

general electron density topology in the surrounding region where a BCP is expected, but not found with an AIMs analysis, using the NCI index yields the desired information that atoms are indeed bonded. This is illustrated in their study on the 'controversial' intramolecular hydrogen bond occurring in ethanediol. When a NCI analysis is performed the RDG is plotted as a function of the electron density times the sign of the second eigen value of the Laplacian (λ_2). At BCPs, RCPs and CCPs the RDG will be equal to zero and form characteristic throughs, *e.g.* regions A and B as indicated in Figure 4.8.

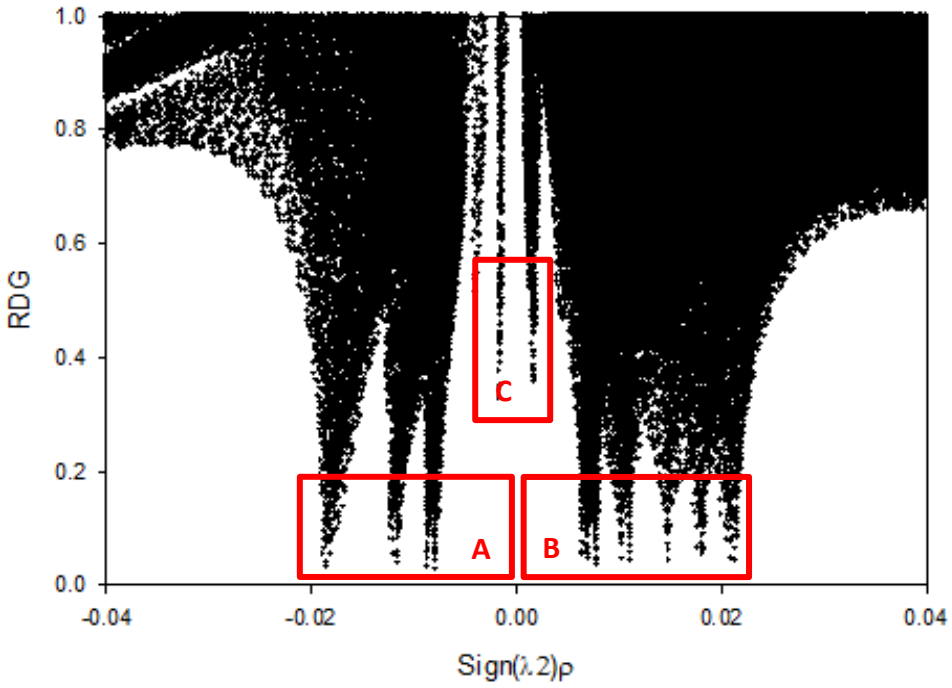

Figure 4.8. Illustrative NCI plot of the fully extended conformerof procyanidin B2 in the gas phase as calculated with the B3LYP/6-311++g** functional

When these troughs occur on the negative side on the x-axis (sign(λ_2)ρ), Figure 4.8 region A, it is an attractive interaction, *i.e.* at the BCP electron accumulation occurs. Conversely for a positive sign(λ_2)ρ, Figure 4.8 region B, the interaction is a repulsive interaction and destabilizing as is expected for RCPs and CCPs [43], due to electron density depletion found there. In this manner similar information to that obtained with an AIMS analysis concerning bonding can be extracted using NCI. The throughs corresponding to 'formal' covalent interactions are not depicted in this or subsequent NCI plots as these occur outside the electron density range scale used for non-covelent interactions, *i.e.* beyond a

electron density of 0.04 au at the BCP or interaction RDG minimum. For several van der Waals interactions the RDG does not tend to zero, and hence QTAIM does not identify a BCP, RCP or CCP. However, the electron density topology is qualitatively the same as would be the case for a BCP, Figure 4.8 region C. Analysis of the the B2 conformers' electron density topology via the NCI index, in regions where the RDG does not tend to zero, grants further insight of electronic stabilization or destabilization. These regions, Figure 4.8 A to C, can be mapped on a three dimensional isosurface, *e.g.* Figure 4.9 a and Figure 4.10, where red and blue regions refer to attractive and repulsive interactions respectively.

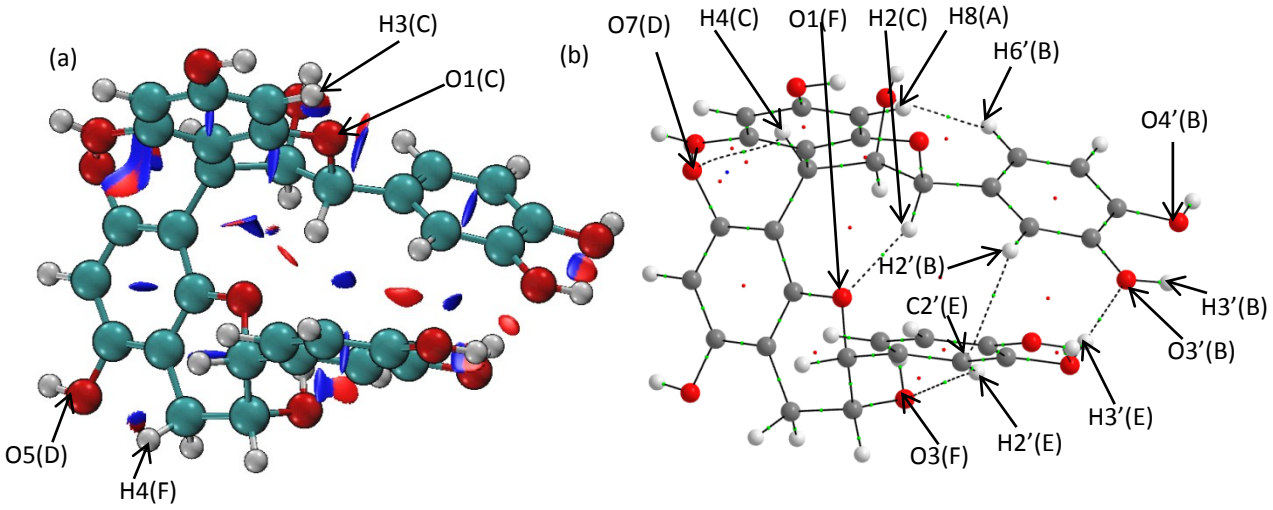

Figure 4.9. Comparison of (a) NCI isosurfaces (isovalue=0.4 showing positive λ_2 as blue and negative as red) with (b) QTAIM interactions for the FC conformer of procyanidin B2 in the gas phase as calculated using B3LYP/6-311++g**

To compare the QTAIM and NCI analyses, the molecular graph (including the BCPs, RCPs and CCPs) and the NCI isosurface plot for the FC conformer is illustrated in Figure 4.9. The corresponding FC conformer RDG versus sign(λ_2) is shown in Figure 4.8. To generate the NCI isosurface plot, the RDG value is set to a maximum of 0.4 and the x-axis range, *i.e.* sign(λ_2), was taken in the electron density region of -0.04 to 0.04, as illustrated in Figure 4.9 a. The blue regions on the isosurfaces correspond to negative sign(λ_2) values and indicate repulsive interactions and the red regions refer to, positive sign(λ_2), attractive regions. The throughs, Figure 4.8 a, that tend towards a RDG of zero correspond to to the BCPs' electron density found with QTAIM, Figure 4.5. The other set of throughs, Figure 4.8 b, corresponds with the RCPs' and CCPs' electron density. The magnitude of the electron density at the

throughs are associated with the strength, destabilizing or stabilizing, of the non-covalent interactions, *e.g.* the O1(F) – H2(C) hydrogen bond being the highest electron density interaction for the FC conformer. In Figure 4.9 the O7(D)-H4(C), O1(F)-H2(C),O3'(B)-H3'(E) and O3(F)-H2'(E) interactions are found by both the NCI and QTAIM analyses. Also, the H8(A) to H6'(C) interaction is shown for both analyses along with the H2'(B) and C2'(E) interaction. However, the H4(F) to O5(D) interaction does not tend to 0 on the NCIplot and consequently does not appear in the AIMS analysis. Steric strain caused by the formation of a ring critical point, seen in Figure 4.9 a as a blue isosurface region, in close proximity to the interaction prevents the formation of a zero RDG value. However, the interaction will still affect the electronic stability of the molecule. One other such interaction is seen between H3(C) and O1(C) and will also have an effect on the electronic stability of the conformation. It is difficult to quantify the effect of these interactions as the destabilization effect of the ring formed may or may not be larger than that of the hydrogen bond's electronic stabilization. In the relatively low electron density range, Figure 4.8 region c, we obtain two relatively weak attractive and repulsive interactions.

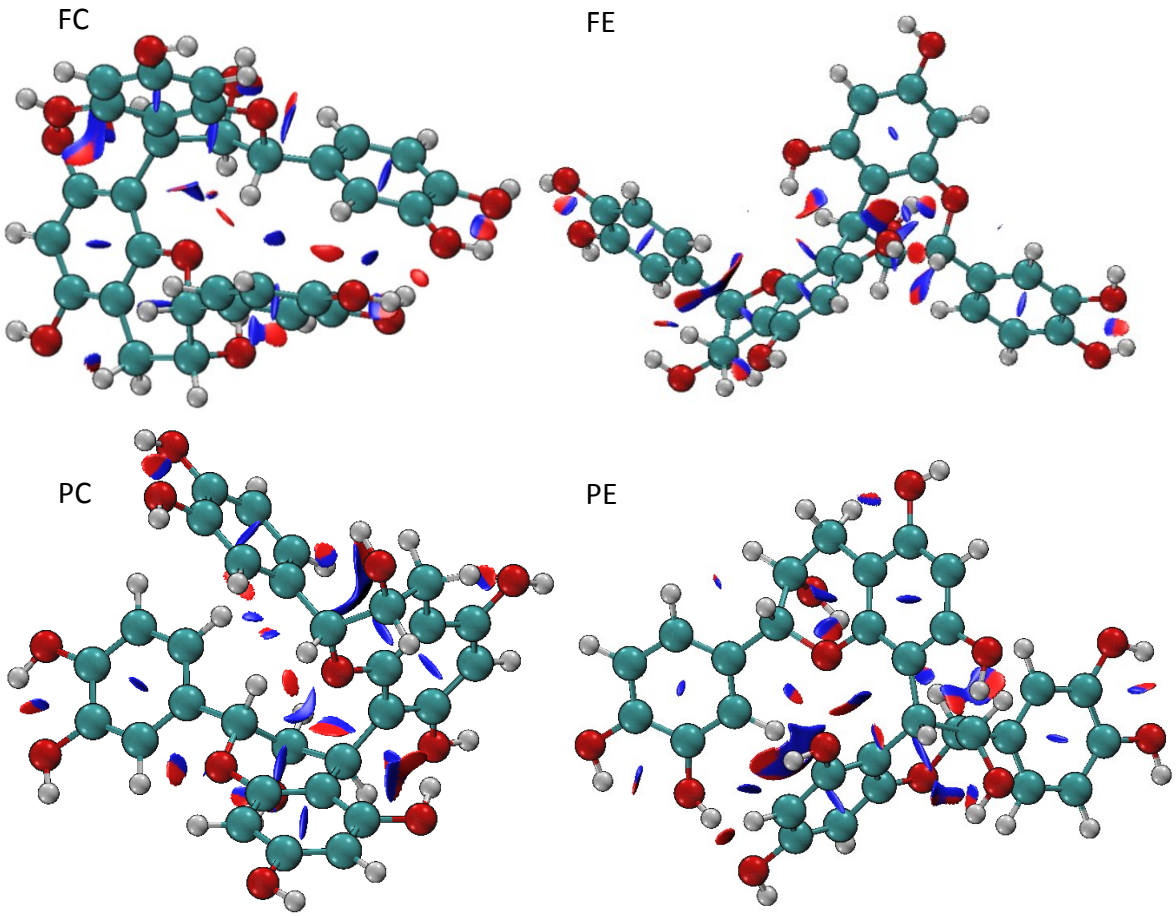

Figure 4.10. Ball and stick representations of procyanidin B2 conformers' non-covalent interaction isosurfaces (RDG iso-value = 0.4) showing positive λ_2 in blue and negative λ_2 in red as calculated using B3LYP/6-311++g**

The ball and stick representations of the NCI isosurfaces for all the procyanidin B2 conformers were generated in Visual Molecular Dynamics (VMD) at a RDG isovalue of 0.4 and colored according to the sign of λ_2 values (positive is red and negative is blue), Figure 4.10. From the ball and stick representation NCI isosurfaces it is observed that the attractive interactions form a web that surrounds areas of steric hindrance that are either true CCPs and RCPs (as defined in QTAIM) or simply non-covalent positive λ_2 steric interactions where the RDG does not tend to zero. It can be observed that there are more repulsive interactions and attractive interactions in total in the FC and PE conformations than seen in the FE and PC conformers.

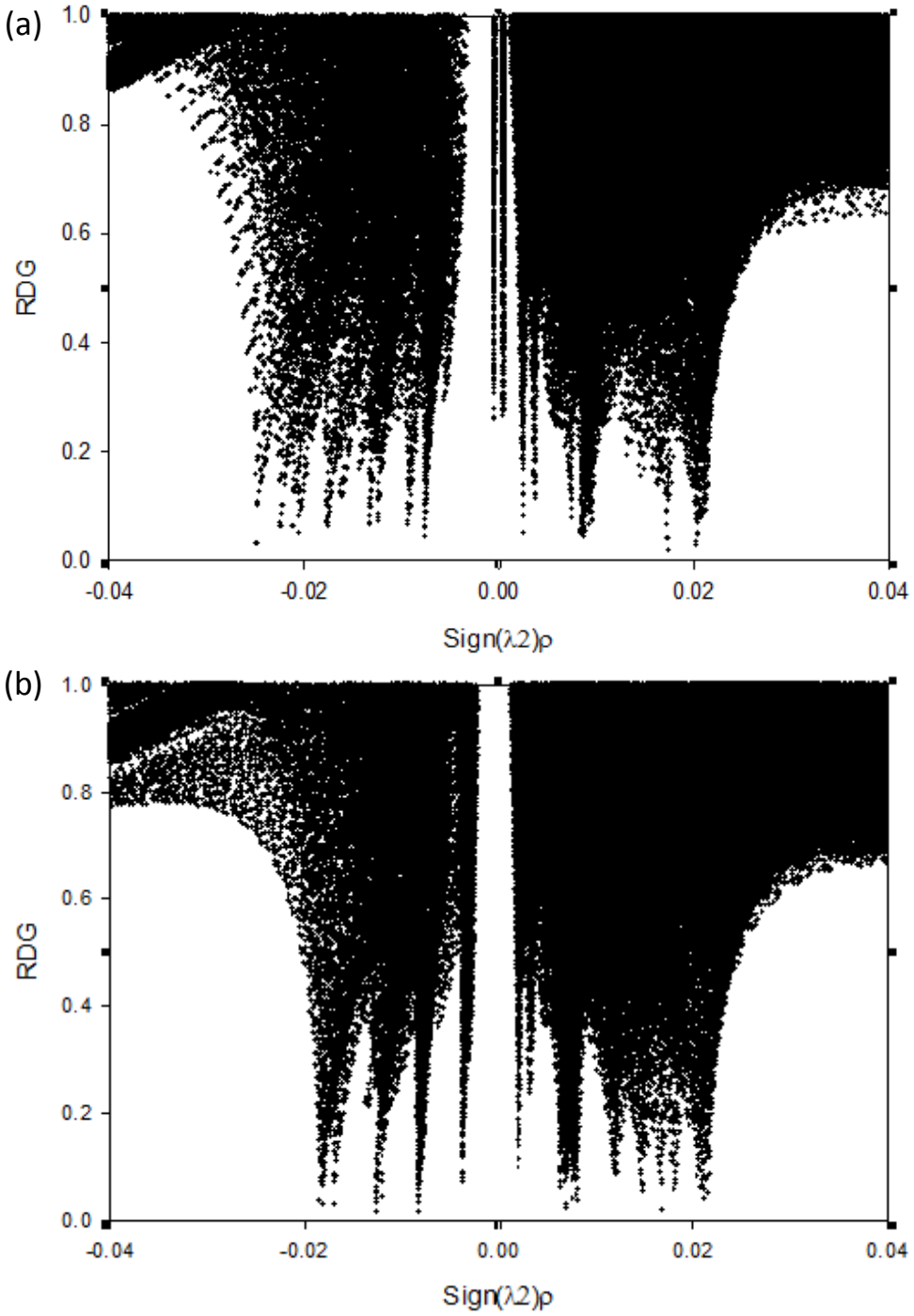

Figure 4.11. NCIplot of the B2 (a) fully compact and (b) partially compact conformations of procyanidin B2 in the gas phase as calculated by B3LYP in G09 with the SCRF acetonitrile solvation model

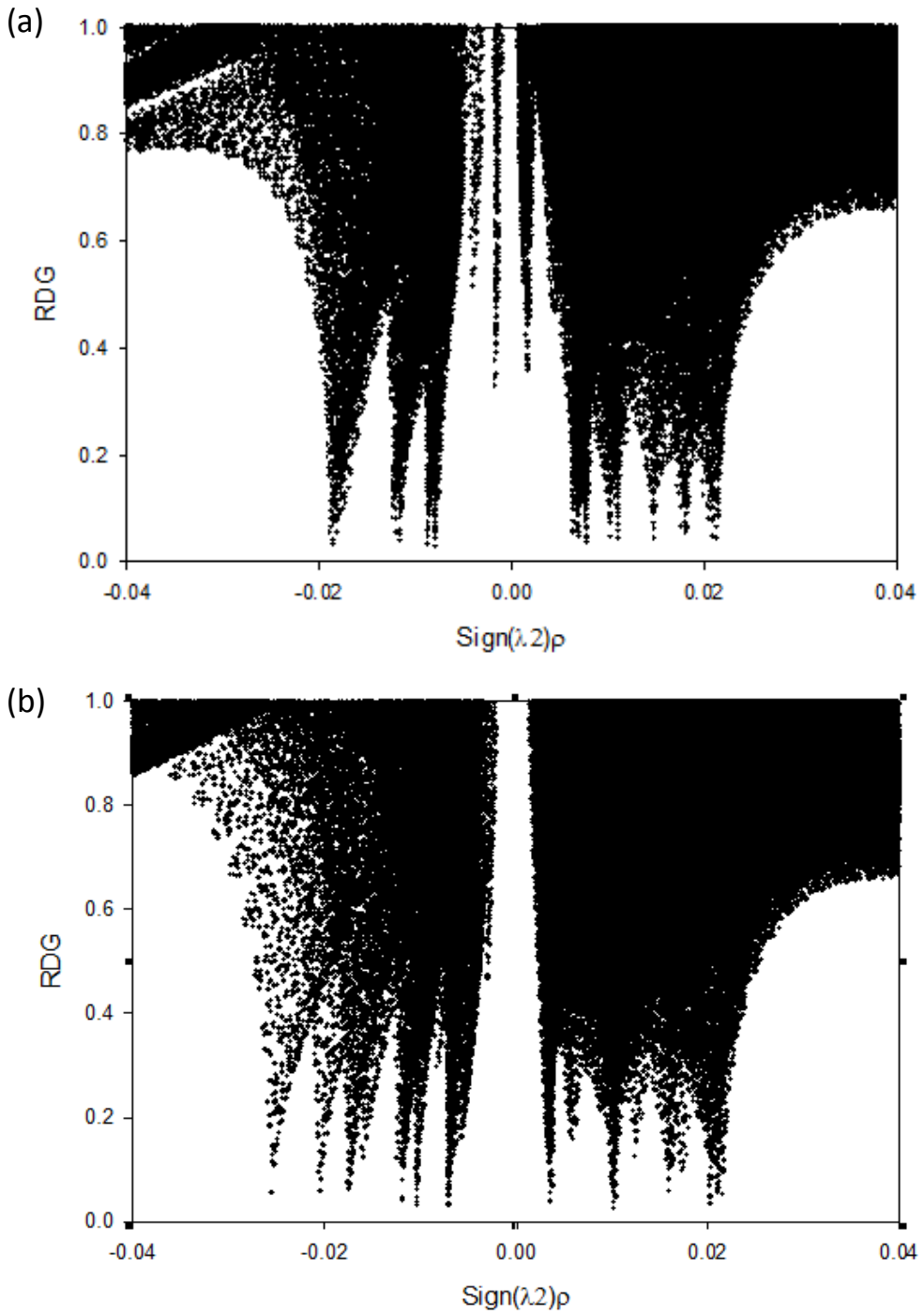

Figure 4.12. NCIplot of the B2 (a) fully extended and (b) partially extended conformations of procyanidin B2 as calculated by B3LYP in G09 with the SCRF acetonitrile solvation model

Another factor that needs to be taken into account for the conformer electronic energy heierarchy is the basis set superposition error (BSSE), by use of counterpoise corrections (CP). In order to calculate the BSSE, two or more fragments of the system must

be selected and then the single point energies of each fragment is calculated. The fragments for counterpoise correction calculations of the procyanidin B2 conformers were the monomers separated by the interflavanoid bond. The results obtained with B3LYP show that the BSSE does not vary significantly between all conformers, *i.e.* less than 2.7 kJ.mol^{-1}, Table 4.5.

Table 4.5. BSSE electronic energies calculated using the B3LYP/6-311++g** functional for procyanidin B2 in gas phase

	B3LYP BSSE (kJ.mol^{-1})	**Counterpoise corrected conformational conformational interchange reaction electronic energy (kJ.mol^{-1}) relative to the PC conformer**
Fully compact	14.84	-7.39
Partially compact	12.98	0
Partially extended	14.36	13.49
Fully extended	11.17	3.02

Moreover, the BSSEs that are listed in Table 4.5 don't change the order of conformer electronic stability, Figure 4.2. The result of the counterpoise correction calculations shows that the BSSE, although very pronounced, does not differ significantly between conformers. It was expected that, if the BSSEs are significant for this system, the BSSE for the FC conformer should be much larger than the FE conformer, where the monomeric units interacts the least. Therefore, BSSEs were not taken into account for subsequent thermodynamic analysis.

4.2.2 Thermodynamic Stability Of Procyanidin B2 Conformers In The Gas Phase

The electronic energies have been shown to consistently favour the FC conformer above the PC and FE conformers and finally the PE conformer, in order of electronic energy hierarchy. However, after taking the entropy and ZPE contributions into account, obtained from the frequency calculations, it was found that the PBE and B3LYP functionals predict that the PC conformer has the lowest relative standard reaction Gibbs free energy. The $\Delta \boldsymbol{G}^{\boldsymbol{0}}_{\boldsymbol{rxn}}$ in Table 4.6 refers to the equilibrium as written in Reaction scheme 4.1.

$$PC \underset{k_{-1}}{\overset{k_1}{\rightleftharpoons}} M \; ; \; M = FC, FE \; or \; PE$$

Reaction scheme 4.1. Conformational interchange reaction relative to the PC conformer

Table 4.6. Relative standard reaction Gibbs free energies for conformers of procyanidin B2 in the gas phase relative to the PC conformer calculated by various functionals and the 6-311++g** basis set

	PBE		PBE-D2		B3LYP	
	ΔG^0_{rxn} (kJ.mol^{-1})	abundance	ΔG^0_{rxn} (kJ.mol^{-1})	abundance	ΔG^0_{rxn} (kJ.mol^{-1})	abundance
fully compact	5.1	9.38%	-5.2	89.45%	6.5	5.60%
partially extended	13.0	0.34%	18.5	0.00%	21.8	0.00%
fully extended	4.2	13.54%	10.9	0.11%	5.0	10.50%
Partially compact	0	76.75%	0	10.44%	0	83.80%

The ΔG^0_{rxn} shown in Table 4.6 don't agree with the trends expected from the electronic stabilizations. By insecting the values calculated, it is apparent that the lowest energy conformer using the PBE and B3LYP functionals is the PC conformer and the second lowest is the FE conformer. In contrast the FC conformer is the most stable conformer when the calculation includes the Grimme D2 dispersion to the PBE functional. The difference in standard reaction Gibbs free energy is not large enough for the FC conformer to have a negligible abundance and would lead to three conformations being visible in NMR. In solvent phase, water and acetonitrile, it was experimentally observed that only two conformations are present in appreciable abundances. If the solvation of the molecules influences the conformational energies in such a way, the conformations may have completely different equilibrium distributions in solvent phase. It appears that only two conformations appear on the VT ^{1}H NMR spectra in solvent phase due to the solvent effects. This would explain that no previous literature have observed more than two conformations. The complete reaction scheme is shown in Reaction scheme 4.2.

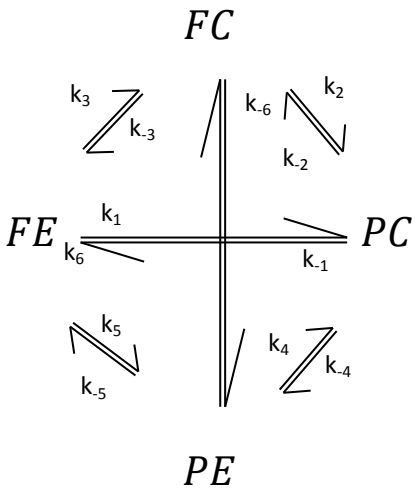

Reaction scheme 4.2. Conformational interchange of the four conformations

From the gas phase relative electronic energies it appears that FC and PC are more electronically stabilized structures than the FE and PE conformers. By looking at the calculations done with the B3LYP functional for the potential energy surface, the electronic energy clearly shows that the FC and PE structures are the lowest points on the surface, but the geometrically reoptimized structures at the PBE/6-311++g** level of theory shows that the PC conformer is electronically more stabilizaed that the FE conformer. The rationale for conformational stability used in procyanidin conformational literature (all done by MM) is that electronic stabilizing interactions, intramolecular hydrogen and π-π bonding, are the determining factor [27, 29]. Using these intramolecular stabilizing interactions as the primary reason for conformational stability, it has been rationalized that the compact structure must be the most stable. However, these conclusions have been made on the basis of MM calculated conformational geometries and energies that do not incorporate electronic interactions, beyond Leonard Jones potentials, into the model. Indeed, the same literature source also stated that the discrepancy between experimental and theoretical values may be due to a inability molecular mechanics models to calculate hydrogen bonds and other interactions [27]. The internal stabilization of the molecules as calculated from DFT is consequently of great interest in determining the effect of electronic interaction on conformational stability. The DFT calculation results show that four conformers exist instead of the two conformers predicted by MM and the MM conformations' geometries do not correspond to any of the DFT conformations' geometries. Moreover, the standard reaction

Gibbs free energies calculated by DFT show that the entropy controbution is essential when considering thermodynamic stability hierarchy. The effects of solvation on the thermodynamic stability hierarchy must also be investigated, as suggested by Terascou *et al.* [27] in hope of better modeling the two conformer system observed in experiment.

Conclusion

The PES of the dihedral angle of the procyanidin B2 molecule has allowed for the determination of four stable conformers in the gas phase, which have been re-optimized in a higher level basis set (6-311++g**) and the PBE, PBE-D2 and B3LYP functionals. Subsequent frequency calcualtions have confirmed that these conformers are equilibrium geometries. QTAIM analysis has been implemented in investigation of the intramolecular interactions formed by each conformation for the rationalization of the electronic and thermodynamic stability hierarchy. The conformations have been electronically ranked as FC>PC>FE>PE for all functionals, but the Gibbs free energy hierarchy has been shown to vary according to functional in the gas phase. The gas phase calculations can not be compared the the equilibrium constants determined in ^{1}H NMR experiments and solvation effects must be studied computationally in order to determine which of the four conformers are the minor and major conformers detected in NMR.

Chapter 5. Solvation Effects on Procyanidin B2

5.1 Introduction

Two procyanidin B2 conformers were found in a relative abundance 3:1 in acetonitrile-D_3 at 303 K by ^{1}H NMR. Subsequent DFT conformational analysis of procyanidin B2 in the gas phase revealed a set of minima on the potential energy surface with respect to rotation about the interflavanoid bond dihedral. It was found that the PC conformer is thermodynamically the most favourable in the gas phase, followed by the FE conformer with the PE and FC conformations the least stable as obtained with the PBE and B3LYP functionals. With the addition of the Grimme D2 dispersion correction the thermodynamic stability hierarchy is FC>PC>FE>PE in gas phase. However, the DFT analysis in the gas phase with the B3LYP and PBE functionals yields conformer abundances that suggest four conformers should be detectable in appreciable abundance via ^{1}H NMR, in contrast to our NMR results.

Procyanidin B2 contains several polar hydroxyl groups and regions where non-polar interactions can occur. The effect of solvation/hydration may then largely influence the thermodynamic stability order of the four B2 conformers found by a DFT analysis in the gas phase. Experimental evidence that illustrates how conformer abundances are drastically influenced by the solvent is clear when comparing the study reported Terascou *et al.* [27] where the conformers of procyanidin B2 were in an approximate 1:1 ratio in water, to the 3:1 ratio found in acetonitrile. In the book written by Cramer [68] it is eloquently illustrated that the electronic PES can significantly change when solvation effects are also taken into account.

Computational methods that take solvation into account can be split into two groups, namely explicit and implicit models. The explicit models consider a “large” number of solvent molecules “placed” around the analyte of interest. Several approaches can then be applied (molecular dynamic molecular mechanics (MD-MM), molecular dynamic quantum mechanics (MD-QM)) that differ in complexity and resource demand and are beyond the ambit of this study [68]. The computational efficiency of the implicit solvation approaches makes this method of great value for the estimation of solvation energies. The

charge distribution of the analyte immersed in a solvent will change upon interaction with the solvent. With a continuum model the charge distribution of the solvent is replaced by a continuous dielectric field. This field around the solute is called the 'reaction field' as it determines the interaction between the solute and the solvent, while the gradient of the electrostatic potential (Ø) at a point in space is equal to the electric field. The work necessary to induce the charge distribution can be calculated from the interaction of the solute charge density (ρ) with the electrostatic potential using equation 5.1.

$$G = -\frac{1}{2}\int \rho(\bar{r})\emptyset(\bar{r})d\bar{r} \tag{5.1}$$

The difference in the work of charging a solute in the solution and in the gas phase is equal to the polarization energy, G_p. Moreover, all that is required is the electrostatic potential in solution and in the gas phase to calculate the polarization energy [40, 69]. It is of some concern that continuum models do not, in some cases, sufficiently take specific interactions between the solvent and the solute into account, *e.g.* intermolecular hydrogen bonding.

In recent years a statistical mechanical theory of molecular solvation, namely the three dimensional reference interaction site model (3DRISM) was introduced [70]. This approach yields the radial pair distribution functions between atomic sites, akin to molecular dynamic simulations, and in this way can account for specific intermolecular interactions. The 3DRISM formalism uses molecular mechanics Leonard-Jones parameters for the solvent and treats the analyte using DFT in a self-consistent field calculation. The DFT part of the calculation can be replaced by *ab initio* methods, e.g. CASSCF as done by Sato *et al.* [70]. The aim of this chapter is to investigate whether solvation effets will change the order of the predicted conformer thermodynamic stability compared to that found with the gas phase DFT calculations.

5.2 Electrostatic Surface Potentials (ESP)

The electrostatic surface potentials, as discussed in chapter 1, allow for the identification of charge polarization and consequently likely sites for intramolecular and intermolecular interactions. From the ESP of the FC conformation of procyanidin B2 in the gas phase, shown in Figure 5.1, it can be observed that there are several regions of negative

charge polarization on the oxygen atoms of the hydroxyl moieties. On the other hand, the hydroxyl hydrogen atoms are positively polarized and will be able to experience Keesom forces when near the polarized oxygen atoms. Similarly, the oxygen atoms that are interacting with other moieties migrate some of their electron density towards those interactions and thereby have a more dispersed negative charge accumulation than if they had not formed said interactions. The reduction in charge polarization intensity can be seen by comparing the O4'(E) with the O3'(E) and the O3'(B) oxygen atoms on Figure 5.1. The self consistent field (SCF) potential on O4'(E) has a maximum around 0, while the O3'(E) and O3'(B) oxygen atoms, that do form interactions with the proximate hydrogen atoms of the nearby hydroxyls moieties, only have SCF potentials of around 0.04. The reduction of the SCF field intensity at these regions should correspond to a reduction in the SCRF reaction field intensity and consequently a less stabilizing solvation energy.

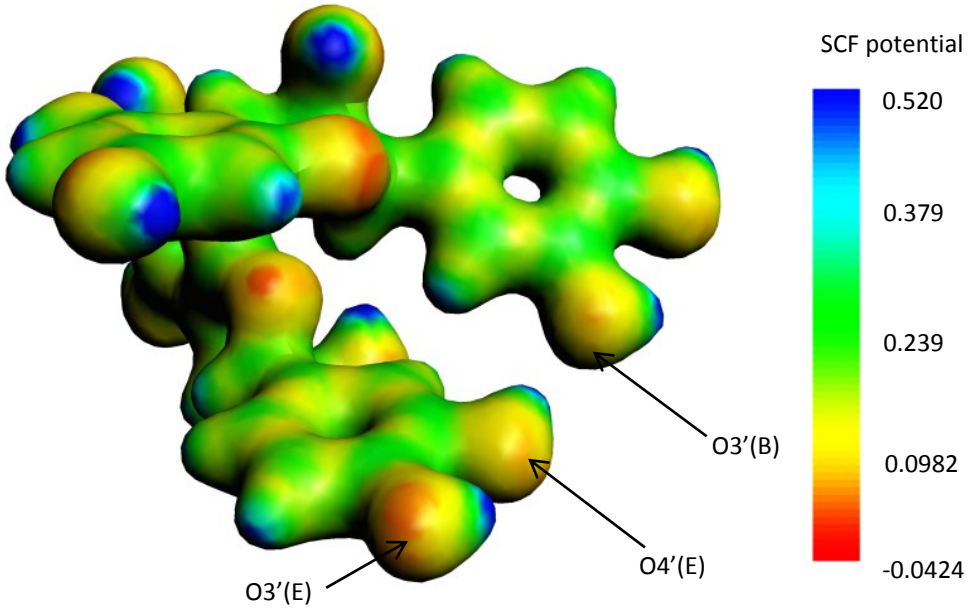

Figure 5.1. Electrostatic surface potential of the fully compact conformer of procyanidin B2 as calculated by PBE/TZ2P in the gash phase with the ADF suite (electron density isovalue=0.03)

The hydroxyl hydrogen atoms have their electrons withdrawn by their respective covalent bond sharing oxygen atoms and consequently have more pronounced positive charge. The hydrogen atoms covalently bonded to oxygen atoms will therefore have larger attractive forces, and consequently higher interaction energies, than their carbon bonded counterparts with negatively polarized groups like other oxygen atoms within the

procyanidin molecule, polarized solvent molecules or negatively charged molecules. However, the principal deduction made from Figure 4.14 is that the hydroxyl O's and H's that do form intramolecular interactions will have less pronounced charge accumulation than their non-interacting counterparts and as a result the more internally electronically stabilized conformers should be less available for polar solvent interaction.

5.3 Implicit Solvation Effects Using the Self Consistent Reaction Field (SCRF)

The four conformers found in the gas phase, from the PES, were re-optimized in G09 (revision B0.1) using the SCRF implicit model in water, acetonitrile and hexane. In all cases frequency calculations were done on the re-optimized structures in the relavant SCRF model to ensure that the optimized structures were indeed minima on the PES. Tables 5.1 to 5.3 list the chosen metric parameters for comparison between gas phase (Table 4.1) and SCRF optimized geometries. The geometry optimization calculations using the PBE-D2 functional rotated the dihedral angle of the FC conformer's interflavanoid bond consistently by approximately 30 degrees with respect to the PBE and B3LYP calculated geometries, in gas phase as well as in all SCRF solvent phases implemented. However, all the other metrics employed, including the position of the herocyclic rings and the bond and interatomic distances, do not change enough between calculated geometries using the different functionals to justify a dinstinction of a new conformation. In fact, the addition of the SCRF solvation model to the calculation does not alter the dihedral angle of the interflavanoid bond appreciably between different solvents. Additionally, inclusion of the SCRF model to the calculation consistently shortens the O1(F) - H2(C) calculated distance with decreasing solvent polarity but has a nearly negligible effect on the interflavanoid bond length. The heterocyclic rings' hydroxyl moiety positions remain the same for the conformers with all functionals and SCRF solvent models.

Table 5.1. Geometry metrics for comparison of procyanidin B2 conformers as calculated in SCRF water solvent using various functionals with the 6-311++g** basis set in G09 revision B0.1

	Conformer	dihedral angle	heterocyclic C ring OH position	heterocyclic F ring OH position	interflavanoid bond length (Å)	O1(F) - H2(C) (Å)
Water	**B3LYP**					
	Fully compact	61.74	quasi-axial	quasi-axial	1.537	2.051
	Partially extended	107.27	quasi-axial	quasi-axial	1.534	3.099
	Fully extended	-85.96	quasi-axial	quasi-equitorial	1.532	4.747
	Partially compact	90.24	quasi-axial	quasi-equitorial	1.532	2.412
	PBE					
	Fully compact	61.38	quasi-axial	quasi-axial	1.536	2.028
	Partially extended	107.82	quasi-axial	quasi-axial	1.531	3.088
	Fully extended	-87.32	quasi-axial	quasi-equitorial	1.530	4.801
	Partially compact	89.57	quasi-axial	quasi-equitorial	1.530	2.389
	PBE-D2					
	Fully compact	87.40	quasi-axial	quasi-axial	1.528	2.076
	Partially extended	107.62	quasi-axial	quasi-axial	1.525	2.971
	Fully extended	-86.90	quasi-axial	quasi-equitorial	1.526	4.700
	Partially compact	87.60	quasi-axial	quasi-equitorial	1.528	2.245

Table 5.2. Geometry metrics for comparison of procyanidin B2 conformers as calculated in SCRF acetonitrile solvent using various functionals with the 6-311++g** basis set in G09 revision B0.1

	Conformer	dihedral angle	heterocyclic C ring OH position	heterocyclic F ring OH position	interflavanoid bond length (Å)	O1(F) - H2(C) (Å)
Acetonitrile	**B3LYP**					
	Fully compact	61.81	quasi-axial	quasi-axial	1.537	2.050
	Partially extended	107.28	quasi-axial	quasi-axial	1.534	3.098
	Fully extended	-86.00	quasi-axial	quasi-equitorial	1.532	4.750
	Partially compact	90.19	quasi-axial	quasi-equitorial	1.532	2.412
	PBE					
	Fully compact	61.38	quasi-axial	quasi-axial	1.536	2.028
	Partially extended	108.53	quasi-axial	quasi-axial	1.531	3.132
	Fully extended	-87.28	quasi-axial	quasi-equitorial	1.530	4.800
	Partially compact	89.53	quasi-axial	quasi-equitorial	1.530	2.386
	PBE-D2					
	Fully compact	89.46	quasi-axial	quasi-axial	1.528	2.078
	Partially extended	107.69	quasi-axial	quasi-axial	1.525	2.973
	Fully extended	-86.86	quasi-axial	quasi-equitorial	1.526	4.700
	Partially compact	87.61	quasi-axial	quasi-equitorial	1.530	2.244

Table 5.3. Geometry metrics for comparison of procyanidin B2 conformers as calculated in SCRF hexane solvent using various functionals with the 6-311++g** basis set in G09 revision B0.1

	Conformer	dihedral angle	heterocyclic C ring OH position	heterocyclic F ring OH position	interflavanoid bond length (Å)	O1(F) - H2(C) (Å)
Hexane	**B3LYP**					
	Fully compact	61.63	quasi-axial	quasi-axial	1.537	2.042
	Partially extended	108.20	quasi-axial	quasi-axial	1.532	3.113
	Fully extended	-85.15	quasi-axial	quasi-equitorial	1.533	4.714
	Partially compact	89.98	quasi-axial	quasi-equitorial	1.533	2.389
	PBE					
	Fully compact	61.41	quasi-axial	quasi-axial	1.536	2.017
	Partially extended	109.03	quasi-axial	quasi-axial	1.529	3.129
	Fully extended	-85.39	quasi-axial	quasi-equitorial	1.531	4.755
	Partially compact	90.40	quasi-axial	quasi-equitorial	1.531	2.354
	PBE-D2					
	Fully compact	89.27	quasi-axial	quasi-axial	1.527	2.071
	Partially extended	108.66	quasi-axial	quasi-axial	1.525	3.034
	Fully extended	-85.62	quasi-axial	quasi-equitorial	1.527	4.666
	Partially compact	89.97	quasi-axial	quasi-equitorial	1.528	2.254

QTAIM analysis of the conformations calculated with the SCRF models were also conducted. The geometries of the reoptimized structures remain largely the same as their gas phase calculated counterparts, as indicated in the metric tables, Tables 5.1 to 5.3. Moreover, the results of the QTAIM analysis, added in the supplementary DVD in the SupBCP.xlsx file, do not show significant deviance from the results obtained for the gas phase analysis. The inclusion of the QTAIM results has been disregarded in this text to avoid tedium. Similarly, the NCIplots are added in the supplementary DVD as they do not yield significant further insights here.

The SCRF implicit solvation model allows for easy comparison of the electronic energies and standard Gibbs free energies of reaction in different solvent systems [69]. The energy differences between conformers in Tables 5.4 to 5.6 refer to the conformational interchange reaction between the PC conformer and the three other conformers, Reaction scheme 5.1.

$$PC \rightleftharpoons M;\ (where\ M = FC, PE, FE)$$

Reaction scheme 5.1. Conformational interchange reaction relative to the PC conformer

The procyanidin molecules interact readily with the solvents due to the polar nature of their hydroxyl moieties [27]. The interaction with solvent can be confirmed from the OH moieties' reaction with residual water in the solvent observed in the NMR experiments discussed in chapter 3. It is evident that the PC conformer remains the primary conformer throughout the solvent systems for all functionals and that FE remains the second most abundant conformer. It is also evident that the conformational abundance ratio between the minor and major conformer approaches 1:1 as the polarity is increased. The FE conformer is a far more geometrically accessible for the solvent than the PC conformer and consequently higher polarity favours the FE conformer due the higher amount of solvation sites available to interact with the solvent.

A comparison of the electrostatic surface potentials calculated with and without the implicit water solvent model, Figure 5.2, shows that there is relatively small effect on the charge polarization when using an implicit solvent model. Slight variation in the electron density isosurface seen at the interaction between the H3(E) and O4(B) atoms, which has an electron density above the iso-value, for the water COSMO model PE conformer isosurface is observed. However, the intensities of the charge dipolarization on the oxygen and hydrogen atoms do not clearly change between gas phase and solvent model PESs. However, the solvation energy is more affected by the dielectric constant used in the SCRF model.

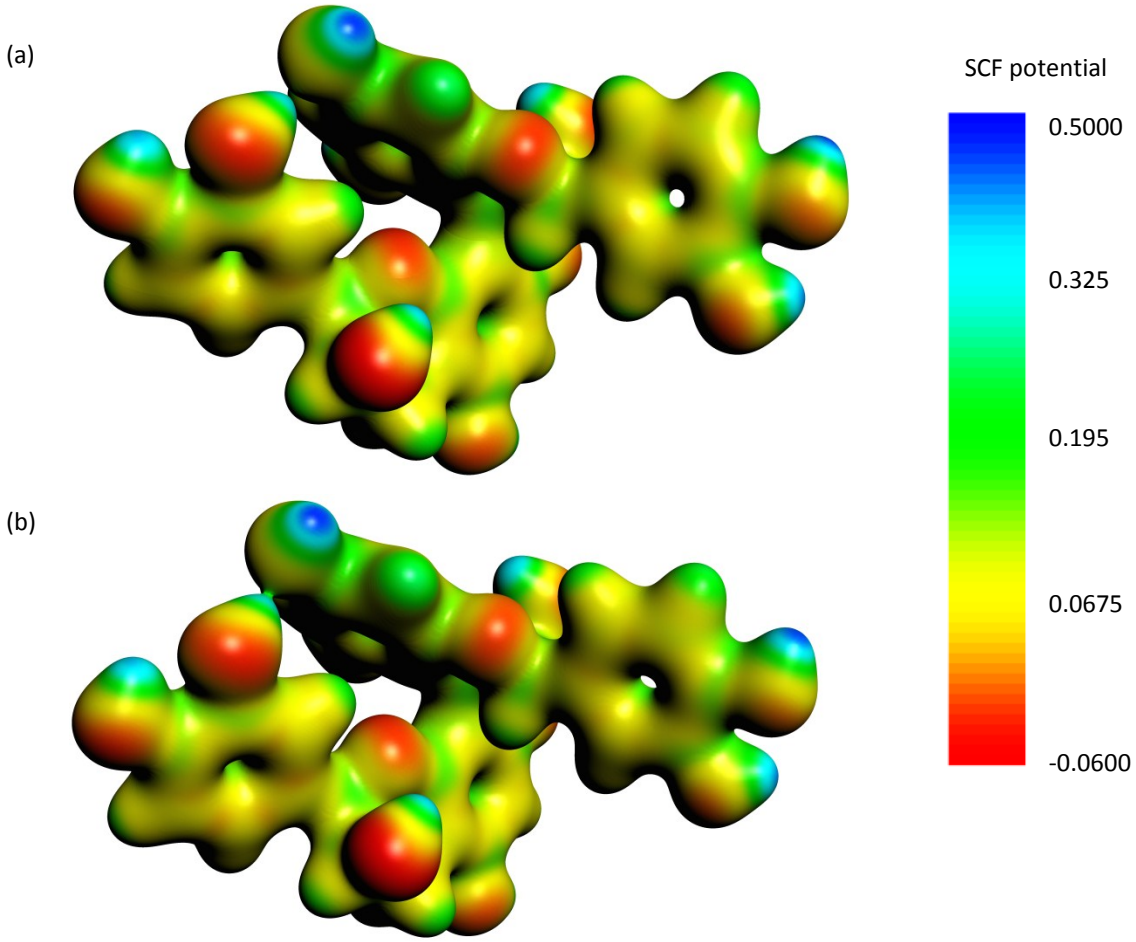

Figure 5.2. Comparison of the electrostatic surface potential of the PE conformer of procyanidin B2 in (a) gas phase and (b) COSMO water implicit solvent model calculated in ADF using the PBE/TZ2P functional

Table 5.4. Relative reaction energies (kJ.mol^{-1}) of interconversion from the PC conformer to the respective product conformers as calculated in various SCRF solvation models using the B3LYP/6-311++g** functional with the solvation Gibbs free energies at 298 K calculated by the difference between the gas phase and SCRF phase conformers' various energies 298 K

Conformer	ΔH^{o}_{rxn}	ΔG^{o}_{rxn}	$\Delta G^{o}_{SCRF}-\Delta G^{o}_{vac}$	%abundance	$T\Delta S^{o}_{rxn}$
Water					
Fully compact	8.67	21.04	-92.82	0.90%	12.28
Partially extended	16.10	24.37	-104.81	0.00%	6.67
Fully extended	5.42	3.93	-108.43	23.60%	-1.83
Partially compact	0	0	-107.37	75.50%	0
Acetonitrile					
Fully compact	8.11	20.07	-90.01	0.00%	11.96
Partially extended	15.87	23.62	-101.79	0.00%	7.74
Fully extended	5.34	3.86	-104.72	16.70%	-1.48
Partially compact	0	0	-103.6	83.30%	0
Hexane					
Fully compact	-1.58	10.69	-30.55	0.00%	12.38
Partially extended	12.18	18.85	-37.71	0.00%	8.27
Fully extended	4.63	2.80	-36.94	16.30%	-1.49
Partially compact	0	0	-34.75	83.70%	0
Vacuum					
Fully compact	-7.26	6.49		5.60%	13.75
Partially extended	12.35	21.81		0.00%	9.46
Fully extended	4.49	4.99		10.50%	0.5
Partially compact	0	0		83.80%	0

Table 5.5. Relative reaction energies (kJ.mol^{-1}) of interconversion from the PC conformer to the respective product conformers as calculated in various SCRF solvation models using the PBE/6-311++g** functional with the solvation Gibbs free energies at 298 K calculated by the difference between the gas phase and SCRF phase conformers' Gibbs free energies at 298 K

Conformer	ΔH^{o}_{rxn}	ΔG^{o}_{rxn}	ΔG^{o}_{SCRF}-ΔG^{o}_{vac}	%abundance	$T\Delta S^{o}_{rxn}$
Water					
Fully compact	8.95	19.15	-91.32	0.03%	10.33
Partially extended	14.53	18.90	-99.56	0.00%	16.28
Fully extended	6.20	2.91	-106.67	29.91%	-4.17
Partially compact	0	0	-105.41	70.06%	0
Acetonitrile					
Fully compact	8.56	18.9	-88.68	0.03%	10.19
Partially extended	11.88	28.16	-87.41	0.03%	4.37
Fully extended	6.22	2.05	-104.65	22.95%	-3.29
Partially compact	0	0	-102.53	77.00%	0
Hexane					
Fully compact	-0.27	13.04	-30.14	9.38%	10.1
Partially extended	11.7	21.11	-30.06	0.34%	3.59
Fully extended	6.50	8.61	-33.7	13.54%	-2.84
Partially compact	0	0	-38.13	76.75%	0
Vacuum					
Fully compact	-5.05	5.05		0.43%	13.31
Partially extended	9.45	13.04		0.01%	9.41
Fully extended	7.01	4.17		2.70%	2.11
Partially compact	0	0		96.86%	0

Table 5.6. Relative reaction energies (kJ.mol^{-1}) of interconversion from the PC conformer to the respective product conformers as calculated in various SCRF solvation models using the PBE-D2/6-311++g** functional with the solvation Gibbs free energies at 298 K calculated by the difference between the gas phase and SCRF phase conformers' various energies at 298 K

Conformer	ΔH^o_{rxn}	ΔG^o_{rxn}	ΔG^o_{SCRF}-ΔG^o_{vac}	%abundance	$T\Delta S^o_{rxn}$
Water					
Fully compact	6.62	12.94	-87.28	0.41%	6.89
Partially extended	16.19	19.49	-104.37	0.02%	4.18
Fully extended	16.61	10.18	-106.14	0.87%	-5.35
Partially compact	0	0	-105.38	98.69%	0
Acetonitrile					
Fully compact	6.29	13.17	-84.72	0.45%	6.32
Partially extended	16.2	20.38	-101.15	0.03%	3.3
Fully extended	16.71	11.36	-102.64	1.42%	-6.43
Partially compact	0	0	-103.05	98.10%	0
Vacuum					
Fully compact	-8.83	-5.16		89.45%	3.67
Partially extended	17.27	18.48		0.00%	1.21
Fully extended	18.93	10.94		0.11%	-7.99
Partially compact	0	0		10.44%	0

Tables 5.4 to 5.6 list the energy differences of the standard reaction enthalpy (ΔH^o_{rxn}), standard reaction gibbs free energy (ΔG^o_{rxn}), temperature multiplied with the standard reaction entropy ($T\Delta S^o_{rxn}$) for the three functionals used as a function of the solvent polarity (water, acetonitrile, hexane and in the gas phase). In addition to these energy differences the calculated solvation/hydration contribution to ΔG^o_{rxn} is also listed as ΔG^o_{SCRF}-ΔG^o_{vac}. The difference ΔG^o_{SCRF}-ΔG^o_{vac} refers to a solvation reaction, Reaction scheme 5.2.

$$M(g) \rightleftharpoons M(solv) \quad ; \quad where\ M = FC, FE, PE\ or\ PC$$

Reaction scheme 5.2. Solvation reaction

The values ΔG^o_{SCRF}-ΔG^o_{vac} are obtained after performing single point and frequency calculations using G09 revision B0.1 for each conformer in both relevant phases. Several distinct trends are noticed in Tables 5.4 to 5.6. As the solvent polarity increases the electronic energy encapsulated in ΔH^o_{rxn} for the three conformers (FE, PE and FC) in general rise with respect to the PC conformer, *i.e.* the electronic stability of the FE, PE and FC

conformers decreases with respect to the PC conformer. The entropy contribution to thermodynamic stability is the highest for the FE conformer and lowest for the FC conformer. This trend is expected considering that the vibrational movement of atoms for the FC conformer must be more sterically hindered compared to the other conformers. The entropy contribution towards thermodynamic stability in all cases except the gas phase follows the order FE>PC>PE>FC. Sifting through 3N-6 (where N is the 68 nuclei in the molecule) vibrational frequencies to identify the higher energy vibrations and comparing them between the four conformers in the three solvent models and gas phase for three functionals is left for future work. The solvation energy decreases as expected as the polarity of the solvent decreases. A clear pattern of the solvation energy magnitude, for water and acetonitrile, is observed with respect to which conformer has the largest to smallest solvation energy, namely FE>PC>PE>FC. With the hexane SCRF solvation model the solvation energy hierarchy is inconsistent between the B3LYP and PBE functionals. The difference in solvation energy trends between the water, acetonitrile and hexane is probably due to the relatively low dielectric constant of hexane, indicating that the different (non-polar) parts of the molecule will now interact more strongly with the solvent. These solvation energy trends can be rationalized when considering that the extended conformers will form more interactions with the solvent "reaction field" and less intramolecular van der Waals interactions compared to the FC conformer.

Apart from the gas phase calculation using PBE-D2 functional, the PC conformer is found to be thermodynamically the most stable in gas and in solvent phases ranging from non-polar (hexane) to polar (water). Interestingly, the thermodynamic stability order of the conformers, PC>FE>FC>PE, remains the same in the gas phase and for the solvents for the PBE and B3LYP functionals. However, the FC and PE conformers' relative abundance, or thermodynamic stability, compared to the PC and FE conformers decreases dramatically as the polarity of the solvent increases. From our experimental work, chapter 2, and the results reported by Terascou *et al.* [27], the ratio of the main conformers found changes from 3:1 to 1:1 as the polarity of the solvent increases at 298 K. The DFT calculations mimics this trend where the amount of minor conformer (FE) increases relative to the major conformer (PC) from about 5% to 20-30% abundances for the PBE and B3LYP functionals. This is relatively close to the relative abundances experimentally found, ±25% at 298 K in

acetonitrile-D_3. For all three functionals the same order of thermodynamic stability are found. However, conformer abundances obtained with the PBE-D2 functional do not agree with experiment.

The DFT calculated equilibrium constants can be compared to the equilibrium constants determined from NMR experiments with the SCRF solvation models. The equilibrium constant for the conformational interchange reaction of the main conformers of procyanidin B2 in acetonitrile-D_3 at 298.15 K is 2.8 as determined from NMR conformational interchange reaction line shape analysis in chapter 3. The equilibrium constant calculated from DFT conformational interconversion between the lowest free energy conformers in SCRF acetonitrile is 2.318 with the PBE/6-311++g** functional and 4.877 with B3LYP/6-311++g** functional. It is clear that the D2 dispersion correction overestimates dispersion as the equilibrium constant calculated from the PBE-D2/6-311++g** functional data with the SCRF (acetonitrile) model is 105 for the same conformer's interconverstion reaction. However, the good agreement between experiment and the PBE and B3LYP equilibrium constants helps to validate that the two conformers experimentally observed (via ^{1}H and ^{13}C NMR) are the most probably PC (major) and FE (minor) conformers.

5.4 Three Dimensional Reference Interaction Site Model (3DRISM)

Specific solvation interaction effects, such as hydrogen bonding, can be estimated by the three dimensional reference interaction site model (3DRISM), which implements a MD solvation model by using a statistical MM calculation for the solvent and DFT for the analyte of interest [42]. The Leonard-Jones potentials implemented in the 3DRISM calculations were all sourced from the ADF manual and are indicated for each set of solvent groups in Table 5.7.

Table 5.7. 3DRISM solvent Leonard-Jones parameters and atomic carthesian spatial coordinates used

Molecular fragment	Z_α (a.u.)	σ_α (Å)	ε_α (kcal.mol^{-1})	X (Å)	Y (Å)	Z (Å)
			Acetonitrile			
CH3	0.269	3.6	0.38	-1.46	0	0
C	0.129	3.4	0.099	0	0	0
N	-0.398	3.3	0.099	-1.17	0	0
			Water			
H	0.4238	0.7	0.046	0.513	0.817	0
H	0.4238	0.7	0.046	0.513	-0.817	0
O	-0.8476	3.166	0.1554	-0.065	0	0
			Hexane			
C	0	3.8	0.294	-1.414	-2.904	0.000
				1.414	2.904	0.000
				1.414	1.373	0.000
				0.006	0.766	0.000
				-0.006	-0.766	0.000
				-1.414	-1.373	0.000
H	0	2.42	0.03	-1.963	-1.008	0.876
				-1.963	-1.008	-0.876
				-2.432	-3.305	0.000
				-0.901	-3.299	-0.883
				0.544	-1.132	-0.877
				-0.544	1.132	-0.877
				1.963	1.008	-0.876
				0.901	3.299	-0.883
				0.901	3.299	0.883
				2.432	3.305	0.000
				-0.544	1.132	0.877
				1.963	1.008	0.876
				0.544	-1.132	0.877
				-0.901	-3.299	0.883

The 3DRISM solvation energies obtained at PBE/TZ2P level of theory for the four B2 conformers are illustrated in Figure 5.3. The conformations used in the 3DRISM calculations were not re-optimized using 3DRISM, but re-optimized in gas phase using PBE/TZ2P in the ADF suite. The SCRF and 3DRISM calculations agree qualitatively that the PC and FE conformers are much more thermodynamically stabilized by solvation energy compared to the FC and PE conformers in all three of the modeled solvents. The variation in solvation energy from polar (water) to non-polar (n-hexane) is unexpectedly small when considering the large change in solvation energy between the more electronically stabilized conformers (PE and FC) and less electronically stabilized (FE and PC) conformers. Moreover, the 3DRISM

solvation energies are significantly larger than those found for the SCRF conformational energies for the PC and FE conformers. As solvent polarity increases, from both the 3DRISM and SCRF results, there is a clear trend towards higher thermodynamic stability due to a larger solvation Gibbs free energy. Moreover, the solvation energies for the PE and FC conformers are much lower than seen in the SCRF calculations. At this point we can't explain the large difference in the solvation energies of the FE and PC conformers in comparison to the FC and PE conformers, but ,qualitatively speaking, the 'large' solvation energies indicate that solvation energy plays a principal role in the conformational stability of procyanidin conformers. Moreover, an increase in solvent polarity increases the solvation energies, presumably due to intermolecular interactions with the polar hydroxyl moieties of the procyanidin conformers. As the solvent polarity is raised, conformations with less sterically restricted polar groups interact more readily with the polar solvent, thereby increasing solvation energy contribution to thermodynamic stabilization. However, the electronic stabilizations reduce the intensity of the charge polarization on the hydroxyl moieties by the electron density donation to the bonding interaction, as seen on the ESP of the FC conformer, Figure 4.14. It is clear from the electrostatic surface potentials in Figure 4.14 that the hydroxyl moieties are the main polar sites and are expected to be the interaction sites between the molecule and the solvent.

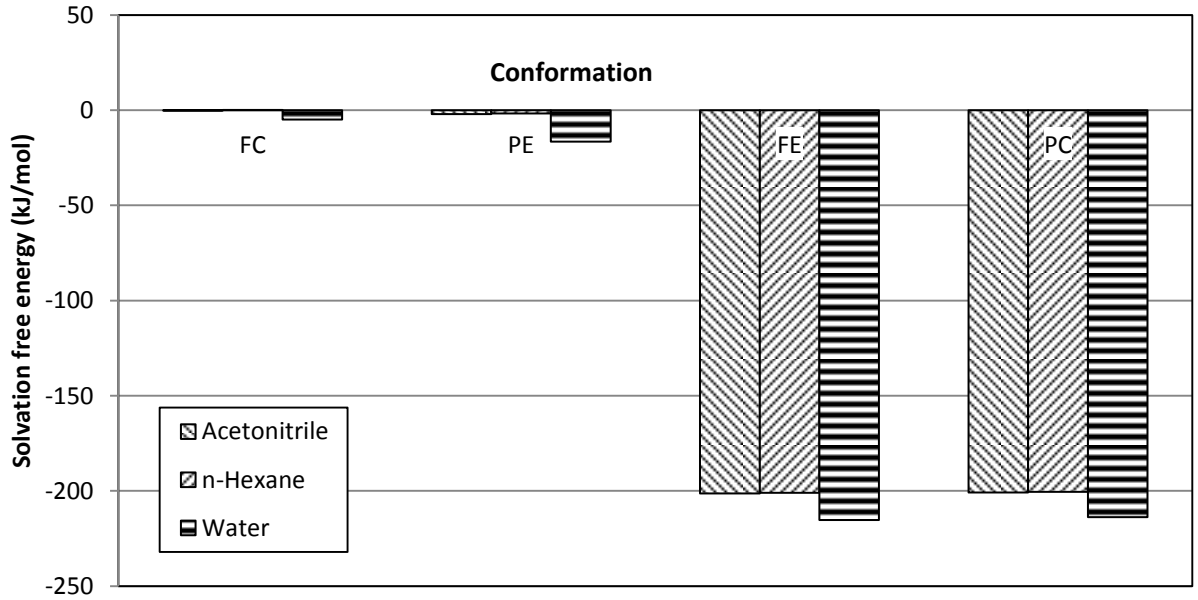

Figure 5.3. 3DRISM solvation energies of various procyanidin B2 conformers

3DRISM allows for the in-depth geometrical study of solvation sites in addition to the total average solvation energies of the conformers. From the radial distribution functions a probability density map can be generated that illustrates when it is most likely that *e.g.* a hydrogen to oxygen atom site-site interaction (using water as solvent) will be found around the analyte, thereby showing the most probable "solvation sites". The 3DRISM calculations also allow for the 3D topology of the interactions to be visualized as shown for two conformers in Figure 5.4.

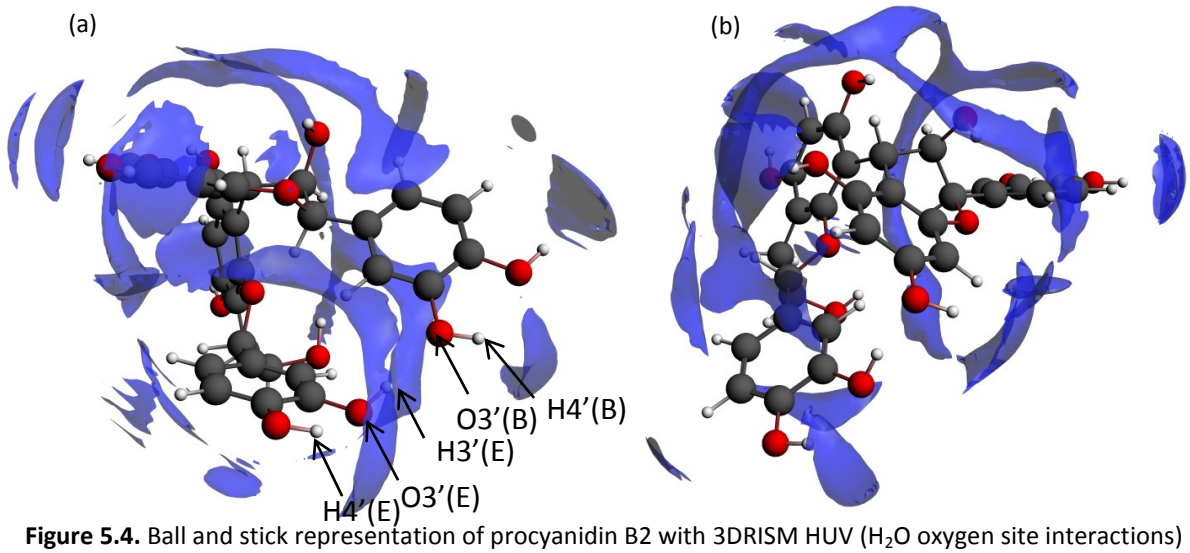

Figure 5.4. Ball and stick representation of procyanidin B2 with 3DRISM HUV (H_2O oxygen site interactions) isosurfaces taken at isovalue 1.5 for the (a) FC and (b) PE conformers

The remaining conformers' isosurfaces in the different solvents could not be visualized as seen in Figure 5.2 due to technical difficulties with the ADF suite. It was attempted to recalculate the 3DRISM solvation site-site interaction isosurfaces in ADF in order to visualize them in this way, but the difficulty persisted and the calculations would not write TAPE41 files for the isosurface visualizations. After persisting issues in the recalculation of the isosurfaces ADF support was queried. The ADF help team replied that the 3DRISM calculations are a specialist option and therefore are not directly supported by ADF. Consequently, the 3DRISM isosurfaces of the FE and PC conformers could not be analyzed for comparison with the FC and PE conformers. Nonetheless, the FC and PE 3DRISM isosurfaces will be discussed. Additionally, the XMU files that report the solvation energies were recalculated, written and reproducible.

It is hypothesized that the more "open" structure of the FE and PC conformations are much more available for these solvent interactions. It should be noted that many nucleophilic solvents will exchange protons with the hydroxyl moieties. However, the effects of deprotonation on solvation energy are beyond the scope of this study. Figure 5.5 shows the 3DRISM solvent hydrogen to procyanidin B2 interaction isosurface around the FC conformer for a water solvation model. The hydrogen atoms of the water solvent molecules have a high probability of being packed around the δ^- side of the hydroxyl moieties. Clustering of hydrogen interactions is also seen around the phenol rings and may be due to electron density accumulation above and below the rings. It should be noted that the isovalues for Figures 5.4 and 5.5 differ and that the interactions on Figure 5.5 are more probable. The hydrogen atoms of the water are therefore more likely to interact with the negative charge accumulations on the procyanidin B2 molecule than the water molecule's oxygen atom is to interact with the positive charge accumulations on the procyanidin B2 molecule. By comparing FC conformers' O4'(E) with O3'(E) it is clear from both the ESP and 3DRISM isosurface plots that the hydrogen bond formed between H4'(E) and O3'(E) reduces the charge accumulation around O3'(E) and consequently reduces the possibility for solvent interaction in comparison to O4'(E). The same reduction in solvation interaction as discussed for the solvent oxygen interactions can be seen for O4'(E) and O3'(E) with the solvent hydrogen interactions. Additionally, the O1(F) oxygen is sterically 'buried' within the molecule and is unavailable to solvation interactions. Although there are unexpected discrepencies in the energies of solvation, 3DRISM can still be used so analyze the sites for solvation. The excess chemical potential (refer to the attached DVD) of site-site interactions calculated by 3DRISM shows that, for water, both the oxygen and hydrogens have negative interaction energies and stabilize the solvation. Consequently the oxygen interaction sites are also of interest and are shown on the isosurface in Figure 5.5 to place preferentially around the oxygen atoms that do not form internal electronic interactions (*i.e*. have the most negatively charged electrostatic surfaces). The difference seen in the acetonitrile 3DRISM calculations is that, although the nitrogen group of the acetonitrile is a repulsive interaction (positive site-site interaction energy) for all conformers, the destabilization is so small that the excess chemical potential from the methane group, as defined by ADF, overpowers this repulsion and will preferentially interact with the analyte. By looking at the interaction surfaces for the highest chemical potential group of each solvent (methane

group for acetonitrile and hydrogen group for hexane) it becomes evident where the molecules are most likely to be solvated. The procyanidin conformers are clearly more solvated around the hydroxyl moieties and the deduction of steric hindrance and electronic stabilization effects is validated.

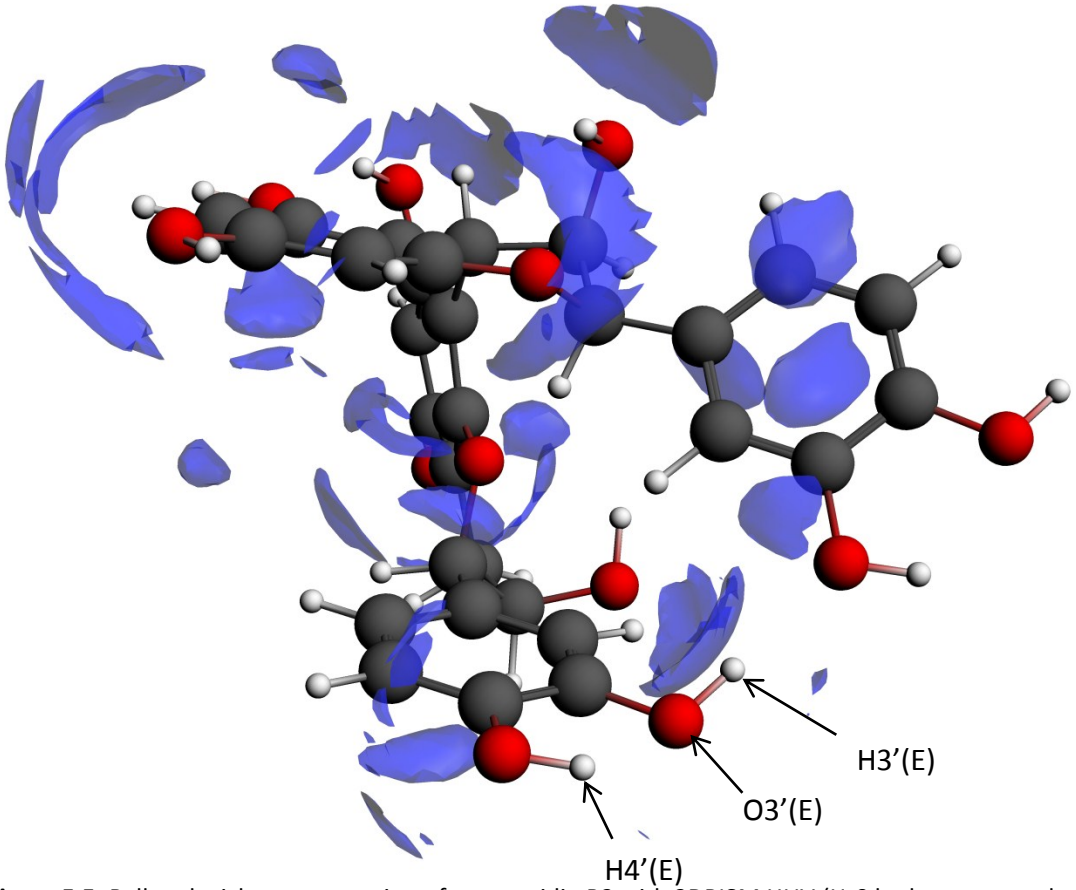

Figure 5.5. Ball and stick representation of procyanidin B2 with 3DRISM HUV (H_20 hydrogen to molecule interaction) isosurface for the FC conformer taken at isovalue of 2.5.

Conclusion

Several procyanidins that include two dimers, four trimers, one tetramer, one pentamer and one hexamer were isolated from a cocoa (*Theobroma Cacao*) sample by means of two dimensional preparative chromatography. The most abundant procyanidin dimer in the cocoa sample was identified as procyanidin B2 (epicathechin4s->8epicathechin). UHPLC-ESI-TOF-MS and ^{1}H NMR were used for structural elucidation and to establish that the collected procyanidins were pure. From the ^{1}H and ^{13}NMR data it is clear that only two conformers of procyanidin B2 are present in acetone and acetonitrile. In acetonitrile the ratio of the two conformers are approximately 4:1 at 253 K. ROESY experiments were used to identify which resonance signals could be associated with the minor and major conformers, respectively. The resonance frequencies for procyanidin B2 in acetonitrile-D_3 could not be found in literature and a novel resonance frequency assignment was performed. Moreover, the chirality of the molecule was determined by use of the NOE of the H3(C) and H2(C) as well as that of the H3(F) and H2(F) protons on the ROESY.

Aggregation of procyanidin B2 does not occur in acetone or in acetonitrile at the concentration used (0.01 g/mL). This was deduced from a ^{1}H DOSY NMR experiment in which the hydrodynamic radius of the molecule was estimated to be 8.5Å in acetone, which corresponds to one procyanidin B2 molecule. Moreover, if aggregation did occur in acetonitrile the ^{1}H NMR resonances would have consistently broadened as temperature decreases, where in contrast sharp resonance signals are observed at 238 K. An NMR line shape analysis program, called NMRfit, was successfully developed in-house in the Matlab environment that can perform non-linear least-squares Bloch-McConnell fits to NMR resonance signals for the determination of 1st order kinetic parameters of symmetric and asymmetric two site exchange reactions. The program NMRfit was validated with a series of test run calculations, where spectra were first generated with analytical solutions and then fitted via a least-squares Nelder-Mead algorithm with NMRfit. A line shape analysis of procyanidin B2 VT ^{1}H NMR spectra, in the temperature range of 252-273 K, using NMRfit yielded linear Eyring plots for the forward and reverse conformational interchange reactions of procyanidin B2. As temperature increases the forward and reverse reaction rate

increases with a corresponding increase in abundance of the minor relative to the major conformer. The good fits obtained for the VT ^{1}H NMR spectra and the linearity of the Eyring plots validated the reversible first order reaction model proposed for the conformational interchange reaction. The positive enthalpies of activation calculated ($\Delta H^{\ddagger}_{forward}$ = 57.03 ± 3.92 kJ.mol^{-1}, $\Delta H^{\ddagger}_{reverse}$ = 53.36 ± 3.82 kJ.mol^{-1}) are indicative of a relatively large electronic energy barrier for procyanidin B2 conformational interchange. The entropies of activation calculated ($\Delta S^{\ddagger}_{forward}$ = -0.3454 ± 14.76 J.mol^{-1}.K^{-1}, $\Delta S^{\ddagger}_{reverse}$ = -4.398 ± 14.39 J.mol^{-1}.K^{-1}) are small negative quantities. Due to the relatively large error interval obtained for the entropies of activation these values should be treated from a more qualitative perspective. The linear van't Hoff plot also gives support that the conformational interchange reaction is a reversible first order reaction. The standard reaction thermodynamic parameters ΔH^{0}_{rxn} equal to 3.670 ± 0.217 kJ.mol^{-1} and ΔS^{0}_{rxn} equal to 4.053 ± 1.57 J.mol^{-1}.K^{-1}) indicate that the forward conformational interchange reaction, the major conformer to the minor conformer, is an endothermic reaction which implies that the abundance of the minor conformer increases with respect to the major conformer as temperature increases, as is indeed observed experiementally. Moreover, the agreement of equilibrium constants obtained from direct integration of conformer spectral areas at a relatively low temperature (253.15 K), where resonance signal overlap is negligible, and those obtained with the NMRfit program further validates the kinetic analysis performed.

Procyanidin B2 has several degrees of conformational freedom w.r.t. hydroxyl moiety rotations, phenol rings rotation, heterocyclic ring orientation and rotation about the interflavonoid bond. A relaxed potential energy surface scan, using the PBE, PBE-D2 and B3LYP functionals with the 6-311++g** basis set in the gas phase, about the interflavonoid bond dihedral angle followed by frequency calculations revealed four conformers of procyanidin B2. The geometries for all the conformers agree well with each other for all functionals used, with the only exception being the FC conformer when using the PBE-D2 functional. In the latter case the interflavonoid dihedral angle is rotated by approximately 30^{o} when compared to the geometries of FC obtained with the PBE and B3LYP functionals. We suspect this is due to an over-estimation of dispersion by PBE-D2. In comparison, previous molecular mechanics studies concerning procyanidin B2 conformational searches

only found two conformers and the geometry of the MM conformers [27] differ significantly from those found in our DFT study.

From an electronic energy perspective, which includes all DFT functionals used, the FC conformer is the most stable, followed by PC>FE>PE. A gas phase QTAIM analyses of the electron density topology showed the existence of several intramolecular bonding interactions, present in all four conformers, which can be classified as closed-shell interactions or more specifically as van der Waals interactions. In all cases the FC conformer has more bond critical points and corresponding bond paths than the other conformers, implying more electronic stabilization. However, the FC conformer also has more RCPs and CCPs compared to the other three conformers, leading to less electronic stabilization. Quantification of these van der Waals interactions in terms of exact energy is not possible at this stage and hence it is difficult to conclude that the hierarchy of electronically stabilized conformers (FC>PC>FE>PE) is directly due to the number or amount of Van der Waals interactions. It is also noteworthy that several different types of Van der Waals intramolecular interactions are found for the procyanidin B2 conformers, e.g. polarized H-O interactions, unpolarized C-C interactions and induced dipole H-H interactions. Furthermore, from NCI analysis even more relatively weak van der Waals interactions could be identified in addition to those found by QTAIM. Unfortunately, due to the lack of resolution of the data (RDG vs. $sign(\lambda_2)\rho$ plots) more detailed NCI analyses were not possible.

Surprisingly, when the standard reaction Gibbs free energies were calculated, *i.e.* addition of the $T\Delta S_{rxn}^{o}$ term to the electronic, nuclear and zero point energies (ZPE) energies, the order of thermodynamic conformational stability, in the gas phase, changed to PC being the most stable followed by FE>FC>PE, for the PBE and B3LYP functionals. With the PBE-D2 functional the thermodynamic stability order is FC>PC>FE>PE in the gas phase. We propose that the PBE-D2 functional over-estimates dispersion interactions or intramolecular Van der Waals interactions for the PC conformer. Previous MM based procyanidin B2 conformational stability studies found that the compact conformer is thermodynamically more stable compared to the extended counterpart [9, 27]. It was suggested by the authors that intramolecular interactions such as hydrogen bonding and π-π stacking occurring in the compact conformer is the reason for this result. Our QTAIM and NCI analyses also suggest that these interactions are the reason for the electronic stability of the conformers.

However, the entropy contribution for the conformers that are not as sterically strained as the PBE-D2 FC conformer, changes the predicted conformer thermodynamic stability order as mentioned above. Experimentally (^{1}H NMR) only two procyanidin B2 conformers are present in appreciable amounts in acetone (conformer ratio of 9:1 at 273 K) and acetonitrile (conformer ratio of 4:1 at 253 K). Computationally, in the gas phase, the abundances of procyanidin B2 conformers found with the B3LYP functional (5.6% FC, 10.3% FE, 83.8 PC), the PBE functional (2.7% FE, 96.9% PC) and with the PBE-D2 functional (89.5% FC, 10.4% PC) do not convey a consistent trend. Only the PC conformer is present in reasonable amounts for the different functionals, which leads us to conclude that one of the two conformers that are experimentally observed is likely to be PC.

The gas phase DFT computational study was extended to include implicit and explicit (3D-RISM) solvation models. When considering the implicit solvent model (SCRF) several distinct trends were noticed as the solvent polarity increases. Firstly, the electronic energy encapsulated in ΔH^o_{rxn} for the three conformers (FE, PE and FC) rises with respect to the PC conformer, *i.e.* the electronic stability of the FE, PE and FC conformers decrease with respect to the PC conformer. The entropy contribution to thermodynamic stability is the highest for the FE conformer and lowest for the FC conformer. This trend is expected considering that the FC conformer is more sterically hindered compared to the other conformers. Moreover, the intensity of the electrostatic surface potential, and in turn the solvent reaction field, decreases as polarized hydroxyl groups form interactions and the electron density is shared across a bond path. Therefore, it is expected that the FC conformer, which forms the most intramolecular van der Waals interactions, should have the least availability to the solvent. The entropic contribution to thermodynamic stability in all solvents and for all functionals follow the trend FE>PC>PE>FC. The solvation energy decreases as expected as the polarity of the solvent decreases. A clear pattern of the solvation energy magnitude for water and acetonitrile is observed with respect to which conformer has the largest to smallest solvation energy namely, FE>PC>PE>FC. Apart from the gas phase calculation using the PBE-D2 functional, the PC conformer is found to be thermodynamically the most stable in gas and in solvent phases ranging from non-polar (hexane) to polar (water). Furthermore, the FC and PE conformers' relative abundance, or thermodynamic stability, compared to the PC and FE conformers decreased dramatically as

the polarity of the solvent increases. From our experimental work and results reported by Terascou *et al.* [27] it is observed that the ratio of the two conformers changes from about 1:3 to 1:1 as the polarity of the solvent increases at 298 K. Results from the DFT calculations mimic this trend where the amount of minor conformer (FE) increases relative to the major conformer (PC) from about 5% to 20-30% abundances for the PBE and B3LYP functionals. This is relatively close to the abundances experimentally found at 298 K in acetonitrile-D_3. For all three functionals the same order of thermodynamic stability are found in acetonitrile (experimental conditions) namely, PC>FE>PE>FC and we conclude that the PC and FE conformers are most likely the two conformers observed experimentally. The DFT calculated equilibrium constants in acetonitrile are 0.43 with the PBE/6-311++g** functional, 0.20 with B3LYP/6-311++g** functional and 0.0095 with PBE-D2/6-311++g** functional data at 298.15 K. These equilibrium constants compare favorably with the experimentally obtained equilibrium constant, 0.36, of the two procyanidin B2 conformers in acetonitrile-D_3 at 298.15 K. The relatively good agreement between experiment and the PBE and B3LYP equilibrium constants lends further support to the conclusion that the two conformers experimentally observed (via ^{1}H and ^{13}C NMR) are the PC (major) and FE (minor) conformers. The 3D-RISM calculations also support that the thermodynamic stability order of the procyanidin B2 conformers are PC>FE>PE>FC. However, the large solvation energy difference between the two sets of conformers PC,FE and PE,FC cast some doubt concerning the validity of the absolute energy values obtained. We believe that the 3D-RISM results must be examined in more detail in order to explain the observed discrepancies.

References

[1] D. Ferreira, D. Slade and J. Marais, "Flavans and Proanthocyanidins," in Flavanoids: Chemistry, Biochemistry and Applications, Boca Raton, CRC Press, 2006, pp. 553-616.

[2] A. A. Shahat, "Procyanidins from Adansonio digitata," Pharmaceutical Biology, vol 44, pp. 445-450, 2006.

[3] Y. Zhang, L. Kong, C. Tin, D. Jiang, J. Jiang, J. He and W. Xiao, "Extraction optimization by response surface methodology, purification and principal antioxidant metabolites of red pigments extracted from bayberry (myrica rubra) pomace," LTW - Food Science and Technology, vol 51, pp. 343-347, 2013.

[4] V. A. P. de Freitas, Y. Glories and M. Laguerre, "Incedence of molecular structure in oxidation of grape seed procyanidins," Journal of agricultural and food chemistry, vol 46, pp. 376-382, 1998.

[5] N. Mateus, E. Carvalho, A. R. F. Carvalho, A. Melo, A. M. Gonzales-Paramas, C. Santos-Buelga, A. M. Silva and V. de Freitas, "Isolation and structural characterization of new acetlyated anthocyanin-vinyl-flavanol pigments occuring in aging red wines," Journal of Agricultural and Food Chemistry, vol 51, pp. 277-282, 2003.

[6] W. Tuckmantel, A. P. Kozikowski and L. J. J. Romanczyk, "Studies in polyphenol chemistry and bioactivity. 1. Preparation of buildingblocks from (+)-Catechin. Procyanidin formation. Synthesis of cancer cell growth inhibitor, 3-O-Galloyl-(2R,3R)-epicatechin-4B,8-[3-O-galloyl-(2R,3R)-epicatechin]," Journal of the American Chemistry Society, vol 121, pp. 12073-12081, 1999.

[7] B. Zhao, X. Li, R. G. He, S. Cheng and X. Wenjureng, "Scavenging effect of extracts of green tea and natural antioxidants on active oxygen radicals," Cell Biochemistry, vol 14, pp. 175, 1989.

[8] S. Matthews, I. Mila, A. Scalbert, B. Pollet, C. Lapierre, C. Herve de Penhoat, C. Rolando and D. Donnelly, "Method for Estimation of Proanthocyanidins Based on Their Acid Depolymerization in the Presence of Nucleophiles," Journal of Agriculture and Chemistry, vol. 45, no. 4, pp. 1195-1201, 1997.

[9] L. Khan, E. Haslam and M. P. Williamson, "Structure and conformation of the Procyanidin B-2 Dimer," Magnetic Resonance in Chemistry, pp. 854-858, 1997.

[10] C. A. Schmidt, R. Murillo, B. Hainzmann, S. Laufer, V. Wray and I. Merfort, "Structural and conformational analysis of proanthocyanidins from Paraptadenia rigida and their wound healing properties," Journal of Natural Products, vol 74, pp. 1427-1436, 2011.

[11] Y. L. Foo, Y. Lu, A. Howell and N. Vorsa, "A-Type proanthocyanidin trimers from cranberry that inhibit adherence of uropathogenic P-fimbriated Eshirichia coli," Journal of Natural Products, vol 63, pp. 1225-1228, 2000.

[12] M. Galleano, S. V. Verstraeten, P. I. Oteiza and C. G. Fraga, "Anti-oxidant actions of flavanoids: Thermodynamic and kinetic analysis," Archives of Biochemistry and Biophysics, pp. 23-30, 2010.

[13] P. Groupy, C. Dufour, M. Loonis and O. Dangles, "Quantitative kinetic analysis of the hydrogen transfer reactions from dietary polyphenols to the DPPH radical," Journal of Agriculture and Food Chemistry, vol 51,pp. 615-622, 2003.

[14] O. Cala, S. Fabre, N. Pinuad, E. Dufourc, M. Laguerre and I. Pianet, "Towards a molecular interpretation of astringency: synthesis, 3D structure, colloidal state, and human saliva protein recognition of procyanidins," Planta Medica, pp. 1116-1122, 2011.

[15] I. Pianet, Y. Andre, M. Ducasse, I. Terascou, J. C. Lartigue, N. Pinaud, E. Fouquet, E. J. Dufourc and M. Laguerre, "Modeling procyanidin self-association processes and understanding their micellar organization: a study by diffusion NMR and molecular mechanics," Langmuir, pp. 11027-11035, 2008.

[16] O. Cala, N. Pinaud, C. Simon, E. Fouquet, M. Laguerre, E. Dufourc and I. Pianet, "NMR and molecular modeling of wine tannins binding to saliva proteins: revisiting astringency from molecular and colloidal prospects," The FASEB Journal, pp. published online: article fj. 10-158741, 2010.

[17] C. Simon, K. Barathieu, M. Laguerre, J. M. Schmitter, E. Fouquet, I. Pianet and E. J. Dufourc, "Three dimensional structure and dynamics of wine tannin- saliva protein complexes. A multitechnique approach," Biochemistry, pp. 10385-10395, 2003.

[18] R. Gonçalves, N. Mateus and V. De Freitas, "Influence of Carbohydrates on the interaction of procyanidin B3 with trypsin," Journal of Agricultural Food Chemistry, volume 59,pp. 11794-11802, 2011.

[19] S. Soares, N. Mateus and V. de Freitas, "Carbohydrates inhibit salivatory proteins precipitation by condensed tannins," Journal of Agricultural and Food Chemistry, vol 60, pp. 3966-3972, 2012.

[20] D. Huang, B. Ou and R. L. Prior, "The chemistry behind antioxidant capacity assays," Journal of Agriculture and Food Chemistry, vol 53, pp. 1841-1856, 2005.

[21] N. Saint-Cricq de Gualejac, C. Provost and N. Vivas, "Comparatice study of polyphenol scavanging activities assessed by different methods," Journal of Agricultural Food Sciences, vol 47, pp. 425-431, 1999.

[22] K. F. Pirker, J. Oliviera, V. de Freitas, B. A. Goodman and N. Mateus, "Antiradical properties of red wine portisins," Joural of Agricultural and Food Chemistry, vol 59, pp. 11833-11837, 2011.

[23] F. Qa'dan, K. Masoor, I. AL-Adham, M. Schmidt and A. Nahrstedt, "Proanthocyanidins from Ginko boloba leaf extract and their radical scavenging activity," Pharmaceutical Biology, vol 49, pp. 471-476, 2011.

[24] T. De Bruyne, L. Pieters, R. Domise, H. Kolodzeij, V. Wray, T. Domke and A. Vlietinck, "Unambiguous assignments for free dimeric proanthocyanidin phenols from 2D NMR," Phytochemistry, vol 43, pp. 265-272, 1996.

[25] T. Esatbeyoglu, B. Jaschik-Kentner, V. Wray and P. Winterhalter, "Structural elucidation of procyanidin oligomers by low temperature 1 H NMR Spectroscopy," Journal of Agricultrual and Food Chemistry, vol 59, pp. 62-69, 2011.

[26] J. Hammerstone, S. Lazarus, M. A.E., R. Rucker and S. H.H., "Identification of Procyanidins in Cacoa (Theobroma cacao) and Chocolate Using High-Performance Liquid Chromatography/Mass Spectrometry," Journal of Agriculture and Food Chemistry, no. 47, pp. 490-496, 1999.

[27] I. Terascou, K. Barathieu, C. Simon, M. A. Ducasse, Y. Andre, E. Fouquet, E. J. Dufourc, V. De Freitas, M. Laguerre and I. Pianet, "A 3D structural and conformational study of procyanidin dimers in water and hydro-alcoholic media as viewed by NMR and molecular modeling," Magnetic Resonance in Chemistry, pp. 44: 868-880, 2006.

[28] F. R. Fronczek, G. Gannuch, W. L. Mattice, F. L. Tobiason, J. L. Broeker and R. W. Hemingway, "Dipole moment, solution and solid state structure of (-)-Epicatechin, a monomer unit of procyanidin polymers," Journal of Chemistry Society: Perkins Transactions, pp. 1611-1616, 1984.

[29] I. Terascou, M. A. Ducasse, E. J. Dufourc, D. Moskau, E. Fouquet, M. Laguerre and I. Pianet, "Structural and conformational analysis of two native procyanidin trimers," Magnetic Resonance in Chemistry, pp. 45:157-166, 2007.

[30] B. Berke and V. A. P. de Freitas, "Influence of procyanidin structures on their ability to complex with oenin," Food Chemstry, pp. 90: 453-460, 2005.

[31] H. Kolodzei, M. Bonefeld, J. F. W. Burger, E. V. Brandt and D. Farreira, "Structure and conformational analysis of procanidin 3-O-rhamnoside from Erythroxylum novogranatense," Phytochemistry, pp. 30: 1255-1258, 1991.

[32] C. WanFei, M. Shuaung, Z. Shu, C. Fei, Z. Hong, L. LaiCai and T. AnMin, "Density functional theory study on the interaction of catechin and cytosine," Science China, vol. 54, no. 7, pp. 1094-1100, July 2011.

[33] A. Mendoza-Wilson, S. Castro-Arredondo and R. Balandran-Quintana, "Computational study of the structure-free radical scavenging relationship of procyanidins," Food Chemistry, no. 161, pp. 155-161, 1 April 2014.

[34] M. Levitt, Spin Dynamics, Stockholm: Wiley, 2000.

[35] H. McConnell, "Reaction rates by nuclear magnetic resonance," Journal of Chemical Physics, vol. 28, no. 3, pp. 430-431, 1958.

[36] M. Gutowski, J. van Lenthe, J. Verbreek and F. van Duijnveldt, "The basis set superposition error in correlated electronic structure calculations," Chemical Physics Letters, vol. 124, no. 4, 1986.

[37] D. Asturiol, M. Duran and P. Salvador, "Intramolecular basis set superposition error effects on the planarity of benze and other aromatic molecules: A solution to the problem," Journal of Chemical Physics, vol. 128, pp. 144108-1 - 144108-5, 2008.

[38] H. Valdez, V. Klusak, M. Pitonak, O. Exner, I. Stary, P. Hobza and L. Rulisek, "Evaluation of the intramolecular basis set superposition error in the calculations of larger molecules: [n]Helicenes and Phe-Gly-Phe Tripeptide," Journal of Computational Chemistry, vol. 29, pp. 861-870, 2008.

[39] R. Balabin, "Communications: Is quantum chemical treatment of biopolymers accurate? Intramamolecular basis set superposition error (BSSE)," Journal of Chemical Physics, vol. 132, pp. 231101- 1 - 231101-4, 2010.

[40] S. Miertus, E. Scrocco and J. Tomasi, "Electrostatic interaction of a solute with a continuum. a Direct utilization of ab initio molecular potentials for the prevision of solvent effects," Chemical Physics, vol. 55, pp. 117-129, 1981.

[41] S. Miertus and J. Tomasi, "Approximate evaluations of the electrostatic free energy and internal energy changes in solution processes," Chemical Physics, vol. 65, pp. 239-245, 1982.

[42] S. Guserov, T. Ziegler and A. Kovalenko, "Self-consistent combination of the three-dimensional RISM theory of molecular solvation with analytical gradients and the Amsterdam Density Functional package," Journal of Physical Chemistry, vol. 110, no. 18, pp. 6083-6090, 2006.

[43] R. Bader, "A quantum theory of molecular structure and its applications," Chemical Reviews, vol. 91, no. 5, pp. 893-928, 1991.

[44] R. Bianchi, G. Gervasio and D. Marabello, "Experimental Electron Density Analysis of the Mn2(CO)10: Metal-Metal and Metal-Ligand Bond Characterization," Inorganic Chemistry, vol. 39, pp. 2360-2366, 2000.

[45] J. Contreras-Garcia, E. Johnson, S. Keinen, R. Chaudret, J. Piquemal, D. Beretan and W. Yang, "NCIPLOT: A program for Plotting Noncovent Interaction Regions," Journal of Chemical Theory and Computation, vol. 7, pp. 625-632, 2011.

[46] L. Lee, Fundamentals of Adhesion, Springer Science and Bussiness Media, 1991.

[47] T. Geissman and N. Yoshimura, "Synthetic procyanidin," Tetrahedron Letters, pp. 24: 2669-2673, 1966.

[48] N. Kohler, V. Wray and P. Winterhalter, "New approach for the synthesis and isolation od dimeric procyanidins," Journal of Agricultural and Food Chemistry, pp. 56:5374-5385, 2008.

[49] K. Oyama, M. Kuwano, M. Ito, K. Yoshida and T. Kondo, "Synthesis of procyanidins by stepwise- and selfcondensation using 3,4-cis-4-acetoxy-3-O-acetyl-4-dehydro-5-7-3'-4'-tetra-O-benzyl-(+)-catechin and (-)-epicatechin as key building monomer," Tetrahedron Letters, pp. 49: 3176-3180, 2008.

[50] A. Saito, N. Nakajima, A. Tanaka and M. Ubukata, "Synthetic studies of proanthocyanidins. Part 2: Stereoselective gram-scale synthesis of procyanidin-B3," Tetrahedron, pp. 58 :7829-7837, 2002.

[51] Y. Mohri, M. Sagehashi, T. Yamada, Y. Hattori, K. Morimura, T. Kamo, M. Hirota and H. Makabe, "An efficient synthesis of procyanidins. Rare earth metal Lewis acid catalyzed equimolar condensation of catechin and epicatechin," Tetrahedron Letters, pp. 48: 5891-5894, 2007.

[52] C. Lozano, J. Bujons and L. Torres, "Novel separation of bioactive catechin derivates from complex plant mixtures by anion exchange chromatography," Separation Purification Technology, pp. 317-322, 2008.

[53] K. Kathithileni M. and D. V. Andre, "Off-line comprehensive 2-dimensional hydrophilic interaction x reversed phase liquid chromatography analysis of procyanidins," Journal of Chromatography A, vol. 1216, pp. 6274-6284, 2009.

[54] Dortmund data bank, "dortmund data bank," [Online]. Available: www.ddbst.com. [Accessed 6 August 2014].

[55] F. Bloch, W. Hansen and M. Packard, "The Nuclear Induction Experiment," Physical Review Letters, vol. 70, no. 474, 1946.

[56] P. Vallurupalli, "Chemical exchange workshop series on NMR and related topics", TIFR Mumbai, 2009.

[57] V. Rimal, H. Stepankova and J. Stepanek, "Analysis of NMR spectra in case of temperature-dependent chemical exchange between two unequally populated sites," Concepts in Magnetic Resonance Part A, vol. 38A, no. 3, pp. 117-127, 2011.

[58] J. Nelder and R. Mead, "A simplex method for function minimization," The Computer Journal, vol. 7, no. 4, pp. 308-313, 1965.

[59] W. Spendley, G. Hext and F. Himsworth, "Sequential application of simplex designs in optimization and evolutionary operation," Technometrics, vol. 4, no. 4, pp. 441-461, 1962.

[60] J. Miller, "Basic statistical methods for analytical chemistry Part 2. calibration and regression methods," Analyst, vol. 116, pp. 3-14, 1991.

[61] T. Claridge, High resolution NMR techniques in organic chemistry, Newnes, 2009.

[62] S. Grimme, "Semiempirical GGA-type density functional constructed with a long-range dispersion correction," Journal of Computational Chemistry, vol. 27, no. 15, pp. 1787-1799, 2006.

[63] S. Grimme, S. Ehrlich and L. Georigk, "Effect of the damping function in dispersion corrected density functional theory," Journal of Computational Chemistry, vol. 32, no. 7, pp. 1456-1465, 2011.

[64] T. Clark, M. Hennemann, J. S. Murray and P. Politzer, "Halogen bonding: the sigma-hole," Journal Of Molecular Modeling, no. 13, pp. 291-296, 2007.

[65] K. Morokuma, "Why do molecules interact? The origin of electron donor-acceptor complexes, hydrogen bonding and proton affinity," Accounts of Chemical Research, vol. 10, pp. 294-300, 1977.

[66] H. Umeyama and K. Morokuma, "The Origin Of Hydrogen Bonding. An Energy Decomposition Study," Journal Of The American Chemical Society, vol. 99, pp. 1316-1332, 1977.

[67] J. Lane, J. Contreras-Garcia, J. Piquemal and B. Miller, "Are Bond Critical Points Really Critical for Hydrogen Bonding?," Journal of Chemical Thoery and Computation, vol. 9, pp. 3263-3266, 2013.

[68] C. Cramer, Essentials of computational chemistry, Second Edition ed., West Sussex: John Wiley & Sons, 2004.

[69] V. Barone and M. Cossi, "Quantum calculation of molecular energies and energy gradients in solution by a conductor solvent model," Journal of Chemical Physics, vol. 102, no. 11, pp. 1995-2001, 1998.

[70] H. Sato, A. Kovalenko and F. Hirata, "Self-Consistent field, ab initio molecular orbital and three-dimensional reference interaction site model study for solvation effect on

carbon monoxide in aqueous solution," Journal of Chemical Physics, vol. 112, no. 21, pp. 9463-9468, 2000.

[71] J. Tirado-Rives and W. Jorgnson, "Performance of B3LYP density functional methods for a large set of organic molecules," Journal of Chemical Theory and Computation, vol. 4, pp. 297-306, 2008.

A. Appendix

A.1. Supplementary NMR Spectra and Plates

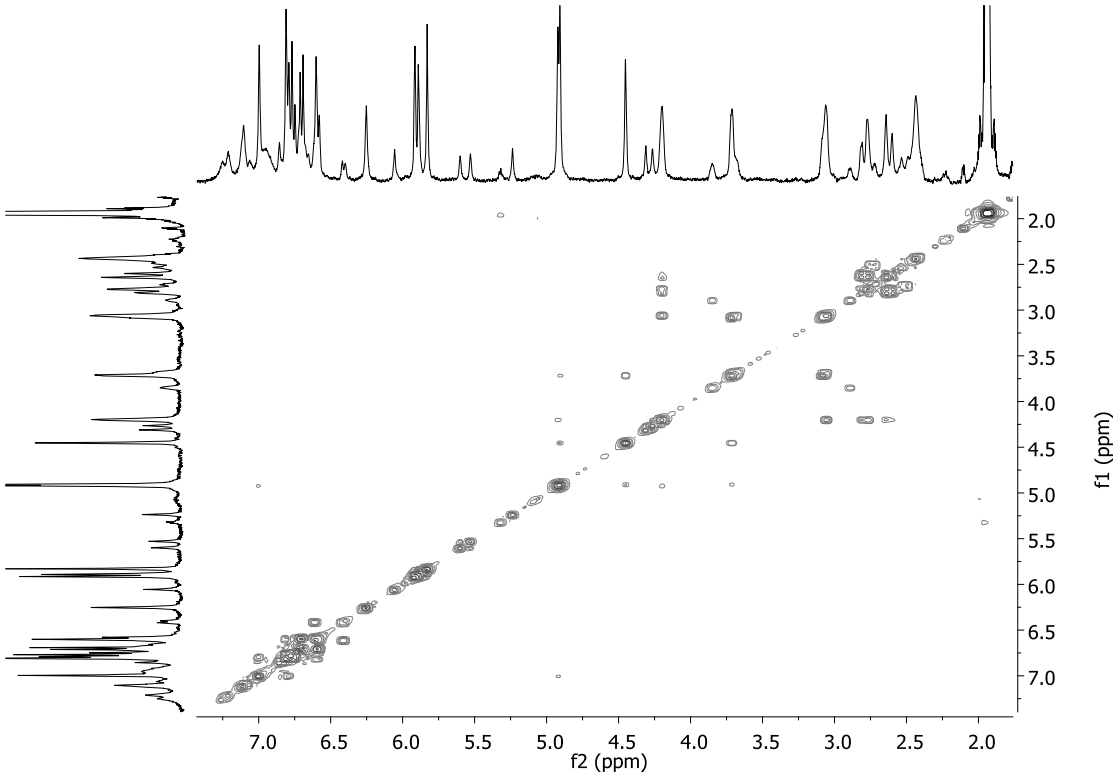

Supplementary plate 1. Full COSY spectrum of procyanidin B2 in acetonitrile-D_3 at 238 K

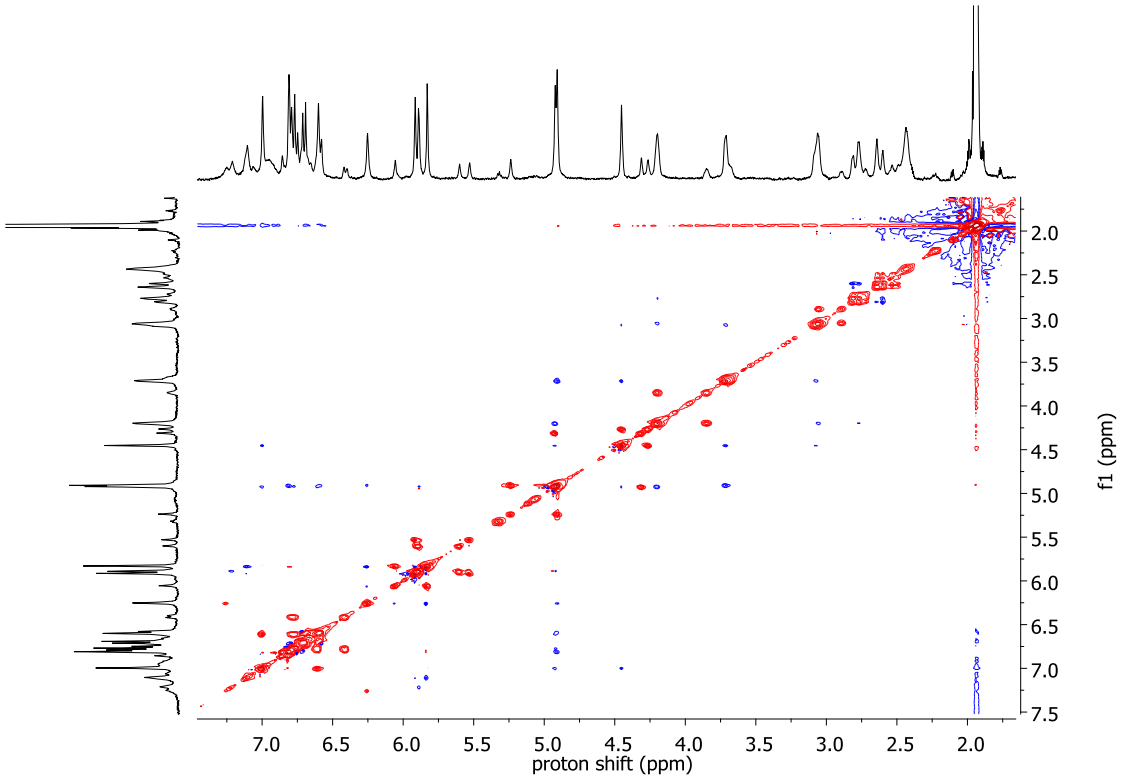

Supplementary plate 2. ROESY spectrum of procyanidin B2 in acetonitrile-D_3 at 238K

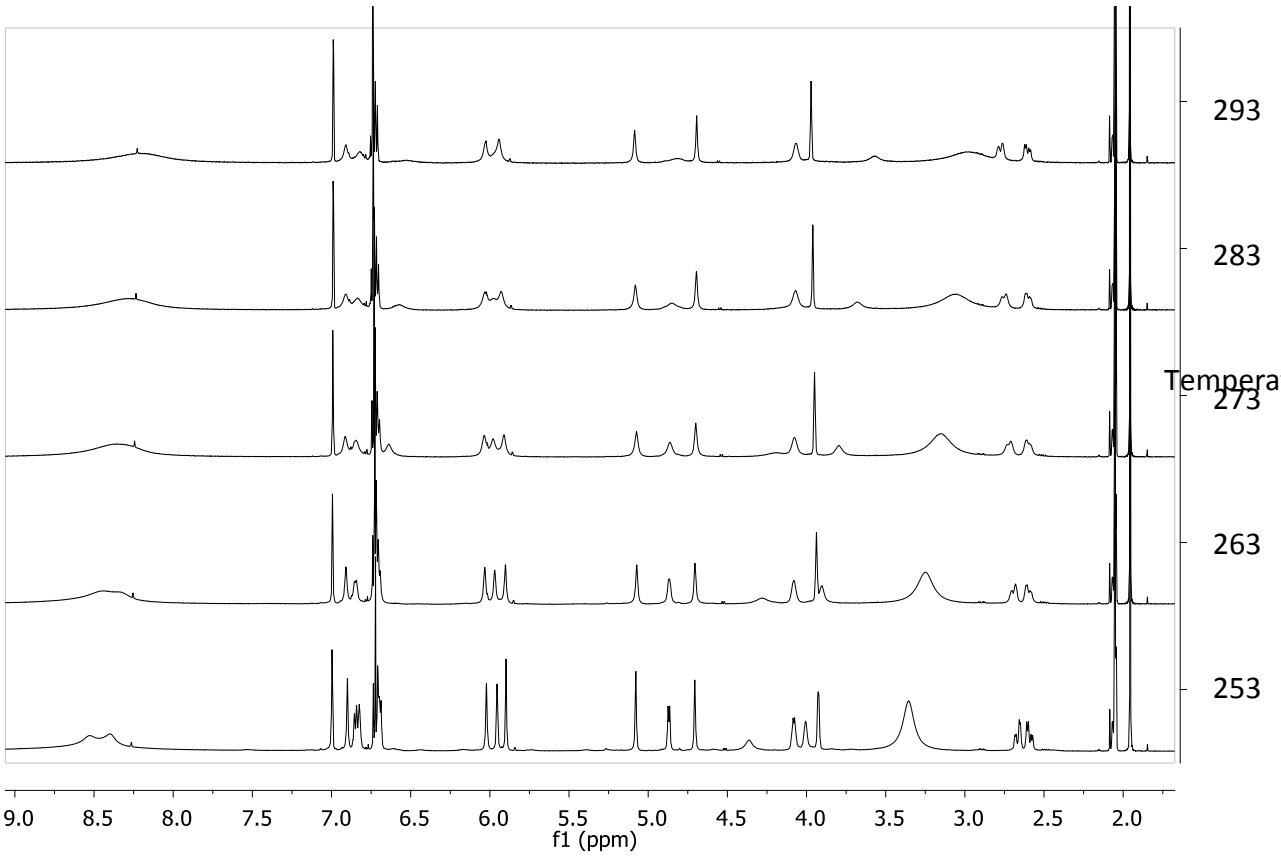

Supplementary figure 1. VT ^{1}H NMR of procyanidin B1 standard purchased from Phytolab GmbH & co. KG in acetone-D_6

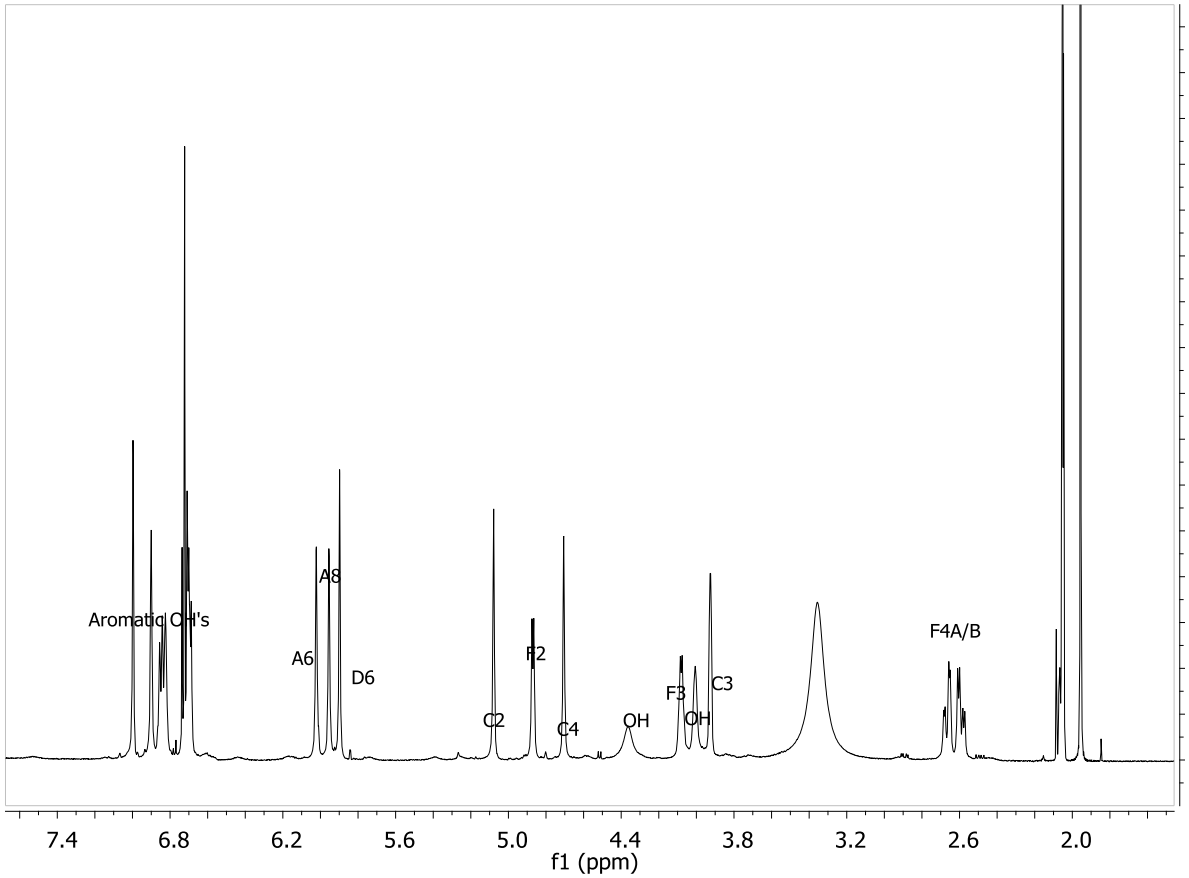

Supplementary figure 2. ^{1}H NMR assignment of procyanidin B2 in acetone-D_6 at 253 K

The assignments shown here were completed via ^{1}H COSY and ROESY spectra.

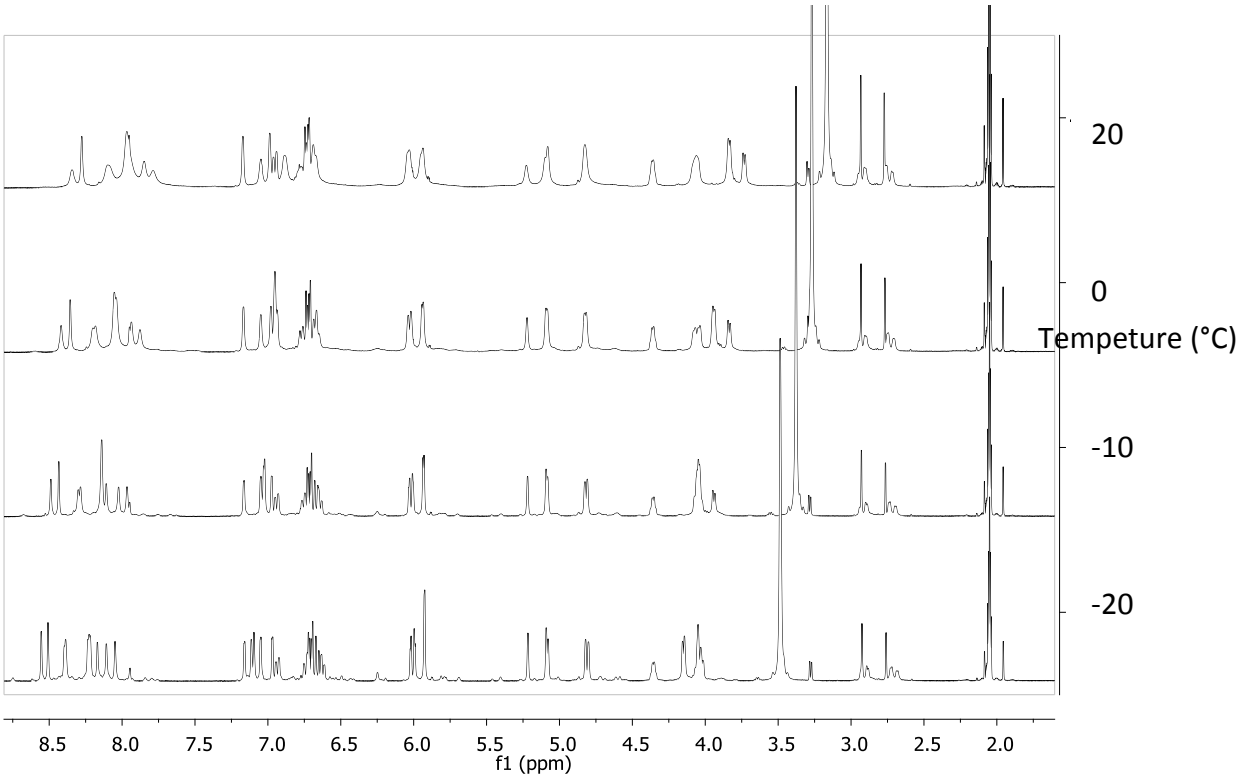

Supplementary figure 3. VT ^{1}H NMR spectra of procyanidin C1(purchased from Phytolab GmbH & co. KG) in acetone-D_6

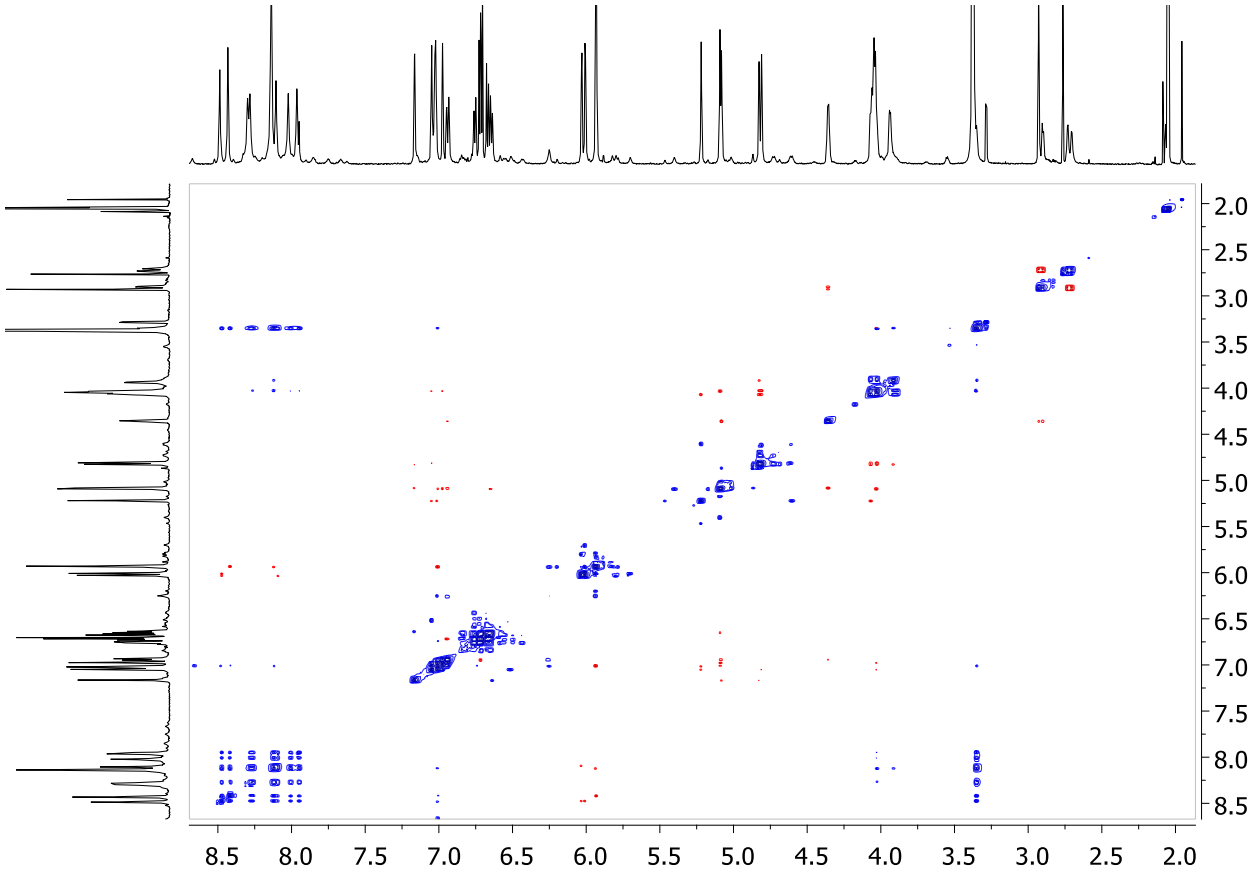

Supplementary plate 3. ^{1}H ROESY of procyanidin C1(purchased from Phytolab GmbH & co. KG) in acetone-D_6 at 253 K

The assignment of the ^{1}H and ^{13}C chemical shifts has been done and corresponds well to literature. The chemical shifts are shown in **Supplementary table 1**.

Supplementary table 1. Procyanidin C1 chemical shift (ppm) assignments

Upper unit				
		^{1}H	^{13}C	
		experimental	experimental	literature
A	5		158.28-153.90	158.28-153.90
	6		95.98	96.41
	7		158.28-153.90	158.28-153.90
	8		95.50	95.85
	9		158.28-153.90	158.28-153.90
	10		101.48	102.10
B	1		132.17	132.20-131.76
	2	6.97	114.89	114.80
	3		145.10	145.23-144.89
	4		144.84	145.23-144.90
	5		115.30	115.44
	6	6.95	118.75	118.78
C	2		76.47	76.78
	3	4.03	72.78	72.93
	4	4.81	36.63	36.81
middle unit				
		^{1}H	^{13}C	
		experimental	experimental	literature
D	5		158.28-153.90	158.28-153.90
	6		96.77	97.13
	7		158.28-153.90	158.28-153.90
	8		106.79	106.84
	9		158.28-153.90	158.28-153.90
	10		100.74	102.10
E	1		132.02	132.20-131.76
	2	7.17	114.64	114.80
	3		145.09	145.23-144.89
	4		144.76	145.23-144.90
	5	6.70	115.25	115.44
	6		118.63	118.78
F	2	5.09	76.64	76.63
	3	4.07	71.85	71.86
	4	4.83	36.55	36.81
terminal unit				
		^{1}H	^{13}C	
		experimental	experimental	literature
G	5		158.28-153.90	158.28-153.90
	6	5.93	96.69	97.13
	7		158.28-153.90	158.28-153.90
	8		107.30	107.13
	9		158.28-153.90	158.28-153.90
	10		100.18	100.45
H	1		131.71	132.20-131.76
	2	7.05	114.52	114.80
	3		145.05	145.23-144.89
	4		144.73	145.23-144.90
	5	6.72	115.25	115.44
	6		118.48	118.78
I	2	5.08	79.00	79.00
	3	4.36	66.24	66.30
	4 A	2.91	28.60	28.88

A.2. Supplementary UHPLC-ESI-TOF-MS Figures

A.2.1. B1

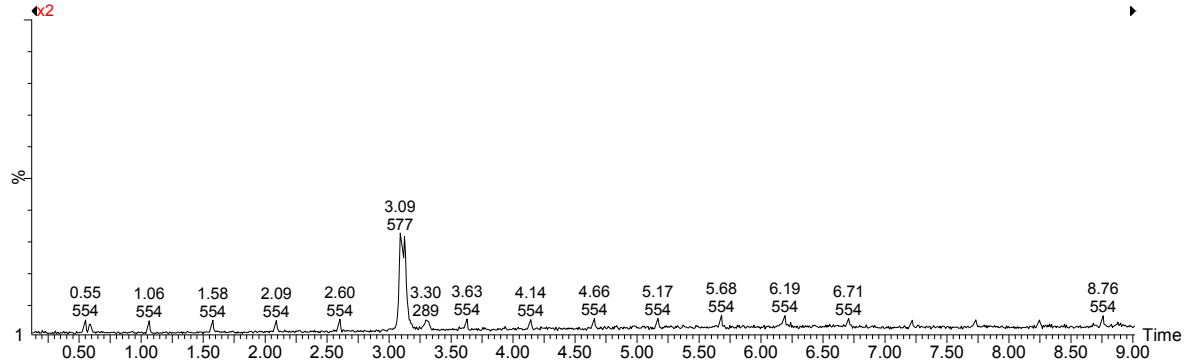

Supplementary figure 4. Procyanidin B1 TIC chromatogram

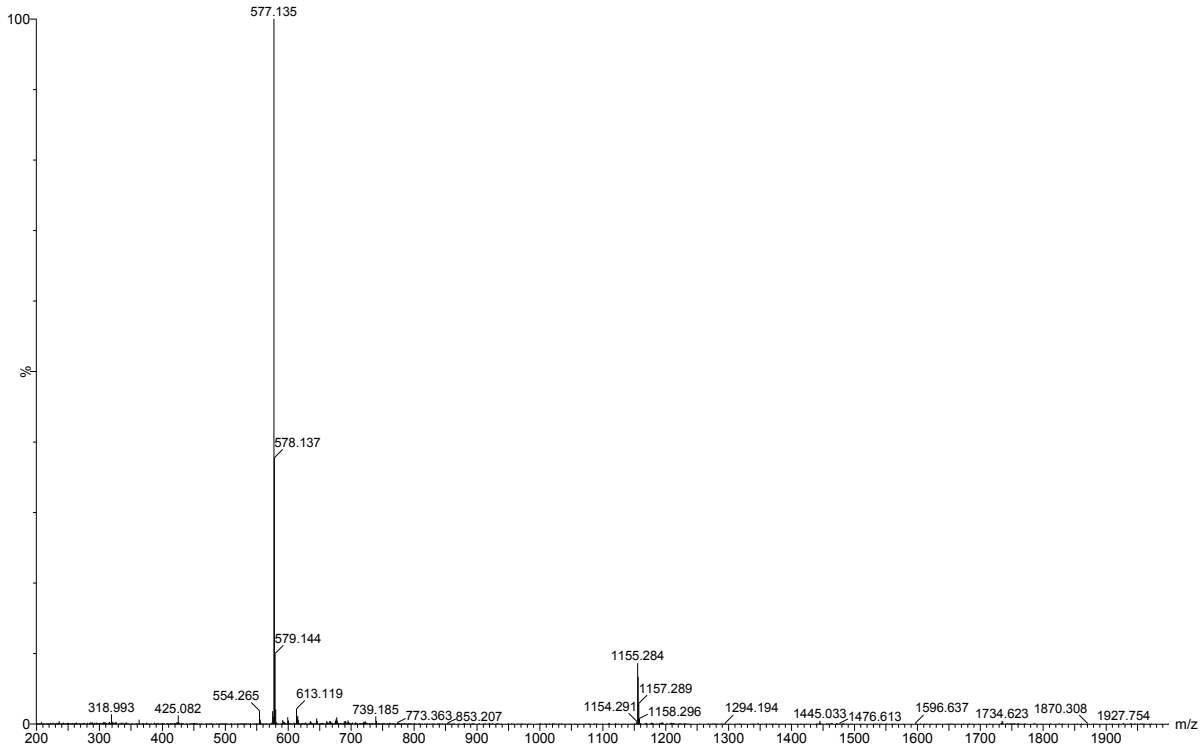

Supplementary figure 5. Procyanidin B1 mass spectrum

The mass spectrum for the procyanidin B1 standard purchased from Phytolab GmbH & co. KG indicates high purity and a $C_{30}H_{26}O_{12}$ empirical formula as is expected for a procyanidin dimer.

A.2.2. Minor Dimer

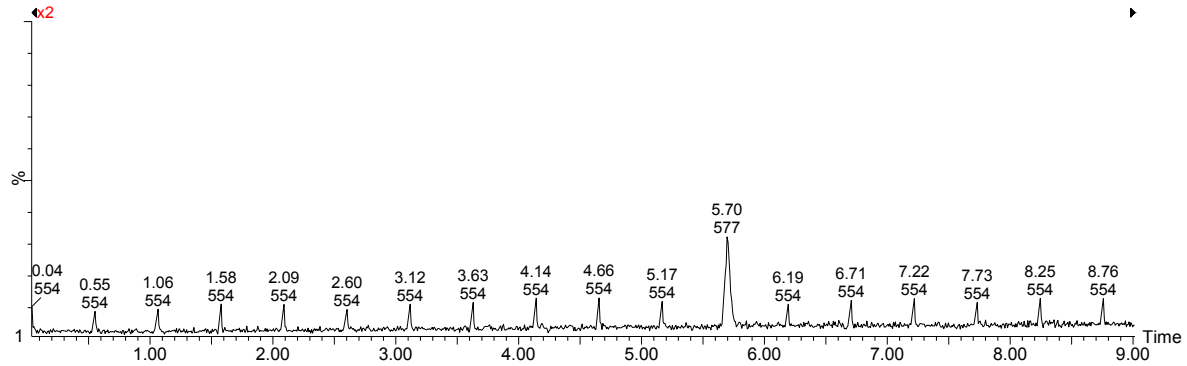

Supplementary figure 6. TIC chromatogram of minor dimeric fraction separated by RP-HPLC

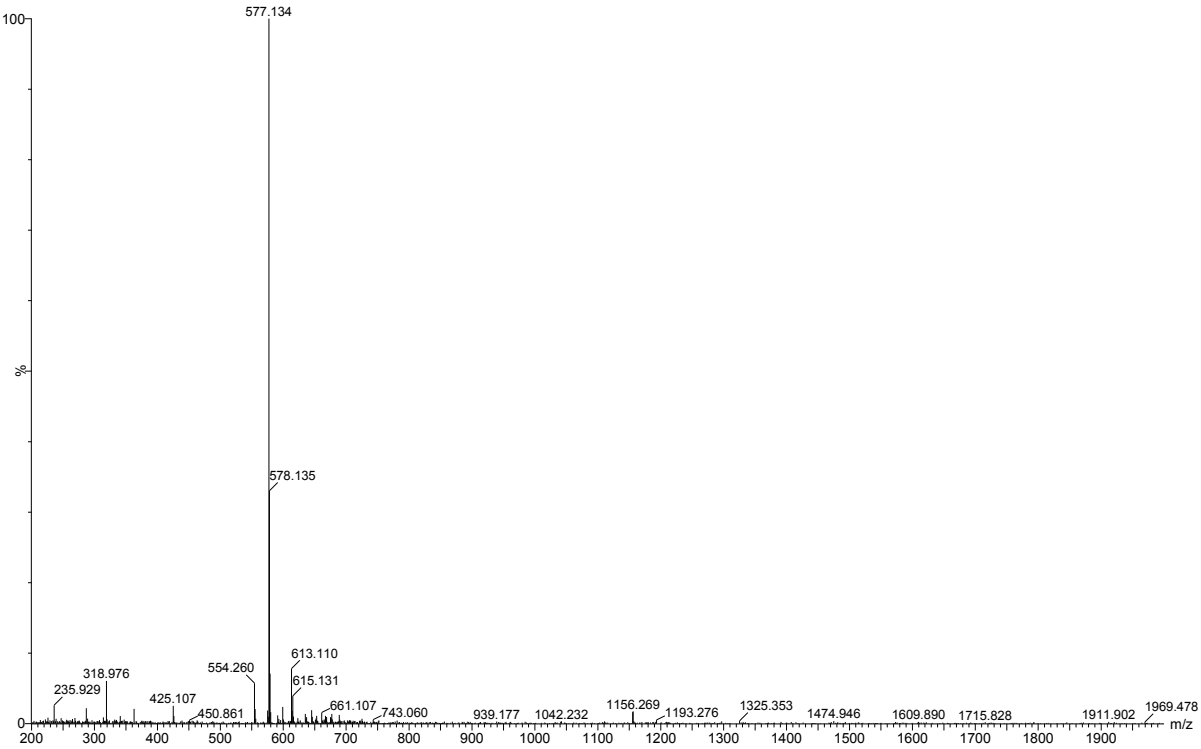

Supplementary figure 7. Mass spectrum of minor dimer fraction separated by RP-HPLC

It is clear that the minor dimer does not correspond to B1 on the TIC and as such must be B3 or B4. The mass spectrum also indicates good purity and the m/z ration indicates a procyanidin dimer.

A.2.3. C1

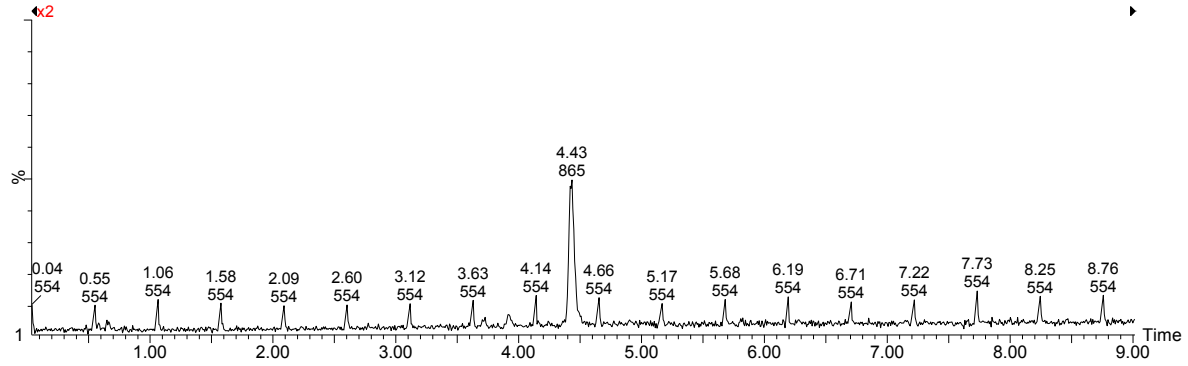

Supplementary figure 8. Procyanidin C1 TIC chromatogram

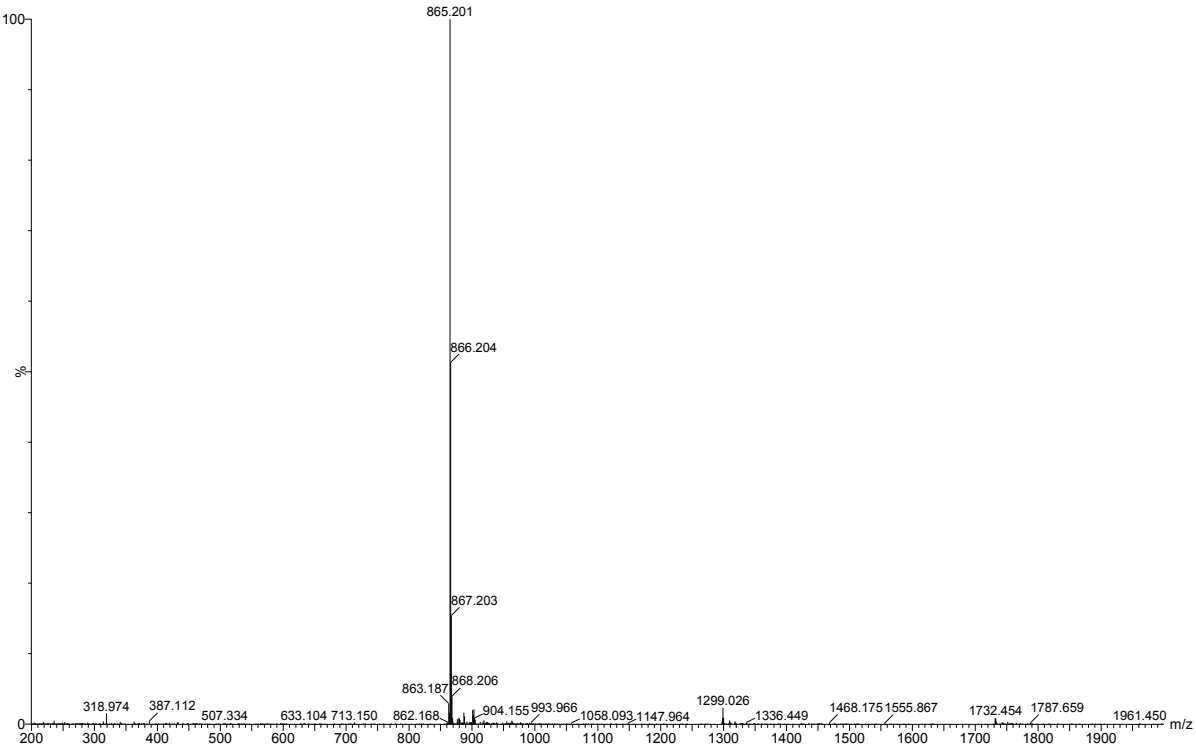

Supplementary figure 9. Procyanidin C1 mass spectrum

The TIC and mass spectrum for procyanidin C1 indicates a trimer from the m/z ratio of 865.201. The mass spectrum also shows high purity.

A.2.4. First Trimer

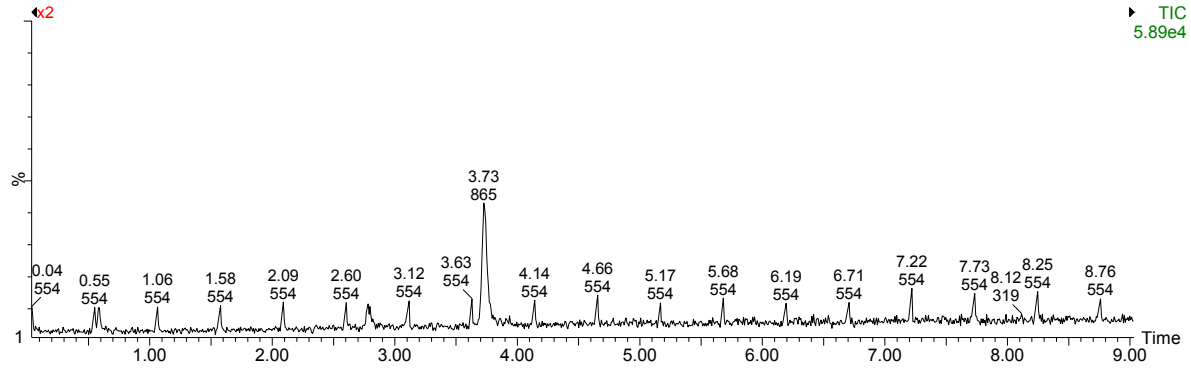

Supplementary figure 10. TIC chromatogram of the first eluting trimer

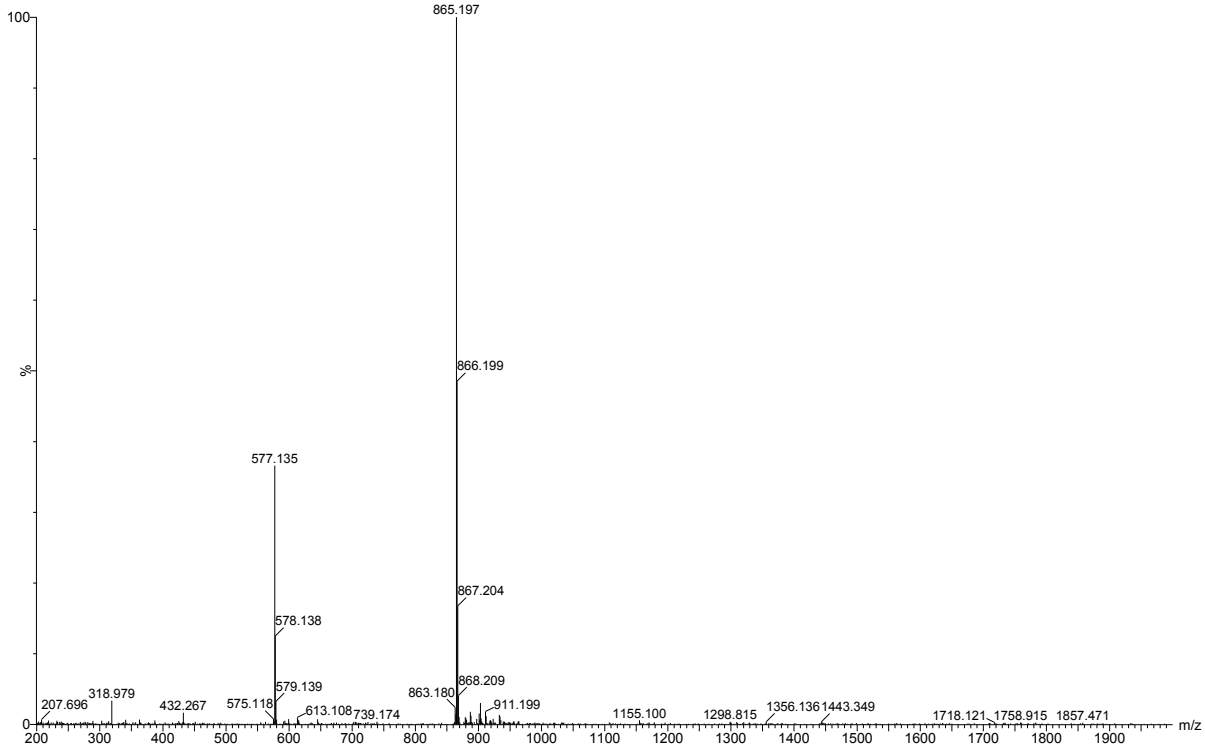

Supplementary figure 11. Mass spectrum of the first eluting trimer

A.2.5. Second Trimer

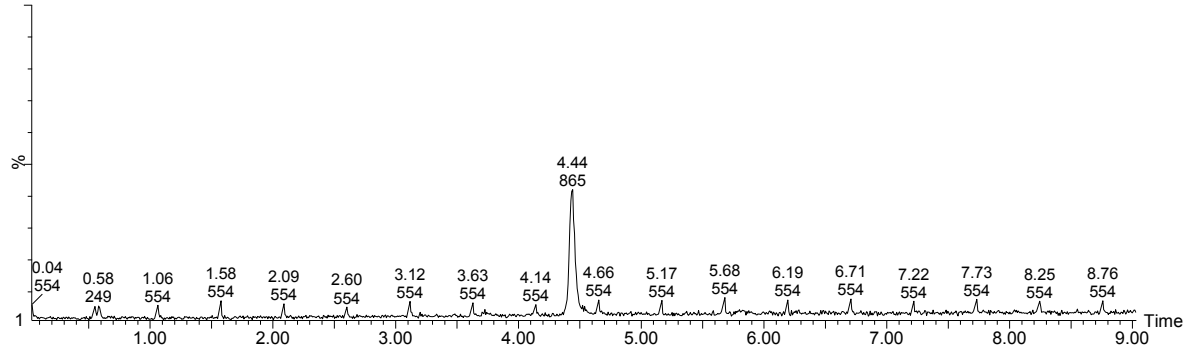

Supplementary figure 12. TIC chromatogram of the second eluting trimer

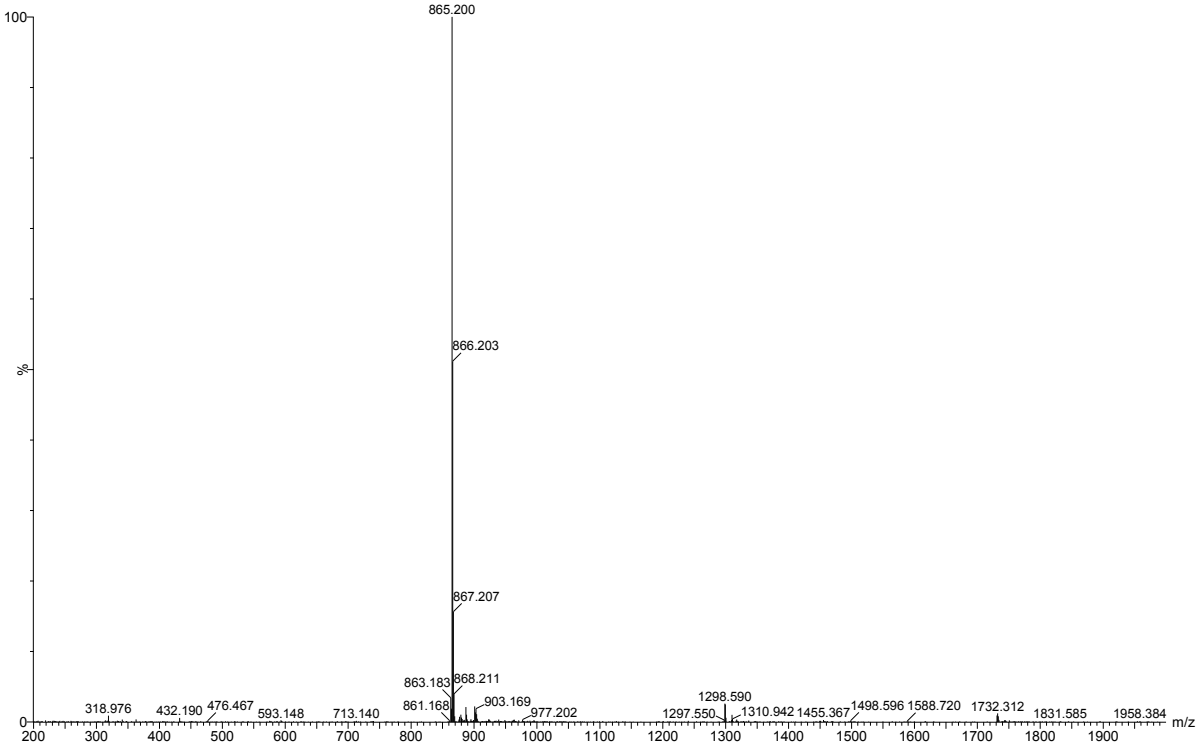

Supplementary figure 13. Mass spectrum of the second eluting trimer

A.2.6. Third Trimer

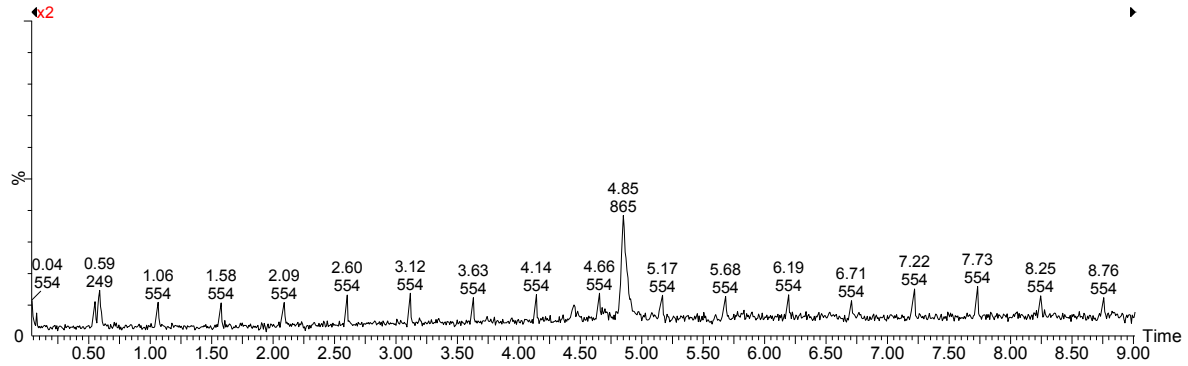

Supplementary figure 14. TIC chromatogram of the third eluting trimer

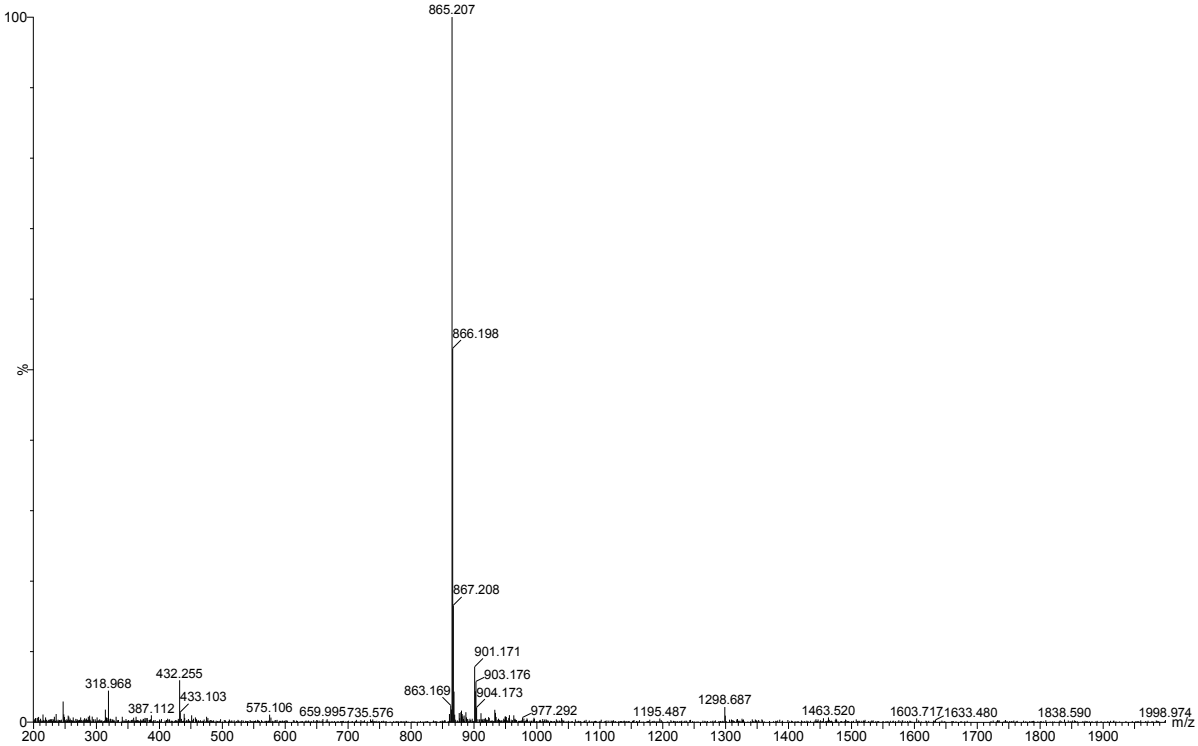

Supplementary figure 15. Mass spectrum of the third eluting trimer

A.2.7. Fourth Trimer

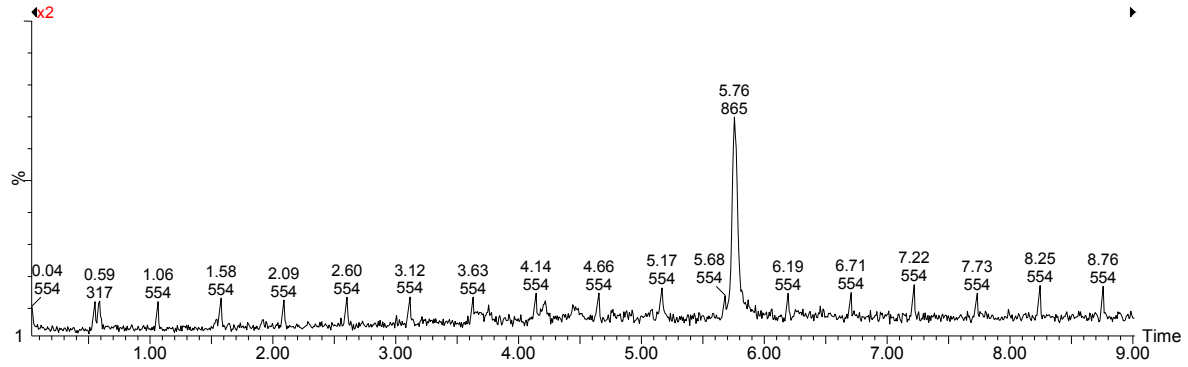

Supplementary figure 16. TIC chromatogram of the fourth eluting trimer

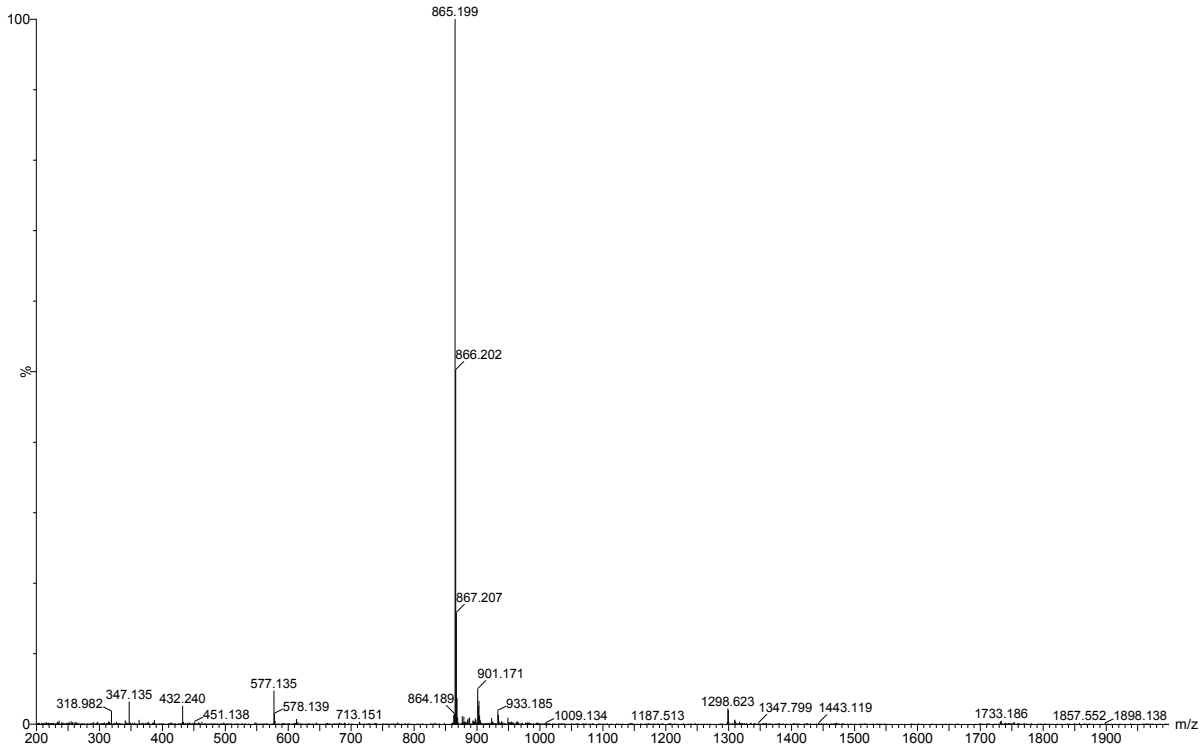

Supplementary figure 17. Mass spectrum of the fourth eluting trimer

From the TIC chromatograms of the four separated trimers it is clear that there are 4 unique chiral trimeric procyanidins. The mass spectrum of the first eluting trimer shows some residual monomer present, but the mass spectra of the remaining three trimers are of a high purity. The second eluting trimer is similar in elution time to that of C1 and may be a C1 fraction but would have to be further investigated to confirm.

A.2.8. Tetramer

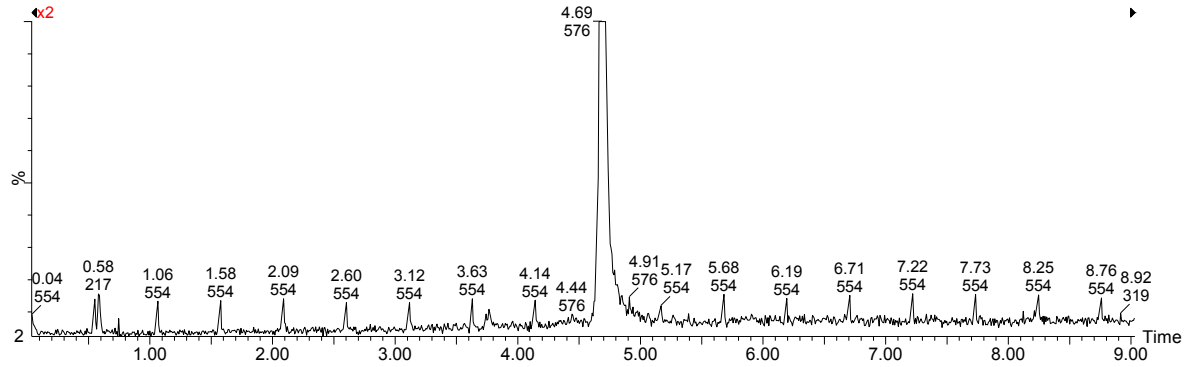

Supplementary figure 18. TIC chromatogram of the tetramer fraction

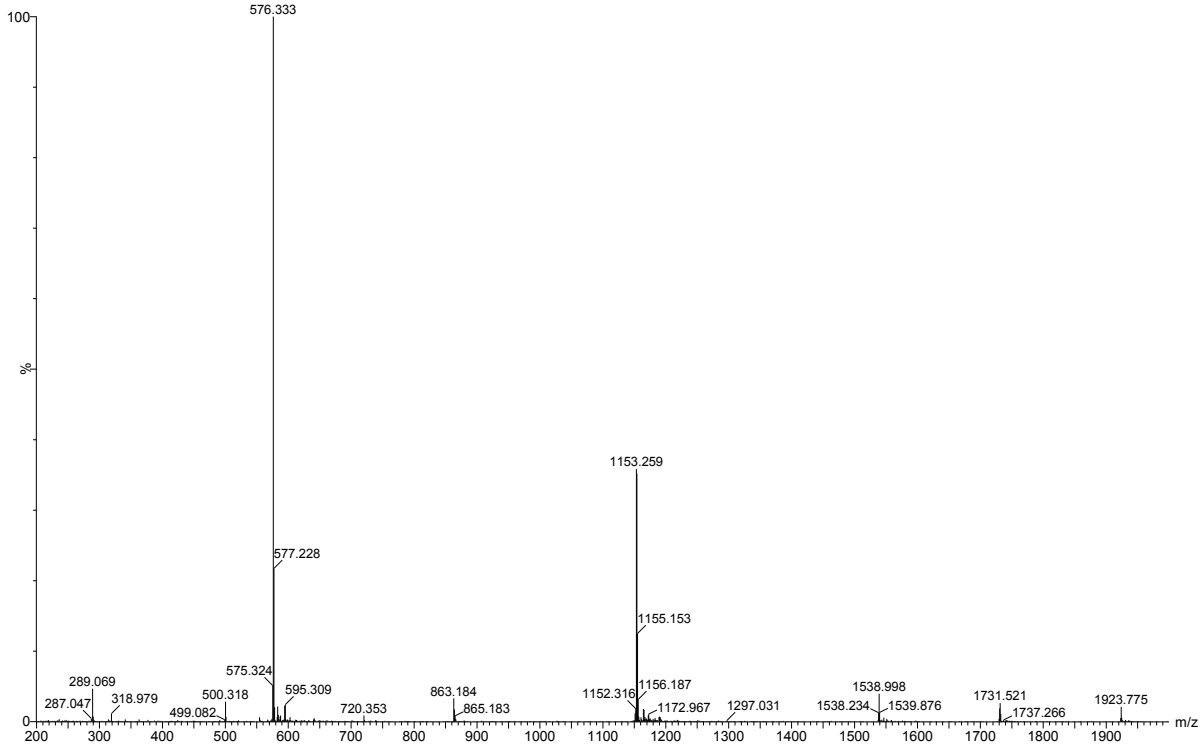

Supplementary figure 19. Mass spectrum of the tetramer fraction

From the mass spectrum of the tetramer it is observed that the 1153.259 m/z ratio corresponds to a procyanidin tetramer ion and the largest abundance ion is the doubly charged 576.333 m/z ratio tetramer ion.

A.2.9. Pentamer

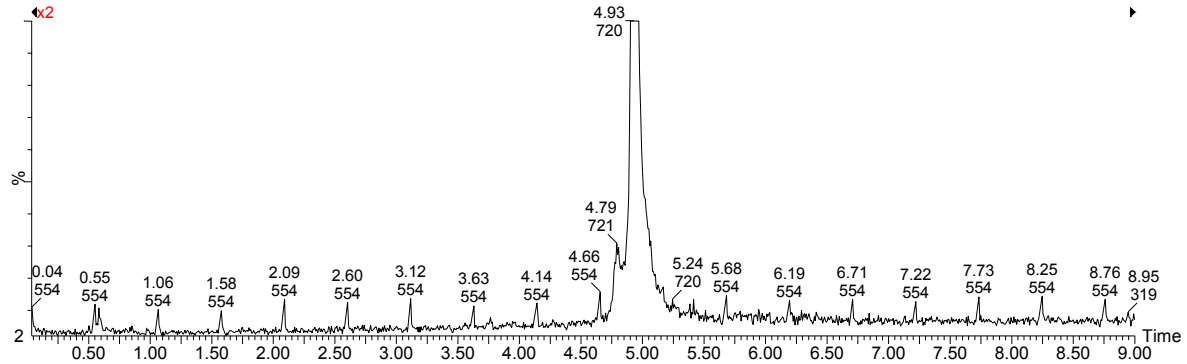

Supplementary figure 20. TIC chromatogram of the pentamer fraction

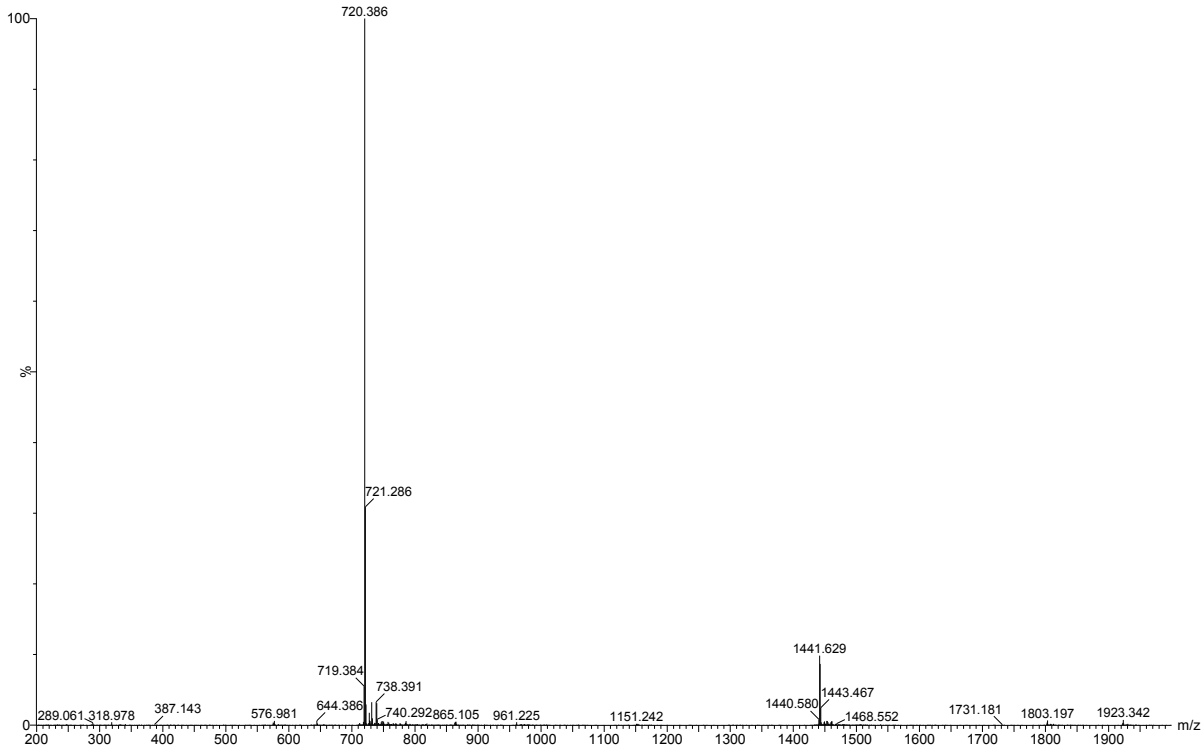

Supplementary figure 21. Mass spectrum of the pentamer fraction

In similar fashion to the tetramer fraction, the pentamer fraction preferentially forms a double charged ion which appears as a 720.386 m/z ratio with the single charge ion shown as a 1441.629 m/z ratio. The mass spectrum shows high purity.

A.2.10. Hexamer

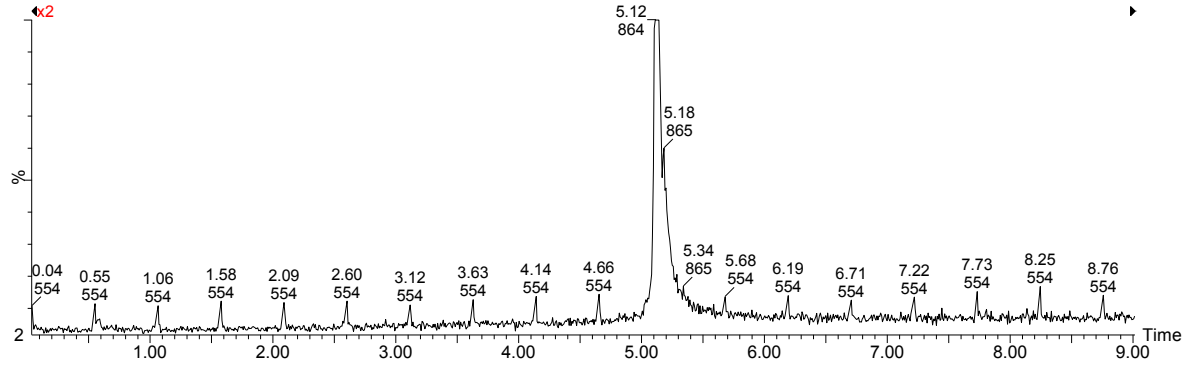

Supplementary figure 22. TIC chromatogram of the hexamer fraction

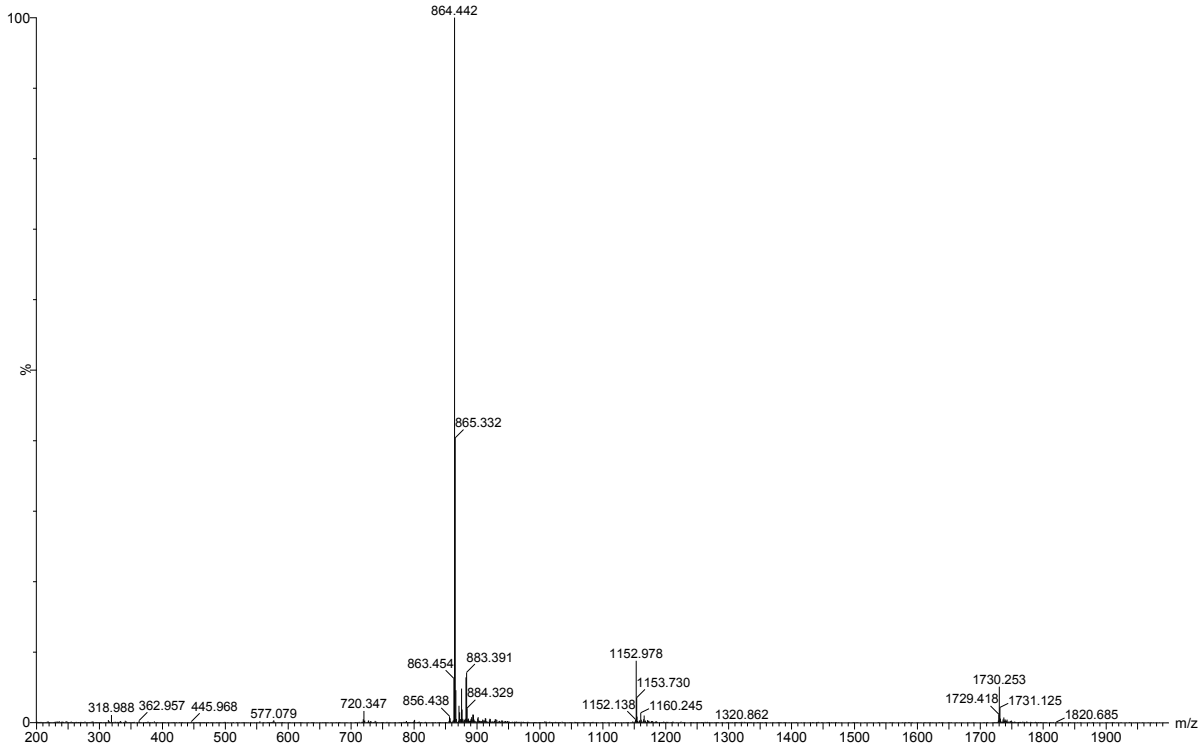

Supplementary figure 23. Mass spectrum of the hexamer fraction

The hexamer fraction's mass spectrum shows a clear impurity at 1152.978 of unknown composition. However, the trend for preferentially double charged ions is continued from the tetramer to the hexamer with increasing ratio of double charged ion to single charged ion as the level of polymerization increases.

A.3. Program Structure

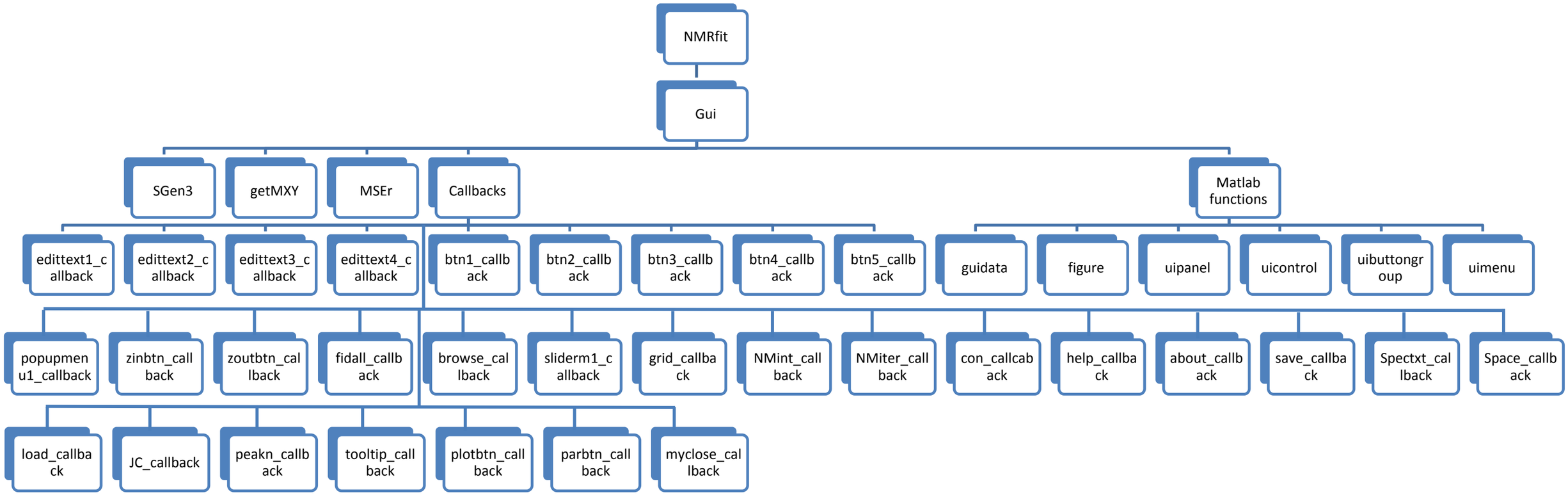

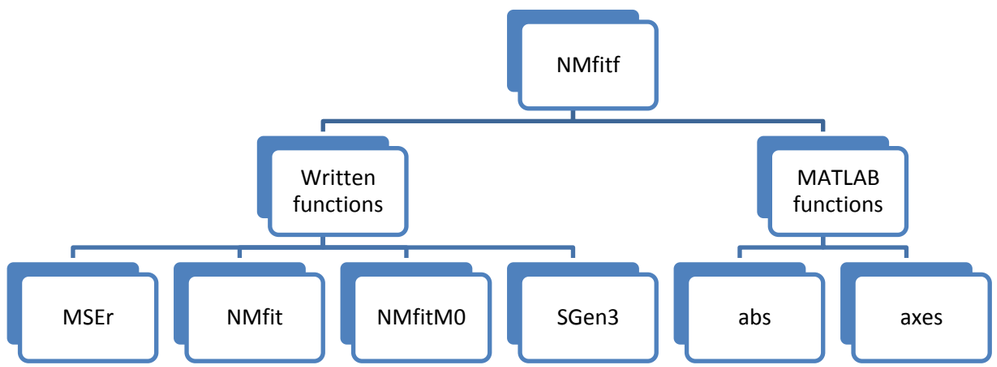

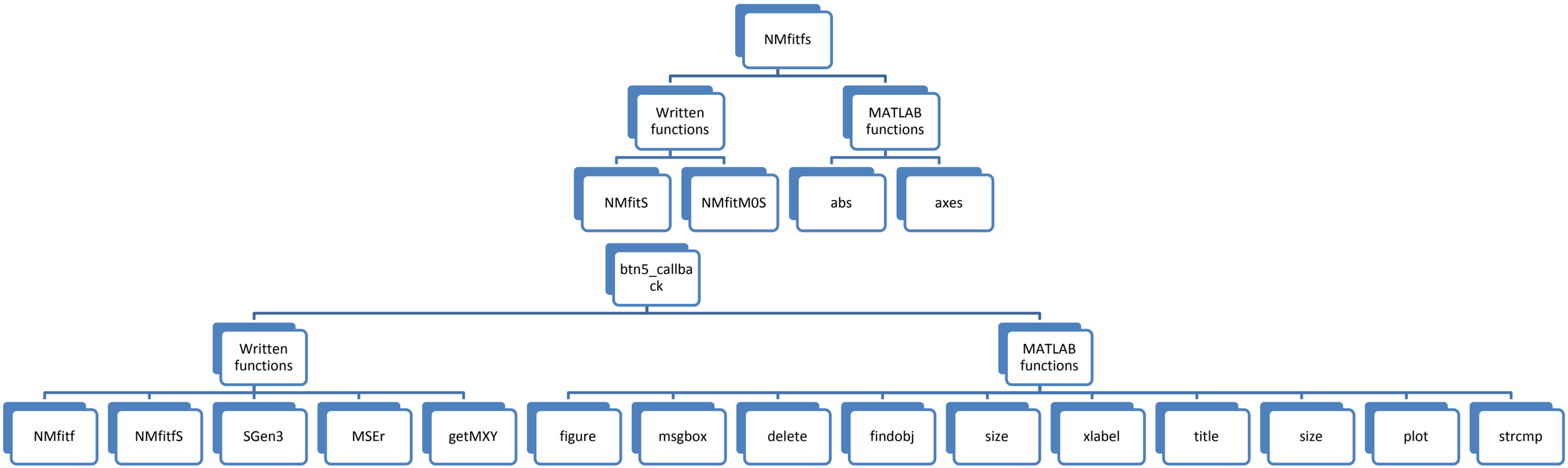

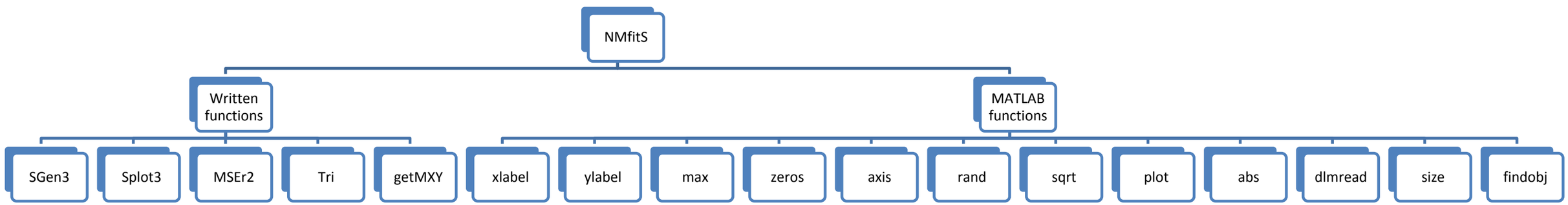

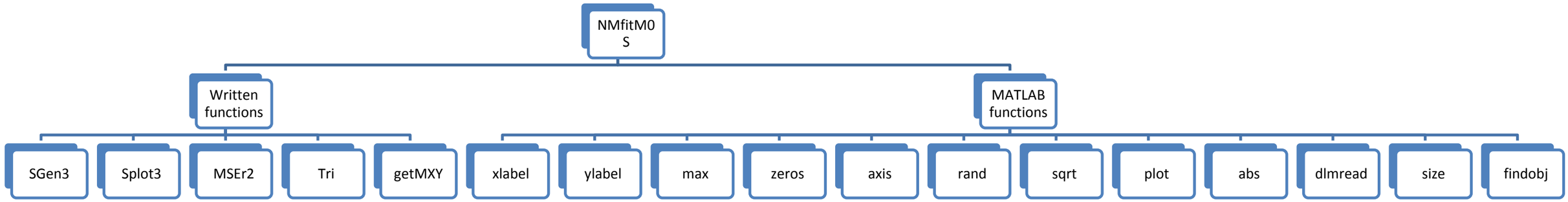

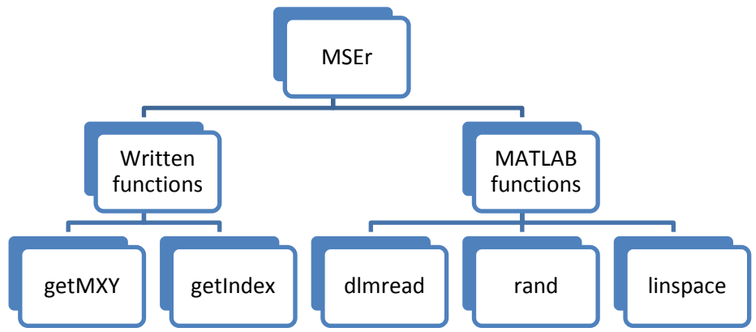

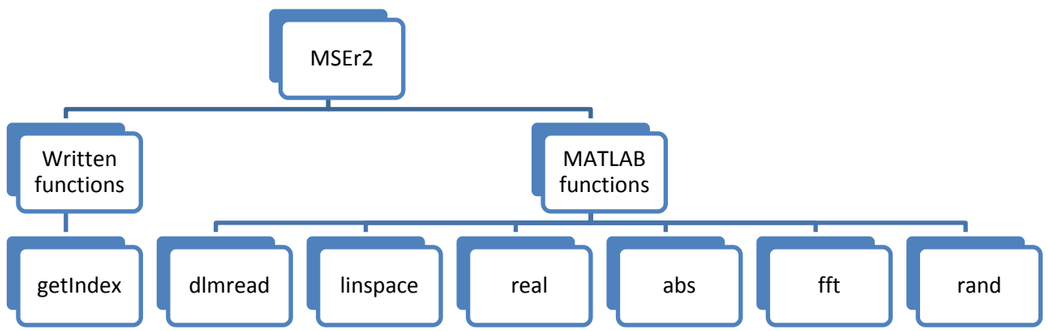

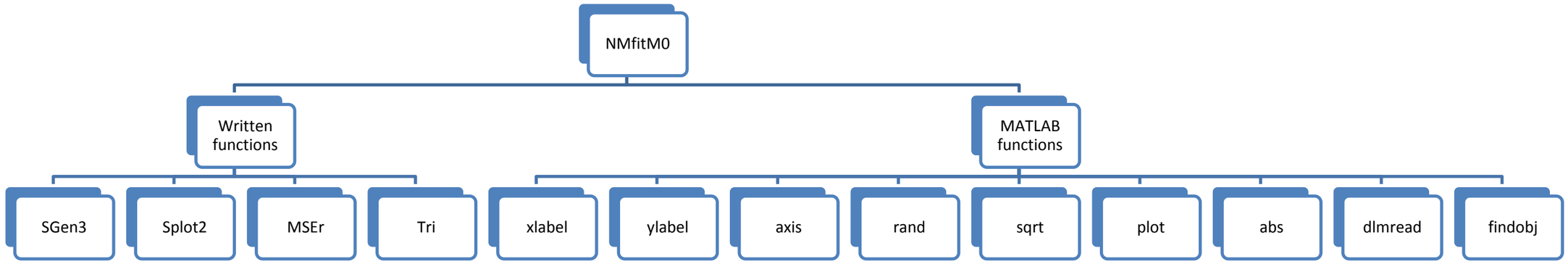

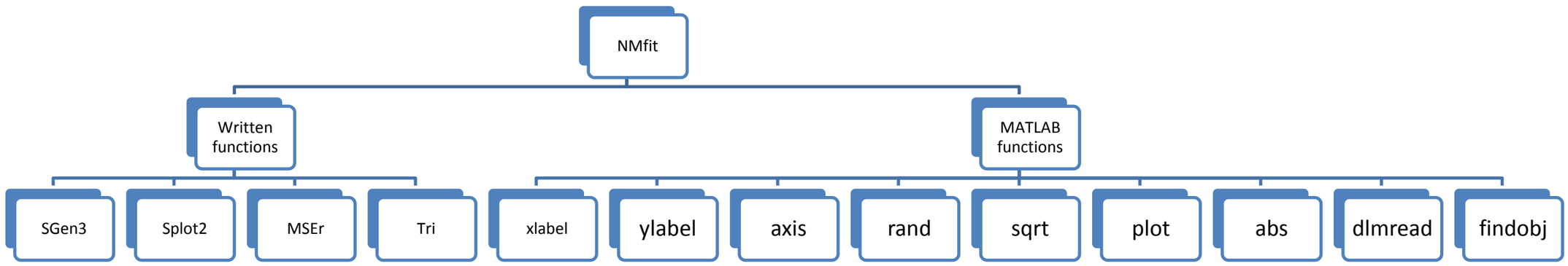

A.4. Program .m Files

The program algorithm implements a Nelder Mead simplex algorithm within the NMfit and NMfitMO. NMfit and NMfitMO files denote the fitting of the kinetic parameters or the magnetic intensity parameters of the Bloch-McConnell equation respectively. The NMfit and NMfitMO are alternated iteratively in turn within the respective full NMfitf.m files. The program iterates and alternates the callback of the NMfit and NMfitMO functions in order to approach a user specified convergence criterion. The addition of an 'S' to the Nelder Mead optimization .m file's name indicates that the optimization can be done on a sum of peaks that are fit using the same set of kinetic and thermodynamic parameters. Similarly, the addition of an 'A' to the .m file name indicates that an analytical solution of the Bloch-McConnell equation is implemented. It should be noted that all callback functions are deemed trivial and are not shown in this text but are attached in the electronic copy.

A.4.1. SGen.m

```
function Ma=SGen(Wi,R,K,M0)
%generates a NMR specra according to the bloch equations
%n- number of exchange states
%t- experimental time
%w- matrix of the chemical shifts of each peak
%R- matrix longitudinal relaxation rate for each species
%K- matrix of input estimations for ki
%M0- initial values of intensity for each peak (general distribution)
Fs = 1e6;
N=2001;

Ts = 1/Fs;
Tm = N*Ts;

t=0:Ts:Tm;

W=[];
n=length(M0);
W=Wi*Fs;
M=[];
K;
R;
W;
X=complex(K-R,W);

for j=1:1:N
   M=[M expm(X*t(j))*M0];
end
Mt=sum(M);
Mw=fft(Mt);


W = (0:1:N-1)*Fs/N;
Ma=[Mt; Mw; W];
```

A.4.2. SGen2.m

```
function Ma=SGen2(Wi,R,K,M0,N,spec)
%generates a NMR specra according to the bloch equations
%n- number of exchange states
%t- experimental time
%w- matrix of the chemical shifts of each peak
%R- matrix longitudinal relaxation rate for each species
%K- matrix of input estimations for ki
%M0- initial values of intensity for each peak (general distribution)
Fs = 1e6*spec;

Ts = 1/Fs;
Tm = N*Ts;

t=0:Ts:Tm;

W=[];
n=length(M0);
W=Wi*Fs/spec;
M=[];
K;
R;
W;
X=complex(K-R,W);

for j=1:1:N
   M=[M expm(X*t(j))*M0];
end

Mt=sum(M);
Mw=fft(Mt)/spec;

W = (0:1:N-1)*Fs/N;

Ma=[Mt; Mw; W];
```

A.4.3. SGen3.m

```
function Ma=SGen3(Wi,R,K,M0,N,spec,J,x,MHz)
%generates a NMR specra according to the bloch equations
%n- number of exchange states
%t- experimental time
%w- matrix of the chemical shifts of each peak
%R- matrix longitudinal relaxation rate for each species
%K- matrix of input estimations for ki
%M0- initial values of intensity for each peak (general distribution)
size(MHz);
size(spec);
Fs = MHz*spec;

Ts = 1/Fs;
Tm = N*Ts;

t=0:Ts:Tm;


n=length(M0);
W=Wi*Fs/spec;
K=K./(2*pi);

X=complex(K-R,W);

M=zeros(2,N);
for j=1:1:N

   M(:,j)=expm(X*t(j))*M0;
end

spl=cos(J(1)*pi*(1:1:N).*Ts).^(x(1)-1).*cos(J(2)*pi*(1:1:N).*Ts).^(x(2)-1).*cos(J(3)*pi*(1:1:N).*Ts).^(x(3)-
1).*cos(J(4)*pi*(1:1:N).*Ts).^(x(4)-1).*cos(J(5)*pi*(1:1:N).*Ts).^(x(5)-1);
spll=size(M0);
for int=1:spll(:,1)
splm(int,:) = spl;
end

Mt=sum(M.*splm);
Mw=fft(Mt)/spec;
```

A.4.4. AnalyticGen.m

```
function Mans=AnalyticGen(Wi,R,K,M0,N,spec,J,x,MHz)
Fs =MHz*spec;
Ts = 1/Fs;
Tm = N*Ts;

t=0:Ts:Tm;

W=Wi*Fs/spec;
K=K./(2*pi);

k2=-K(2,2);
k1=-K(1,1);
B1=R(1,1)-i*(W(1,1));
B2=R(2,2)-i*(W(2,2));
D=(B1-B2+k1-k2)^2+4*k1*k2;
a=k2;
b=a;
c=0.5*(B1-B2+k1-k2+D^0.5);
d=0.5*(B1-B2+k1-k2-D^0.5);
U=[a b; c d];
U1=(1/(a*d-b*c))*[d -b; -c a];
L1=0.5*(-(B1+B2+k1+k2)+D^0.5);
L2=0.5*(-(B1+B2+k1+k2)-D^0.5);
T=exp(L1*t);
C=zeros(2,2,N);
for j= 1:N
Xa=[exp(L1*t(j)) 0;0 exp(L2*t(j))];
Mall(:,j)=U*Xa*U1*M0;
end
Ma=Mall(1,:);
Mb=Mall(2,:);
M=Ma +Mb;
W = (0:1:N-1)*Fs/N;
W=W;

spl=cos(J(1)*pi*(1:1:N).*Ts).^(x(1)-1).*cos(J(2)*pi*(1:1:N).*Ts).^(x(2)-1).*cos(J(3)*pi*(1:1:N).*Ts).^(x(3)-
1).*cos(J(4)*pi*(1:1:N).*Ts).^(x(4)-1).*cos(J(5)*pi*(1:1:N).*Ts).^(x(5)-1);

Mt=M.*spl;
Mw=fft(Mt)/spec;
Mans=[Mt;(real(Mw)); W];
```

A.4.5. GUI.m

```
function GUI
%A function to display spectra and fit them theoretically
%
%  The fit works by using a Bloch McConnel matrix of the given peaks
%    where:
%           M(t)=exp(Wi-R+K)*(M0)
%        Wi is a square matrix of the chemical shifts
%        R is a square matrix of the relaxation constants
%        K is a square matrix of the reaction constants
%        M0 is the initial magnetic intensities of the species that are
%        proportional to the concentrations of the protons
%
%
%
%
%originalLnF = javax.swing.UIManager.getLookAndFeel;
%javax.swing.UIManager.setLookAndFeel('com.jtattoo.plaf.noire.NoireLookAndFeel');
% Create and then hide GUI----------------------------

f= figure('Color',[.1 .1
.1],'Visible','off','units','normalized','Position',[.05,.07,.9,.85],'NumberTitle','off','Name','NMRFit','Renderer','OpenG
L');
set(f,'menubar','none');
tm=javax.swing.ToolTipManager.sharedInstance;
txtchk='Test3.txt';

%add handle fields-----------------------------------

handle = guihandles(f);
handle.npeaks=1;
for num=1:handle.npeaks

handle.cpb(num)=1;%current parameter button
end
handle.ccpb=1;%current chosen parameter button
handle.cps=1;%current peak set
handle.text=txtchk;
%handle.n=2;
handle.N=10001;
handle.W1=1;
handle.W2=1.5;
W=[handle.W1 0; 0 handle.W2];
handle.R=0.5;
R=[handle.R 0; 0 handle.R];
handle.k1=10;
handle.k2=10;
K=[-handle.k1 handle.k2;handle.k1 -handle.k2];
handle.M1=2;
handle.M2=1;
M=[handle.M1; handle.M2];
handle.C1=0.9;
```

```
handle.C2=1.1;
handle.C3=1.4;
handle.C4=1.6;
handle.JC1=0;
handle.JC2=0;
handle.JC3=0;
handle.JC4=0;
handle.JC5=0;
handle.X1=1;
handle.X2=1;
handle.X3=1;
handle.X4=1;
handle.X5=1;
J=[handle.JC1 , handle.JC2 , handle.JC3, handle.JC4 , handle.JC5];
x=[handle.X1 , handle.X2 , handle.X3, handle.X4 , handle.X5];
C=[handle.C1 handle.C2; handle.C3 handle.C4];
handle.Mhz=400;
handle.space=100;
handle.grid=5;
handle.spec=1;
handle.NMint=0.001;
handle.NMiter=5;
handle.converge=0.01;
handle.d=100;
handle.mse=MSEr(AnalyticGen(W,R,K,M,handle.N,handle.spec,J,x,handle.Mhz),handle.text,C,handle.space,handle.
Mhz,handle.d);
handle.btntxt1='plot';
handle.btntxt2='set';
handle.btntxt3='initial fit';
handle.h=plot([1 1]);
handle.method='Select Method';
sliderWidth=30;
sliderspacing=sliderWidth+10;
hold on
set(handle.h,'Visible','off')
handle.fit=plot([1 1]);
set(handle.fit,'Visible','off')
set(gca,'Visible','off','Position',[.1,.1,.85,.3])
hold off
guidata(f,handle)

%Construct components
%--------------------------------------
%uip= uipanel('Position',[0,0.8,1,0.2],'BackgroundColor',[0.4 0.4 0.5]);
%UIpanel 1 components
textdataset= uicontrol('Style','text','BackgroundColor',[.2 .2 .2],'ForegroundColor',[1 1
1],'String','Datafile','units','normalized','Position',[0.06,.98,.1,0.02],'TooltipString','The file directory and name of
the text file(xy column format) that you would like to be fit');
textmethod= uicontrol('Style','text','BackgroundColor',[.2 .2 .2],'ForegroundColor',[1 1 1],'String','Optimization
method','units','normalized','Position',[0.02,.93,.1,0.02],'TooltipString','Choose your fit method (to be expanded in
future)');
%textSites= uicontrol('Style','text','BackgroundColor',[.2 .2 .2],'ForegroundColor',[1 1 1],'String','Number of
exchange sites','Position',[420, 480,130,18]);
```

```
boxdataset= uicontrol('Style','edit','BackgroundColor',[.2 .2 .2],'ForegroundColor',[1 1
1],'String',txtchk,'units','normalized','units','normalized','Position',[0.060,.95,.14,0.03],'callback',@edittext1_Callba
ck,'TooltipString','Input the file directory and name of the text file(xy column format) that you would like to be
fit','Tag','boxdataset');

browsebtn= uicontrol('Style','pushbutton','BackgroundColor',[.2 .2 .2],'ForegroundColor',[1 1
1],'String','browse','units','normalized','Position',[0.02,.95,.04,0.03],'callback',@browse_Callback,'TooltipString','Br
owse for the text file(xy column format) that you would like to be fit');
dropmethod= uicontrol('Style','popupmenu','BackgroundColor',[0.1 0.1 0.1],'ForegroundColor',[1 1
1],'String','Select Method|Nelder Mead|all peak Nelder mead|Analytical Nelder Mead|Analytical all peak Nelder
Mead|Analytical  Nelder Mead
Symmetric','units','normalized','Position',[0.02,.90,.1,0.03],'callback',@popupmenu1_Callback,'TooltipString','Choo
se your fit method (to be expanded in future)');
%boxSites= uicontrol('Style','edit','BackgroundColor',[.2 .2 .2],'ForegroundColor',[1 1
1],'units','normalized','Position',[420, 455,130,30]);
plotbtn= uicontrol('Style','pushbutton','BackgroundColor',[.2 .2 .2],'ForegroundColor',[1 1
1],'String',handle.btntxt1,'units','normalized','Position',[0.2,.95,.05,0.03],'callback',@btn1_Callback,'TooltipString','
Plot the data','Tag', 'plot1');
%setbtn= uicontrol('Style','pushbutton','BackgroundColor',[.2 .2 .2],'ForegroundColor',[1 1
1],'String',handle.btntxt2,'units','normalized','Position',[550, 455,35,30],'callback',@btn2_Callback);
plotbtn2= uicontrol('Style','pushbutton','BackgroundColor',[.2 .2 .2],'ForegroundColor',[1 1
1],'String',handle.btntxt3,'units','normalized','Position',[0.02,.70,.05,0.03],'callback',@btn3_Callback,'TooltipString',
'Add the fit','Tag','plot2');
fidbtn= uicontrol('Style','pushbutton','BackgroundColor',[.2 .2 .2],'ForegroundColor',[1 1
1],'String','FID','units','normalized','Position',[0.07,.70,.05,0.03],'callback',@btn4_Callback,'TooltipString','Show the
fit equation time domain');
fidallbtn= uicontrol('Style','pushbutton','BackgroundColor',[.2 .2 .2],'ForegroundColor',[1 1 1],'String','FID
all','units','normalized','Position',[0.07,.67,.05,0.03],'callback',@fidall_Callback,'TooltipString','Show the fit
equation time domain of all peak sets');
fitbtn= uicontrol('Style','pushbutton','BackgroundColor',[.2 .2 .2],'ForegroundColor',[1 1 1],'String','Engage
fit','units','normalized','Position',[0.12,.70,.05,0.03],'callback',@btn5_Callback,'TooltipString','Engage the chosen fit
method');
zinbtn= uicontrol('Style','pushbutton','BackgroundColor',[.2 .2 .2],'ForegroundColor',[1 1 1],'String','zoom
in','units','normalized','Position',[0.62,.62,.05,0.03],'callback',@zinbtn_Callback,'TooltipString','Select or deselect
the zoom cursor');
zoutbtn= uicontrol('Style','pushbutton','BackgroundColor',[.2 .2 .2],'ForegroundColor',[1 1 1],'String','zoom
out','units','normalized','Position',[0.67,.62,.05,0.03],'callback',@zoutbtn_Callback,'TooltipString','Return to the full
figure zoom');


sPanel=uipanel(f,'Title','Spectrum variables','Position',[0.12,.76,.10,.14],'BackGroundColor',[0.2 0.2
0.2],'ForegroundColor','w','ShadowColor',[0.4 0.4 0.4],'BorderType','beveledout');
boxSpectral= uicontrol(sPanel,'Style','edit','BackgroundColor',[.2 .2 .2],'ForegroundColor',[1 1
1],'String',sprintf('%0.3g
ppm',handle.spec*2*pi),'units','normalized','Position',[0,1/15*10,1,1/15*2.5],'callback',@spectxt_Callback,'Tooltip
String','Input the spectral width in ppm (it must stretch from 0)','Tag','spec');
boxSpectraltxt= uicontrol(sPanel,'Style','text','BackgroundColor',[.2 .2 .2],'ForegroundColor',[1 1 1],'String','spectral
width','units','normalized','Position',[0,1/15*12.5,1,1/15*2.5],'TooltipString','The spectral width in ppm (it must
stretch from 0)');
Rtxt= uicontrol(sPanel,'Style','text','BackgroundColor',[.2 .2 .2],'ForegroundColor',[1 1
1],'String','R','units','normalized','Position',[0,1/15*7.5,1,1/15*2.5],'TooltipString','Relaxation constant T2');
```

```
Rvtext= uicontrol(sPanel,'Style','edit','BackgroundColor',[.2 .2 .2],'ForegroundColor',[1 1
1],'String',handle.R,'units','normalized','Position',[0,1/15*5,1,1/15*2.5],'callback',@edittext4_Callback,'TooltipStrin
g','Input the relaxation constant T2 in Hz','Tag','Rvtext');
MseSpacetxt= uicontrol(sPanel,'Style','text','BackgroundColor',[.2 .2 .2],'ForegroundColor',[1 1 1],'String','Mse
spacing','units','normalized','Position',[0,1/15*2.5,1,1/15*2.5],'TooltipString','Number of points in a mean square
error fit range');
MseSpacevtext= uicontrol(sPanel,'Style','edit','BackgroundColor',[.2 .2 .2],'ForegroundColor',[1 1
1],'String',handle.space,'units','normalized','Position',[0,0,1,1/15*2.5],'callback',@space_Callback,'TooltipString','N
umber of points in a mean square error fit range');

%-------------Scrollbars----------------------
%uip2=uipanel('units','normalized','Position',[0,0.5,1,0.3],'BackgroundColor',[0.4 0.4 0.5]);
m1Scroll= uicontrol('Style','slider','units','normalized','Position',[.37,0.75,.04,.2],'SliderStep',[0.01
0.01],'Min',0,'Max',500000000,'Value',handle.M1,'Callback',@sliderm1_callback,'TooltipString','Magnetization
concentration for conformer 1','Tag','slideM1');
w1Scroll= uicontrol('Style','slider','units','normalized','Position',[.37+0.05*1,0.75,.04,.2],'SliderStep',[0.0001
0.0001],'Min',0,'Max',10000,'Value',handle.W1,'Callback',@sliderm1_callback,'TooltipString','Chemical shift of
conformer 1 in ppm','Tag','slideW1');
k1Scroll= uicontrol('Style','slider','units','normalized','Position',[.37+0.05*2,0.75,.04,.2],'SliderStep',[0.000001
0.000001],'Min',0,'Max',600000,'Value',str2num(sprintf('%.1g',handle.k1)),'Callback',@sliderm1_callback,'TooltipSt
ring','Kinetic constant k1','Tag','slidek1');
m2Scroll= uicontrol('Style','slider','units','normalized','Position',[.37+0.05*3,0.75,.04,.2],'SliderStep',[0.01
0.01],'Min',0,'Max',500000000,'Value',handle.M2,'Callback',@sliderm1_callback,'TooltipString','Magnetization
concentration for conformer 2','Tag','slideM2');
w2Scroll= uicontrol('Style','slider','units','normalized','Position',[.37+0.05*4,0.75,.04,.2],'SliderStep',[0.0001
0.0001],'Min',0,'Max',10000,'Value',handle.W2,'Callback',@sliderm1_callback,'TooltipString','Chemical shift of
conformer 2 in ppm','Tag','slideW2');
k2Scroll= uicontrol('Style','slider','units','normalized','Position',[.37+0.05*5,0.75,.04,.2],'SliderStep',[0.000001
0.000001],'Min',0,'Max',600000,'Value',str2num(sprintf('%.1g',handle.k2)),'Callback',@sliderm1_callback,'TooltipSt
ring','Kinetic constant k2','Tag','slidek2');
resScroll= uicontrol('Style','slider','units','normalized','Position',[.37+0.05*6,0.75,.04,.2],'SliderStep',[0.01
0.01],'Min',1000,'Max',20000,'Value',handle.N,'Callback',@sliderm1_callback,'TooltipString','Number of points
generated','Tag','slideRes');

peak1= uicontrol('Style','text','BackgroundColor',[.2 .2 .2],'ForegroundColor',[1 1 1],'String','peak
1','units','normalized','Position',[.37+0.05*0,0.98,.14,.02]);
m1text= uicontrol('Style','text','BackgroundColor',[.2 .2 .2],'ForegroundColor',[1 1
1],'String','M1','units','normalized','Position',[.37+0.05*0,0.95,.04,.02],'TooltipString','Magnetization concentration
for conformer 1');
w1text= uicontrol('Style','text','BackgroundColor',[.2 .2 .2],'ForegroundColor',[1 1
1],'String','W1','units','normalized','Position',[.37+0.05*1,0.95,.04,.02],'TooltipString','Chemical shift of conformer 1
in ppm');
k1text= uicontrol('Style','text','BackgroundColor',[.2 .2 .2],'ForegroundColor',[1 1
1],'String','k1','units','normalized','Position',[.37+0.05*2,0.95,.04,.02],'TooltipString','Kinetic constant k1');
peak2= uicontrol('Style','text','BackgroundColor',[.2 .2 .2],'ForegroundColor',[1 1 1],'String','peak
2','units','normalized','Position',[.37+0.05*3,0.98,.14,.02]);
m2text= uicontrol('Style','text','BackgroundColor',[.2 .2 .2],'ForegroundColor',[1 1
1],'String','M2','units','normalized','Position',[.37+0.05*3,0.95,.04,.02],'TooltipString','Magnetization concentration
for conformer 2');
w2text= uicontrol('Style','text','BackgroundColor',[.2 .2 .2],'ForegroundColor',[1 1
1],'String','W2','units','normalized','Position',[.37+0.05*4,0.95,.04,.02],'TooltipString','Chemical shift of conformer 2
in ppm');
```

```
k2text= uicontrol('Style','text','BackgroundColor',[.2 .2 .2],'ForegroundColor',[1 1
1],'String','k2','units','normalized','Position',[.37+0.05*5,0.95,.04,.02],'TooltipString','Kinetic constant k2');
restxt= uicontrol('Style','text','BackgroundColor',[.2 .2 .2],'ForegroundColor',[1 1
1],'String','Resolution','units','normalized','Position',[.37+0.05*6,0.95,.04,.02],'TooltipString','Number of points
generated');

m1vtext= uicontrol('Style','edit','BackgroundColor',[.2 .2 .2],'ForegroundColor',[1 1
1],'String',handle.M1,'units','normalized','Position',[.37+0.05*0,.73,.04,.02],'callback',@edittext2_Callback,'Tooltip
String','Magnetization concentration for conformer 1','Tag','editM1');
w1vtext= uicontrol('Style','edit','BackgroundColor',[.2 .2 .2],'ForegroundColor',[1 1
1],'String',handle.W1,'units','normalized','Position',[.37+0.05*1,.73,.04,.02],'callback',@edittext2_Callback,'Tooltip
String','Chemical shift of conformer 1 in ppm','Tag','editW1');
k1vtext= uicontrol('Style','edit','BackgroundColor',[.2 .2 .2],'ForegroundColor',[1 1
1],'String',handle.k1,'units','normalized','Position',[.37+0.05*2,.73,.04,.02],'callback',@edittext2_Callback,'TooltipSt
ring','Kinetic constant k1','Tag','editk1');
m2vtext= uicontrol('Style','edit','BackgroundColor',[.2 .2 .2],'ForegroundColor',[1 1
1],'String',handle.M2,'units','normalized','Position',[.37+0.05*3,.73,.04,.02],'callback',@edittext2_Callback,'Tooltip
String','Magnetization concentration for conformer 2','Tag','editM2');
w2vtext= uicontrol('Style','edit','BackgroundColor',[.2 .2 .2],'ForegroundColor',[1 1
1],'String',handle.W2,'units','normalized','Position',[.37+0.05*4,.73,.04,.02],'callback',@edittext2_Callback,'Tooltip
String','Chemical shift of conformer 2 in ppm','Tag','editW2');
k2vtext= uicontrol('Style','edit','BackgroundColor',[.2 .2 .2],'ForegroundColor',[1 1
1],'String',handle.k2,'units','normalized','Position',[.37+0.05*5,.73,.04,.02],'callback',@edittext2_Callback,'TooltipSt
ring','Kinetic constant k2','Tag','editk2');
resvtxt= uicontrol('Style','edit','BackgroundColor',[.2 .2 .2],'ForegroundColor',[1 1
1],'String',handle.N,'units','normalized','Position',[.37+0.05*6,.73,.04,.02],'callback',@edittext2_Callback,'TooltipStr
ing','Number of points generated','Tag','editRes');

% Bounds for MSE
Cpanel=uipanel(f,'Title','MSE ranges','Position',[0.02,.80,.10,.1],'BackGroundColor',[0.2 0.2
0.2],'ForegroundColor','w','ShadowColor',[0.4 0.4 0.4],'BorderType','beveledout');
%Ctext= uicontrol('Style','text','BackgroundColor',[.2 .2 .2],'ForegroundColor',[1 1 1],'String','MSE
range','units','normalized','Position',[.02,.80,.1,.02],'TooltipString','spectral ranges to be included during tht fit');
C1text= uicontrol(Cpanel,'Style','text','BackgroundColor',[.2 .2 .2],'ForegroundColor',[1 1
1],'String','start','units','normalized','Position',[0.,0.75,0.5,0.25]);
C2text= uicontrol(Cpanel,'Style','text','BackgroundColor',[.2 .2 .2],'ForegroundColor',[1 1
1],'String','end','units','normalized','Position',[0.5,0.75,0.5,0.25]);
C1vtext= uicontrol(Cpanel,'Style','edit','BackgroundColor',[.2 .2 .2],'ForegroundColor',[1 1
1],'String',handle.C1,'units','normalized','Position',[0.0,0.5,0.5,0.25],'callback',@edittext3_Callback,'TooltipString','s
tart of the first peak fit range','Tag','C1vtext');
C2vtext= uicontrol(Cpanel,'Style','edit','BackgroundColor',[.2 .2 .2],'ForegroundColor',[1 1
1],'String',handle.C2,'units','normalized','Position',[0.5,0.5,0.5,0.25],'callback',@edittext3_Callback,'TooltipString','
end of the first peak fit range','Tag','C2vtext');
C3text= uicontrol(Cpanel,'Style','text','BackgroundColor',[.2 .2 .2],'ForegroundColor',[1 1
1],'String','start','units','normalized','Position',[0.0,0.25,0.5,0.25]);
C4text= uicontrol(Cpanel,'Style','text','BackgroundColor',[.2 .2 .2],'ForegroundColor',[1 1
1],'String','end','units','normalized','Position',[0.5,0.25,0.5,0.25]);
C3vtext= uicontrol(Cpanel,'Style','edit','BackgroundColor',[.2 .2 .2],'ForegroundColor',[1 1
1],'String',handle.C3,'units','normalized','Position',[0.0,0.0,0.5,0.25],'callback',@edittext3_Callback,'TooltipString','s
tart of the second peak fit range','Tag','C3vtext');
C4vtext= uicontrol(Cpanel,'Style','edit','BackgroundColor',[.2 .2 .2],'ForegroundColor',[1 1
1],'String',handle.C4,'units','normalized','Position',[0.5,0.0,0.5,0.25],'callback',@edittext3_Callback,'TooltipString','
end of the second peak fit range','Tag','C4vtext');
```

```
MseGridtxt= uicontrol('Style','text','BackgroundColor',[.2 .2 .2],'ForegroundColor',[1 1
1],'String','Grid','units','normalized','Position',[.28,.80,.05,0.02],'Visible','off','TooltipString','Number of points in a
MSE fit method grid axis');
MseGridvtext= uicontrol('Style','edit','BackgroundColor',[.2 .2 .2],'ForegroundColor',[1 1
1],'String',handle.grid,'units','normalized','Position',[.28,.75,.05,0.05],'callback',@grid_Callback,'Visible','off','Toolti
pString','Input the number of points in a MSE fit method grid axis');
MSEtext= uicontrol('Style','text','BackgroundColor',[.2 .2 .2],'ForegroundColor',[1 1 1],'String',['MSE: ',
num2str(handle.mse)],'units','normalized','Position',[.88,.63,.1,0.02],'Visible','on','Tag','MSE');

nmPanel=uipanel(f,'Title','Nelder Mead variables','Position',[0.22,.76,.10,.14],'BackGroundColor',[0.2 0.2
0.2],'ForegroundColor','w','ShadowColor',[0.4 0.4 0.4],'BorderType','beveledout','Visible','off','Tag','NM');
NMinttxt= uicontrol(nmPanel,'Style','text','BackgroundColor',[.2 .2 .2],'ForegroundColor',[1 1 1],'String','NM
interval','units','normalized','Position',[0,1/15*12.5,1,1/15*2.5],'TooltipString','starting fraction of current variable
for a Nelder Mead initial step','Tag','NMintext');
NMintvtext= uicontrol(nmPanel,'Style','edit','BackgroundColor',[.2 .2 .2],'ForegroundColor',[1 1
1],'String',handle.NMint,'units','normalized','Position',[0,1/15*10,1,1/15*2.5],'callback',@NMint_Callback,'TooltipS
tring','starting fraction of current variable for a Nelder Mead initial step','Tag','NMinvtext');
NMitertxt= uicontrol(nmPanel,'Style','text','BackgroundColor',[.2 .2 .2],'ForegroundColor',[1 1 1],'String','NM
iterations','units','normalized','Position',[0,1/15*7.5,1,1/15*2.5],'TooltipString','Iterations for the Nelder Mead
Optimization','Tag','NMittext');
NMitervtext= uicontrol(nmPanel,'Style','edit','BackgroundColor',[.2 .2 .2],'ForegroundColor',[1 1
1],'String',handle.NMiter,'units','normalized','Position',[0,1/15*5,1,1/15*2.5],'callback',@NMiter_Callback,'Tooltip
String','Iterations for the Nelder Mead Optimization','Tag','NMitvtext');
convergetxt= uicontrol(nmPanel,'Style','text','BackgroundColor',[.2 .2 .2],'ForegroundColor',[1 1 1],'String','Conv
%','units','normalized','Position',[0,1/15*2.5,1,1/15*2.5],'Visible','on','ToolTipString','Convergence criteria for
optimized variables in percentage change','Tag','crittext');
convergebox= uicontrol(nmPanel,'Style','edit','BackgroundColor',[.2 .2 .2],'ForegroundColor',[1 1
1],'String',num2str(sprintf('%.2g%%',handle.converge*100)),'units','normalized','Position',[0,0,1,1/15*2.5],'callback
',@con_Callback,'Visible','on','ToolTipString','Convergence criteria for optimized variables in percentage
change','Tag','critvtext');

nm1Panel=uipanel(f,'Title','Nelder Mead variables','Position',[0.22,.72,.10,.18],'BackGroundColor',[0.2 0.2
0.2],'ForegroundColor','w','ShadowColor',[0.4 0.4 0.4],'BorderType','beveledout','Visible','off','Tag','NM1');
NM1inttxt= uicontrol(nm1Panel,'Style','text','BackgroundColor',[.2 .2 .2],'ForegroundColor',[1 1 1],'String','NM
interval','units','normalized','Position',[0,7/8.5,1,1/8],'TooltipString','starting fraction of current variable for a
Nelder Mead initial step','Tag','NM1intext');
NM1intvtext= uicontrol(nm1Panel,'Style','edit','BackgroundColor',[.2 .2 .2],'ForegroundColor',[1 1
1],'String',handle.NMint,'units','normalized','Position',[0,6/8,1,1/8],'callback',@NMint_Callback,'TooltipString','star
ting fraction of current variable for a Nelder Mead initial step','Tag','NM1invtext');
NM1itertxt= uicontrol(nm1Panel,'Style','text','BackgroundColor',[.2 .2 .2],'ForegroundColor',[1 1 1],'String','NM
iterations','units','normalized','Position',[0,5/8,1,1/8],'TooltipString','Iterations for the Nelder Mead
Optimization','Tag','NM1ittext');
NM1itervtext= uicontrol(nm1Panel,'Style','edit','BackgroundColor',[.2 .2 .2],'ForegroundColor',[1 1
1],'String',handle.NMiter,'units','normalized','Position',[0,4/8,1,1/8],'callback',@NMiter_Callback,'TooltipString','Ite
rations for the Nelder Mead Optimization','Tag','NM1itvtext');
converge1txt= uicontrol(nm1Panel,'Style','text','BackgroundColor',[.2 .2 .2],'ForegroundColor',[1 1 1],'String','Conv
%','units','normalized','Position',[0,3/8,1,1/8],'Visible','on','ToolTipString','Convergence criteria for optimized
variables in percentage change','Tag','crittext1');
converge1box= uicontrol(nm1Panel,'Style','edit','BackgroundColor',[.2 .2 .2],'ForegroundColor',[1 1
1],'String',num2str(sprintf('%.2g%%',handle.converge*100)),'units','normalized','Position',[0,2/8,1,1/8],'callback',@
```

```
con_Callback,'Visible','on','ToolTipString','Convergence criteria for optimized variables in percentage
change','Tag','critvtext1');
chosenvartxt= uicontrol(nm1Panel,'Style','text','BackgroundColor',[.2 .2 .2],'ForegroundColor',[1 1
1],'String','chosen parameter set','units','normalized','Position',[0,1/8,1,1/8],'Visible','on','ToolTipString','Parameter
set to optimize','Tag','chosenvartxt');
chosenvarbox= uicontrol(nm1Panel,'Style','edit','BackgroundColor',[.2 .2 .2],'ForegroundColor',[1 1
1],'String',num2str(handle.ccpb),'units','normalized','Position',[0,0/8,1,1/8],'callback',@con_Callback,'Visible','on','
ToolTipString','Parameter set to optimize','Tag','chosenvarbox');

decPanel=uipanel(f,'Title','decimal places','Position',[.72,.72,.10,.06],'BackGroundColor',[0.2 0.2
0.2],'ForegroundColor','w','ShadowColor',[0.4 0.4 0.4],'BorderType','beveledout','Visible','on','Tag','dec1');
decedit=uicontrol(decPanel,'Style','edit','BackgroundColor',[.2 .2 .2],'ForegroundColor',[1 1
1],'String',log10(handle.d),'units','normalized','Position',[0,0,1,1],'callback',@dec_Callback,'Visible','on','ToolTipStri
ng','Convergence criteria for optimized variables in percentage change','Tag','dect1');
MHzPanel=uipanel(f,'Title','Machine frequency','Position',[.72,.78,.10,.06],'BackGroundColor',[0.2 0.2
0.2],'ForegroundColor','w','ShadowColor',[0.4 0.4 0.4],'BorderType','beveledout','Visible','on','Tag','MHz1');
MHzedit=uicontrol(MHzPanel,'Style','edit','BackgroundColor',[.2 .2 .2],'ForegroundColor',[1 1
1],'String',handle.Mhz,'units','normalized','Position',[0,0,1,1],'callback',@MHz_Callback,'Visible','on','ToolTipString',
'Convergence criteria for optimized variables in percentage change','Tag','MHzt1');

%uimenu-----------------------------------------------------------------
File= uimenu('Label','File');
options= uimenu('Label','Options');
%peakSet = uimenu('Label','Peak sets');
%peak1= uimenu(peakSet,'Label','Peak set 1','Callback',@peak_Callback);

help= uimenu('Label','Help','Callback',@help_Callback);
about= uimenu('Label','About','Callback',@about_Callback);
save= uimenu(File,'Label','Save parameters','Callback',@save_Callback);
load= uimenu(File,'Label','Load parameters','Callback',@load_Callback);
savespec= uimenu(File,'Label','Save the spectrum','Callback',@savespec_Callback);

%J coupling
cplingP = uipanel(f,'Title','JCoupling','Position',[0.22,.70,.15,.1],'BackGroundColor',[0.2 0.2
0.2],'ForegroundColor','w','ShadowColor',[0.4 0.4 0.4],'BorderType','beveledout','Visible','off','Tag','cplingP');
jcoupling= uicontrol('Style','togglebutton','BackgroundColor',[.2 .2 .2],'ForegroundColor',[1 1 1],'String','J-
Coupling','units','normalized','Position',[.17,.70,.05,0.03],'Value',0,'callback',@JC_Callback,'Visible','on','TooltipStrin
g','is there any J-Coupling?','Tag','Jtoggle');

Jedit1 = uicontrol(cplingP,'Style','edit','BackgroundColor',[.2 .2 .2],'ForegroundColor',[1 1
1],'String',handle.JC1,'units','normalized','Position',[.0,.5,.2,.25],'callback',@JC_Callback,'TooltipString','Coupling
constant 1','Tag','JC1');
Jedit2 = uicontrol(cplingP,'Style','edit','BackgroundColor',[.2 .2 .2],'ForegroundColor',[1 1
1],'String',handle.JC2,'units','normalized','Position',[.2,.5,.2,.25],'callback',@JC_Callback,'TooltipString','Coupling
constant 2','Tag','JC2');
Jedit3 = uicontrol(cplingP,'Style','edit','BackgroundColor',[.2 .2 .2],'ForegroundColor',[1 1
1],'String',handle.JC3,'units','normalized','Position',[.4,.5,.2,.25],'callback',@JC_Callback,'TooltipString','Coupling
constant 3','Tag','JC3');
Jedit4 = uicontrol(cplingP,'Style','edit','BackgroundColor',[.2 .2 .2],'ForegroundColor',[1 1
1],'String',handle.JC4,'units','normalized','Position',[.6,.5,.2,.25],'callback',@JC_Callback,'TooltipString','Coupling
constant 4','Tag','JC4');
```

```
Jedit5 = uicontrol(cplingP,'Style','edit','BackgroundColor',[.2 .2 .2],'ForegroundColor',[1 1
1],'String',handle.JC5,'units','normalized','Position',[.8,.5,.2,.25],'callback',@JC_Callback,'TooltipString','Coupling
constant 5','Tag','JC5');

Jtxt1 = uicontrol(cplingP,'Style','text','BackgroundColor',[.2 .2 .2],'ForegroundColor',[1 1
1],'String','JC1','units','normalized','Position',[.0,.75,.2,.25],'TooltipString','Coupling constant 1','Tag','JT1');
Jtxt2 = uicontrol(cplingP,'Style','text','BackgroundColor',[.2 .2 .2],'ForegroundColor',[1 1
1],'String','JC2','units','normalized','Position',[.2,.75,.2,.25],'TooltipString','Coupling constant 2','Tag','JT2');
Jtxt3 = uicontrol(cplingP,'Style','text','BackgroundColor',[.2 .2 .2],'ForegroundColor',[1 1
1],'String','JC3','units','normalized','Position',[.4,.75,.2,.25],'TooltipString','Coupling constant 3','Tag','JT3');
Jtxt4 = uicontrol(cplingP,'Style','text','BackgroundColor',[.2 .2 .2],'ForegroundColor',[1 1
1],'String','JC4','units','normalized','Position',[.6,.75,.2,.25],'TooltipString','Coupling constant 4','Tag','JT4');
Jtxt5 = uicontrol(cplingP,'Style','text','BackgroundColor',[.2 .2 .2],'ForegroundColor',[1 1
1],'String','JC5','units','normalized','Position',[.8,.75,.2,.25],'TooltipString','Coupling constant 5','Tag','JT5');

Xedit1 = uicontrol(cplingP,'Style','edit','BackgroundColor',[.2 .2 .2],'ForegroundColor',[1 1
1],'String',handle.X1,'units','normalized','Position',[.0,.0,.2,.25],'callback',@JC_Callback,'TooltipString','Coupling
constant 1 order','Tag','X1');
Xedit2 = uicontrol(cplingP,'Style','edit','BackgroundColor',[.2 .2 .2],'ForegroundColor',[1 1
1],'String',handle.X2,'units','normalized','Position',[.2,.0,.2,.25],'callback',@JC_Callback,'TooltipString','Coupling
constant 2 order','Tag','X2');
Xedit3 = uicontrol(cplingP,'Style','edit','BackgroundColor',[.2 .2 .2],'ForegroundColor',[1 1
1],'String',handle.X3,'units','normalized','Position',[.4,.0,.2,.25],'callback',@JC_Callback,'TooltipString','Coupling
constant 3 order','Tag','X3');
Xedit4 = uicontrol(cplingP,'Style','edit','BackgroundColor',[.2 .2 .2],'ForegroundColor',[1 1
1],'String',handle.X4,'units','normalized','Position',[.6,.0,.2,.25],'callback',@JC_Callback,'TooltipString','Coupling
constant 4 order','Tag','X4');
Xedit5 = uicontrol(cplingP,'Style','edit','BackgroundColor',[.2 .2 .2],'ForegroundColor',[1 1
1],'String',handle.X5,'units','normalized','Position',[.8,.0,.2,.25],'callback',@JC_Callback,'TooltipString','Coupling
constant 5 order','Tag','X5');

Xtxt1 = uicontrol(cplingP,'Style','text','BackgroundColor',[.2 .2 .2],'ForegroundColor',[1 1
1],'String','X1','units','normalized','Position',[.0,.25,.2,.25],'callback',@JC_Callback,'TooltipString','Coupling constant
1 order','Tag','XT1');
Xtxt2 = uicontrol(cplingP,'Style','text','BackgroundColor',[.2 .2 .2],'ForegroundColor',[1 1
1],'String','X2','units','normalized','Position',[.2,.25,.2,.25],'callback',@JC_Callback,'TooltipString','Coupling constant
2 order','Tag','XT2');
Xtxt3 = uicontrol(cplingP,'Style','text','BackgroundColor',[.2 .2 .2],'ForegroundColor',[1 1
1],'String','X3','units','normalized','Position',[.4,.25,.2,.25],'callback',@JC_Callback,'TooltipString','Coupling constant
3 order','Tag','XT3');
Xtxt4 = uicontrol(cplingP,'Style','text','BackgroundColor',[.2 .2 .2],'ForegroundColor',[1 1
1],'String','X4','units','normalized','Position',[.6,.25,.2,.25],'callback',@JC_Callback,'TooltipString','Coupling constant
4 order','Tag','XT4');
Xtxt5 = uicontrol(cplingP,'Style','text','BackgroundColor',[.2 .2 .2],'ForegroundColor',[1 1
1],'String','X5','units','normalized','Position',[.8,.25,.2,.25],'callback',@JC_Callback,'TooltipString','Coupling constant
5 order','Tag','XT5');

tooltips= uimenu(options,'Label','Disable tooltips','Callback',@tooltip_Callback);

peaksnP = uipanel(f,'Title','Peak sets','Position',[0.02,.73,.1,.07],'BackGroundColor',[0.2 0.2
0.2],'ForegroundColor','w','ShadowColor',[0.4 0.4 0.4],'BorderType','beveledout','Visible','on','Tag','peaksnP');
```

```
peakntxt= uicontrol(peaksnP,'Style','edit','BackgroundColor',[.2 .2 .2],'ForegroundColor',[1 1
1],'String',1,'units','normalized','Position',[0,0,1,1],'callback',@peakn_Callback,'TooltipString','Number of peak
sets','Tag','peakntext');

parbtngroup= uibuttongroup(f,'Title','Parameter
set','SelectionChangeFcn',@parbtn_Callback,'Tag','parbtngroup','BackGroundColor',[0.2 0.2
0.2],'ForegroundColor','w','BorderType','beveledout','Position',[0.37,.68,.34,.05]);
plotbtngroup= uibuttongroup(f,'Title','peak
set','SelectionChangeFcn',@plotbtn_Callback,'Tag','plotbtngroup','BackGroundColor',[0.2 0.2
0.2],'ForegroundColor','w','BorderType','beveledout','Position',[0.10,.60,.34,.05]);
if(handle.npeaks==1)
   set(parbtngroup,'Visible','off')
   set(plotbtngroup,'Visible','off')
end



set(f, 'Visible', 'on');
drawnow
        W=[handle.W1 0; 0 handle.W2];
        R=[handle.R 0; 0 handle.R];
        K=[-handle.k1 handle.k2; handle.k1 -handle.k2];
        M=[handle.M1;handle.M2];
        C=[handle.C1 handle.C2; handle.C3 handle.C4];
        J=[handle.JC1 , handle.JC2 , handle.JC3, handle.JC4 , handle.JC5];
        x=[handle.X1 , handle.X2 , handle.X3, handle.X4 , handle.X5];
        fitM=SGen3(W,R,K,M,handle.N,handle.spec,J,x,handle.Mhz);
        [y,x]=getMXY(fitM,handle.Mhz);
        handle.fitPlot(:,:,1)=[x;y];
%javax.swing.UIManager.setLookAndFeel(originalLnF);
%assign values
```

A.4.6. MSEr.m

```
function MSEr= MSEr(M,txt,C,spacing,MHz,d)
% caclulates the mean square error for a spectra as compared to a x y text file between a set of spectral shifts
% C interval of fit in ppm [w1start w1end; w2start w2end]
% text document to be fit
exper=dlmread(txt);
x=exper(:,1)';
y=exper(:,2)';
[y2,W]=getMXY(M,MHz);

we1=linspace(getIndex(x,C(1,1),d),getIndex(x,C(1,2),d),spacing);
we2=linspace(getIndex(x,C(2,1),d),getIndex(x,C(2,2),d),spacing);
wt1=linspace(getIndex(W,C(1,1),d),getIndex(W,C(1,2),d),spacing);
wt2=linspace(getIndex(W,C(2,1),d),getIndex(W,C(2,2),d),spacing);

MSEr=0;
for count = 1:1:spacing
```

```
   d1=(y(round(we1(count)))-y2(round(wt1(count))));
   d2=(y(round(we2(count)))-y2(round(wt2(count))));
   MSEr= MSEr+(d1^2+d2^2)/spacing;
end
end
```

A.4.7. getIndex.m

```
function i=getIndex(x,xi,d)
%gets the index value for a specific x axis value
found=false;
for j= 1:1:length(x)
   if(round(x(j)*d)/d==round(xi*d)/d)
      i=j;
      %round(x(j)*d)/d;
      %round(xi*d)/d;
      found=true;
   end
end
if (~found)
   error('never finds match');
end
end
```

A.4.8. getMtY.m

```
function [x,y]=getMtY(M,MHz)
%returns the frequency variable as x in ppm and the magnetization in the
%frequency domain in x
x=(M(1,:));
x=x;
y=M(3,:)*(2*pi)/MHz;
end
```

A.4.9. getMXY.m

```
function [x,y]=getMXY(M,MHz)
%returns the frequency variable as x in ppm and the magnetization in the
%frequency domain in x
x=abs(real(M(2,:)));
x=x-min(x);
y=M(3,:)*(2*pi)/MHz;
end
```

A.4.10. getMXY2.m

```
function [x,y]=getMXY2(M,MHz)
%returns the frequency variable as x in ppm and the magnetization in the
%frequency domain in x
x=abs(real(M(2,:)));
x=x-min(x);
y=M(3,:);
end
```

A.4.11. NMfit.m

```
function [k1,k2,M01,M02,dK]=NMfit(k1,k2,M01,M02,int,txt,Cg,W1,W2,R1,R2,N,Spec,conv,J,xn,MHz,d)
   Ri=[R1 0 ; 0 R2];
   Wi=[W1 0; 0 W2];
   M0=[M01;M02];
   Ki=[-k1 k2;k1 -k2];
   Mplot=SGen3(Wi,Ri,Ki,M0,N,Spec,J,xn,MHz);
   ax2=findobj('Position',[0.1,0.1,0.8,0.35]);
   set(gca,'XColor',[1 1 1],'YColor',[1 1 1],'ZColor',[1 1 1],'Color',[0.25 0.25 0.25])
   ax1=findobj('Position',[0.1,0.575,0.8,0.35]);
   xlabel('k1')
   ylabel('k2')
   Splot2(ax1,Mplot,txt,MHz);
   set(gca,'XDir','reverse','XColor',[1 1 1],'YColor',[1 1 1],'ZColor',[1 1 1],'Color',[0.25 0.25 0.25])
   axis([Cg(1,1) Cg(2,2) -0.05*max(Mplot(2,:)) 1.2*max(Mplot(2,:))])
   drawnow
%termination variables
K1= k1;
K2= k2;
dK1= 1;
dK2= 1;
dK= dK1+dK2;
contract=false;

SB=MSEr(Mplot,txt,Cg,100,MHz,d);
dSB=10;
count=1;
xy=dlmread(txt);
x=xy(:,1)';
y=xy(:,2)';

   if(k1==0 || k2==0)
      A=[k1 ; k2+int*rand()];
      B=[k1+int*rand()*sqrt(3)/2 ; k2-int*rand()*0.5];
      C=[k1-int*rand()*sqrt(3)/2 ; k2-int*rand()*0.5];
   else
      A=[k1 ; k2+int*rand()*k2];
      B=[k1+int*k1*sqrt(3)/2 ; k2-int*0.5*k2];
      C=[k1-int*k1*sqrt(3)/2 ; k2-int*0.5*k2];
   end
   %triplot
   trix=[];
   triy=[];
   [trix(:,count),triy(:,count)]=Tri(A,B,C);
   set(gcf,'CurrentAxes',ax2)
   plot(trix,triy);
   set(gca,'XColor',[1 1 1],'YColor',[1 1 1],'ZColor',[1 1 1],'Color',[0.25 0.25 0.25]);
   axis([-5,5,-5,5]);
   KA=[-A(1) A(2);A(1) -A(2)];
   KB=[-B(1) B(2);B(1) -B(2)];
   KC=[-C(1) C(2);C(1) -C(2)];
```

```
    Ri=[R1 0 ; 0 R2];
    Wi=[W1 0; 0 W2];
    M0=[M01;M02];
while (dK>conv)
    contract=false;
    j=SB;
    count=count+1;

    MA=SGen3(Wi,Ri,KA,M0,N,Spec,J,xn,MHz);
    MB=SGen3(Wi,Ri,KB,M0,N,Spec,J,xn,MHz);
    MC=SGen3(Wi,Ri,KC,M0,N,Spec,J,xn,MHz);

    SA=MSEr(MA,txt,Cg,100,MHz,d);
    SB=MSEr(MB,txt,Cg,100,MHz,d);
    SC=MSEr(MC,txt,Cg,100,MHz,d);
    %rank system
    %-------------------------------------------------------
    %%
    BB=B;
    if(SA<SB)
       if(SB<SC)
          W=C;
          MW=MC;
          SW=SC;
          G=B;
          MG=MB;
          SG=SB;
          B=A;
          MB=MA;
          SB=SA;
       else
          if(SC<SA)
             W=B;
             MW=MB;
             SW=SB;
             G=A;
             MG=MA;
             SG=SA;
             B=C;
             MB=MC;
             SB=SC;
          else
             W=B;
             MW=MB;
             SW=SB;
             G=C;
             MG=MC;
             SG=SC;
             B=A;
             MB=MA;
             SB=SA;
          end
       end
```

```
else
   if(SA<SC)
      W=C;
      MW=MC;
      SW=SC;
      G=A;
      MG=MA;
      SG=SA;
      B=B;
      MB=MB;
      SB=SB;
   else
      if(SC<SB)
         W=A;
         MW=MA;
         SW=SA;
         G=B;
         MG=MB;
         SG=SB;
         B=C;
         MB=MC;
         SB=SC;
      else
         W=A;
         MW=MA;
         SW=SA;
         G=C;
         MG=MC;
         SG=SC;
         B=B;
         MB=MB;
         SB=SB;
      end
   end
end

KG=[-G(1) G(2);G(1) -G(2)];
KB=[-B(1) B(2);B(1) -B(2)];
KW=[-W(1) W(2);W(1) -W(2)];

M=(G+B)/2;
R=2*M-W;
KR=[-R(1) R(2);R(1) -R(2)];
MR=SGen3(Wi,Ri,KR,M0,N,Spec,J,xn,MHz);
SR=MSEr(MR,txt,Cg,100,MHz,d);

%%
%nelder mead algorithm
if (SR<SG)
   if(SB<SR)
      W=R;
   else
      E=2*R-M;
```

```
      KE=[-E(1) E(2);E(1) -E(2)];
      ME=SGen3(Wi,Ri,KE,M0,N,Spec,J,xn,MHz);
      SE=MSEr(ME,txt,Cg,100,MHz,d);

      if(SE<SR)%rather than SE<SB because R might be smaller than E
         W=E;
      else
         W=R;
      end

   end
else
   if(SR<SW)
      W=R;

   else
      contract=true;
      C1=(M+W)/2;
      C2=(M+R)/2;
      KC1=[-C1(1) C1(2);C1(1) -C1(2)];
      KC2=[-C2(1) C2(2);C2(1) -C2(2)];
      MC1=SGen3(Wi,Ri,KC1,M0,N,Spec,J,xn,MHz);
      MC2=SGen3(Wi,Ri,KC2,M0,N,Spec,J,xn,MHz);
      SC1=MSEr(MC1,txt,Cg,100,MHz,d);
      SC2=MSEr(MC2,txt,Cg,100,MHz,d);
      if(SC1<SC2)
         C=C1;
         SC=SC1;
      else
         C=C2;
         SC=SC2;
      end
      if(SC<SW)
         W=C;
      else
         S=(B+W)/2;
         W=S;
         G=M;
      end
   end
end
k1=B(1);
k2=B(2);
Avg=(W+G+B)/3;
if(~contract)
   dK1=abs(1-k1/K1);
   dK2=abs(1-k2/K2);
   dK=dK1+dK2;
   K1=k1;
   K2=k2;
else
   dK1=abs(1-k1/Avg(1));
   dK2=abs(1-k2/Avg(2));
```

```
    dK=dK1+dK2;
  end


  KI=[-k1 k2; k1 -k2];
  MI=SGen3(Wi,Ri,KI,M0,N,Spec,J,xn,MHz);
  SB=MSEr(MI,txt,Cg,100,MHz,d);

  if(W~=C)

    dSB=j-SB;
  end

  A=G;
  KA= [-A(1) A(2);A(1) -A(2)];
  B=B;
  KB= [-B(1) B(2);B(1) -B(2)];
  C=W;
  KC= [-C(1) C(2);C(1) -C(2)];

  [trix(:,count),triy(:,count)]=Tri(A,B,C);
  set(gcf,'CurrentAxes',ax2)
  plot(trix,triy)
  set(gca,'XColor',[1 1 1],'YColor',[1 1 1],'ZColor',[1 1 1],'Color',[0.25 0.25 0.25])
  xlabel('k1')
  ylabel('k2')
  set(gcf,'CurrentAxes',ax1)
  Mplot=SGen3(Wi,Ri,[-k1 k2;k1 -k2],M0,N,Spec,J,xn,MHz);
  Splot2(ax1,Mplot,txt,MHz);
  set(gca,'XDir','reverse','XColor',[1 1 1],'YColor',[1 1 1],'ZColor',[1 1 1],'Color',[0.25 0.25 0.25])
  axis([Cg(1,1) Cg(2,2) -0.05*max(Mplot(2,:)) 1.2*max(Mplot(2,:))])
  drawnow


end
count;
set(gcf,'CurrentAxes',ax2)
plot(trix,triy)
set(gca,'XColor',[1 1 1],'YColor',[1 1 1],'ZColor',[1 1 1],'Color',[0.25 0.25 0.25]);
xlabel('k1')
ylabel('k2')
set(gcf,'CurrentAxes',ax1)
Splot2(ax1,Mplot,txt,MHz);
set(gca,'XDir','reverse','XColor',[1 1 1],'YColor',[1 1 1],'ZColor',[1 1 1],'Color',[0.25 0.25 0.25])
end
```

A.4.12. NMfitM0.m

```
function [k1,k2,M01,M02,SB]=NMfitM0(k1,k2,M01,M02,int,txt,Cg,W1,W2,R1,R2,N,Spec,conv,J,xn,MHz)
  Ri=[R1 0 ; 0 R2];
  Wi=[W1 0; 0 W2];
  M0=[M01;M02];
  Ki=[-k1 k2;k1 -k2];
```

```
   Mplot=SGen3(Wi,Ri,Ki,M0,N,Spec,J,xn,MHz);
   ax2=findobj('Position',[0.1,0.1,0.8,0.35]);
   set(gca,'XColor',[1 1 1],'YColor',[1 1 1],'ZColor',[1 1 1],'Color',[0.25 0.25 0.25])
   ax1=findobj('Position',[0.1,0.575,0.8,0.35]);
   xlabel('M01')
   ylabel('M02')
   Splot2(ax1,Mplot,txt,MHz);
   set(gca,'XDir','reverse','XColor',[1 1 1],'YColor',[1 1 1],'ZColor',[1 1 1],'Color',[0.25 0.25 0.25])
   axis([Cg(1,1) Cg(2,2) -0.05*max(Mplot(2,:)) 1.2*max(Mplot(2,:))])
   drawnow
%termination variables
M1= M01;
M2= M02;
dM1= 1;
dM2= 1;
dM= dM1+dM2;
contract=false;

SB=MSEr(Mplot,txt,Cg,100,MHz);
dSB=10;
count=1;
xy=dlmread(txt);
x=xy(:,1)';
y=xy(:,2)';

   if(M01==0 || M02==0)
      A=[M01 ; M02+int*rand()];
      B=[M01+int*rand()*sqrt(3)/2 ; M02-int*rand()*0.5];
      C=[M01-int*rand()*sqrt(3)/2 ; M02-int*rand()*0.5];
   else
      A=[M01 ; M02+int*rand()*M02];
      B=[M01+int*M01*rand()*sqrt(3)/2 ; M02-int*0.5*rand()*M02];
      C=[M01-int*M01*rand()*sqrt(3)/2 ; M02-int*0.5*rand()*M02];
   end
   %triplot
   trix=[];
   triy=[];
   [trix(:,count),triy(:,count)]=Tri(A,B,C);
   set(gcf,'CurrentAxes',ax2)
   plot(trix,triy);
   set(gca,'XDir','reverse','XColor',[1 1 1],'YColor',[1 1 1],'ZColor',[1 1 1],'Color',[0.25 0.25 0.25])
   xlabel('M01')
   ylabel('M02')
   axis([-5,5,-5,5]);

while (dM>conv)
   contract=false;
   j=SB;
   count=count+1;

   MA=SGen3(Wi,Ri,Ki,A,N,Spec,J,xn,MHz);
   MB=SGen3(Wi,Ri,Ki,B,N,Spec,J,xn,MHz);
   MC=SGen3(Wi,Ri,Ki,C,N,Spec,J,xn,MHz);
```

```
SA=MSEr(MA,txt,Cg,100,MHz);
SB=MSEr(MB,txt,Cg,100,MHz);
SC=MSEr(MC,txt,Cg,100,MHz);
%rank system
%-------------------------------------------------------
%%
BB=B;
if(SA<SB)
   if(SB<SC)
      W=C;
      G=B;
      B=A;
   else
      if(SC<SA)
         W=B;
         G=A;
         B=C;
      else
         W=B;
         G=C;
         B=A;
      end
   end
else
   if(SA<SC)
      W=C;
      G=A;
      B=B;
   else
      if(SC<SB)
         W=A;
         G=B;
         B=C;
      else
         W=A;
         G=C;
         B=B;
      end
   end
end


MG=SGen3(Wi,Ri,Ki,G,N,Spec,J,xn,MHz);
MB=SGen3(Wi,Ri,Ki,B,N,Spec,J,xn,MHz);
MW=SGen3(Wi,Ri,Ki,W,N,Spec,J,xn,MHz);
SG=MSEr(MG,txt,Cg,100,MHz);


SB=MSEr(MB,txt,Cg,100,MHz);
SW=MSEr(MW,txt,Cg,100,MHz);

%%
```

```
M=(G+B)/2;
R=2*M-W;
MR=SGen3(Wi,Ri,Ki,R,N,Spec,J,xn,MHz);
SR=MSEr(MR,txt,Cg,100,MHz);

%%
%nelder mead algorithm
if (SR<SG)
   if(SB<SR)
      W=R;
   else
      E=2*R-M;
      ME=SGen3(Wi,Ri,Ki,E,N,Spec,J,xn,MHz);
      SE=MSEr(ME,txt,Cg,100,MHz);
      if(SE<SR)%rather than SE<SB because R might be smaller than E
         W=E;
      else
         W=R;
      end

   end
else
   if(SR<SW)
      W=R;

   else
      contract=true;
      C1=(M+W)/2;
      C2=(M+R)/2;
      MC1=SGen3(Wi,Ri,Ki,C1,N,Spec,J,xn,MHz);
      MC2=SGen3(Wi,Ri,Ki,C2,N,Spec,J,xn,MHz);
      SC1=MSEr(MC1,txt,Cg,100,MHz);
      SC2=MSEr(MC2,txt,Cg,100,MHz);
      if(SC1<SC2)
         C=C1;
         SC=SC1;
      else
         C=C2;
         SC=SC2;
      end
      if(SC<SW)
         W=C;

      else
            S=(B+W)/2;

            W=S;
            G=M;

      end
   end
end
M01=B(1);
```

```
   M02=B(2);
   Avg=(W+G+B)/3;
   if(~contract)
      dM1=abs(1-M01/M1);
      dM2=abs(1-M02/M2);
      dM=dM1+dM2;
      M1=M01;
      M2=M02;
   else
      dM1=abs(1-M01/Avg(1));
      dM2=abs(1-M02/Avg(2));
      dM=dM1+dM2;
   end

   MB=SGen3(Wi,Ri,Ki,Avg,N,Spec,J,xn,MHz);
   SB=MSEr(MB,txt,Cg,100,MHz);

   if(W~=C)
      dSB=j-SB;
   end
   A=G;
   B=B;
   C=W;

   [trix(:,count),triy(:,count)]=Tri(A,B,C);
   set(gcf,'CurrentAxes',ax2)
   plot(trix,triy)
   set(gca,'XColor',[1 1 1],'YColor',[1 1 1],'ZColor',[1 1 1],'Color',[0.25 0.25 0.25])
   xlabel('M01')
   ylabel('M02')
   set(gcf,'CurrentAxes',ax1)
   Mx=SGen3(Wi,Ri,Ki,[M01;M02],N,Spec,J,xn,MHz);
   Splot2(ax1,Mx,txt,MHz);
   set(gca,'XDir','reverse','XColor',[1 1 1],'YColor',[1 1 1],'ZColor',[1 1 1],'Color',[0.25 0.25 0.25])
   axis([Cg(1,1) Cg(2,2) -0.05*max(Mplot(2,:)) max(Mx(2,:))])
   drawnow


end
count;
set(gcf,'CurrentAxes',ax2)
plot(trix,triy)
set(gca,'XColor',[1 1 1],'YColor',[1 1 1],'ZColor',[1 1 1],'Color',[0.25 0.25 0.25]);
xlabel('M01')
ylabel('M02')
set(gcf,'CurrentAxes',ax1)
Splot2(ax1,Mx,txt,MHz);
set(gca,'XDir','reverse','XColor',[1 1 1],'YColor',[1 1 1],'ZColor',[1 1 1],'Color',[0.25 0.25 0.25])
end
```

A.4.13. NMfitf.m

```
function [k1,k2,M01,M02,SB]=NMfitf(k1,k2,M01,M02,int,txt,Cg,W1,W2,R1,R2,N,Spec,conv,iter,J,x,MHz,d)
```

```
W=[W1 0;0 W2];
R=[R1 0 ; 0 R2];
K=[-k1 k2;k1 -k2];
M0=[M01;M02];
%SB=MSEr(SGen3(W,R,K,M0,N,Spec,J,x,MHz),txt,Cg,100,MHz);
SB=100;
dM=conv*2;
dK=conv*2;
  if(SB>0)
    inc=0;
    ax2=axes('Position',[0.1,0.1,0.8,0.35]);
    set(gca,'XColor',[1 1 1],'YColor',[1 1 1],'ZColor',[1 1 1],'Color',[0.25 0.25 0.25])
    ax1=axes('Position',[0.1,0.575,0.8,0.35]);
    set(gca,'XColor',[1 1 1],'YColor',[1 1 1],'ZColor',[1 1 1],'Color',[0.25 0.25 0.25])
    while((dM>conv||dK>conv)&&inc<=iter)
      inc=inc+1;
      [k1,k2,M01,M02,dK]=NMfit(k1,k2,M01,M02,int,txt,Cg,W1,W2,R1,R2,N,Spec,conv,J,x,MHz,d);
      dK=abs(1+K(1,1)/k1)+abs(1+K(2,2)/k2);
      K=[-k1 k2;k1 -k2];
      [k1,k2,M01,M02,SB]=NMfitM0(k1,k2,M01,M02,int,txt,Cg,W1,W2,R1,R2,N,Spec,conv,J,x,MHz,d);
      dM=abs(1-M0(1)/M01)+abs(1-M0(2)/M02);
      M0=[M01;M02];
    end
  end

end
```

A.4.14. NMfitS.m

```
function [k1,k2,M01,M02,dK]=NMfitS(k1,k2,M01,M02,inte,txt,Cg,W1,W2,R1,N,Spec,conv,J,xn,MHz,var,cpb,d)

  M_main=zeros(1,N);
  M_otherpeaks=zeros(1,N);
  for int=1:size(squeeze(W1'))
    Ri(int,:,:)=[R1 0;0 R1];
    Wi(int,:,:)=[W1(int) 0; 0 W2(int)];
    Ki(int,:,:)=[-k1(cpb(int)) k2(cpb(int));k1(cpb(int)) -k2(cpb(int))];
    M0(int,:,:)=[M01(cpb(int));M02(cpb(int))]';
    if(var==cpb(int))

Mc=SGen3(squeeze(Wi(int,:,:)),squeeze(Ri(int,:,:)),squeeze(Ki(cpb(int),:,:)),squeeze(M0(cpb(int),:,:)),N,Spec,squeez
e(J(int,:)),squeeze(xn(int,:)),MHz);
      M_main=M_main+squeeze(Mc(1,:));
    else

Mc=SGen3(squeeze(Wi(int,:,:)),squeeze(Ri(int,:,:)),squeeze(Ki(cpb(int),:,:)),squeeze(M0(cpb(int),:,:)),N,Spec,squeez
e(J(int,:)),squeeze(xn(int,:)),MHz);
      M_otherpeaks=M_otherpeaks+squeeze(Mc(1,:));
    end
  end
  M_full=M_main+M_otherpeaks;
  [y,Wshift]=getMXY(Mc,MHz);
  M_full=abs(real(fft(M_full)));
```

```
    M_full=M_full-min(M_full);
    Cg=[0 max(Wshift)/2; max(Wshift)/2 max(Wshift)];
    ax2=findobj('Position',[0.1,0.1,0.8,0.35]);
    set(ax2,'ColorOrder',[1 1 1; 1 0 0; 0 1 0; 0 0 1],'nextplot','replacechildren')
    set(gca,'XColor',[1 1 1],'YColor',[1 1 1],'ZColor',[1 1 1],'Color',[0.25 0.25 0.25])
    ax1=findobj('Position',[0.1,0.575,0.8,0.35]);
    xlabel('k1')
    ylabel('k2')
    Splot3(ax1,M_full,Wshift,txt,MHz);
    set(gca,'XDir','reverse','XColor',[1 1 1],'YColor',[1 1 1],'ZColor',[1 1 1],'Color',[0.25 0.25 0.25])
    axis([Cg(1,1) Cg(2,2) -0.5 1.2*max(M_full)])
    drawnow
%termination variables
K1= k1(cpb(var));
K2= k2(cpb(var));
dK1= 1;
dK2= 1;
dK= dK1+dK2;
contract=false;

SB=MSEr2(M_full,txt,Cg,100,MHz,Wshift,d);
dSB=10;
count=1;
xy=dlmread(txt);
x=xy(:,1)';
y=xy(:,2)';

    if(k1(cpb(var))==0 || k2(cpb(var))==0)
        A=[k1(cpb(var)) ; k2(cpb(var))+inte*rand()];
        B=[k1(cpb(var))+inte*rand()*sqrt(3)/2 ; k2(cpb(var))-inte*rand()*0.5];
        C=[k1(cpb(var))-inte*rand()*sqrt(3)/2 ; k2(cpb(var))-inte*rand()*0.5];
    else
        A=[k1(cpb(var)) ; k2(cpb(var))+inte*rand()*k2(cpb(var))];
        B=[k1(cpb(var))+inte*k1(cpb(var))*sqrt(3)/2 ; k2(cpb(var))-inte*0.5*k2(cpb(var))];
        C=[k1(cpb(var))-inte*k1(cpb(var))*sqrt(3)/2 ; k2(cpb(var))-inte*0.5*k2(cpb(var))];
    end
    %triplot
    trix=[];
    triy=[];
    [trix(:,count),triy(:,count)]=Tri(A,B,C);
    set(gcf,'CurrentAxes',ax2)
    set(ax2,'ColorOrder',[1 1 1; 1 0 0; 0 1 0; 0 0 1],'nextplot','replacechildren')
    plot(trix,triy);
    set(gca,'XColor',[1 1 1],'YColor',[1 1 1],'ZColor',[1 1 1],'Color',[0.25 0.25 0.25]);

    KA=[-A(1) A(2);A(1) -A(2)];
    KB=[-B(1) B(2);B(1) -B(2)];
    KC=[-C(1) C(2);C(1) -C(2)];
while (dK>conv)
    contract=false;
    j=SB;
    count=count+1;
    M_fullA=zeros(1,N);
```

```
M_fullB=zeros(1,N);
M_fullC=zeros(1,N);
M_mainA=zeros(1,N);
M_mainB=zeros(1,N);
M_mainC=zeros(1,N);

for int=1:size(W1')
   Ri(int,:,:)=[R1 0;0 R1];
   Wi(int,:,:)=[W1(int) 0; 0 W2(int)];
   M0(int,:,:)=[M01(cpb(int));M02(cpb(int))]';
   if(var==cpb(int))

Mc=SGen3(squeeze(Wi(int,:,:)),squeeze(Ri(int,:,:)),KA,squeeze(M0(cpb(int),:,:)),N,Spec,squeeze(J(int,:)),squeeze(xn(
int,:)),MHz);
      M_mainA=M_mainA+squeeze(Mc(1,:));

Mc=SGen3(squeeze(Wi(int,:,:)),squeeze(Ri(int,:,:)),KB,squeeze(M0(cpb(int),:,:)),N,Spec,squeeze(J(int,:)),squeeze(xn(
int,:)),MHz);
      M_mainB=M_mainB+squeeze(Mc(1,:));

Mc=SGen3(squeeze(Wi(int,:,:)),squeeze(Ri(int,:,:)),KC,squeeze(M0(cpb(int),:,:)),N,Spec,squeeze(J(int,:)),squeeze(xn(
int,:)),MHz);
      M_mainC=M_mainC+squeeze(Mc(1,:));
   end
end
M_fullA=M_mainA+M_otherpeaks;
M_fullA=abs(real(fft(M_fullA)));
M_fullA=M_fullA-min(M_fullA);
M_fullB=M_mainB+M_otherpeaks;
M_fullB=abs(real(fft(M_fullB)));
M_fullB=M_fullB-min(M_fullB);
M_fullC=M_mainC+M_otherpeaks;
M_fullC=abs(real(fft(M_fullC)));
M_fullC=M_fullC-min(M_fullC);


SA=MSEr2(M_fullA,txt,Cg,100,MHz,Wshift,d);
SB=MSEr2(M_fullB,txt,Cg,100,MHz,Wshift,d);
SC=MSEr2(M_fullC,txt,Cg,100,MHz,Wshift,d);
%rank system
%-------------------------------------------------------
%%
BB=B;
if(SA<SB)
   if(SB<SC)
      W=C;
      MW=M_fullC;
      SW=SC;
      G=B;
      MG=M_fullB;
      SG=SB;
      B=A;
      MB=M_fullA;
```

```
        SB=SA;
    else
        if(SC<SA)
            W=B;
            MW=M_fullB;
            SW=SB;
            G=A;
            MG=M_fullA;
            SG=SA;
            B=C;
            MB=M_fullC;
            SB=SC;
        else
            W=B;
            MW=M_fullB;
            SW=SB;
            G=C;
            MG=M_fullC;
            SG=SC;
            B=A;
            MB=M_fullA;
            SB=SA;
        end
    end
else
    if(SA<SC)
        W=C;
        MW=M_fullC;
        SW=SC;
        G=A;
        MG=M_fullA;
        SG=SA;
        B=B;
        MB=M_fullB;
        SB=SB;
    else
        if(SC<SB)
            W=A;
            MW=M_fullA;
            SW=SA;
            G=B;
            MG=M_fullB;
            SG=SB;
            B=C;
            MB=M_fullC;
            SB=SC;
        else
            W=A;
            MW=M_fullA;
            SW=SA;
            G=C;
            MG=M_fullC;
            SG=SC;
```

```
            B=B;
            MB=M_fullB;
            SB=SB;
        end
    end
end

KG=[-G(1) G(2);G(1) -G(2)];
KB=[-B(1) B(2);B(1) -B(2)];
KW=[-W(1) W(2);W(1) -W(2)];

M=(G+B)/2;
R=2*M-W;
KR=[-R(1) R(2);R(1) -R(2)];
M_mainR=zeros(1,N);
M_fullR=zeros(1,N);

for int=1:size(W1')
    Ri(int,:,:)=[R1 0;0 R1];
    Wi(int,:,:)=[W1(int) 0; 0 W2(int)];
    M0(int,:,:)=[M01(cpb(int));M02(cpb(int))]';
    if(var==cpb(int))

Mc=SGen3(squeeze(Wi(int,:,:)),squeeze(Ri(int,:,:)),KR,squeeze(M0(cpb(int),:,:)),N,Spec,squeeze(J(int,:)),squeeze(xn(
int,:)),MHz);
        M_mainR=M_mainR+squeeze(Mc(1,:));
    end
end
M_fullR=M_mainR+M_otherpeaks;
M_fullR=abs(real(fft(M_fullR)));
M_fullR=M_fullR-min(M_fullR);

SR=MSEr2(M_fullR,txt,Cg,100,MHz,Wshift,d);

%%
%nelder mead algorithm
if (SR<SG)
    if(SB<SR)
        W=R;
    else
        E=2*R-M;
        KE=[-E(1) E(2);E(1) -E(2)];
        M_mainE=zeros(1,N);
        M_fullE=zeros(1,N);

        for int=1:size(W1')
            Ri(int,:,:)=[R1 0;0 R1];
            Wi(int,:,:)=[W1(int) 0; 0 W2(int)];
            M0(int,:,:)=[M01(cpb(int));M02(cpb(int))]';
            if(var==cpb(int))

Mc=SGen3(squeeze(Wi(int,:,:)),squeeze(Ri(int,:,:)),KE,squeeze(M0(cpb(int),:,:)),N,Spec,squeeze(J(int,:)),squeeze(xn(
int,:)),MHz);
```

```
            M_mainE=M_mainE + squeeze(Mc(1,:));
          end
        end
        M_fullE=M_mainE+M_otherpeaks;
        M_fullE=abs(real(fft(M_fullE)));
        M_fullE=M_fullE-min(M_fullE);
        SE=MSEr2(M_fullE,txt,Cg,100,MHz,Wshift,d);

        if(SE<SR)%rather than SE<SB because R might be smaller than E
          W=E;
        else
          W=R;
        end

    end
  else
    if(SR<SW)
      W=R;

    else
      contract=true;
      C1=(M+W)/2;
      C2=(M+R)/2;
      KC1=[-C1(1) C1(2);C1(1) -C1(2)];
      KC2=[-C2(1) C2(2);C2(1) -C2(2)];
      M_mainC1=zeros(1,N);
      M_fullC1=zeros(1,N);
      M_mainC2=zeros(1,N);
      M_fullC2=zeros(1,N);

      for int=1:size(W1')
        Ri(int,:,:)=[R1 0;0 R1];
        Wi(int,:,:)=[W1(int) 0; 0 W2(int)];
        M0(int,:,:)=[M01(cpb(int));M02(cpb(int))]';
        if(var==cpb(int))

Mc=SGen3(squeeze(Wi(int,:,:)),squeeze(Ri(int,:,:)),KC1,squeeze(M0(cpb(int),:,:)),N,Spec,squeeze(J(int,:)),squeeze(x
n(int,:)),MHz);
            M_mainC1=M_mainC1+squeeze(Mc(1,:));

Mc=SGen3(squeeze(Wi(int,:,:)),squeeze(Ri(int,:,:)),KC2,squeeze(M0(cpb(int),:,:)),N,Spec,squeeze(J(int,:)),squeeze(x
n(int,:)),MHz);
            M_mainC2=M_mainC2+squeeze(Mc(1,:));
          end
        end
        M_fullC1=M_mainC1+M_otherpeaks;
        M_fullC1=abs(real(fft(M_fullC2)));
        M_fullC1=M_fullC1-min(M_fullC1);
        SC1=MSEr2(M_fullC1,txt,Cg,100,MHz,Wshift,d);
        M_fullC2=M_mainC2+M_otherpeaks;
        M_fullC2=abs(real(fft(M_fullC2)));
        M_fullC2=M_fullC2-min(M_fullC2);
        SC2=MSEr2(M_fullC2,txt,Cg,100,MHz,Wshift,d);
```

```
        if(SC1<SC2)
           C=C1;
           SC=SC1;
        else
           C=C2;
           SC=SC2;
        end
        if(SC<SW)
           W=C;
        else
           S=(B+W)/2;
           W=S;
           G=M;
        end
     end
  end
  Avg=(W+G+B)/3;
  if(~contract)
     dK1=abs(1-B(1)/K1);
     dK2=abs(1-B(2)/K2);
     dK=dK1+dK2;
     K1=B(1);
     K2=B(2);
  else
     dK1=abs(1-k1(cpb(var))/Avg(1));
     dK2=abs(1-k2(cpb(var))/Avg(2));
     dK=dK1+dK2;
  end


  KI=[-k1(cpb(var)) k2(cpb(var)); k1(cpb(var)) -k2(cpb(var))];
        M_mainI=zeros(1,N);
        M_fullI=zeros(1,N);

        for int=1:size(W1')
           Ri(int,:,:)=[R1 0;0 R1];
           Wi(int,:,:)=[W1(int) 0; 0 W2(int)];
           M0(int,:,:)=[M01(cpb(int));M02(cpb(int))]';
           if(var==cpb(int))

Mc=SGen3(squeeze(Wi(int,:,:)),squeeze(Ri(int,:,:)),KI,squeeze(M0(cpb(int),:,:)),N,Spec,squeeze(J(int,:)),squeeze(xn(i
nt,:)),MHz);
              M_mainI=M_mainI + squeeze(Mc(1,:));
           end
        end
        M_fullI=M_mainI+M_otherpeaks;
        M_fullI=abs(real(fft(M_fullI)));
        M_fullI=M_fullI-min(M_fullI);
        SB=MSEr2(M_fullI,txt,Cg,100,MHz,Wshift,d);
```

```
   if(W~=C)

      dSB=j-SB;
   end

   A=G;
   KA= [-A(1) A(2);A(1) -A(2)];
   B=B;
   KB= [-B(1) B(2);B(1) -B(2)];
   C=W;
   KC= [-C(1) C(2);C(1) -C(2)];

   [trix(:,count),triy(:,count)]=Tri(A,B,C);
   set(gcf,'CurrentAxes',ax2)
   set(ax2,'ColorOrder',[1 1 1; 1 0 0; 0 1 0; 0 0 1],'nextplot','replacechildren')
   plot(trix,triy)
   set(gca,'XColor',[1 1 1],'YColor',[1 1 1],'ZColor',[1 1 1],'Color',[0.25 0.25 0.25])
   xlabel('k1')
   ylabel('k2')
   set(gcf,'CurrentAxes',ax1)
   M_main=zeros(1,N);
   M_otherpeaks=zeros(1,N);
   for int=1:size(W1')
      Ri(int,:,:)=[R1 0;0 R1];
      Wi(int,:,:)=[W1(int) 0; 0 W2(int)];
      M0(int,:,:)=[M01(cpb(int));M02(cpb(int))]';
      if(var==cpb(int))

Mc=SGen3(squeeze(Wi(int,:,:)),squeeze(Ri(int,:,:)),KB,squeeze(M0(cpb(int),:,:)),N,Spec,squeeze(J(int,:)),squeeze(xn(
int,:)),MHz);
         M_main=M_main+squeeze(Mc(1,:));
      end
   end
   M_full=M_main+M_otherpeaks;
   M_full=abs(real(fft(M_full)));
   M_full=M_full-min(M_full);
   Splot3(ax1,M_full,Wshift,txt,MHz);
   set(gca,'XDir','reverse','XColor',[1 1 1],'YColor',[1 1 1],'ZColor',[1 1 1],'Color',[0.25 0.25 0.25])
   axis([Cg(1,1) Cg(2,2) -0.5 1.2*max(M_full)])
   drawnow


end
count;
set(gcf,'CurrentAxes',ax2)
set(ax2,'ColorOrder',[1 1 1; 1 0 0; 0 1 0; 0 0 1])
plot(trix,triy)
set(gca,'XColor',[1 1 1],'YColor',[1 1 1],'ZColor',[1 1 1],'Color',[0.25 0.25 0.25]);
xlabel('k1')
ylabel('k2')
set(gcf,'CurrentAxes',ax1)
Splot3(ax1,M_full,Wshift,txt,MHz);
set(gca,'XDir','reverse','XColor',[1 1 1],'YColor',[1 1 1],'ZColor',[1 1 1],'Color',[0.25 0.25 0.25])
```

```
k1(cpb(var))=-KB(1,1);
k2(cpb(var))=-KB(2,2);
end
```

A.4.15. NMfitMOS.m

```
function [k1,k2,M01,M02,SB]=NMfitM0S(k1,k2,M01,M02,inte,txt,Cg,W1,W2,R1,N,Spec,conv,J,xn,MHz,var,cpb,d)
   M_main=zeros(1,N);
   M_otherpeaks=zeros(1,N);
   for int=1:size(W1')
      Ri(int,:,:)=[R1 0;0 R1];
      Wi(int,:,:)=[W1(int) 0; 0 W2(int)];
      Ki(int,:,:)=[-k1(cpb(int)) k2(cpb(int));k1(cpb(int)) -k2(cpb(int))];
      M0(int,:,:)=[M01(cpb(int));M02(cpb(int))]';
      if(var==cpb(int))

Mc=SGen3(squeeze(Wi(int,:,:)),squeeze(Ri(int,:,:)),squeeze(Ki(cpb(int),:,:)),squeeze(M0(cpb(int),:,:)),N,Spec,squeez
e(J(int,:)),squeeze(xn(int,:)),MHz);
         M_main=M_main+squeeze(Mc(1,:));
      else

Mc=SGen3(squeeze(Wi(int,:,:)),squeeze(Ri(int,:,:)),squeeze(Ki(cpb(int),:,:)),squeeze(M0(cpb(int),:,:)),N,Spec,squeez
e(J(int,:)),squeeze(xn(int,:)),MHz);
         M_otherpeaks=M_otherpeaks+squeeze(Mc(1,:));
      end
   end
   M_full=M_main+M_otherpeaks;
   [y,Wshift]=getMXY(Mc,MHz);
   Cg=[0 max(Wshift)/2; max(Wshift)/2 max(Wshift)];
   M_full=abs(real(fft(M_full)));
   M_full=M_full-min(M_full);
   ax2=findobj('Position',[0.1,0.1,0.8,0.35]);
   set(ax2,'ColorOrder',[1 1 1; 1 0 0; 0 1 0; 0 0 1],'nextplot','replacechildren')
   set(gca,'XColor',[1 1 1],'YColor',[1 1 1],'ZColor',[1 1 1],'Color',[0.25 0.25 0.25])
   ax1=findobj('Position',[0.1,0.575,0.8,0.35]);
   xlabel('M01')
   ylabel('M02')
   Splot3(ax1,M_full,Wshift,txt,MHz);
   set(gca,'XDir','reverse','XColor',[1 1 1],'YColor',[1 1 1],'ZColor',[1 1 1],'Color',[0.25 0.25 0.25])
   axis([Cg(1,1) Cg(2,2) -0.5 1.2*max(M_full)])
   drawnow
%termination variables
M1= M01(cpb(var));
M2= M02(cpb(var));
dM1= 1;
dM2= 1;
dM= dM1+dM2;
contract=false;

SB=MSEr2(M_main,txt,Cg,100,MHz,Wshift,d);
dSB=10;
count=1;
xy=dlmread(txt);
```

```
x=xy(:,1)';
y=xy(:,2)';

   if(M01(cpb(var))==0 || M02(cpb(var))==0)
      A=[M01(cpb(var)) ; M02(cpb(var))+inte*rand()];
      B=[M01(cpb(var))+inte*rand()*sqrt(3)/2 ; M02(cpb(var))-inte*rand()*0.5];
      C=[M01(cpb(var))-inte*rand()*sqrt(3)/2 ; M02(cpb(var))-inte*rand()*0.5];
   else
      A=[M01(cpb(var)) ; M02(cpb(var))+inte*rand()*M02(cpb(var))];
      B=[M01(cpb(var))+inte*M01(cpb(var))*rand()*sqrt(3)/2 ; M02(cpb(var))-inte*0.5*rand()*M02(cpb(var))];
      C=[M01(cpb(var))-inte*M01(cpb(var))*rand()*sqrt(3)/2 ; M02(cpb(var))-inte*0.5*rand()*M02(cpb(var))];
   end
   %triplot
   trix=[];
   triy=[];
   [trix(:,count),triy(:,count)]=Tri(A,B,C);
   set(gcf,'CurrentAxes',ax2)
   set(ax2,'ColorOrder',[1 1 1; 1 0 0; 0 1 0; 0 0 1],'nextplot','replacechildren')
   plot(trix,triy);
   set(gca,'XColor',[1 1 1],'YColor',[1 1 1],'ZColor',[1 1 1],'Color',[0.25 0.25 0.25]);
   xlabel('M01')
   ylabel('M02')

while (dM>conv)
   contract=false;
   j=SB;
   count=count+1;
   M_fullA=zeros(1,N);
   M_fullB=zeros(1,N);
   M_fullC=zeros(1,N);
   M_mainA=zeros(1,N);
   M_mainB=zeros(1,N);
   M_mainC=zeros(1,N);

   for int=1:size(W1')
      Ri(int,:,:)=[R1 0;0 R1];
      Wi(int,:,:)=[W1(int) 0; 0 W2(int)];
      Ki(int,:,:)=[-k1(cpb(int)) k2(cpb(int));k1(cpb(int)) -k2(cpb(int))];

      if(var==cpb(int))

Mc=SGen3(squeeze(Wi(int,:,:)),squeeze(Ri(int,:,:)),squeeze(Ki(cpb(int),:,:)),A,N,Spec,squeeze(J(int,:)),squeeze(xn(int
,:)),MHz);
         M_mainA=M_mainA+squeeze(Mc(1,:));

Mc=SGen3(squeeze(Wi(int,:,:)),squeeze(Ri(int,:,:)),squeeze(Ki(cpb(int),:,:)),B,N,Spec,squeeze(J(int,:)),squeeze(xn(int
,:)),MHz);
         M_mainB=M_mainB+squeeze(Mc(1,:));

Mc=SGen3(squeeze(Wi(int,:,:)),squeeze(Ri(int,:,:)),squeeze(Ki(cpb(int),:,:)),C,N,Spec,squeeze(J(int,:)),squeeze(xn(int
,:)),MHz);
         M_mainC=M_mainC+squeeze(Mc(1,:));
      end
```

```
end
M_fullA=M_mainA+M_otherpeaks;
M_fullA=abs(real(fft(M_fullA)));
M_fullA=M_fullA-min(M_fullA);
M_fullB=M_mainB+M_otherpeaks;
M_fullB=abs(real(fft(M_fullB)));
M_fullB=M_fullB-min(M_fullB);
M_fullC=M_mainC+M_otherpeaks;
M_fullC=abs(real(fft(M_fullC)));
M_fullC=M_fullC-min(M_fullC);

SA=MSEr2(M_fullA,txt,Cg,100,MHz,Wshift,d);
SB=MSEr2(M_fullB,txt,Cg,100,MHz,Wshift,d);
SC=MSEr2(M_fullC,txt,Cg,100,MHz,Wshift,d);
%rank system
%-------------------------------------------------------
%%
BB=B;
if(SA<SB)
   if(SB<SC)
      W=C;
      MW=M_fullC;
      SW=SC;
      G=B;
      MG=M_fullB;
      SG=SB;
      B=A;
      MB=M_fullA;
      SB=SA;
   else
      if(SC<SA)
         W=B;
         MW=M_fullB;
         SW=SB;
         G=A;
         MG=M_fullA;
         SG=SA;
         B=C;
         MB=M_fullC;
         SB=SC;
      else
         W=B;
         MW=M_fullB;
         SW=SB;
         G=C;
         MG=M_fullC;
         SG=SC;
         B=A;
         MB=M_fullA;
         SB=SA;
      end
   end
else
```

```
    if(SA<SC)
      W=C;
      MW=M_fullC;
      SW=SC;
      G=A;
      MG=M_fullA;
      SG=SA;
      B=B;
      MB=M_fullB;
      SB=SB;
    else
      if(SC<SB)
        W=A;
        MW=M_fullA;
        SW=SA;
        G=B;
        MG=M_fullB;
        SG=SB;
        B=C;
        MB=M_fullC;
        SB=SC;
      else
        W=A;
        MW=M_fullA;
        SW=SA;
        G=C;
        MG=M_fullC;
        SG=SC;
        B=B;
        MB=M_fullB;
        SB=SB;
      end
    end
  end

  %%
  M=(G+B)/2;
  R=2*M-W;
  M_mainR=zeros(1,N);
  M_fullR=zeros(1,N);

  for int=1:size(W1')
    Ri(int,:,:)=[R1 0;0 R1];
    Wi(int,:,:)=[W1(int) 0; 0 W2(int)];
    Ki(int,:,:)=[-k1(cpb(int)) k2(cpb(int));k1(cpb(int)) -k2(cpb(int))];

    if(var==cpb(int))

Mc=SGen3(squeeze(Wi(int,:,:)),squeeze(Ri(int,:,:)),squeeze(Ki(cpb(int),:,:)),R,N,Spec,squeeze(J(int,:)),squeeze(xn(int
,:)),MHz);
      M_mainR=M_mainR+squeeze(Mc(1,:));
    end
  end
```

```
M_fullR=M_mainR+M_otherpeaks;
M_fullR=abs(real(fft(M_fullR)));
M_fullR=M_fullR-min(M_fullR);

SR=MSEr2(M_fullR,txt,Cg,100,MHz,Wshift,d);

%%
%nelder mead algorithm
if (SR<SG)
   if(SB<SR)
      W=R;
   else
      E=2*R-M;
      M_mainE=zeros(1,N);
      M_fullE=zeros(1,N);

      for int=1:size(W1')
         Ri(int,:,:)=[R1 0;0 R1];
         Wi(int,:,:)=[W1(int) 0; 0 W2(int)];
         Ki(int,:,:)=[-k1(cpb(int)) k2(cpb(int));k1(cpb(int)) -k2(cpb(int))];

         if(var==cpb(int))

Mc=SGen3(squeeze(Wi(int,:,:)),squeeze(Ri(int,:,:)),squeeze(Ki(cpb(int),:,:)),E,N,Spec,squeeze(J(int,:)),squeeze(xn(int
,:)),MHz);
            M_mainE=M_mainE + squeeze(Mc(1,:));
         end
      end
      M_fullE=M_mainE+M_otherpeaks;
      M_fullE=abs(real(fft(M_fullE)));
      M_fullE=M_fullE-min(M_fullE);
      SE=MSEr2(M_fullE,txt,Cg,100,MHz,Wshift,d);

      if(SE<SR)%rather than SE<SB because R might be smaller than E
         W=E;
      else
         W=R;
      end

   end
else
   if(SR<SW)
      W=R;

   else
      contract=true;
      C1=(M+W)/2;
      C2=(M+R)/2;
      M_mainC1=zeros(1,N);
      M_fullC1=zeros(1,N);
      M_mainC2=zeros(1,N);
      M_fullC2=zeros(1,N);
```

```
        for int=1:size(W1')
           Ri(int,:,:)=[R1 0;0 R1];
           Wi(int,:,:)=[W1(int) 0; 0 W2(int)];
           Ki(int,:,:)=[-k1(cpb(int)) k2(cpb(int));k1(cpb(int)) -k2(cpb(int))];

           if(var==cpb(int))

Mc=SGen3(squeeze(Wi(int,:,:)),squeeze(Ri(int,:,:)),squeeze(Ki(cpb(int),:,:)),C1,N,Spec,squeeze(J(int,:)),squeeze(xn(i
nt,:)),MHz);
              M_mainC1=M_mainC1+squeeze(Mc(1,:));

Mc=SGen3(squeeze(Wi(int,:,:)),squeeze(Ri(int,:,:)),squeeze(Ki(cpb(int),:,:)),C2,N,Spec,squeeze(J(int,:)),squeeze(xn(i
nt,:)),MHz);
              M_mainC2=M_mainC2+squeeze(Mc(1,:));
           end
        end
        M_fullC1=M_mainC1+M_otherpeaks;
        M_fullC1=abs(real(fft(M_fullC2)));
        M_fullC1=M_fullC1-min(M_fullC1);
        SC1=MSEr2(M_fullC1,txt,Cg,100,MHz,Wshift,d);
        M_fullC2=M_mainC2+M_otherpeaks;
        M_fullC2=abs(real(fft(M_fullC2)));
        M_fullC2=M_fullC2-min(M_fullC2);
        SC2=MSEr2(M_fullC2,txt,Cg,100,MHz,Wshift,d);

        if(SC1<SC2)
           C=C1;
           SC=SC1;
        else
           C=C2;
           SC=SC2;
        end
        if(SC<SW)
           W=C;

        else
              S=(B+W)/2;

              W=S;
              G=M;

        end
     end
  end

  Avg=(W+G+B)/3;
  if(~contract)
     dM1=abs(1-B(1)/M1);
     dM2=abs(1-B(1)/M2);
     dM=dM1+dM2;
     M1=B(1);
     M2=B(2);
  else
```

```
    dM1=abs(1-B(1)/Avg(1));
    dM2=abs(1-B(2)/Avg(2));
    dM=dM1+dM2;
  end

  M_mainI=zeros(1,N);
  M_fullI=zeros(1,N);

      for int=1:size(W1')
        Ri(int,:,:)=[R1 0;0 R1];
        Wi(int,:,:)=[W1(int) 0; 0 W2(int)];
        Ki(int,:,:)=[-k1(cpb(int)) k2(cpb(int));k1(cpb(int)) -k2(cpb(int))];

        if(var==cpb(int))

Mc=SGen3(squeeze(Wi(int,:,:)),squeeze(Ri(int,:,:)),squeeze(Ki(cpb(int),:,:)),B,N,Spec,squeeze(J(int,:)),squeeze(xn(int
,:)),MHz);
          M_mainI=M_mainI + squeeze(Mc(1,:));
        end
      end
      M_fullI=M_mainI+M_otherpeaks;
      M_fullI=abs(real(fft(M_fullI)));
      M_fullI=M_fullI-min(M_fullI);
      SB=MSEr2(M_fullI,txt,Cg,100,MHz,Wshift,d);

  if(W~=C)
    dSB=j-SB;
  end
  A=G;
  B=B;
  C=W;

  [trix(:,count),triy(:,count)]=Tri(A,B,C);
  set(gcf,'CurrentAxes',ax2)
  set(ax2,'ColorOrder',[1 1 1; 1 0 0; 0 1 0; 0 0 1],'nextplot','replacechildren')
  plot(trix,triy)
  set(gca,'XColor',[1 1 1],'YColor',[1 1 1],'ZColor',[1 1 1],'Color',[0.25 0.25 0.25])
  xlabel('M01')
  ylabel('M02')
  set(gcf,'CurrentAxes',ax1)
  M_main=zeros(1,N);
  M_otherpeaks=zeros(1,N);
  for int=1:size(W1')
    Ri(int,:,:)=[R1 0;0 R1];
    Wi(int,:,:)=[W1(int) 0; 0 W2(int)];
    M0(int,:,:)=[M01(cpb(int));M02(cpb(int))]';
    if(var==cpb(int))

Mc=SGen3(squeeze(Wi(int,:,:)),squeeze(Ri(int,:,:)),squeeze(Ki(cpb(int),:,:)),B,N,Spec,squeeze(J(int,:)),squeeze(xn(int
,:)),MHz);
      M_main=M_main+squeeze(Mc(1,:));
    end
  end
```

```
   M_full=M_main+M_otherpeaks;
   M_full=abs(real(fft(M_full)));
   M_full=M_full-min(M_full);
   Splot3(ax1,M_full,Wshift,txt,MHz);
   set(gca,'XDir','reverse','XColor',[1 1 1],'YColor',[1 1 1],'ZColor',[1 1 1],'Color',[0.25 0.25 0.25])
   axis([Cg(1,1) Cg(2,2) -0.5 1.2*max(M_full)])
   drawnow


end
count;
set(gcf,'CurrentAxes',ax2)
set(ax2,'ColorOrder',[1 1 1; 1 0 0; 0 1 0; 0 0 1])
plot(trix,triy)
set(gca,'XColor',[1 1 1],'YColor',[1 1 1],'ZColor',[1 1 1],'Color',[0.25 0.25 0.25]);
xlabel('M01')
ylabel('M02')
set(gcf,'CurrentAxes',ax1)
Splot3(ax1,M_full,Wshift,txt,MHz);
set(gca,'XDir','reverse','XColor',[1 1 1],'YColor',[1 1 1],'ZColor',[1 1 1],'Color',[0.25 0.25 0.25])
M01(cpb(var))=B(1);
M02(cpb(var))=B(2);
end
```

A.4.16. NMfitfS.m

```
function [k1,k2,M01,M02,SB]=NMfitfS(k1,k2,M01,M02,int,txt,Cg,W1,W2,R1,N,Spec,conv,iter,J,x,MHz,var,cpb,d)
W=[W1 0;0 W2];
R=[R1 0 ; 0 R1];
K=[-k1 k2;k1 -k2];
M0=[M01;M02];
%SB=MSEr(SGen3(W,R,K,M0,N,Spec,J,x,MHz),txt,Cg,100,MHz);
dM=conv*2;
dK=conv*2;
   %if(SB>20)
      inc=0;
      ax2=axes('Position',[0.1,0.1,0.8,0.35],'ColorOrder',[1 1 1; 1 0 0; 0 1 0; 0 0 1]);
      set(gca,'XColor',[1 1 1],'YColor',[1 1 1],'ZColor',[1 1 1],'Color',[0.25 0.25 0.25],'ColorOrder',[1 1 1; 1 0 0; 0 1 0; 0
0 1])
      ax1=axes('Position',[0.1,0.575,0.8,0.35]);
      set(gca,'XColor',[1 1 1],'YColor',[1 1 1],'ZColor',[1 1 1],'Color',[0.25 0.25 0.25])
      while((dM>conv||dK>conv)&&inc<=iter)
         inc=inc+1;
         [k1,k2,M01,M02,dK]=NMfitS(k1,k2,M01,M02,int,txt,Cg,W1,W2,R1,N,Spec,conv,J,x,MHz,var,cpb,d);
         dK=abs(1+K(1,1)/k1(cpb(var)))+abs(1+K(2,2)/k2(cpb(var)));
         K=[-k1(cpb(var)) k2(cpb(var));k1(cpb(var)) -k2(cpb(var))];
         [k1,k2,M01,M02,SB]=NMfitM0S(k1,k2,M01,M02,int,txt,Cg,W1,W2,R1,N,Spec,conv,J,x,MHz,var,cpb,d);
         dM=abs(1-M0(1)/M01(cpb(var)))+abs(1-M0(2)/M02(cpb(var)));
         M0=[M01(cpb(var));M02(cpb(var))];
      end
   %end

end
```

A.4.17. NMfitA.m

```
function [k1,k2,M01,M02,dK]=NMfitA(k1,k2,M01,M02,int,txt,Cg,W1,W2,R1,R2,N,Spec,conv,J,xn,MHz,Spacing,d)
   Ri=[R1 0 ; 0 R2];
   Wi=[W1 0; 0 W2];
   M0=[M01;M02];
   Ki=[-k1 k2;k1 -k2];
   Mplot=AnalyticGen(Wi,Ri,Ki,M0,N,Spec,J,xn,MHz);
   ax2=findobj('Position',[0.1,0.1,0.8,0.35]);
   set(gca,'XColor',[1 1 1],'YColor',[1 1 1],'ZColor',[1 1 1],'Color',[0.25 0.25 0.25])
   ax1=findobj('Position',[0.1,0.575,0.8,0.35]);
   xlabel('k1')
   ylabel('k2')
   Splot2(ax1,Mplot,txt,MHz);
   set(gca,'XDir','reverse','XColor',[1 1 1],'YColor',[1 1 1],'ZColor',[1 1 1],'Color',[0.25 0.25 0.25])
   axis([Cg(1,1) Cg(2,2) -0.05*max(Mplot(2,:)) 1.2*max(Mplot(2,:))])
   drawnow
%termination variables
K1= k1;
K2= k2;
dK1= 1;
dK2= 1;
dK= dK1+dK2;
contract=false;

SB=MSEr(Mplot,txt,Cg,Spacing,MHz,d);
dSB=10;
count=1;
xy=dlmread(txt);
x=xy(:,1)';
y=xy(:,2)';

   if(k1==0 || k2==0)
      A=[k1 ; k2+int*rand()];
      B=[k1+int*rand()*sqrt(3)/2 ; k2-int*rand()*0.5];
      C=[k1-int*rand()*sqrt(3)/2 ; k2-int*rand()*0.5];
   else
      A=[k1 ; k2+int*rand()*k2];
      B=[k1+int*k1*sqrt(3)/2 ; k2-int*0.5*k2];
      C=[k1-int*k1*sqrt(3)/2 ; k2-int*0.5*k2];
   end
   %triplot
   trix=[];
   triy=[];
   [trix(:,count),triy(:,count)]=Tri(A,B,C);
   set(gcf,'CurrentAxes',ax2)
   plot(trix,triy);
   set(gca,'XColor',[1 1 1],'YColor',[1 1 1],'ZColor',[1 1 1],'Color',[0.25 0.25 0.25]);
   axis([-5,5,-5,5]);
   KA=[-A(1) A(2);A(1) -A(2)];
   KB=[-B(1) B(2);B(1) -B(2)];
   KC=[-C(1) C(2);C(1) -C(2)];
```

```
    Ri=[R1 0 ; 0 R2];
    Wi=[W1 0; 0 W2];
    M0=[M01;M02];
while (dK>conv)
    contract=false;
    j=SB;
    count=count+1;

    MA=AnalyticGen(Wi,Ri,KA,M0,N,Spec,J,xn,MHz);
    MB=AnalyticGen(Wi,Ri,KB,M0,N,Spec,J,xn,MHz);
    MC=AnalyticGen(Wi,Ri,KC,M0,N,Spec,J,xn,MHz);

    SA=MSEr(MA,txt,Cg,Spacing,MHz,d);
    SB=MSEr(MB,txt,Cg,Spacing,MHz,d);
    SC=MSEr(MC,txt,Cg,Spacing,MHz,d);
    %rank system
    %-------------------------------------------------------
    %%
    BB=B;
    if(SA<SB)
       if(SB<SC)
          W=C;
          MW=MC;
          SW=SC;
          G=B;
          MG=MB;
          SG=SB;
          B=A;
          MB=MA;
          SB=SA;
       else
          if(SC<SA)
             W=B;
             MW=MB;
             SW=SB;
             G=A;
             MG=MA;
             SG=SA;
             B=C;
             MB=MC;
             SB=SC;
          else
             W=B;
             MW=MB;
             SW=SB;
             G=C;
             MG=MC;
             SG=SC;
             B=A;
             MB=MA;
             SB=SA;
          end
       end
```

```
else
   if(SA<SC)
      W=C;
      MW=MC;
      SW=SC;
      G=A;
      MG=MA;
      SG=SA;
      B=B;
      MB=MB;
      SB=SB;
   else
      if(SC<SB)
         W=A;
         MW=MA;
         SW=SA;
         G=B;
         MG=MB;
         SG=SB;
         B=C;
         MB=MC;
         SB=SC;
      else
         W=A;
         MW=MA;
         SW=SA;
         G=C;
         MG=MC;
         SG=SC;
         B=B;
         MB=MB;
         SB=SB;
      end
   end
end

KG=[-G(1) G(2);G(1) -G(2)];
KB=[-B(1) B(2);B(1) -B(2)];
KW=[-W(1) W(2);W(1) -W(2)];

M=(G+B)/2;
R=2*M-W;
KR=[-R(1) R(2);R(1) -R(2)];
MR=AnalyticGen(Wi,Ri,KR,M0,N,Spec,J,xn,MHz);
SR=MSEr(MR,txt,Cg,Spacing,MHz,d);

%%
%nelder mead algorithm
if (SR<SG)
   if(SB<SR)
      W=R;
   else
      E=2*R-M;
```

```
      KE=[-E(1) E(2);E(1) -E(2)];
      ME=AnalyticGen(Wi,Ri,KE,M0,N,Spec,J,xn,MHz);
      SE=MSEr(ME,txt,Cg,Spacing,MHz,d);

      if(SE<SR)%rather than SE<SB because R might be smaller than E
         W=E;
      else
         W=R;
      end

   end
else
   if(SR<SW)
      W=R;

   else
      contract=true;
      C1=(M+W)/2;
      C2=(M+R)/2;
      KC1=[-C1(1) C1(2);C1(1) -C1(2)];
      KC2=[-C2(1) C2(2);C2(1) -C2(2)];
      MC1=AnalyticGen(Wi,Ri,KC1,M0,N,Spec,J,xn,MHz);
      MC2=AnalyticGen(Wi,Ri,KC2,M0,N,Spec,J,xn,MHz);
      SC1=MSEr(MC1,txt,Cg,Spacing,MHz,d);
      SC2=MSEr(MC2,txt,Cg,Spacing,MHz,d);
      if(SC1<SC2)
         C=C1;
         SC=SC1;
      else
         C=C2;
         SC=SC2;
      end
      if(SC<SW)
         W=C;
      else
         S=(B+W)/2;
         W=S;
         G=M;
      end
   end
end
k1=B(1);
k2=B(2);
Avg=(W+G+B)/3;
if(~contract)
   dK1=abs(1-k1/K1);
   dK2=abs(1-k2/K2);
   dK=dK1+dK2;
   K1=k1;
   K2=k2;
else
   dK1=abs(1-k1/Avg(1));
   dK2=abs(1-k2/Avg(2));
```

```
    dK=dK1+dK2;
  end


  KI=[-k1 k2; k1 -k2];
  MI=AnalyticGen(Wi,Ri,KI,M0,N,Spec,J,xn,MHz);
  SB=MSEr(MI,txt,Cg,Spacing,MHz,d);

  if(W~=C)

    dSB=j-SB;
  end

  A=G;
  KA= [-A(1) A(2);A(1) -A(2)];
  B=B;
  KB= [-B(1) B(2);B(1) -B(2)];
  C=W;
  KC= [-C(1) C(2);C(1) -C(2)];

  [trix(:,count),triy(:,count)]=Tri(A,B,C);
  set(gcf,'CurrentAxes',ax2)
  plot(trix,triy)
  set(gca,'XColor',[1 1 1],'YColor',[1 1 1],'ZColor',[1 1 1],'Color',[0.25 0.25 0.25])
  xlabel('k1')
  ylabel('k2')
  set(gcf,'CurrentAxes',ax1)
  Mplot=AnalyticGen(Wi,Ri,[-k1 k2;k1 -k2],M0,N,Spec,J,xn,MHz);
  Splot2(ax1,Mplot,txt,MHz);
  set(gca,'XDir','reverse','XColor',[1 1 1],'YColor',[1 1 1],'ZColor',[1 1 1],'Color',[0.25 0.25 0.25])
  axis([Cg(1,1) Cg(2,2) -0.05*max(Mplot(2,:)) 1.2*max(Mplot(2,:))])
  drawnow



end
count;
set(gcf,'CurrentAxes',ax2)
plot(trix,triy)
set(gca,'XColor',[1 1 1],'YColor',[1 1 1],'ZColor',[1 1 1],'Color',[0.25 0.25 0.25]);
xlabel('k1')
ylabel('k2')
set(gcf,'CurrentAxes',ax1)
Splot2(ax1,Mplot,txt,MHz);
set(gca,'XDir','reverse','XColor',[1 1 1],'YColor',[1 1 1],'ZColor',[1 1 1],'Color',[0.25 0.25 0.25])
end
```

A.4.18. NMfitAM0.m

```
function
[k1,k2,M01,M02,SB]=NMfitAM0(k1,k2,M01,M02,int,txt,Cg,W1,W2,R1,R2,N,Spec,conv,J,xn,MHz,Spacing,d)
  Ri=[R1 0 ; 0 R2];
```

```
   Wi=[W1 0; 0 W2];
   M0=[M01;M02];
   Ki=[-k1 k2;k1 -k2];
   Mplot=AnalyticGen(Wi,Ri,Ki,M0,N,Spec,J,xn,MHz);
   ax2=findobj('Position',[0.1,0.1,0.8,0.35]);
   set(gca,'XColor',[1 1 1],'YColor',[1 1 1],'ZColor',[1 1 1],'Color',[0.25 0.25 0.25])
   ax1=findobj('Position',[0.1,0.575,0.8,0.35]);
   xlabel('M01')
   ylabel('M02')
   Splot2(ax1,Mplot,txt,MHz);
   set(gca,'XDir','reverse','XColor',[1 1 1],'YColor',[1 1 1],'ZColor',[1 1 1],'Color',[0.25 0.25 0.25])
   axis([Cg(1,1) Cg(2,2) -0.05*max(Mplot(2,:)) 1.2*max(Mplot(2,:))])
   drawnow
%termination variables
M1= M01;
M2= M02;
dM1= 1;
dM2= 1;
dM= dM1+dM2;
contract=false;

SB=MSEr(Mplot,txt,Cg,Spacing,MHz,d);
dSB=10;
count=1;
xy=dlmread(txt);
x=xy(:,1)';
y=xy(:,2)';

   if(M01==0 || M02==0)
      A=[M01 ; M02+int*rand()];
      B=[M01+int*rand()*sqrt(3)/2 ; M02-int*rand()*0.5];
      C=[M01-int*rand()*sqrt(3)/2 ; M02-int*rand()*0.5];
   else
      A=[M01 ; M02+int*rand()*M02];
      B=[M01+int*M01*rand()*sqrt(3)/2 ; M02-int*0.5*rand()*M02];
      C=[M01-int*M01*rand()*sqrt(3)/2 ; M02-int*0.5*rand()*M02];
   end
   %triplot
   trix=[];
   triy=[];
   [trix(:,count),triy(:,count)]=Tri(A,B,C);
   set(gcf,'CurrentAxes',ax2)
   plot(trix,triy);
   set(gca,'XDir','reverse','XColor',[1 1 1],'YColor',[1 1 1],'ZColor',[1 1 1],'Color',[0.25 0.25 0.25])
   xlabel('M01')
   ylabel('M02')
   axis([-5,5,-5,5]);

while (dM>conv)
   contract=false;
   j=SB;
   count=count+1;
```

```
MA=AnalyticGen(Wi,Ri,Ki,A,N,Spec,J,xn,MHz);
MB=AnalyticGen(Wi,Ri,Ki,B,N,Spec,J,xn,MHz);
MC=AnalyticGen(Wi,Ri,Ki,C,N,Spec,J,xn,MHz);

SA=MSEr(MA,txt,Cg,Spacing,MHz,d);
SB=MSEr(MB,txt,Cg,Spacing,MHz,d);
SC=MSEr(MC,txt,Cg,Spacing,MHz,d);
%rank system
%-------------------------------------------------------
%%
BB=B;
if(SA<SB)
   if(SB<SC)
      W=C;
      G=B;
      B=A;
   else
      if(SC<SA)
         W=B;
         G=A;
         B=C;
      else
         W=B;
         G=C;
         B=A;
      end
   end
else
   if(SA<SC)
      W=C;
      G=A;
      B=B;
   else
      if(SC<SB)
         W=A;
         G=B;
         B=C;
      else
         W=A;
         G=C;
         B=B;
      end
   end
end


MG=AnalyticGen(Wi,Ri,Ki,G,N,Spec,J,xn,MHz);
MB=AnalyticGen(Wi,Ri,Ki,B,N,Spec,J,xn,MHz);
MW=AnalyticGen(Wi,Ri,Ki,W,N,Spec,J,xn,MHz);
SG=MSEr(MG,txt,Cg,Spacing,MHz,d);


SB=MSEr(MB,txt,Cg,Spacing,MHz,d);
```

```
SW=MSEr(MW,txt,Cg,Spacing,MHz,d);

%%
M=(G+B)/2;
R=2*M-W;
MR=AnalyticGen(Wi,Ri,Ki,R,N,Spec,J,xn,MHz);
SR=MSEr(MR,txt,Cg,Spacing,MHz,d);

%%
%nelder mead algorithm
if (SR<SG)
   if(SB<SR)
      W=R;
   else
      E=2*R-M;
      ME=AnalyticGen(Wi,Ri,Ki,E,N,Spec,J,xn,MHz);
      SE=MSEr(ME,txt,Cg,Spacing,MHz,d);
      if(SE<SR)%rather than SE<SB because R might be smaller than E
         W=E;
      else
         W=R;
      end

   end
else
   if(SR<SW)
      W=R;

   else
      contract=true;
      C1=(M+W)/2;
      C2=(M+R)/2;
      MC1=AnalyticGen(Wi,Ri,Ki,C1,N,Spec,J,xn,MHz);
      MC2=AnalyticGen(Wi,Ri,Ki,C2,N,Spec,J,xn,MHz);
      SC1=MSEr(MC1,txt,Cg,Spacing,MHz,d);
      SC2=MSEr(MC2,txt,Cg,Spacing,MHz,d);
      if(SC1<SC2)
         C=C1;
         SC=SC1;
      else
         C=C2;
         SC=SC2;
      end
      if(SC<SW)
         W=C;

      else
            S=(B+W)/2;

            W=S;
            G=M;

      end
```

```
    end
  end
  M01=B(1);
  M02=B(2);
  Avg=(W+G+B)/3;
  if(~contract)
    dM1=abs(1-M01/M1);
    dM2=abs(1-M02/M2);
    dM=dM1+dM2;
    M1=M01;
    M2=M02;
  else
    dM1=abs(1-M01/Avg(1));
    dM2=abs(1-M02/Avg(2));
    dM=dM1+dM2;
  end

  MB=AnalyticGen(Wi,Ri,Ki,Avg,N,Spec,J,xn,MHz);
  SB=MSEr(MB,txt,Cg,Spacing,MHz,d);

  if(W~=C)
    dSB=j-SB;
  end
  A=G;
  B=B;
  C=W;

  [trix(:,count),triy(:,count)]=Tri(A,B,C);
  set(gcf,'CurrentAxes',ax2)
  plot(trix,triy)
  set(gca,'XColor',[1 1 1],'YColor',[1 1 1],'ZColor',[1 1 1],'Color',[0.25 0.25 0.25])
  xlabel('M01')
  ylabel('M02')
  set(gcf,'CurrentAxes',ax1)
  Mx=AnalyticGen(Wi,Ri,Ki,[M01;M02],N,Spec,J,xn,MHz);
  Splot2(ax1,Mx,txt,MHz);
  set(gca,'XDir','reverse','XColor',[1 1 1],'YColor',[1 1 1],'ZColor',[1 1 1],'Color',[0.25 0.25 0.25])
  axis([Cg(1,1) Cg(2,2) -0.05*max(Mplot(2,:)) max(Mx(2,:))])
  drawnow


end
count;
set(gcf,'CurrentAxes',ax2)
plot(trix,triy)
set(gca,'XColor',[1 1 1],'YColor',[1 1 1],'ZColor',[1 1 1],'Color',[0.25 0.25 0.25]);
xlabel('M01')
ylabel('M02')
set(gcf,'CurrentAxes',ax1)
Splot2(ax1,Mx,txt,MHz);
set(gca,'XDir','reverse','XColor',[1 1 1],'YColor',[1 1 1],'ZColor',[1 1 1],'Color',[0.25 0.25 0.25])
end
```

A.4.19. NMfitAf.m

```
function
[k1,k2,M01,M02,SB]=NMfitAf(k1,k2,M01,M02,int,txt,Cg,W1,W2,R1,R2,N,Spec,conv,iter,J,x,MHz,spacing,d)
W=[W1 0;0 W2];
R=[R1 0 ; 0 R2];
K=[-k1 k2;k1 -k2];
M0=[M01;M02];
SB=MSEr(AnalyticGen(W,R,K,M0,N,Spec,J,x,MHz),txt,Cg,spacing,MHz,d);
dM=conv*2;
dK=conv*2;
  if(SB>0)
    inc=0;
    ax2=axes('Position',[0.1,0.1,0.8,0.35]);
    set(gca,'XColor',[1 1 1],'YColor',[1 1 1],'ZColor',[1 1 1],'Color',[0.25 0.25 0.25])
    ax1=axes('Position',[0.1,0.575,0.8,0.35]);
    set(gca,'XColor',[1 1 1],'YColor',[1 1 1],'ZColor',[1 1 1],'Color',[0.25 0.25 0.25])
    while((dM>conv||dK>conv)&&inc<=iter)
      inc=inc+1;
      [k1,k2,M01,M02,dK]=NMfitA(k1,k2,M01,M02,int,txt,Cg,W1,W2,R1,R2,N,Spec,conv,J,x,MHz,spacing,d);
      dK=abs(1+K(1,1)/k1)+abs(1+K(2,2)/k2);
      K=[-k1 k2;k1 -k2];
      [k1,k2,M01,M02,SB]=NMfitAM0(k1,k2,M01,M02,int,txt,Cg,W1,W2,R1,R2,N,Spec,conv,J,x,MHz,spacing,d);
      dM=abs(1-M0(1)/M01)+abs(1-M0(2)/M02);
      M0=[M01;M02];
    end
  end

end
```

A.4.20. NMfitAS.m

```
function [k1,k2,M01,M02,dK]=NMfitAS(k1,k2,M01,M02,inte,txt,Cg,W1,W2,R1,N,Spec,conv,J,xn,MHz,var,cpb,d)

  M_main=zeros(1,N);
  M_otherpeaks=zeros(1,N);
  for int=1:size(squeeze(W1'))
    Ri(int,:,:)=[R1 0;0 R1];
    Wi(int,:,:)=[W1(int) 0; 0 W2(int)]
    Ki(int,:,:)=[-k1(cpb(int)) k2(cpb(int));k1(cpb(int)) -k2(cpb(int))];
    M0(int,:,:)=[M01(cpb(int));M02(cpb(int))]';
    if(var==cpb(int))

Mc=AnalyticGen(squeeze(Wi(int,:,:)),squeeze(Ri(int,:,:)),squeeze(Ki(cpb(int),:,:)),squeeze(M0(cpb(int),:,:)),N,Spec,sq
ueeze(J(int,:)),squeeze(xn(int,:)),MHz);
      M_main=M_main+squeeze(Mc(1,:));
    else

Mc=AnalyticGen(squeeze(Wi(int,:,:)),squeeze(Ri(int,:,:)),squeeze(Ki(cpb(int),:,:)),squeeze(M0(cpb(int),:,:)),N,Spec,sq
ueeze(J(int,:)),squeeze(xn(int,:)),MHz);
      M_otherpeaks=M_otherpeaks+squeeze(Mc(1,:));
    end
  end
```

```
    M_full=M_main+M_otherpeaks;
    [y,Wshift]=getMXY(Mc,MHz);
    M_full=abs(real(fft(M_full)));
    M_full=M_full-min(M_full);
    Cg=[0 max(Wshift)/2; max(Wshift)/2 max(Wshift)];
    ax2=findobj('Position',[0.1,0.1,0.8,0.35]);
    set(ax2,'ColorOrder',[1 1 1; 1 0 0; 0 1 0; 0 0 1],'nextplot','replacechildren')
    set(gca,'XColor',[1 1 1],'YColor',[1 1 1],'ZColor',[1 1 1],'Color',[0.25 0.25 0.25])
    ax1=findobj('Position',[0.1,0.575,0.8,0.35]);
    xlabel('k1')
    ylabel('k2')
    Splot3(ax1,M_full,Wshift,txt,MHz);
    set(gca,'XDir','reverse','XColor',[1 1 1],'YColor',[1 1 1],'ZColor',[1 1 1],'Color',[0.25 0.25 0.25])
    axis([Cg(1,1) Cg(2,2) -0.5 1.2*max(M_full)])
    drawnow
%termination variables
K1= k1(cpb(var));
K2= k2(cpb(var));
dK1= 1;
dK2= 1;
dK= dK1+dK2;
contract=false;

SB=MSEr2(M_full,txt,Cg,100,MHz,Wshift,d);
dSB=10;
count=1;
xy=dlmread(txt);
x=xy(:,1)';
y=xy(:,2)';

    if(k1(cpb(var))==0 || k2(cpb(var))==0)
        A=[k1(cpb(var)) ; k2(cpb(var))+inte*rand()];
        B=[k1(cpb(var))+inte*rand()*sqrt(3)/2 ; k2(cpb(var))-inte*rand()*0.5];
        C=[k1(cpb(var))-inte*rand()*sqrt(3)/2 ; k2(cpb(var))-inte*rand()*0.5];
    else
        A=[k1(cpb(var)) ; k2(cpb(var))+inte*rand()*k2(cpb(var))];
        B=[k1(cpb(var))+inte*k1(cpb(var))*sqrt(3)/2 ; k2(cpb(var))-inte*0.5*k2(cpb(var))];
        C=[k1(cpb(var))-inte*k1(cpb(var))*sqrt(3)/2 ; k2(cpb(var))-inte*0.5*k2(cpb(var))];
    end
    %triplot
    trix=[];
    triy=[];
    [trix(:,count),triy(:,count)]=Tri(A,B,C);
    set(gcf,'CurrentAxes',ax2)
    set(ax2,'ColorOrder',[1 1 1; 1 0 0; 0 1 0; 0 0 1],'nextplot','replacechildren')
    plot(trix,triy);
    set(gca,'XColor',[1 1 1],'YColor',[1 1 1],'ZColor',[1 1 1],'Color',[0.25 0.25 0.25]);

    KA=[-A(1) A(2);A(1) -A(2)];
    KB=[-B(1) B(2);B(1) -B(2)];
    KC=[-C(1) C(2);C(1) -C(2)];
while (dK>conv)
    contract=false;
```

```
   j=SB;
   count=count+1;
   M_fullA=zeros(1,N);
   M_fullB=zeros(1,N);
   M_fullC=zeros(1,N);
   M_mainA=zeros(1,N);
   M_mainB=zeros(1,N);
   M_mainC=zeros(1,N);

   for int=1:size(W1')
      Ri(int,:,:)=[R1 0;0 R1];
      Wi(int,:,:)=[W1(int) 0; 0 W2(int)];
      M0(int,:,:)=[M01(cpb(int));M02(cpb(int))]';
      if(var==cpb(int))

Mc=AnalyticGen(squeeze(Wi(int,:,:)),squeeze(Ri(int,:,:)),KA,squeeze(M0(cpb(int),:,:)),N,Spec,squeeze(J(int,:)),squee
ze(xn(int,:)),MHz);
         M_mainA=M_mainA+squeeze(Mc(1,:));

Mc=AnalyticGen(squeeze(Wi(int,:,:)),squeeze(Ri(int,:,:)),KB,squeeze(M0(cpb(int),:,:)),N,Spec,squeeze(J(int,:)),squee
ze(xn(int,:)),MHz);
         M_mainB=M_mainB+squeeze(Mc(1,:));

Mc=AnalyticGen(squeeze(Wi(int,:,:)),squeeze(Ri(int,:,:)),KC,squeeze(M0(cpb(int),:,:)),N,Spec,squeeze(J(int,:)),squee
ze(xn(int,:)),MHz);
         M_mainC=M_mainC+squeeze(Mc(1,:));
      end
   end
   M_fullA=M_mainA+M_otherpeaks;
   M_fullA=abs(real(fft(M_fullA)));
   M_fullA=M_fullA-min(M_fullA);
   M_fullB=M_mainB+M_otherpeaks;
   M_fullB=abs(real(fft(M_fullB)));
   M_fullB=M_fullB-min(M_fullB);
   M_fullC=M_mainC+M_otherpeaks;
   M_fullC=abs(real(fft(M_fullC)));
   M_fullC=M_fullC-min(M_fullC);


   SA=MSEr2(M_fullA,txt,Cg,100,MHz,Wshift,d);
   SB=MSEr2(M_fullB,txt,Cg,100,MHz,Wshift,d);
   SC=MSEr2(M_fullC,txt,Cg,100,MHz,Wshift,d);
   %rank system
   %-------------------------------------------------------
   %%
   BB=B;
   if(SA<SB)
      if(SB<SC)
         W=C;
         MW=M_fullC;
         SW=SC;
         G=B;
         MG=M_fullB;
```

```
        SG=SB;
        B=A;
        MB=M_fullA;
        SB=SA;
    else
        if(SC<SA)
            W=B;
            MW=M_fullB;
            SW=SB;
            G=A;
            MG=M_fullA;
            SG=SA;
            B=C;
            MB=M_fullC;
            SB=SC;
        else
            W=B;
            MW=M_fullB;
            SW=SB;
            G=C;
            MG=M_fullC;
            SG=SC;
            B=A;
            MB=M_fullA;
            SB=SA;
        end
    end
else
    if(SA<SC)
        W=C;
        MW=M_fullC;
        SW=SC;
        G=A;
        MG=M_fullA;
        SG=SA;
        B=B;
        MB=M_fullB;
        SB=SB;
    else
        if(SC<SB)
            W=A;
            MW=M_fullA;
            SW=SA;
            G=B;
            MG=M_fullB;
            SG=SB;
            B=C;
            MB=M_fullC;
            SB=SC;
        else
            W=A;
            MW=M_fullA;
            SW=SA;
```

```
            G=C;
            MG=M_fullC;
            SG=SC;
            B=B;
            MB=M_fullB;
            SB=SB;
        end
    end
end

KG=[-G(1) G(2);G(1) -G(2)];
KB=[-B(1) B(2);B(1) -B(2)];
KW=[-W(1) W(2);W(1) -W(2)];

M=(G+B)/2;
R=2*M-W;
KR=[-R(1) R(2);R(1) -R(2)];
M_mainR=zeros(1,N);
M_fullR=zeros(1,N);

for int=1:size(W1')
    Ri(int,:,:)=[R1 0;0 R1];
    Wi(int,:,:)=[W1(int) 0; 0 W2(int)];
    M0(int,:,:)=[M01(cpb(int));M02(cpb(int))]';
    if(var==cpb(int))

Mc=AnalyticGen(squeeze(Wi(int,:,:)),squeeze(Ri(int,:,:)),KR,squeeze(M0(cpb(int),:,:)),N,Spec,squeeze(J(int,:)),squee
ze(xn(int,:)),MHz);
        M_mainR=M_mainR+squeeze(Mc(1,:));
    end
end
M_fullR=M_mainR+M_otherpeaks;
M_fullR=abs(real(fft(M_fullR)));
M_fullR=M_fullR-min(M_fullR);

SR=MSEr2(M_fullR,txt,Cg,100,MHz,Wshift,d);

%%
%nelder mead algorithm
if (SR<SG)
    if(SB<SR)
        W=R;
    else
        E=2*R-M;
        KE=[-E(1) E(2);E(1) -E(2)];
        M_mainE=zeros(1,N);
        M_fullE=zeros(1,N);

        for int=1:size(W1')
            Ri(int,:,:)=[R1 0;0 R1];
            Wi(int,:,:)=[W1(int) 0; 0 W2(int)];
            M0(int,:,:)=[M01(cpb(int));M02(cpb(int))]';
            if(var==cpb(int))
```

```
Mc=AnalyticGen(squeeze(Wi(int,:,:)),squeeze(Ri(int,:,:)),KE,squeeze(M0(cpb(int),:,:)),N,Spec,squeeze(J(int,:)),squee
ze(xn(int,:)),MHz);
                M_mainE=M_mainE + squeeze(Mc(1,:));
              end
            end
            M_fullE=M_mainE+M_otherpeaks;
            M_fullE=abs(real(fft(M_fullE)));
            M_fullE=M_fullE-min(M_fullE);
            SE=MSEr2(M_fullE,txt,Cg,100,MHz,Wshift,d);

            if(SE<SR)%rather than SE<SB because R might be smaller than E
              W=E;
            else
              W=R;
            end

        end
    else
        if(SR<SW)
            W=R;

        else
            contract=true;
            C1=(M+W)/2;
            C2=(M+R)/2;
            KC1=[-C1(1) C1(2);C1(1) -C1(2)];
            KC2=[-C2(1) C2(2);C2(1) -C2(2)];
            M_mainC1=zeros(1,N);
            M_fullC1=zeros(1,N);
            M_mainC2=zeros(1,N);
            M_fullC2=zeros(1,N);

            for int=1:size(W1')
              Ri(int,:,:)=[R1 0;0 R1];
              Wi(int,:,:)=[W1(int) 0; 0 W2(int)];
              M0(int,:,:)=[M01(cpb(int));M02(cpb(int))]';
              if(var==cpb(int))

Mc=AnalyticGen(squeeze(Wi(int,:,:)),squeeze(Ri(int,:,:)),KC1,squeeze(M0(cpb(int),:,:)),N,Spec,squeeze(J(int,:)),sque
eze(xn(int,:)),MHz);
                M_mainC1=M_mainC1+squeeze(Mc(1,:));

Mc=AnalyticGen(squeeze(Wi(int,:,:)),squeeze(Ri(int,:,:)),KC2,squeeze(M0(cpb(int),:,:)),N,Spec,squeeze(J(int,:)),sque
eze(xn(int,:)),MHz);
                M_mainC2=M_mainC2+squeeze(Mc(1,:));
              end
            end
            M_fullC1=M_mainC1+M_otherpeaks;
            M_fullC1=abs(real(fft(M_fullC2)));
            M_fullC1=M_fullC1-min(M_fullC1);
            SC1=MSEr2(M_fullC1,txt,Cg,100,MHz,Wshift,d);
            M_fullC2=M_mainC2+M_otherpeaks;
```

```
        M_fullC2=abs(real(fft(M_fullC2)));
        M_fullC2=M_fullC2-min(M_fullC2);
        SC2=MSEr2(M_fullC2,txt,Cg,100,MHz,Wshift,d);


        if(SC1<SC2)
           C=C1;
           SC=SC1;
        else
           C=C2;
           SC=SC2;
        end
        if(SC<SW)
           W=C;
        else
           S=(B+W)/2;
           W=S;
           G=M;
        end
     end
  end
  Avg=(W+G+B)/3;
  if(~contract)
     dK1=abs(1-B(1)/K1);
     dK2=abs(1-B(2)/K2);
     dK=dK1+dK2;
     K1=B(1);
     K2=B(2);
  else
     dK1=abs(1-k1(cpb(var))/Avg(1));
     dK2=abs(1-k2(cpb(var))/Avg(2));
     dK=dK1+dK2;
  end


  KI=[-k1(cpb(var)) k2(cpb(var)); k1(cpb(var)) -k2(cpb(var))];
        M_mainI=zeros(1,N);
        M_fullI=zeros(1,N);

        for int=1:size(W1')
           Ri(int,:,:)=[R1 0;0 R1];
           Wi(int,:,:)=[W1(int) 0; 0 W2(int)];
           M0(int,:,:)=[M01(cpb(int));M02(cpb(int))]';
           if(var==cpb(int))

Mc=AnalyticGen(squeeze(Wi(int,:,:)),squeeze(Ri(int,:,:)),KI,squeeze(M0(cpb(int),:,:)),N,Spec,squeeze(J(int,:)),squeez
e(xn(int,:)),MHz);
              M_mainI=M_mainI + squeeze(Mc(1,:));
           end
        end
        M_fullI=M_mainI+M_otherpeaks;
        M_fullI=abs(real(fft(M_fullI)));
        M_fullI=M_fullI-min(M_fullI);
```

```
        SB=MSEr2(M_fullI,txt,Cg,100,MHz,Wshift,d);


   if(W~=C)

      dSB=j-SB;
   end

   A=G;
   KA= [-A(1) A(2);A(1) -A(2)];
   B=B;
   KB= [-B(1) B(2);B(1) -B(2)];
   C=W;
   KC= [-C(1) C(2);C(1) -C(2)];

   [trix(:,count),triy(:,count)]=Tri(A,B,C);
   set(gcf,'CurrentAxes',ax2)
   set(ax2,'ColorOrder',[1 1 1; 1 0 0; 0 1 0; 0 0 1],'nextplot','replacechildren')
   plot(trix,triy)
   set(gca,'XColor',[1 1 1],'YColor',[1 1 1],'ZColor',[1 1 1],'Color',[0.25 0.25 0.25])
   xlabel('k1')
   ylabel('k2')
   set(gcf,'CurrentAxes',ax1)
   M_main=zeros(1,N);
   M_otherpeaks=zeros(1,N);
   for int=1:size(W1')
      Ri(int,:,:)=[R1 0;0 R1];
      Wi(int,:,:)=[W1(int) 0; 0 W2(int)];
      M0(int,:,:)=[M01(cpb(int));M02(cpb(int))]';
      if(var==cpb(int))

Mc=AnalyticGen(squeeze(Wi(int,:,:)),squeeze(Ri(int,:,:)),KB,squeeze(M0(cpb(int),:,:)),N,Spec,squeeze(J(int,:)),squee
ze(xn(int,:)),MHz);
         M_main=M_main+squeeze(Mc(1,:));
      end
   end
   M_full=M_main+M_otherpeaks;
   M_full=abs(real(fft(M_full)));
   M_full=M_full-min(M_full);
   Splot3(ax1,M_full,Wshift,txt,MHz);
   set(gca,'XDir','reverse','XColor',[1 1 1],'YColor',[1 1 1],'ZColor',[1 1 1],'Color',[0.25 0.25 0.25])
   axis([Cg(1,1) Cg(2,2) -0.5 1.2*max(M_full)])
   drawnow


end
count;
set(gcf,'CurrentAxes',ax2)
set(ax2,'ColorOrder',[1 1 1; 1 0 0; 0 1 0; 0 0 1])
plot(trix,triy)
set(gca,'XColor',[1 1 1],'YColor',[1 1 1],'ZColor',[1 1 1],'Color',[0.25 0.25 0.25]);
xlabel('k1')
ylabel('k2')
```

```
set(gcf,'CurrentAxes',ax1)
Splot3(ax1,M_full,Wshift,txt,MHz);
set(gca,'XDir','reverse','XColor',[1 1 1],'YColor',[1 1 1],'ZColor',[1 1 1],'Color',[0.25 0.25 0.25])
k1(cpb(var))=-KB(1,1);
k2(cpb(var))=-KB(2,2);
end
```

A.4.21. NMfitAM0S.m

```
function [k1,k2,M01,M02,SB]=NMfitAM0S(k1,k2,M01,M02,inte,txt,Cg,W1,W2,R1,N,Spec,conv,J,xn,MHz,var,cpb,d)
   M_main=zeros(1,N);
   M_otherpeaks=zeros(1,N);
   for int=1:size(W1')
      Ri(int,:,:)=[R1 0;0 R1];
      Wi(int,:,:)=[W1(int) 0; 0 W2(int)];
      Ki(int,:,:)=[-k1(cpb(int)) k2(cpb(int));k1(cpb(int)) -k2(cpb(int))];
      M0(int,:,:)=[M01(cpb(int));M02(cpb(int))]';
      if(var==cpb(int))

Mc=AnalyticGen(squeeze(Wi(int,:,:)),squeeze(Ri(int,:,:)),squeeze(Ki(cpb(int),:,:)),squeeze(M0(cpb(int),:,:)),N,Spec,sq
ueeze(J(int,:)),squeeze(xn(int,:)),MHz);
         M_main=M_main+squeeze(Mc(1,:));
      else

Mc=AnalyticGen(squeeze(Wi(int,:,:)),squeeze(Ri(int,:,:)),squeeze(Ki(cpb(int),:,:)),squeeze(M0(cpb(int),:,:)),N,Spec,sq
ueeze(J(int,:)),squeeze(xn(int,:)),MHz);
         M_otherpeaks=M_otherpeaks+squeeze(Mc(1,:));
      end
   end
   M_full=M_main+M_otherpeaks;
   [y,Wshift]=getMXY(Mc,MHz);
   Cg=[0 max(Wshift)/2; max(Wshift)/2 max(Wshift)];
   M_full=abs(real(fft(M_full)));
   M_full=M_full-min(M_full);
   ax2=findobj('Position',[0.1,0.1,0.8,0.35]);
   set(ax2,'ColorOrder',[1 1 1; 1 0 0; 0 1 0; 0 0 1],'nextplot','replacechildren')
   set(gca,'XColor',[1 1 1],'YColor',[1 1 1],'ZColor',[1 1 1],'Color',[0.25 0.25 0.25])
   ax1=findobj('Position',[0.1,0.575,0.8,0.35]);
   xlabel('M01')
   ylabel('M02')
   Splot3(ax1,M_full,Wshift,txt,MHz);
   set(gca,'XDir','reverse','XColor',[1 1 1],'YColor',[1 1 1],'ZColor',[1 1 1],'Color',[0.25 0.25 0.25])
   axis([Cg(1,1) Cg(2,2) -0.5 1.2*max(M_full)])
   drawnow
%termination variables
M1= M01(cpb(var));
M2= M02(cpb(var));
dM1= 1;
dM2= 1;
dM= dM1+dM2;
contract=false;

SB=MSEr2(M_main,txt,Cg,100,MHz,Wshift,d);
```

```
dSB=10;
count=1;
xy=dlmread(txt);
x=xy(:,1)';
y=xy(:,2)';

   if(M01(cpb(var))==0 || M02(cpb(var))==0)
      A=[M01(cpb(var)) ; M02(cpb(var))+inte*rand()];
      B=[M01(cpb(var))+inte*rand()*sqrt(3)/2 ; M02(cpb(var))-inte*rand()*0.5];
      C=[M01(cpb(var))-inte*rand()*sqrt(3)/2 ; M02(cpb(var))-inte*rand()*0.5];
   else
      A=[M01(cpb(var)) ; M02(cpb(var))+inte*rand()*M02(cpb(var))];
      B=[M01(cpb(var))+inte*M01(cpb(var))*rand()*sqrt(3)/2 ; M02(cpb(var))-inte*0.5*rand()*M02(cpb(var))];
      C=[M01(cpb(var))-inte*M01(cpb(var))*rand()*sqrt(3)/2 ; M02(cpb(var))-inte*0.5*rand()*M02(cpb(var))];
   end
   %triplot
   trix=[];
   triy=[];
   [trix(:,count),triy(:,count)]=Tri(A,B,C);
   set(gcf,'CurrentAxes',ax2)
   set(ax2,'ColorOrder',[1 1 1; 1 0 0; 0 1 0; 0 0 1],'nextplot','replacechildren')
   plot(trix,triy);
   set(gca,'XColor',[1 1 1],'YColor',[1 1 1],'ZColor',[1 1 1],'Color',[0.25 0.25 0.25]);
   xlabel('M01')
   ylabel('M02')

while (dM>conv)
   contract=false;
   j=SB;
   count=count+1;
   M_fullA=zeros(1,N);
   M_fullB=zeros(1,N);
   M_fullC=zeros(1,N);
   M_mainA=zeros(1,N);
   M_mainB=zeros(1,N);
   M_mainC=zeros(1,N);

   for int=1:size(W1')
      Ri(int,:,:)=[R1 0;0 R1];
      Wi(int,:,:)=[W1(int) 0; 0 W2(int)];
      Ki(int,:,:)=[-k1(cpb(int)) k2(cpb(int));k1(cpb(int)) -k2(cpb(int))];

      if(var==cpb(int))

Mc=AnalyticGen(squeeze(Wi(int,:,:)),squeeze(Ri(int,:,:)),squeeze(Ki(cpb(int),:,:)),A,N,Spec,squeeze(J(int,:)),squeeze(
xn(int,:)),MHz);
         M_mainA=M_mainA+squeeze(Mc(1,:));

Mc=AnalyticGen(squeeze(Wi(int,:,:)),squeeze(Ri(int,:,:)),squeeze(Ki(cpb(int),:,:)),B,N,Spec,squeeze(J(int,:)),squeeze(
xn(int,:)),MHz);
         M_mainB=M_mainB+squeeze(Mc(1,:));
```

```
Mc=AnalyticGen(squeeze(Wi(int,:,:)),squeeze(Ri(int,:,:)),squeeze(Ki(cpb(int),:,:)),C,N,Spec,squeeze(J(int,:)),squeeze(
xn(int,:)),MHz);
        M_mainC=M_mainC+squeeze(Mc(1,:));
      end
   end
   M_fullA=M_mainA+M_otherpeaks;
   M_fullA=abs(real(fft(M_fullA)));
   M_fullA=M_fullA-min(M_fullA);
   M_fullB=M_mainB+M_otherpeaks;
   M_fullB=abs(real(fft(M_fullB)));
   M_fullB=M_fullB-min(M_fullB);
   M_fullC=M_mainC+M_otherpeaks;
   M_fullC=abs(real(fft(M_fullC)));
   M_fullC=M_fullC-min(M_fullC);

   SA=MSEr2(M_fullA,txt,Cg,100,MHz,Wshift,d);
   SB=MSEr2(M_fullB,txt,Cg,100,MHz,Wshift,d);
   SC=MSEr2(M_fullC,txt,Cg,100,MHz,Wshift,d);
   %rank system
   %-------------------------------------------------------
   %%
   BB=B;
   if(SA<SB)
      if(SB<SC)
         W=C;
         MW=M_fullC;
         SW=SC;
         G=B;
         MG=M_fullB;
         SG=SB;
         B=A;
         MB=M_fullA;
         SB=SA;
      else
         if(SC<SA)
            W=B;
            MW=M_fullB;
            SW=SB;
            G=A;
            MG=M_fullA;
            SG=SA;
            B=C;
            MB=M_fullC;
            SB=SC;
         else
            W=B;
            MW=M_fullB;
            SW=SB;
            G=C;
            MG=M_fullC;
            SG=SC;
            B=A;
```

```
        MB=M_fullA;
        SB=SA;
      end
    end
else
    if(SA<SC)
      W=C;
      MW=M_fullC;
      SW=SC;
      G=A;
      MG=M_fullA;
      SG=SA;
      B=B;
      MB=M_fullB;
      SB=SB;
    else
      if(SC<SB)
        W=A;
        MW=M_fullA;
        SW=SA;
        G=B;
        MG=M_fullB;
        SG=SB;
        B=C;
        MB=M_fullC;
        SB=SC;
      else
        W=A;
        MW=M_fullA;
        SW=SA;
        G=C;
        MG=M_fullC;
        SG=SC;
        B=B;
        MB=M_fullB;
        SB=SB;
      end
    end
end

%%
M=(G+B)/2;
R=2*M-W;
M_mainR=zeros(1,N);
M_fullR=zeros(1,N);

for int=1:size(W1')
    Ri(int,:,:)=[R1 0;0 R1];
    Wi(int,:,:)=[W1(int) 0; 0 W2(int)];
    Ki(int,:,:)=[-k1(cpb(int)) k2(cpb(int));k1(cpb(int)) -k2(cpb(int))];

    if(var==cpb(int))
```

```
Mc=AnalyticGen(squeeze(Wi(int,:,:)),squeeze(Ri(int,:,:)),squeeze(Ki(cpb(int),:,:)),R,N,Spec,squeeze(J(int,:)),squeeze(
xn(int,:)),MHz);
        M_mainR=M_mainR+squeeze(Mc(1,:));
      end
    end
    M_fullR=M_mainR+M_otherpeaks;
    M_fullR=abs(real(fft(M_fullR)));
    M_fullR=M_fullR-min(M_fullR);

    SR=MSEr2(M_fullR,txt,Cg,100,MHz,Wshift,d);

    %%
    %nelder mead algorithm
    if (SR<SG)
      if(SB<SR)
        W=R;
      else
        E=2*R-M;
        M_mainE=zeros(1,N);
        M_fullE=zeros(1,N);

        for int=1:size(W1')
          Ri(int,:,:)=[R1 0;0 R1];
          Wi(int,:,:)=[W1(int) 0; 0 W2(int)];
          Ki(int,:,:)=[-k1(cpb(int)) k2(cpb(int));k1(cpb(int)) -k2(cpb(int))];

          if(var==cpb(int))

Mc=AnalyticGen(squeeze(Wi(int,:,:)),squeeze(Ri(int,:,:)),squeeze(Ki(cpb(int),:,:)),E,N,Spec,squeeze(J(int,:)),squeeze(
xn(int,:)),MHz);
            M_mainE=M_mainE + squeeze(Mc(1,:));
          end
        end
        M_fullE=M_mainE+M_otherpeaks;
        M_fullE=abs(real(fft(M_fullE)));
        M_fullE=M_fullE-min(M_fullE);
        SE=MSEr2(M_fullE,txt,Cg,100,MHz,Wshift,d);

        if(SE<SR)%rather than SE<SB because R might be smaller than E
          W=E;
        else
          W=R;
        end

      end
    else
      if(SR<SW)
        W=R;

      else
        contract=true;
        C1=(M+W)/2;
```

```
        C2=(M+R)/2;
        M_mainC1=zeros(1,N);
        M_fullC1=zeros(1,N);
        M_mainC2=zeros(1,N);
        M_fullC2=zeros(1,N);

        for int=1:size(W1')
           Ri(int,:,:)=[R1 0;0 R1];
           Wi(int,:,:)=[W1(int) 0; 0 W2(int)];
           Ki(int,:,:)=[-k1(cpb(int)) k2(cpb(int));k1(cpb(int)) -k2(cpb(int))];

           if(var==cpb(int))

Mc=AnalyticGen(squeeze(Wi(int,:,:)),squeeze(Ri(int,:,:)),squeeze(Ki(cpb(int),:,:)),C1,N,Spec,squeeze(J(int,:)),squeez
e(xn(int,:)),MHz);
              M_mainC1=M_mainC1+squeeze(Mc(1,:));

Mc=AnalyticGen(squeeze(Wi(int,:,:)),squeeze(Ri(int,:,:)),squeeze(Ki(cpb(int),:,:)),C2,N,Spec,squeeze(J(int,:)),squeez
e(xn(int,:)),MHz);
              M_mainC2=M_mainC2+squeeze(Mc(1,:));
           end
        end
        M_fullC1=M_mainC1+M_otherpeaks;
        M_fullC1=abs(real(fft(M_fullC2)));
        M_fullC1=M_fullC1-min(M_fullC1);
        SC1=MSEr2(M_fullC1,txt,Cg,100,MHz,Wshift,d);
        M_fullC2=M_mainC2+M_otherpeaks;
        M_fullC2=abs(real(fft(M_fullC2)));
        M_fullC2=M_fullC2-min(M_fullC2);
        SC2=MSEr2(M_fullC2,txt,Cg,100,MHz,Wshift,d);

        if(SC1<SC2)
           C=C1;
           SC=SC1;
        else
           C=C2;
           SC=SC2;
        end
        if(SC<SW)
           W=C;

        else
              S=(B+W)/2;

              W=S;
              G=M;

        end
     end
  end

  Avg=(W+G+B)/3;
  if(~contract)
```

```
    dM1=abs(1-B(1)/M1);
    dM2=abs(1-B(1)/M2);
    dM=dM1+dM2;
    M1=B(1);
    M2=B(2);
  else
    dM1=abs(1-B(1)/Avg(1));
    dM2=abs(1-B(2)/Avg(2));
    dM=dM1+dM2;
  end

  M_mainI=zeros(1,N);
  M_fullI=zeros(1,N);

      for int=1:size(W1')
        Ri(int,:,:)=[R1 0;0 R1];
        Wi(int,:,:)=[W1(int) 0; 0 W2(int)];
        Ki(int,:,:)=[-k1(cpb(int)) k2(cpb(int));k1(cpb(int)) -k2(cpb(int))];

        if(var==cpb(int))

Mc=AnalyticGen(squeeze(Wi(int,:,:)),squeeze(Ri(int,:,:)),squeeze(Ki(cpb(int),:,:)),B,N,Spec,squeeze(J(int,:)),squeeze(
xn(int,:)),MHz);
          M_mainI=M_mainI + squeeze(Mc(1,:));
        end
      end
      M_fullI=M_mainI+M_otherpeaks;
      M_fullI=abs(real(fft(M_fullI)));
      M_fullI=M_fullI-min(M_fullI);
      SB=MSEr2(M_fullI,txt,Cg,100,MHz,Wshift,d);

  if(W~=C)
    dSB=j-SB;
  end
  A=G;
  B=B;
  C=W;

  [trix(:,count),triy(:,count)]=Tri(A,B,C);
  set(gcf,'CurrentAxes',ax2)
  set(ax2,'ColorOrder',[1 1 1; 1 0 0; 0 1 0; 0 0 1],'nextplot','replacechildren')
  plot(trix,triy)
  set(gca,'XColor',[1 1 1],'YColor',[1 1 1],'ZColor',[1 1 1],'Color',[0.25 0.25 0.25])
  xlabel('M01')
  ylabel('M02')
  set(gcf,'CurrentAxes',ax1)
  M_main=zeros(1,N);
  M_otherpeaks=zeros(1,N);
  for int=1:size(W1')
    Ri(int,:,:)=[R1 0;0 R1];
    Wi(int,:,:)=[W1(int) 0; 0 W2(int)];
    M0(int,:,:)=[M01(cpb(int));M02(cpb(int))]';
    if(var==cpb(int))
```

```
Mc=AnalyticGen(squeeze(Wi(int,:,:)),squeeze(Ri(int,:,:)),squeeze(Ki(cpb(int),:,:)),B,N,Spec,squeeze(J(int,:)),squeeze(
xn(int,:)),MHz);
        M_main=M_main+squeeze(Mc(1,:));
      end
   end
   M_full=M_main+M_otherpeaks;
   M_full=abs(real(fft(M_full)));
   M_full=M_full-min(M_full);
   Splot3(ax1,M_full,Wshift,txt,MHz);
   set(gca,'XDir','reverse','XColor',[1 1 1],'YColor',[1 1 1],'ZColor',[1 1 1],'Color',[0.25 0.25 0.25])
   axis([Cg(1,1) Cg(2,2) -0.5 1.2*max(M_full)])
   drawnow


end
count;
set(gcf,'CurrentAxes',ax2)
set(ax2,'ColorOrder',[1 1 1; 1 0 0; 0 1 0; 0 0 1])
plot(trix,triy)
set(gca,'XColor',[1 1 1],'YColor',[1 1 1],'ZColor',[1 1 1],'Color',[0.25 0.25 0.25]);
xlabel('M01')
ylabel('M02')
set(gcf,'CurrentAxes',ax1)
Splot3(ax1,M_full,Wshift,txt,MHz);
set(gca,'XDir','reverse','XColor',[1 1 1],'YColor',[1 1 1],'ZColor',[1 1 1],'Color',[0.25 0.25 0.25])
M01(cpb(var))=B(1);
M02(cpb(var))=B(2);
end
```

A.4.22. NMfitAfS.m

```
function [k1,k2,M01,M02,SB]=NMfitAfS(k1,k2,M01,M02,int,txt,Cg,W1,W2,R1,N,Spec,conv,iter,J,x,MHz,var,cpb,d)
W=[W1 0;0 W2];
R=[R1 0 ; 0 R1];
K=[-k1 k2;k1 -k2];
M0=[M01;M02];
dM=conv*2;
dK=conv*2;
   %if(SB>20)
      inc=0;
      ax2=axes('Position',[0.1,0.1,0.8,0.35],'ColorOrder',[1 1 1; 1 0 0; 0 1 0; 0 0 1]);
      set(gca,'XColor',[1 1 1],'YColor',[1 1 1],'ZColor',[1 1 1],'Color',[0.25 0.25 0.25],'ColorOrder',[1 1 1; 1 0 0; 0 1 0; 0
0 1])
      ax1=axes('Position',[0.1,0.575,0.8,0.35]);
      set(gca,'XColor',[1 1 1],'YColor',[1 1 1],'ZColor',[1 1 1],'Color',[0.25 0.25 0.25])
      while((dM>conv||dK>conv)&&inc<=iter)
         inc=inc+1;
         [k1,k2,M01,M02,dK]=NMfitAS(k1,k2,M01,M02,int,txt,Cg,W1,W2,R1,N,Spec,conv,J,x,MHz,var,cpb,d);
         dK=abs(1+K(1,1)/k1(cpb(var)))+abs(1+K(2,2)/k2(cpb(var)));
         K=[-k1(cpb(var)) k2(cpb(var));k1(cpb(var)) -k2(cpb(var))];
         [k1,k2,M01,M02,SB]=NMfitAM0S(k1,k2,M01,M02,int,txt,Cg,W1,W2,R1,N,Spec,conv,J,x,MHz,var,cpb,d);
         dM=abs(1-M0(1)/M01(cpb(var)))+abs(1-M0(2)/M02(cpb(var)));
```

```
        M0=[M01(cpb(var));M02(cpb(var))];
      end
   %end

end
```

A.4.23. Tri.m

```
function [X,Y]=Tri(X1,X2,X3)
%receives the coordinates for a triangle and gives the x and y vectors to be plot for the triangle
X= [X1(1),X2(1),X3(1), X1(1)];
Y= [X1(2),X2(2),X3(2), X1(2)];

end
```